DEPARTAMENT OF
PHYSICS

Software Development for Material Analysis by PIGE (Proton Induced Gamma Emission)

VASCO MIGUEL ROLDÃO MANTEIGAS

Master in Engineering Physics

DOCTORATE IN PHYSICS ENGINEERING

NOVA University Lisbon
March, 2024

DEPARTAMENT OF
PHYSICS

Software Development for Material Analysis by PIGE (Proton Induced Gamma Emission)

Vasco Miguel Roldão Manteigas

Master in Engineering Physics

Adviser: Maria Adelaide Pedro de Almeida Jesus
Full Professor, NOVA University Lisbon

Co-adviser: João Duarte Neves Cruz
Associate Professor, NOVA University Lisbon

Examination Committee:

Chair: Orlando Manuel Neves Duarte Teodoro
Full Professor, FCT-NOVA

Rapporteurs: Luís Filipe dos Santos Garcia Peralta
Associate Professor, FCT-UL

Rui Manuel Coelho da Silva
Main Researcher, IST-UL

Advisers: Maria Adelaide Pedro de Almeida Jesus
Full Professor, NOVA University Lisbon

Members: Daniel Galaviz Redondo
Assistant Professor, FCT-UL

Nuno Pessoa Barradas
Main Researcher, IST-UL

Orlando Manuel Neves Duarte Teodoro
Full Professor, FCT-NOVA

DOCTORATE IN ENGINEERING PHYSICS

NOVA University Lisbon
March, 2024

Software Development for Material Analysis by PIGE (Proton Induced Gamma Emission)

Dedicatory to the researches of CTN

ACKNOWLEDGMENTS

This thesis is about the implementation of the ERYA software, which was only possible due to the combined collaboration of several institutions.

I would like to thank everyone related to this project, starting from my advisers. Through them I gained access to the CTN Research Center and the NOVA University for guidance of the thesis project.

Also, I would like to thank for the opportunity given by the IAEA for the Inter-Codes Meeting, which was important for ERYA recognition.

Also, the author gratefully acknowledges the family support during the elaboration of this project.

“Nothing in life is to be feared,
it is only to be understood.” (Marie Curie).

ABSTRACT

PIGE (Proton Induced Gamma Emission) is an analytical technique based on accelerated proton beams (with most common energies around 1.5 to 3.0 MeV), hindered by the lack of availability of software tools derived from first principles for sample analysis, which have only been on active research in the last twenty years.

Previously, sample composition was determined using the assumption of homogeneity in terms of area and depth and comparing with a standard sample (bulk analysis). For in-depth heterogeneous samples, depth profiling analysis was accomplished by the use of a single isolated resonance for which the concentration profile was easily deduced.

To perform PIGE analysis using first principles, it was required to obtain all relevant cross-sections of many nuclear reactions for a wide range of energies, building a database of them, which became a major endeavor of the research team including the author of this thesis.

From this foundation, the main objective was the development of software capable of performing bulk and depth analysis. Based on first efforts of the research team, recently a decision was made to upgrade to two versions: ERYA-Bulk for homogeneous bulk samples, and ERYA-Profiling for in-depth heterogeneous samples (the ERYA acronym meaning Emitted Radiation Yield Analysis) designed with the following requirements: compatibility with the major operating systems, a user-friendly graphical user interface with re-sizable windows and automatic scaling for different screen sizes, with support of different input and output file formats for relevant contexts. It also should be intuitive and easy to use.

While ERYA-Bulk performs the analysis by direct integration using interpolation of the excitation function, a generalization was made for ERYA-Profiling so that for a specific resonance, overriding the excitation function, a set of parameters that models a resonance by a Lorentzian can be defined either by a Breit-Wigner or a Resonance Strength by filling the necessary parameters.

Since ERYA-Profiling depth profiling analysis requires to take account of the energy dispersion effects (straggling) of proton beams due to the stochastic nature of beam energy loss in the interaction

between the beam and the sample, it would require a elaborate numerical analysis of the energy distributions to perform the heavy computational task to evaluate them.

Keywords: IBA, PIGE, ERYA, Multi-Platform, Vavilov Distribution, Depth Profiling

RESUMO

PIGE (Emissão Gama Induzida por Protões) é uma das técnicas analíticas baseada em feixes de protões acelerados (em geral 1.5 a 3.0 MeV) que para a qual, contrariamente a outras, até há cerca de duas décadas não houve desenvolvimento de software baseado em princípios físicos para o cálculo da composição das amostras a analisar. No pressuposto que as amostras eram homogéneas em área e profundidade era usado um método comparativo com padrões para análise em bloco (*bulk analysis*); para análise em profundidade eram usadas ressonâncias isoladas para as quais a obtenção do perfil era imediata.

Para avançar com cálculos era necessário obter as secções eficazes das reacções nucleares relevantes que se tornou um dos objetivos do grupo de investigação em que esta tese se insere. O grande passo seguinte seria o desenvolvimento de software para análise em bloco e em profundidade.

Recentemente os primeiros esforços de desenvolvimento foram objeto de uma transformação no sentido de criar uma versão para cada caso (ERYA-Bulk e ERYA-Profiling, sendo ERYA o acrónimo de *Emitted Radiation Yield Analysis*) obedecendo a: compatibilidade com todos os sistemas operativos; interface amiga do utilizador com rescalonamento automático para diferentes écrans; aceitação de vários formatos de entrada para os dados físicos pertinentes; produção de vários formatos de saída.

Para a análise de amostras heterogéneas em profundidade, foi feita a generalização de trabalhar uma dada ressonância (para a qual a entrada pode ser dado independentemente em parâmetros de uma Lorentziana definida quer por uma Breit-Wigner ou por uma amplitude de ressonância) em conjunto com a restante função de excitação. Foi necessário fazer um grande investimento para a compreensão e computação da dispersão em energia (straggling) do feixe de protões, devida ao aspeto estocástico da sua perda de energia, e das distribuições que a descrevem, as quais, nomeadamente para pequenas perdas de energia são matematicamente elaboradas e computacionalmente pesadas.

Palavras chave: IBA, PIGE, ERYA, Multi-Plataforma, Distribuição de Vavilov, Análise em Profundidade

CONTENTS

LIST OF FIGURES

LIST OF TABLES

GLOSSARY

Gamma Profiling	Measurement of the composition of the material using the gamma ray yield as function of depth and energy.
Nuclear Yield	Measurable quantity obtained from a nuclear reaction, like the number of gamma rays induced by the reaction.
Analytical Technique	A method to determine the chemical composition of a material using dedicated spectroscopy methods, like the gamma ray emission due to use of an ion beam to irradiate the sample.
Gamma Spectroscopy	The method of quantification and identification of nuclides by the analysis of the gamma-ray spectrum emitted from a source.
Cross-Section	Measurement of probability of a specific reaction between two or more particles.
Differential Cross-Section	Measurement of probability within a certain small area of a specific reaction between two or more particles.
Detector	An electronic device designed to produce a signal from the interaction medium due to a physical interaction from a phenomenon. In this thesis context, a semiconductor gamma detector, use a semiconductor crystal as interaction medium with the gamma ray radiation. The electronic signal is directly proportional to the number of gamma rays and quantified in terms of energy.

ACRONYMS

ERYA	Emitted Radiation Yield Analysis
NGR	Nuclear Reactions Group
CTN	Nuclear Technological Campus / Campus Tecnológico e Nuclear
IAEA	International Atomic Energy Agency
SRIM	The Stopping and Range of Ions in Matter
NRA	Nuclear Reaction Analysis
SPACES	Stochastic Particle Energy Loss
PIGRECO	Particle Induced Gamma Ray Emission Code
NDF	Nuno Data Furnace
PIGE	Particle Induced Gamma-Ray Emission
PIXE	Particle Induced X-Ray Emission

SYMBOLS

$\boldsymbol{\kappa}$	Also known as k-factor. Represents the Vavilov Maximum Transfer Ratio during collisions between the incident beams and the material atoms.
$\boldsymbol{\xi}$	Bethe-Bloch parameter.
$\boldsymbol{\epsilon_{MAX}}$	Maximum Transferable Energy from a collision.
$\boldsymbol{\lambda}$	Landau Parameter. All approximations of Vavilov distribution can be computed in terms of this parameter.
$\boldsymbol{\beta}$	Relativistic Velocity using natural units: $0<\beta<1$
$\boldsymbol{\gamma}$	Lorentz Factor, defined as: $\gamma^2 = 1/(1-\beta^2)$
$\boldsymbol{\gamma_{EM}}$	Euler-Mascheroni constant. $\gamma_{EM} = 0.57721$
$\boldsymbol{\Omega}$, $\boldsymbol{\Omega(\theta,\phi)}$	Solid angle. Solid angle in terms of angular variables.
$\boldsymbol{\Omega_a}$	Standard Deviation of a quantity designed by the subscript "a". It can be “D” or “th” for Thermal Doppler, “Beam” for beam resolution, “S” for Straggling.
$\boldsymbol{\Gamma}$, $\boldsymbol{\Gamma(E)}$	Resonance Width, which in general is a function of energy "E"
$\boldsymbol{\Gamma_a}$	Resonance Width relative to the channel “a”. The subscript letter can be different.
$\boldsymbol{\Gamma(x)}$	Gamma Function of an argument "x", which cannot be confused with the Resonance Width.
$\boldsymbol{\sigma}$, $\boldsymbol{\sigma_T}$	Cross-Section. Total Cross-Section.
$\boldsymbol{\sigma(E,\theta)}$	Cross-Section in function of energy at a certain angle.
$\boldsymbol{\frac{d\sigma}{d\Omega}}$	Differential Cross-Section

$\mathbf{f_i}$	Isotopic Abundance
$\mathbf{f_m}$	Mass Fraction
$\mathbf{N_p}$	Number of Protons
N, n	Number of particles. Number of particles over area when indicated.
j	Density current.
n	Depth of a layer with 10^{15} at/cm^2 units.
$\mathbf{N_{av}}$	Avogrado's Number, equal to $6.022*10^{23}$
$\boldsymbol{\varepsilon_{abs}(E_\gamma)}$	Detector's Efficiency at gamma-ray energy.
$\mathbf{S_m}$	Stopping-Power
F(E)	Distribution function in terms of energy
$\mathbf{F_D(E)}$	Doppler Distribution
$\mathbf{F_{DB}(E)}$	Doppler and Beam Convoluted Distribution
$\mathbf{F_{Beam}(E)}$	Beam Resolution Distribution
$\mathbf{F_S(E)}$	Straggling Distribution.
$\boldsymbol{\overline{E}_k}$	Average Energy at layer k.
$\boldsymbol{(\Delta E)_k}$	Energy loss at layer k.
$\mathbf{I_a}$, $\mathbf{I_b}$, **J**	Spin of a nuclide from channel "a" or "b". Total Spin "J" of a compound.
$\boldsymbol{\omega}$	Statistical Spin Factor
$\boldsymbol{\gamma}$	Width ratio when appears on the product $\omega\gamma$ only.
$\boldsymbol{\delta_0}$	Phase Shift
$\boldsymbol{\psi}$	Wave Function in Quantum Mechanics
$\hbar$	Planck's Constant. The thesis assumes $\hbar = 1$.
$\lambda\!\!\!^{-}$	Compton's Wavelength.
c	Speed of light. This thesis assumes c=1.

1

INTRODUCTION

1.1 Brief Introduction of PIGE Methodology

Along the last century until today, different analytical methods were designed, tested and extended to find the composition of a sample. Methods based on the physics of atomic and nuclear interactions with matter form a rich group of techniques which were exploited by institutions and companies.

Among those techniques, PIGE (Particle-Induced Gamma-Ray Emission) is based on nuclear reactions induced by the beam (composed usually by protons although ionized deuterium and helium may be also used) in the nuclei of the sample. The induced nuclear reaction could produce a new kind of nuclide or a new configuration of the original nuclide, in an excited state, which decays to a more stable configuration, by emission of gamma radiation.

Measuring the energy and the number of emitted photons, the relevant nuclides may be identified and their concentration in the sample may be determined. This constitutes the basis of the PIGE analytical technique, namely for samples considered homogeneous in depth (along the beam direction), being then the technique specified by the adjective Bulk. The cross sections (directly related to the reaction probability) of most nuclear reactions exhibit resonances at certain beam energies, allowing the in-depth scan of a sample, i.e., allowing the depth profiling of a sample. This method measures the number of gammas in function of beam energy. In this case we refer to PIGE Profiling or (p,γ) Profiling.

The origins of PIGE can be traced back to 1950s when the gamma ray emission of fluorine samples due to proton bombardment was discovered. The nuclear reaction $^{19}F(p,\gamma\alpha)^{16}O$ has a significant nuclear reaction rate, making fluorine detectable even for trace amounts on samples. The first measurement of ion beam (proton) analysis of fluorine is credited to Sippel and Glover in 1960 [1] and was done to measure the presence of some trace elements in silicate rocks.

The first comprehensive work on the theory and measurement related to PIGE analysis of fluorine (and following later, of lithium, chlorine and other light elements in between.) was done in 1969 by Bewers and Flack [2]. This work laid the first tools for quantitative evaluation, opening the PIGE Bulk methodology of comparison with a sample (standard) with certified amounts of relevant elements. This methodology was and still is used often for PIGE analysis, although with limitations concerning the availability of standards, and the fact that the major composition of the samples to be analyzed must be known beforehand.

During the late 1980s and early 1990s PIGE Bulk was extended (continuing today) for light multielement analysis in many fields as archaeology, mineralogy, environment, culture heritage and medicine.

Several efforts were made to provide the PIGE community with thick target gamma-ray yields, helping the pursuit of the PIGE comparative methodology, which were later compiled [3].

More recently a movement towards a standard-free methodology appeared. It is important to give credit to Boni work (1988) on the measurement of cross-sections for a set of nuclear reactions [4]. Boni main objective was to create a library of cross-sections to implement a standard free PIGE methodology. The same purpose led the Nuclear Reaction Group (NRG) of LIBPhys to perform detailed measurements of cross-sections concerning light elements [5-20]. This was accompanied by development of software to support a PIGE standard free methodology as detailed later.

During the transition from the 20th to the 21st century, IAEA has funded and encouraged the development of PIGE as a standard-free analytical methodology [21]. A joint CRP Project led to the compilation and measurement (when needed) of proton (and deuteron) induced nuclear reactions in light elements. This data is now part of the IBANDL database [22].

The capability of resonance profiling was first introduced by Möller and Starfelt (1967) [23] for fluorine to test the contamination of Zircaloy cladding of a reactor fuel, and the theory of

depth profiling was developed in 1973 by Mandler [24] using tooth enamel (rich in fluorine) as main sample of study.

The method of resonant depth profiling was based on narrow and isolated resonances of nuclear reactions induced in light elements, mainly (p,γ) resonances. The measured gamma-ray yield obtained by scanning the resonance along the sample is then directly proportional to the relevant element concentration, simplifying the needed calculations. The limitation of this method concerns the availability of adequate resonances and the low cross sections associated with (p,γ) resonances.

Until 1990's several experimental studies led to a set of published resonances with their own physical properties [3], in order to support the PIGE profiling work that meanwhile extended to several light and medium elements.

At this period, depth profiling slowly made the transition from a single dominated element (fluorine) to multiple elements analysis with a broad range of applications, including medicine, geology and material science and technology.

An effort was done to simulate PIGE Profiling from first principles leading to the SPACES program [25]. However, a public version of this program is not available.

Concerning PIGE Bulk and PIGE Profiling, the situation at the beginning of the thesis work was that no public program was available, but the ones developed by the NRG, although the codes SIMNRA [26] (proprietary) and NDF [27] (proprietary) were available for other Ion Beam Analytical Techniques. Using the first version of the PIGE Bulk code developed by the NRG, as described below, NDF program extended later its functionality to PIGE.

Recently, programs SIMNRA (around 2019) and PiGreco (around 2017) also implemented bulk PIGE analysis.

To ensure proper validation and credibility of those different programs, IAEA promoted a joint Inter Code comparison for PIGE Bulk [28], and IAEA just started another inter-code comparison concerning PIGE-Profiling.

In relation to the computation efforts of NRG where the work for this theses is inserted, the very first effort developed was made before by Rodrigo Mateus [29], written in C and running on MS-DOS, called ERYA. Although some data tables (cross-sections and other relevant

quantities) were developed, manual inputs for physical parameters concerning the element were needed. The program itself was not intended for public release.

Around the 2000's the first ERYA program served as template for Micaela Fonseca to implement a GUI version of ERYA [30] that used the proprietary LabView framework. This program was designed as ERYA-Bulk. Some improvements were done to handle the user inputs, and the capability to handle samples with more than one element. It was also capable of performing the fitting procedure of the sample composition from the experimental yields and initial composition guess introduced by the user.

Around 2010, NRG started to work on a more realistic physical model that takes into consideration the beam energy dispersion due to the finite initial beam resolution and due to statistical fluctuations associated with energy loss (i.e. energy straggling) of the beam interacting with the sample. This extended model would allow to perform depth profiling, and layered sample analysis.

Luis Martins [31] created a prototype program using the LabView version of Micaela as a template, introducing new features, including the straggling effects by implementing various approximations of the Vavilov distribution, and an option to the user handle more complex heterogeneous samples with layers made by multielemental compositions.

Since the depth profiling depends on heavy numerical routines, the actual numerical simulation was offloaded to a console program which handled this task and communicated with the LabView program to receive the databases and layers matrix and send the results back to the LabView to be displayed. (A Server/Client pair of programs in a nutshell.)

While the bulk analysis program made with LabView had published results by the scientific community despite compatibility issues, the depth profiling prototype program was confined for Luis Martins graduate thesis and was never used outside also due to several compatibility problems.

1.2 Main Objectives

In this situation, a decision was taken to perform a project where the ERYA programs for bulk and profiling analysis, renamed ERYA-Bulk and ERYA-Profiling, should be remade with the following requirements:

1. Portability and Native Building with a Graphical User Interface. This should ensure compatibility of the code to build and run on different operating systems and architectures. Native compiling is needed to the computer processor to run the critical numerical routines as natively as possible. A Graphical User Interface is also required for user easiness but needed to use open GUI frameworks to avoid proprietary ones like LabView. This requirement favors the use of cross-platform tools to fulfill the development needs.
2. It should handle different types of data files, either by reading and saving them. The LabView version only handled the database files but lacked direct import or export of certain useful files without manual work, apart of copy and paste some text based content. Also, it did not save the results to files.
3. It should follow a Modular Implementation Approach. This simplifies adding new features as needed without wrecking the code.
4. Refined version of the beam straggling energy distributions, to improve accuracy and minimize computation time.
5. Compliance with IAEA format data standards, due to the large nuclear data compilation of this institution.

The development of programs obeying these requirements constitutes the objective of this thesis. Additionally, the writing down of manuals [32] of both programs was also required.

The modularity and native building requirements were fulfilled by choosing C++ language as option by the author of this work.

To ensure portability, including the GUI, wxWidgets framework was chosen to implement the graphical elements of the program, since it provides a multi-plaform GUI toolkit, that was originally a clone of Microsoft MFC (Microsoft Foundation Class) over Windows Win32 API and then later extended for other operating systems.

This thesis uses a format approach based on papers, starting by providing in Ch. 2 a general context of the work done, introducing the framework of PIGE (theoretical basis and brief description of experimental set-up); theoretical aspects concerning nuclear resonances and

energy distributions and main points of the implementation of ERYA-Bulk and ERYA-Profiling. Also, a resume of results obtained in relation to the implementation and performance of both programs and applications is presented. Ch. 3 contains the most important papers concerning the implementation and performance of both programs. Ch. 4 provides general conclusions of the developed work and hints for future work.

2

PIGE FRAMEWORK AND ERYA IMPLEMENTATION

2.1 Background

As stated before, PIGE is one of the ion-beam based techniques relying on gamma-ray producing nuclear reactions – (p, γ), (p,p'γ) (p,αγ) or even (p,nγ) due to the interactions of charged particles (usually protons) with the sample's nuclei.

The gamma-rays energies point to a specific nuclear reaction and isotope involved in that reaction.

The number of produced gamma-rays (gamma yield) is directly proportional to the number of protons impinging on the target, on the number of atoms of the relevant isotope seen by the beam, which for a thin layer is equal to the number of atoms per area unit multiplied by the layer thickness (or areal atomic density), and on the relevant reaction cross section (translating the probability of reaction occurrence).

Hence, if the cross section is known and the number of protons and correspondent produced gamma-rays are measured, the number of atoms of the relevant isotope (element) may be determined, and this constitutes the basis of the PIGE technique.

In the next sections we describe briefly a typical PIGE experimental set-up and explain the analytical methodologies.

2.2 PIGE Experimental Setup

2.2.1 The main Components of an Experimental Setup for PIGE

In general, PIGE requires three major components, as depicted in fig. 2.1: a particle accelerator that delivers the ion beam (usually protons), a vacuum chamber to place the sample to be irradiated, and the gamma ray detector with the associated electronics. In general, the path between the ion source and the target is under high vacuum ($\sim 10^{-7}$ mbar).

The most common accelerators used for PIGE experiments are linear accelerators that commonly provide particle beams with energies up to 10 MeV, which complies with the PIGE analysis commonly performed under 4 MeV.

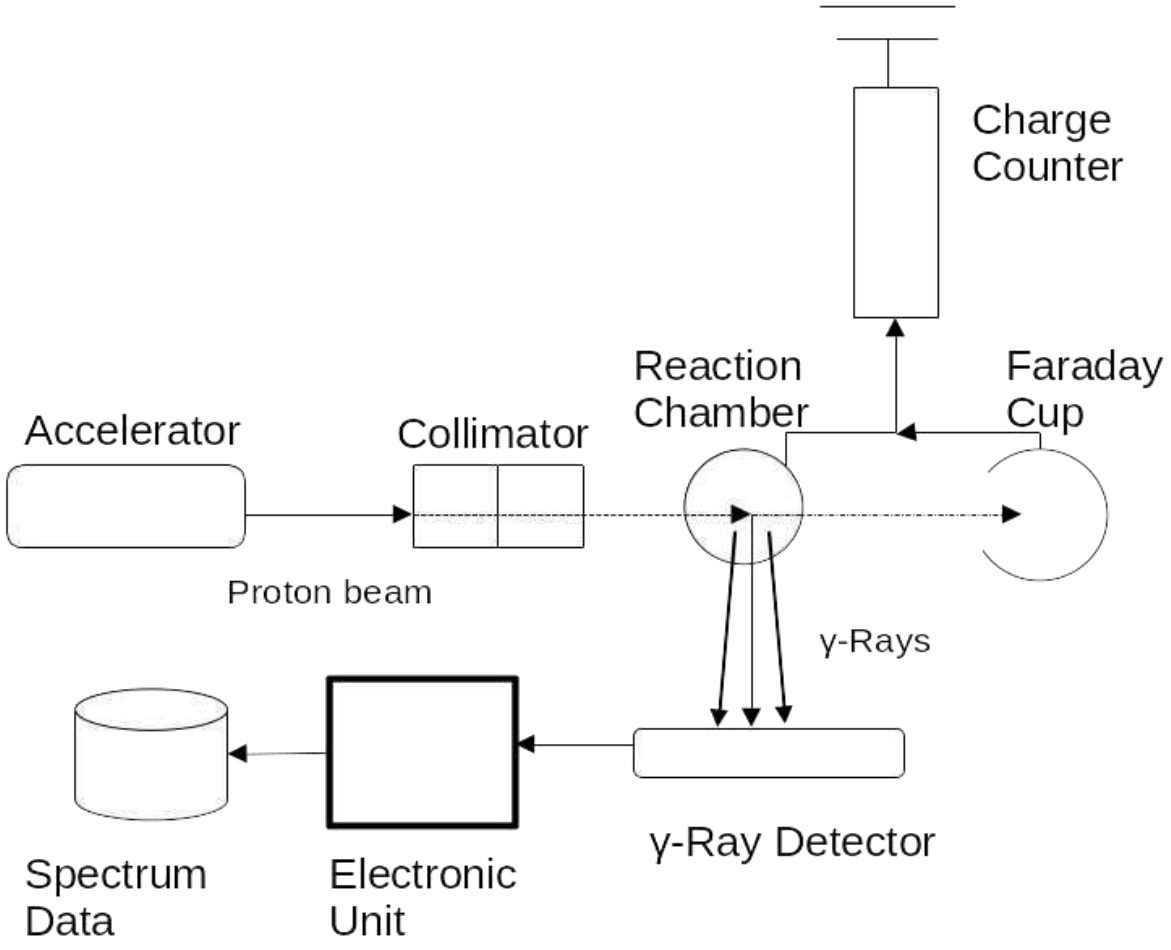

Figure 2.1. A simple sketch of the generic PIGE instrumentation.

Once the proton beam hits the target at the reaction chamber it will produce gamma-ray radiation which will be detected by a proper device called detector, and the electric charge, correspondent to the number of incident projectiles, is measured by a charge counter (Which is a dedicated electronic device. Older laboratories uses a current integrator made from electronic components.). The gamma-ray spectrum is obtained by an electronic unit coupled with the detector, being the main components shown in fig. 2.2.

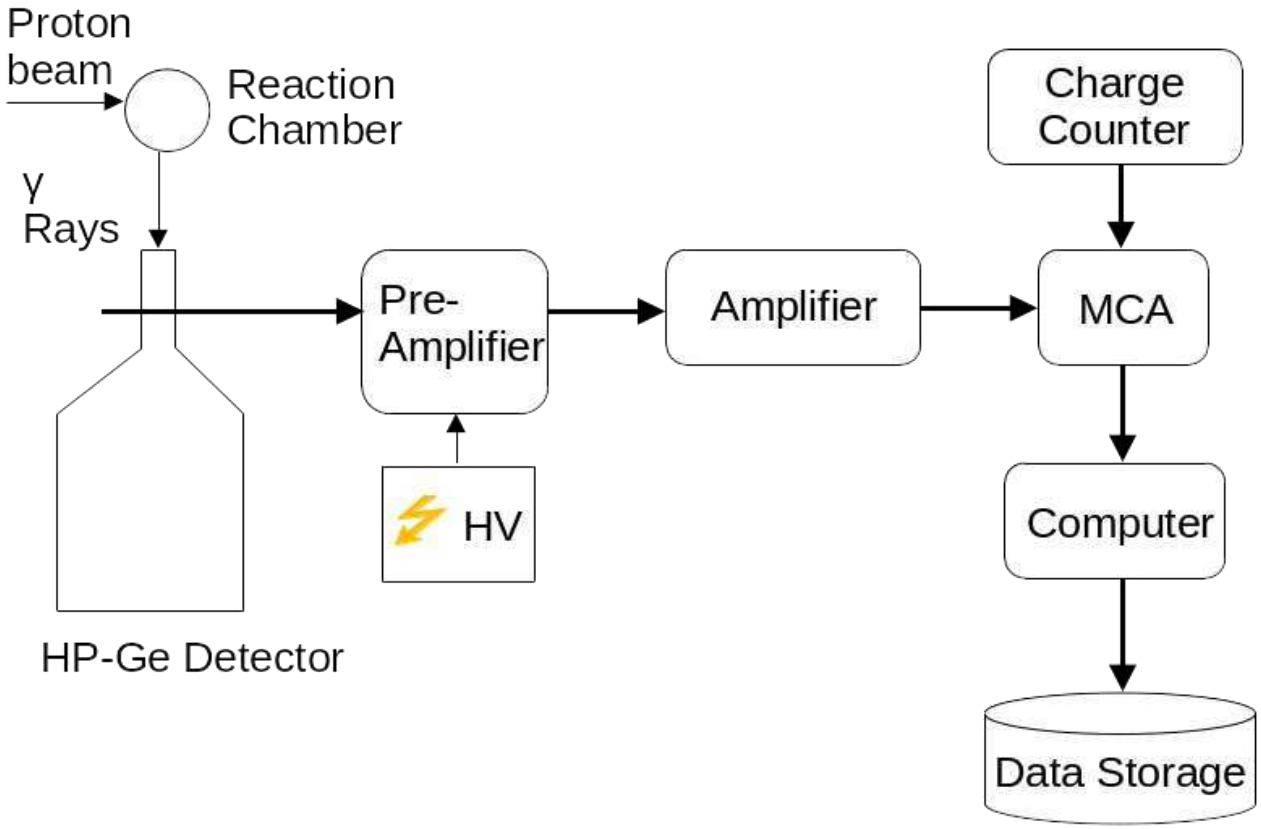

Figure 2.2. Description of the major electronic components of the Electronic Unit mentioned in fig. 2.1, where MCA refers to Multi-Channel Analyzer.

The widespread application of gamma detectors based on semiconductors are mainly to their high energy resolution and fair efficiency. The HP-Ge (High Purity Germanium) detectors have the additional advantage of having a good efficiency for gamma rays (above 100 keV).

Semiconductor detectors work by placing a pure semiconductor crystal (germanium is this case, with specific dopants added to the crystal) under a high-voltage electric field, where the gamma-ray radiation excite the electrons from the crystal atoms and produces free electrons and holes which are

in number proportional to the energy of the radiation. These excited electrons will transfer from the valence band to the conduction band of the semiconductor, and an equal number of holes is created in the valence band. The electric field will guide the electrons and holes to the electrodes, creating a charge pulse.

The electronic unit of fig. 2 will treat the conversion of the electric signal to digital data.
Since the energy required to produce electron-holes pairs is lower compared to the one required to create ions in a gas detector, the statistic variation of the electric pulse height is lower and the energy resolution is better, while the time resolution due to the higher electron speed is also better. This physical advantage of semiconductor detectors, with higher density compared to gaseous detectors, enables to create a small detector. Germanium crystals can also be very thick, with some centimeters compared to silicon (which cannot be thicker than some millimeters), which make them viable for radiation energies up to few MeV gamma-ray detection.

2.2.2 The PIGE Setup at CTN

At national level, a PIGE set-up was developed at the CTN institution provided with an accelerator laboratory. The installations use a Tandem accelerator whose internal components can be read on [1, 2]. To this work is it more worth to give a brief explanation about the complete experimental setup where the accelerator is the main device.
The Tandem has two main channels related to the particle beams, where the left side is linked to the particle beam intake, and the right side handles the beam propagation.
Since the left side handles the ion sources and other devices under low energy physics, it is also known as the Low Energy (LE) side of Tandem. For PIGE perspective, the LE is responsible to produce the ions to create a beam and steer it into the accelerator.
The right side contains all the instrumentation devices which focus and steer the beam into several reaction lines, where PIGE (named NRA in fig. 2.3) is one of them. Since the particle beam travels at higher energies, it is referred to as High Energy (HE) side of the Tandem.
Also, along those lines Faraday Cups (FC) are placed on certain points to measure the beam intensity.

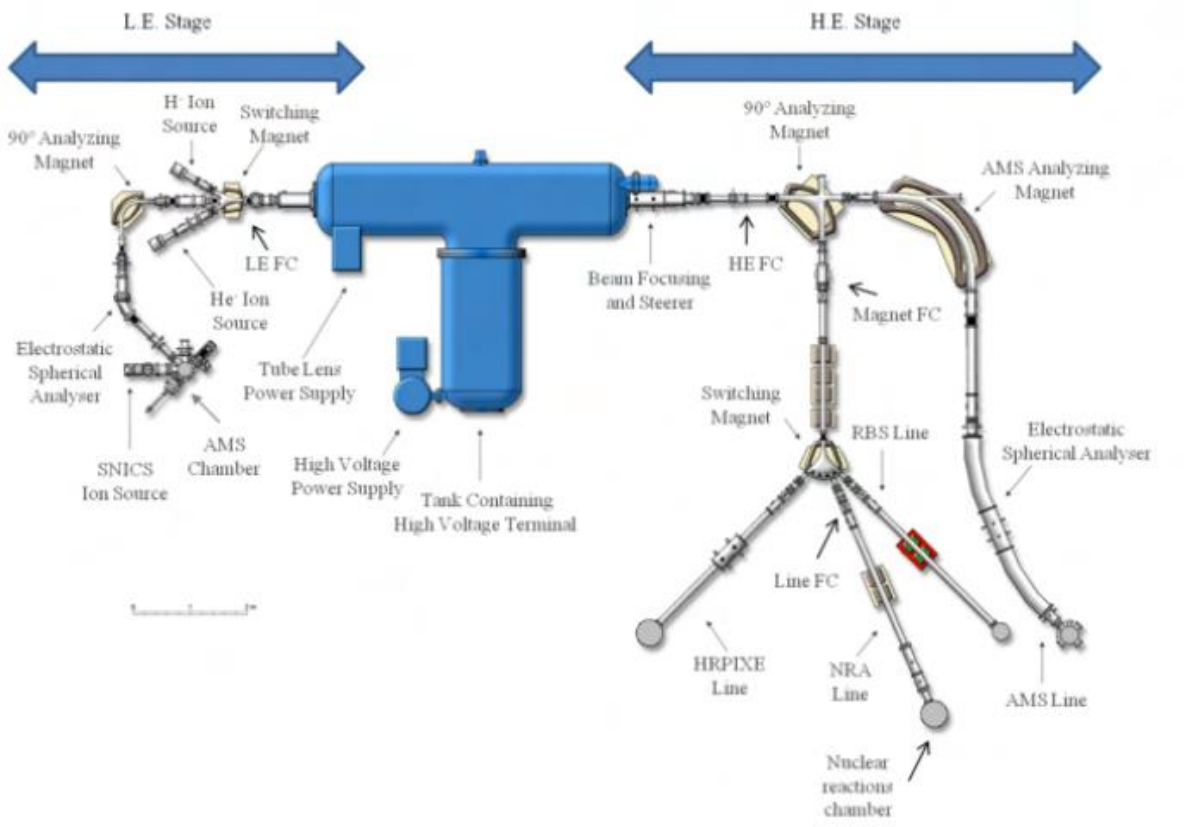

Figure 2.3. Full Description of CTN Tandem accelerator, adapted from [1, 2]

Describing now the reaction chamber we point out:

- Since the sample chamber is isolated from electronics and the accelerator (acting as a Faraday Shield device), it is possible to evaluate the collected charge by integrating the current from the target holder and the chamber itself.
- The gamma detector mounted at the target chamber is a commercial one manufactured by Ametek Ortec which is high HP-Ge, with a resolution of 1.76 keV at the 1332 keV peak of ^{60}Co and 45% relative efficiency.

The detector's absolute efficiency curve was determined from radioactive calibration sources, ^{152}Eu, ^{56}Co and ^{133}Ba, with specific gamma peaks with 5% uncertainty in their activity. Fig. 2.4 shows the efficiency curve obtained by measuring a set of experimental values from the calibration samples at the target position, and then fit the results as displayed.

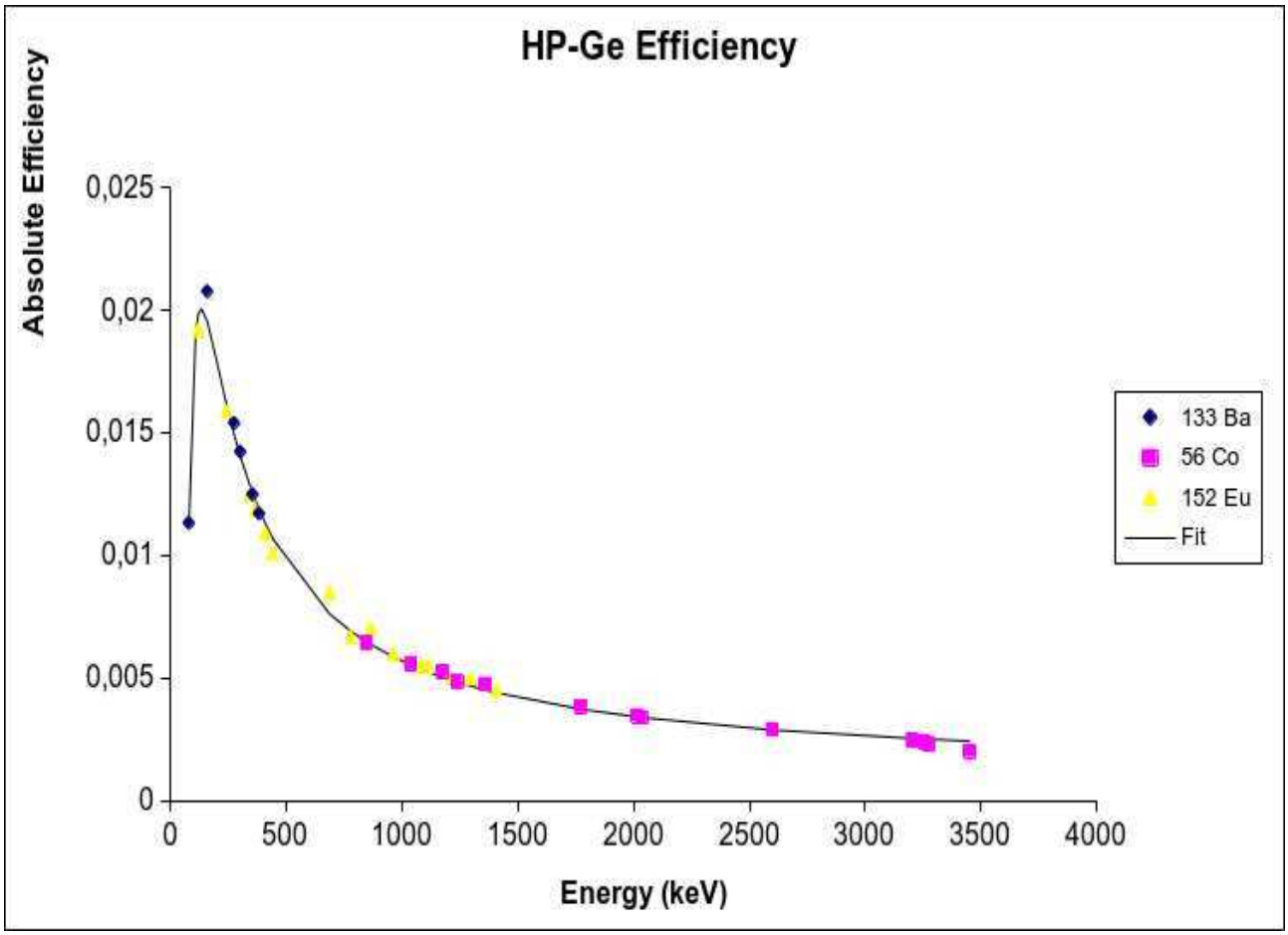

Figure 2.4. HP(Ge) Efficiency curve plotted from radioactive source data.

The black line (fit) is the polynomial fit of this experimental detector efficiency data, using the following model:

$$\epsilon_{\text{abs}}(E_\gamma) = a_3x^3 + a_2x^2 + a_1x + a_0 \qquad x = \frac{1}{E_\gamma}$$

This cubic function composed with the reciprocal of energy ensures a single maximum for the efficiency and a long tail for higher energies than the peak. Also, this function was chosen in the context of the IAEA CRP mentioned before.

2.3 Description of the PIGE methods

As mentioned in the introduction chapter PIGE as a quantitative methodology has evolved from a standard-based technique to a standard-free one. In the following paragraphs we will discuss these two approaches.

2.3.1 PIGE Methodology using Standard Samples

From the interaction of N_p protons with energy E with a thin layer having an areal density Nidx of a relevant isotope species, the corresponding gamma yield dY(E,θ) detected at an angle θ in relation to the beam direction is given by:

$$dY(E,\theta) = 4\pi.\varepsilon_{\text{abs}}(E_\gamma).N_p.\sigma(E,\theta).N_i.dx \quad (2.1)$$

where Ni is the number of isotopes per unit volume, dx is the thickness of the thin layer, $\varepsilon_{abs}(E\gamma)$ is the absolute efficiency of the detector for γ rays with energy Eγ, and σ(E,θ) the differential cross-section at proton energy E and detection angle θ. Considering that, for a thick target, a beam with initial energy E_0 will steadily lose energy as it crosses the sample, the total yield will be, for in-depth homogeneous samples:

$$Y(E_0,\theta) = 4\pi.\varepsilon_{\text{abs}}(E_\gamma).N_p.f_m.f_i.N_{av}.A^{-1}\int_0^{E_0}\sigma\,(E,\theta)/S_m\,(E)\,dE \quad (2.2)$$

where $S_m(E)$ is the mass stopping power at energy E; f_m is the relevant element mass fraction; f_i, and A are the isotopic abundance and atomic mass of the relevant element, respectively, and N_{av} is the Avogadro number. The factor $N_i/\rho = f_m.f_i.N_{av}.A_{-1}$, where ρ is the mass density of the sample, transforms the atomic density into mass fraction also changing the linear stopping power to mass stopping power.

The yield (2.2) may also be given by the following sum:

$$Y(E_0,\theta) = 4\pi.\varepsilon_{\text{abs}}(E_\gamma).N_p.f_m.f_i.N_{av}.A^{-1}\left[\int_{E_1}^{E_0}\sigma\,(E,\theta)/S_m\,(E)\,dE + \int_{E_2}^{E_1}\sigma\,(E,\theta)/S_m\,(E)\,dE+\ldots\right] \quad (2.3)$$

The energy intervals may be chosen small enough so that there is a negligible variation of the stopping power within each interval. Then (2.3) can be written as:

$$Y(E_0,\theta) = 4\pi.\varepsilon_{\text{abs}}(E_\gamma).N_p.f_m.f_i.N_{av}.A^{-1}.\left[S_{m0}^{-1}\int_{E_1}^{E_0}\sigma(E,\theta)\,dE + S_{m1}^{-1}\int_{E_2}^{E_1}\sigma(E,\theta)\,dE+\ldots\right] \quad (2.4)$$

The cross-section integrals will become smaller as the energy is decreased, so that a minimum energy value may be considered for the calculations.

As the stopping-power behaves smoothly by large energies scales, in first approximation, it may be assumed constant in the energy interval E_0-E_{min} and equal to its value at incident energy E_0.

$$Y(E_0,\theta) \approx 4\pi\varepsilon_{\text{abs}}(E_\gamma).N_p.f_m.f_i.N_{av}.A^{-1}S_m^{-1}(E_0)\int_{E_{min}}^{E_0}\sigma(E,\theta)\,dE \tag{2.5}$$

The integral of the differential cross-section in (2.5) is the total cross-section, represented by σ_T:

$$Y(E_0,\theta) \approx 4\pi\varepsilon_{\text{abs}}(E_\gamma).N_p.f_m.f_i.N_{av}.A^{-1}.S_m^{-1}(E_0).\sigma_T(E_0) \tag{2.6}$$

Hence, the gamma yield from a given sample compared with the corresponding yield from a standard sample (std) for an initial beam energy E_0, would be given by

$$\frac{Y_s(E_0,\theta)}{Y_{std}(E_0,\theta)} = \frac{\varepsilon_{\text{abs}}(E_\gamma).N_p.f_s.f_i.N_{av}.A^{-1}.S_m^{std}(E_0).\sigma_T(E_0,\theta)}{\varepsilon_{\text{abs}}(E_\gamma).N_p.f_{std}.f_i.N_{av}.A^{-1}.S_m^{S}(E_0).\sigma_T(E_0,\theta)} = \frac{f_s}{f_{std}}\frac{S_m^{std}(E_0)}{S_m^{S}(E_0)} \tag{2.7}$$

A better approximation is often employed replacing in (2.7) $S_m(E_0)$ by $Sm(E_{1/2})$, being $E_{1/2}$ the proton energy correspondent to half the value of the yield obtained at E_0.

With this simple formula (2.7) it is possible to solve the problem of finding the concentration fs of an element in a given sample in terms of a standard f_{std} concentration.

Note that the cross-sections are related to the element (isotope) to be analyzed, while the stopping power aggregates all elements in the sample, which means the stopping power of a standard sample compared to an experimental sample, for the same beam energy, will have different values.

Although the approximations behind the calculation algorithm are acceptable, this methodology relies on the knowledge of both sample and standard major compositions (which determine the stopping power), which constitutes its weakness. For some so-called standard samples, standard mass fractions are given for some elements, but the exact major composition is not known. In relation to samples to be analyzed, their major composition is often unknown.

2.3.2 Standard-free Methodology

One could start from (2.3), solving the integral, implying the knowledge of the energy functions describing the stopping power and the nuclear cross section. Although the first quantity is a smooth function of energy, the same is not true for the second. The function describing the variation of nuclear reaction cross sections with energy (called the excitation function) often exhibits resonances over a continuum and cannot easily be described by an analytical equation. However, considering that the total yield is the sum of yields corresponding to infinitesimal layers (for each layer both the stopping power and cross section are constant) (2.3) leads to:

$$Y(E_0,\theta) = \sum_{k=1}^{N} \Delta Y_k(E_k,\theta) = 4\pi\varepsilon_{\text{abs}}(E_\gamma).N_p.f_i.f_m.N_{av}.A^{-1}\sum_{k=1}^{N}\sigma(E_k,\theta).S_m^{-1}(E_k)\underbrace{(E_{k+1}-E_k)}_{\Delta E} \qquad (2.8)$$

To perform a standard-free PIGE method of in depth-homogeneous samples, it is necessary to evaluate numerically the integral in (2.4) using (2.8) as template for the algorithm, whose accuracy depends on the detailed knowledge of the cross section. The wider the energy range and density of values of the cross-section available, the higher the accuracy of the yield calculation. Once available a full description from low energies to the initial beam energy, it is possible to scan the entire excitation function to perform the theoretical yield evaluation.

As stated in the introduction chapter, the Nuclear Reaction Group (NRG) started around the year 2000 to measure relevant nuclear cross sections and recently IAEA lead a joint effort of experimental measurements and gathering from the literature of relevant data [3], which were compiled in IBANDL [4].

The uncertainty of mass fractions (or concentrations), determined from (2.8), depends on the uncertainties of the detector efficiency, beam collected charge, and absolute values of the cross sections and stopping powers.

The combined uncertainty of these quantities is rather large, but may be reduced by a calibration procedure, relying on standard samples. Hence, this standard-free methodology has a moment in time, the calibration process, when standard samples are used. Once the calibration factors are measured and introduced in the code or user editable databases the analytical work may proceed without further use of standards.

The existence of a computational program translates in other advantages. A fitting algorithm may be introduced to allow the search of the best possible composition description of the sample, together with individual element mass fractions. Ratios between mass fractions of elements belonging to a given chemical compound may be fixed during the fitting process.
ERYA-Bulk, one of the programs developed during this thesis, performs yield calculations from (2.8), implementing all the advantages mentioned before for the analysis of in depth-homogeneous (or bulk) samples.

2.3.3 Extending for in depth-heterogeneous samples

Equation (2.3) may be again the starting point, but to deal with in heterogeneous samples along the depth, mass fractions must be inside the integral, as protons going through the sample (and losing their energy in the process) will interact with potential different elemental (isotopic) concentrations. Also, within a given layer the protons will have an energy distribution around an average energy calculated from the average energy loss.
Hence the starting equation for yield calculation is:

$$Y(E_0,\theta) = 4\pi\varepsilon_{\text{abs}}(E_\gamma).N_p.N_{av}.A^{-1}\int_0^{E_0}\sigma\,(E,\theta).f_i(E).f_m(E)/S\,(E)\,dE \qquad (2.9a)$$

Where the following quantity is evaluated by the following integral in terms of distributions of energy:

$$\sigma\,(E,\theta) = \int_{-\infty}^{\infty}\int_{-\infty}^{\infty}\sigma\,(E-E',\theta)\,F_S(E''-E')F_{DB}(E'')dE'dE'' \qquad (2.9b)$$

ERYA-Profiling, the other program developed during this thesis was designed to tackle this calculation.
One specific aim of this program is to simulate a resonance-scanning depth-profile as this is one of the ion beam techniques to analyze heterogeneous samples.
In order to implement numerically the calculation of (2.9a) and (2.9b), two problems had to be solved:

1. How to describe the proton energy distribution, where in particular for the first layers of the material corresponds to very small energy losses?
2. How to deal with a specific resonance?
    a) Information about thin resonances cannot be taken directly from excitation functions for the case where the target thickness is larger than the resonance width. In this

case the excitation function gives the integration of the resonance along the target thickness.

b) For resonant depth-profiling isolated very thin resonances have been used, being the information related to them resumed to resonance width and strength.

The following paragraphs address these two problems.

2.4 ERYA-Profiling Yield Calculation

Starting from (2.9), ERYA-Profiling takes the following assumptions:

- It considers the sample as a composition of homogeneous layers, with mass fraction f_{mk}, where each layer is perpendicular to the beam direction.
- For each individual layer or integration layer k the variable E is approximately constant, equal to $\overline{E}_k$, which is the initial energy E_0 subtracted by the average energy loss of the protons till that specific layer, $\overline{E_k} = E_0 - (\Delta E)_0 - \ldots - (\Delta E)_k$.
- The stopping-power at an individual layer may be treated as constant, as the energy variation within each layer is small.

Using those three principles, the yield for a given element is represented by the following sum:

$$Y(E_0, \theta) = \sum_{k=1}^{n} Y_k\left(\overline{E}_k, \theta\right) \tag{2.10}$$

where each partial yield may be calculated by:

$$Y_k\left(\overline{E}_k, \theta\right) = 4\pi\varepsilon_{\text{abs}}\left(E_\gamma\right).N_{av}.N_p.A^{-1}.f_{mk}.f_i.F\left(\overline{E}_k\right)/S\left(\overline{E}_k\right) \tag{2.11}$$

where $F(E)$ refers to the proton energy distribution and the quantity ΔE_k represents the energy lost in layer k, which is related to:

$$\overline{E}_{k+1} = \overline{E}_k - (\Delta E)_k \tag{2.12}$$

The energy function, $F(E)$, is given by a convolution of three separated distributions:

$$F(E) = F_D(E) * F_{Beam}(E) * F_S(E) \tag{2.13}$$

where $F_D(E)$ is the Doppler Distribution, a gaussian distribution with thermal standard deviation given by:

$$\sigma_{th} = 2.355\sqrt{\frac{2m_H kTE_k}{M}} \quad (2.14)$$

Where kT is the temperature of the sample (directly converted to keV), m_H is the hydrogen mass, M the isotopic mass and E_k the beam energy at layer k, with all quantities set in keV.
$F_{beam}(E)$ represents the beam initial energy dispersion or beam resolution (assumed also as gaussian) $F_S(E)$, the Straggling Distribution, is the energy distribution resulting from the stochastic character of the energy loss suffered by the beam. It may be described by energy distributions, Landau [5], Vavilov [6] or Gaussian, depending on the amount of energy loss. Actually, Landau and Gaussian approximations may be found as limits (for very small and very large energy losses, respectively) of the Vavilov approach.

Due to the complexity of the Vavilov analytical solution, leading to calculations which are computer-time consuming [7], different approaches have been used to include this distribution in Monte Carlo codes programs dealing with transport of charged particles through matter [8-12].
We chose to follow the approach of Rotondi and Montagna [9], who derived several analytical expressions to cover the domain of energy loss where the Landau and Vavilov approximations are relevant. We found some continuity issues regarding the frontier between different functions, which motivated the development of several modifications.
The fluctuations in the energy loss may be characterized by the significance parameter κ, which is proportional to the ratio of mean energy loss to the maximum allowed energy transfer in a single collision with an atomic electron, ϵ_{MAX} [6]:

$$\kappa = \xi/\epsilon_{MAX} \quad (2.15)$$

where the parameter ξ comes from the Bethe-Bloch formula and is defined as [6]:

$$\xi = 2\pi\left(\frac{e^2}{4\pi\varepsilon_0}\right)^2 \frac{{Z_1}^2 Z_2 N_A \rho x}{m_e \beta^2 c^2 A} = \frac{2.5496*10^{-10} {Z_1}^2 Z_2 n}{\beta^2 A}\,[\text{keV}] \quad (2.16)$$

And ϵ_{MAX} itself is given by the following relativistic formula, as it includes the relativistic velocity β and the Lorentz factor γ [6]:

$$\epsilon_{MAX} = \frac{2m_e\beta^2\gamma^2}{1+2\gamma\frac{m_e}{m_p}+\left(\frac{m_e}{m_p}\right)^2} \quad (2.17)$$

All previous formulas (2.15-2.17) assume c=1 and all masses in keV as implemented on ERYA. The layer depth n uses SRIM units, which is 10^{15} at. /cm^2. A is the atomic mass of the target and Z_1 with Z_2 corresponds to the atomic number of the ion beam and target respectively.

The value of the significance parameter determines the choice of the adequate straggling energy distribution, as indicated in table 2.1, also showing the modifications implemented in this work.

Rotondi and Montagna	**Our work**
Landau Distribution $\kappa \leq 0.02$ Moyal Function $0.02 \leq \kappa < 0.27$ Split in 3 intervals: $0.02 \leq \kappa < 0.12$ $0.12 \leq \kappa < 0.22$ $0.22 \leq \kappa < 0.29$	Landau Distribution $\kappa \leq 0.02$ Moyal Function $0.02 \leq \kappa < 0.29$ Split in 3 intervals: $0.02 \leq \kappa < 0.11$ $0.11 \leq \kappa < 0.22$ $0.22 \leq \kappa < 029$
Edgeworth Expansion $0.29 \leq \kappa < 5$	Airy Function $0.29 < \kappa < 22$
Gaussian Distribution $\kappa > 5$	Gaussian Distribution $\kappa > 22$

Table 2.1 The different regimes and functions used to emulate the Vavilov distribution in the previous work of Rotondi and Montagna (where our work was based) and in our work.

The major modification is the implementation of the Airy function of First Kind to replace the Edgeworth Expansion. The Airy function numerical approximation was derived by the author of this thesis. Details may be found in Appendix 1. This function assures a better continuity between the Moyal and Gaussian regimes.

More details of the physics/mathematics of the distributions as well as some computation details are given in the paper "ERYA-Profiling Energy Straggling Distributions", part of the chapter 3 of this thesis.

2.5 Resonances

Under the context of nuclear reactions, a resonance is a physical phenomenon that occurs when the energy of an incident particle matches (almost) exactly the energy of a specific state of the compound nuclide, composed by the target nuclide with the projectile. The resonance translates into a peak of the excitation function.

Under the realm of Nuclear Physics, as it would be explored in detail under the *Theory of Resonances and Scattering* paragraph, all nuclear resonances are modeled by a Lorentz-like function:

$$f(E) = \frac{\Gamma^2/4}{(E-E_R)^2+\Gamma^2/4} \tag{2.18}$$

the function *f(E)* depending on the resonance energy E_R and the width of the resonance Γ.

From elemental calculus, (2.18) goes to a single maximum equal to one when $E=E_R$ and decreases towards zero when $E < E_R$ or $E > E_R$.

It is worth to notice that the function can be rewritten as a function of a universal scale ε, given by:

$$\epsilon = \frac{2(E-E_R)}{\Gamma} \tag{2.19}$$

Resulting the universal Cauchy-Lorentz distribution:

$$f(\epsilon) = \frac{1}{1+\epsilon^2} \tag{2.20}$$

The cross-section of a nuclear excitation function that has a resonance can be evaluated by this simpler formula:

$$\sigma(E) = \sigma_R f(E) = \frac{\sigma_R \Gamma^2/4}{(E-E_R)^2+\Gamma^2/4} \tag{2.21}$$

where σ_R is the maximum cross-section of the resonance as modeled. With (2.21) in mind, any resonance can be modeled only by their maximum, width and resonance energy.

To derive a Lorentz-like resonance from experimental data, an adequate fit in terms of the parameters of (2.21) should be performed using adequate software.

A more careful derivation follows.

2.6 Theory of Scattering and Resonances

Till now the key concepts of PIGE and the physical measurements were elucidated. To understand the formal derivation of the nuclear yield, the excitation function and the resonances, it is needed to review the Theory of Scattering under a mixture of Classic and Quantum Mechanics concepts.

2.6.1 Definitions of Cross-Section

The interaction of a low energy projectile (a few MeV proton, deuteron or helium beam) with a target nucleus may be treated as a classical collision between the two nuclei, where the first correction of the classic model is provided by wave mechanics formalism. The quantum mechanics derivation may be done without considering the nuclear forces between projectile and nucleus.

Physically the probability of interaction is directly proportional to the cross-section of the interaction of the two nuclei, which is equal to the ratio between the number of scattered particles *N* per time unit and the incident beam current flux *j*:

$$\sigma = \frac{N}{j} \tag{2.22}$$

Since the process is generally not isotropic, it is useful to define a differential cross section given by:

$$\frac{d\sigma}{d\Omega} = \frac{n}{j} \tag{2.23}$$

where *n* is the number of scattered particles per unit angle and also by unit time. By integrating (2.23) the total cross-section is obtained:

$$\sigma = \int_0^{2\pi} \int_0^{\pi} sin\,(\theta) \left(\frac{d\sigma}{d\Omega}\right) d\theta d\phi = \int_0^{2\pi} \int_0^{\pi} \frac{n(\theta,\phi) sin(\theta)}{j(\theta,\phi)} d\theta d\phi \tag{2.24}$$

When the cross-section is isotropic, the integration of (2.24) is trivial, leading to:

$$\sigma = \frac{4\pi n}{j} = 4\pi \left(\frac{d\sigma}{d\Omega}\right) \tag{2.25}$$

This simple result explains the "4π" conversion factor between the total cross-section used on ERYA databases and the differential cross-section used on IBANDL files.

2.6.2 First Approach to derive the Cross-Section around a Resonance

To develop a model required to evaluate the cross-section of a nuclear reaction, especially around a resonance, one may follow the basic reasoning of Krane [13] and Rolfs [14] crossing the key concepts with Merzbacher [15].

Since the nuclear interaction can be approximated by central forces at distances larger that the size of the nuclide itself, the interaction of a particle and a nuclide may be described by a Schrodinger's equation on spherical coordinates:

$$\left[-\frac{\hbar^2\nabla^2}{2m} + V(r)\right]\psi(r) = \frac{\hbar^2 k^2}{2m}\psi(r) \tag{2.26}$$

From the long-range perspective, only the radial part of (2.26) dominates, which simplifies to:

$$\left[\frac{\partial^2}{\partial r^2} + \frac{1}{r}\frac{\partial}{\partial r} - V(r) + k^2\right]\psi(r) = 0 \tag{2.27}$$

Assuming that the interaction between the projectile and the nuclide only happens inside a potential well within a certain radius *R*, with a constant potential *Q*, defined by:

$$V(r) = -Q : 0 < r < R, Q > 0 \tag{2.28}$$

Using the scaling factor $u(r) = r\psi(r)$, (2.27) reduces to a trivial solvable differential equation:

$$\left[\frac{\partial^2}{\partial r^2} - V(r) + k^2\right]u(r) = 0 \tag{2.29}$$

leading to different wave-functions for different zones:

$$u_0(r) = u_0 sin(kr), r < R: \psi_i(r) = u_0\,(r)/r \tag{2.30}$$

$$u_1(r) = u_1 sin(kr + \delta_0), r > R: \psi_f(r) = u_1\,(r)/r \tag{2.31}$$

This result also provides incident and final wave formulas, which are similar to a free particle wave function, being the only difference between the final and incident waves a phase shift δ_0. Since no destruction or creation of particles (at lower energy scales it is meaningless) happen during the interaction of the target nuclide with the projectile, the density current is conserved;

$$j_f = j_s + j_i \tag{2.32}$$

which means that the final current is equal to the sum of the scattered and initial currents. Density currents are calculable from the wave-function as following:

$$j = \frac{\hbar}{2mi}\left(\psi^* \frac{\partial \psi}{\partial r} - \psi \frac{\partial \psi^*}{\partial r}\right) \tag{2.33}$$

And, due to the conservation law in (2.32) and the presence of a phase shift on (2.31), the scattered wave-function may be given by:

$$\psi_s = \psi_f - \psi_i = \frac{(u_1 sin(kr+\delta_0) - u_0 sin(kr))}{r} = \frac{Ae^{ikr}(e^{2i\delta_0}-1)}{2ikr}, A = u_0 = ku_1 e^{-ik\delta_0} \tag{2.34}$$

To derive the cross-section at (2.23) it only requires evaluating the scattering current density by applying (2.34) and (2.33), to obtain:

$$n = j_s = \frac{\hbar |A|^2}{mkr^2} sin^2(\delta_0) \tag{2.35}$$

while the incident current density is evaluated in a similar fashion:

$$j = j_i = \frac{\hbar k |A|^2}{m} \tag{2.36}$$

Since the terms on (2.35) and (2.36) do not have explicit angular dependencies, it is straightforward to apply (2.25) to obtain the total cross-section formula:

$$\sigma = \frac{4\pi}{k^2} sin^2(\delta_0) \tag{2.37}$$

This simple result implies that the cross-section only depends on the phase shift and wave number.

However, at the boundary condition of (2.30) and (2.31) the incident energy matches the compound nuclide energy state, where the scattering cross section reaches its maximum. This resonance condition is equivalent to the wave amplitude reaching its maximum or diverging to infinity, which happens when $tan(\delta_0) \to \infty$, which is equal to $\delta_0 = \pi/2$ or $cot(\delta_0) \to 0$, but in general the maximum do not diverge and a finite $tan(\delta_0)$ value occurs. This happens when the resonance had a finite time duration, that are related to the half-life of a given state.

Due to this special condition, it is wise to make a Taylor expansion of $cot\big(\delta_0(E)\big)$ for $E = E_R$, where the first non-zero term is the following derivative:

$$cot\big(\delta_0(E)\big) \approx (E - E_R)\frac{\partial\big(cot(\delta(E_R))\big)}{\partial E} = -(E - E_R)\frac{\partial(\delta(E_R))}{\partial E} \equiv \frac{E_R - E}{\Gamma/2} \tag{2.38}$$

where Γ, the resonance width, is defined as the derivative of the angle shift at the resonance energy. It is also related to the half-life ($t_{1/2}$) by been inversely proportional of the resonance with, defined as, $\Gamma = \log(2)\ \hbar / t_{1/2}$, with $\hbar$ been the Planck constant.

By applying the following trigonometric identity:

$$sin^2(\delta) = \frac{tan^2(\delta)}{1 + tan^2(\delta)} \tag{2.39}$$

From (2.37) one obtains the cross-section within the vicinity of a resonance:

$$\sigma(E) = \frac{4\pi}{k^2}\frac{\Gamma^2}{4(E_R - E)^2 + \Gamma^2} \tag{2.40}$$

This formula represents a Breit-Wigner resonance, which is also known as a Lorentzian distribution.

A more general but equivalent treatment could have been done for any value of the scattering angular momentum $\vec{l}$ leading to

$$\sigma(E) = \frac{4\pi}{k^2}(2l + 1)\frac{\Gamma^2}{4(E_R - E)^2 + \Gamma^2} \tag{2.41}$$

A generalization must be performed to allow for the intrinsic spin of the interacting particles. Referring to the spins as $\vec{I}_a$ and $\vec{I}_b$ for the incident and target particles, respectively being $\vec{J}$ the total angular momentum of the resonance state, we have

$$\vec{J} = \overrightarrow{I_a} + \overrightarrow{I_b} + \vec{l} \tag{2.42}$$

Then the statistical factor $(2l + 1)$ related with the number of substates must be replaced by

$$\omega = \frac{(2J+1)}{(2I_a+1)(2I_b+1)} \tag{2.43}$$

Following an intuitive approach (a theoretical deductions is given in appendix 2), by comparing a nuclear excited state with a damped oscillator, the quantity ω in the numerator of (2.40) must be related with the strength of the reaction, i, e. the formation of the compound nucleus and its decay into a specific channel, while the quantity ω in the denominator must be related with the decay of the compound nucleus, which has a finite life-time, with an energy width related to the life-time by the Heisenberg uncertainty principle. If there are many ways to decay the total width is equal to the sum of the width related with each way. Hence, the Breit-Wigner formula for a single-level resonance is given by:

$$\sigma(E) = \frac{\pi}{k^2}\,\omega\,\frac{\Gamma_a\Gamma_b}{4(E_R-E)^2+\Gamma^2} \tag{2.44}$$

Notice that the resonance widths from the resonance or related to all projectile channels are functions of energy, which is true at larger energy intervals, but can be approximated as constants for the vicinity of the resonance energy.

2.6.3 Special cases of the General Breit-Wigner

The most obvious limit happens for pure inelastic reactions; it makes the resonance widths measured at initial and final states equal. Considering also the proton energy range related to PIGE, one may assume the statistical spin factor to be dominated by the compound nuclide, resulting:

$$\omega = \frac{2J+1}{(2I_a+1)(2I_b+1)} \approx \frac{2J+1}{2J+1} = 1 \tag{2.45}$$

And the fact of $\Gamma_b \approx \Gamma_a \approx \Gamma$ on (2.44) will lead to:

$$\sigma(E) = \frac{4\pi\lambda^2\Gamma^2(E)}{4(E-E_R)^2+\Gamma^2(E)} \tag{2.46}$$

According to the literature [14] the term "resonance strength" refers to the quantity:

$$\omega\gamma = \underbrace{\frac{2J+1}{(2I_a+1)(2I_b+1)}}_{\omega}\underbrace{\frac{\Gamma_a\Gamma_b}{\Gamma}}_{\gamma} \tag{2.47}$$

which is the product of the statistical spin factor already defined on (2.43), and the width ratio γ of the resonance states. This term reduces to a trivial value when all resonance states widths are equal.

This allows to derive the ERYA-Profiling formula for a resonance strength Briet-Wigner requiring the user to input the resonance strength value as defined by (2.47), along the resonance width and resonance energy:

$$\sigma(E) = \frac{4\pi\lambda^2\omega\gamma(E)\Gamma(E)}{4(E-E_R)^2+\Gamma^2(E)} \tag{2.48}$$

The Briet-Wigner may also be defined in terms of a maximum cross-section value which is by definition the cross section value at the resonance energy:

$$\sigma_{MAX}(E_R) = 4\pi\lambda^2 \tag{2.49}$$

And the ERYA-Profiling implemented formula is simply given by the following expression:

$$\sigma(E) = \frac{\sigma_{MAX}\Gamma^2(E)}{4(E-E_R)^2+\Gamma^2(E)} \tag{2.50}$$

A similar strategy can be used to derive the resonance strength from (2.48) at the resonance energy, resulting a maximum cross-section to be equal to:

$$\sigma_{MAX} = \frac{4\pi\lambda^2\omega\gamma(E_R)\Gamma(E_R)}{4(E_R-E_R)^2+\Gamma^2(E_R)} = \frac{4\pi\lambda^2\omega\gamma(E_R)}{\Gamma(E_R)} \tag{2.51}$$

This means that the resonance strength is equal to:

$$\omega\gamma(E_R) = \frac{\sigma_{MAX}\Gamma(E_R)}{4\pi\lambda^2} \tag{2.52}$$

which is the conversion factor used by ERYA-Profiling whenever, for thin resonances, the resonant strength is the only measured parameter available. When a resonance strength Briet-Wigner is introduced by the user, (2.50) is used with the conversion factor defined by (2.52).

For ERYA-Profiling perform the calculation of (2.52) it was needed to derive an expression for the Compton wavelength. For the energy range of the projectile with energy E been few MeV, it was enough to considering classic kinematics, and taking the mass M of the target as $M \approx Am_p$, being m_p the proton mass to derive the following formula:

$$\lambda\!\!\!^{-2} = \frac{\hbar^2(A+1)}{2AEm_p} \tag{2.53}$$

and replacing in (2.50), for all energy terms given in keV, becomes equal to:

$$\sigma(E[keV]) \approx \frac{2607472.5(A+1)\omega\gamma(E)\Gamma(E)}{AE\left(4(E-E_R)^2+\Gamma^2(E)\right)}[mb] \tag{2.54}$$

2.7 ERYA Code Implementation

This paragraph will detail the ERYA-Bulk and ERYA-Profiling program routines which are the main work of this thesis. When the text uses the denomination ERYA alone it refers to a routine shared by the two programs.

2.7.1 ERYA Bulk and ERYA Profiling Description

ERYA-Bulk is a new version of the ERYA (Emitted Radiation Yield Analysis) program designed to evaluate the gamma-ray yields coming from homogeneous samples bombarded by charged particles (namely protons), implemented by two different software versions: a MS-DOS version, and later a Windows version based on LabView Runtime, which are currently discontinued.

ERYA-Profiling is an extension of ERYA-Bulk designed to deal with depth-heterogeneous samples. There was a first version of ERYA-Profiling, which never reached beyond a prototype stage.

As explained in the introduction chapter, the objective of the new ERYA programs was the implementation of functional and portable codes, free of proprietary libraries, and this was done with the cross-platform framework wxWidgets to implement the GUI and the use of the C++11 language. Additionally, the full implementation of energy straggling was revised and upgraded.

The major advantage of wxWidgets was the possibility to ease the port to several operating systems, since it acts as a wrapper library to make the code compile to different operating systems, including different computer architectures. The current code, once linked with the adequate wxWidgets libraries for each target system, compile it without changing a single line of code.

Both ERYA-Bulk and ERYA-Profiling executable can be analyzed as a merge of three main modules:

1. A GUI which handles all events related to the several tools available to the user, using the wxWidgets model framework.
2. A series of auxiliary routines, called *library* routines, dedicated to managing the databases, user inputs and other structured data from the GUI handlers to the memory.
3. The physical numerical evaluation routine that is a module by his own right. It gathers the user inputs, and the Databases loaded into memory, and then handles the actual numerical simulation code. ERYA-Bulk and ERYA-Profiling had two different implementations within this module.

2.7.2 Brief Description of Main Program Modules

2.7.2.1 GUI Module

The GUI module of both programs is implemented according to the wxWidgets coding Standards. Each major window and its contents are defined by each own C++ class, and may contain the function handlers to call to another C++ class corresponding to another window.

The cross-platform framework allows to use the same GUI code for all the operating systems.

2.7.2.2 Library Module

Some tasks are not easily implemented on the GUI module source code files. Instead, a set of separated files was created as a library to handle those tasks, making the code more readable by assigning specific routines. This is the case, for example, of saving data to a file.

This library module uses the wxWidgets framework libraries to create a series of specific routines for ERYA to handle special types of data, offloading from the GUI components code.

We will describe with some detail two specific library modules that demonstrate the use of modular programming, which are related to the Databases and the File Formats, for then also depend on other components detailed later.

2.7.2.3 Database Library

The Databases were implemented as overridden vector C++ classes or single C++ classes.
The Elements Database is an example of an overridden vector C++ class, where each individual register (called Element) contains the contents of each physical characteristic of an element. Each Element register is identified by a name and gamma peak, and also four physical quantities (abundance, isotopic and atomic mass, and also the atomic number). An entire table of four columns (related to the experimental cross-section for each energy value, and the relative measurement uncertainties) of numerical data is also linked to the element register. The vector class that handles the entire Element Database, contains a series of custom functions to manage several operations, such as to find an element by name or gamma peak, add new elements, delete some of them, find duplicates, or sorting the entire database.
A second example relates to the SRIM tables (more precisely the tables of stopping powers calculated by the SRIM program and loaded and converted to the ERYA database by the user employing the Stopping-Power widget tool; SRIM itself is not needed to run at all to use ERYA), where each register contains a two columns table (for an experimental value of the stopping-power for each energy), and the atomic number to label it. A global overridden vector class takes control of the entire array of SRIM tables, enabling to implement routines to detect duplicates, search for a table by a certain atomic number, or update the changed data of an element when request by the user.
Other Databases files, such as the Detector Efficiency or the Stopping-Power (for approximations of stopping power calculation other than SRIM) are single C++ classes.

2.7.2.4 File Format Library

The next important (and more complex in terms of code) library module is the **File Format Library** that contains the C++ classes to host the function to handle the actual loading and saving of Databases classes contents on memory to a file on a storage device.

This was implemented along some C++ source files which contain special auxiliary functions linked to the main File Format Library, where each one implements a specific file format, in order to make the implementation and debugging more efficient.

Since wxWidgets contains support to create XML documents (as their own C++ classes and methods), and XML files are an excellent choice to store text files with a formatted tree structure, but also human readable, it was decided by program design to all native Database files were implemented as XML files.

Following the previous standard, the configuration file of ERYA is also implemented as a XML file, but due to their short content the functions to load and save a configuration file were placed on the GUI class that manages the main screen, since it was simpler to implement in this way.

2.7.2.5 Compatibility with non-native File Formats

For the user convenience and also justified previously, ERYA support implemented the import or export of data by reading directly ASCII and Excel files.

For ASCII files consisting of numerical rows, ERYA will load and decode accordingly. Some special ASCII files, such as IBANDL and SRIM table files had special import routines to parse non-numeric and numerical data. ERYA can also store data on IBANDL format, in order to ease interchanging.

In relation to Excel files, since these files are in reality zip files with a strict structure of folders, filled with mandatory XML files, it was an author decision to create an implementation to read those files using the wxWidgets library support for zip files and XML documents.

Using this specific library routine, ERYA reads the first spreadsheet of any Excel files, and only parse pure numerical and strings cell contents to a temporary matrix on memory, that later will be processed by the adequate ERYA Library methods, according to the program context.

ERYA can also save tabular data as Excel files, storing everything in a single spreadsheet.

The only issues driven by this implementation was the lack of proper documentation from Microsoft itself, requiring further testing to fix the major flaws.

2.7.2.6 ERYA Macro Language

An auxiliary library which deserves to be mentioned is the Parser and Macro Library, where a small programming language was implemented for some advanced options of ERYA to support some user inputs.

ERYA Macro implementation resembles a runtime compiler, with an internal stack interpreter. The syntax was inspired by programmable calculators (CASIO and Texas Instruments), acting as a derivative of the Basic language, while the variable names follow the C standards.

When ERYA reads a string that should act as a macro, such as the Detector's Efficiency custom function, it parses into a chain of words (tokens) and converts them into a postfix chain of commands (using the shunting yard algorithm [16]). Then a interpreter (similar to the FORTH language logic), runs the postfix chain of commands, achieving the pretended results.

2.7.2.7 Physics Module

The evaluation of all numerical evaluation derived from the physics is handled by this module, and since ERYA-Bulk and ERYA-Profiling correspond to different implementations, each version is exclusive of each program.

In both cases the simulation C++ class handles the user inputs and Databases and coordinates all the processes until the results are displayed on the GUI.

When the simulation procedure starts when requested by the user, ERYA makes a check of the validity of the inputs, and the Database consistency before starting the simulation. In case of an error the program will abort the procedure, giving an error information in order to the user fix it before try again.

From there, the procedure of two programs diverge and this will be explained on next sections.

2.7.3 ERYA-Bulk simulation

Once ERYA-Bulk validates all inputs, the next step is to compile the sample in terms of memory data structures and import from database the required numerical tables.

The basic numerical object is the numerical vector that handles all elements selected by the user on the main screen, that combine the contents related to the Element Database, with the

Stopping-Power, not forgetting to evaluate the Detector's Efficiency when needed. If the user uses any custom functions as inputs or any databases, they are compiled by the internal ERYA Macro interpreter, and stored as a stack of operators ready to be used when needed.

After the compilation of this information, a vector of Yield's Elements is created. Each Yield object evaluates the individual yields according to the theory exposed in earlier paragraphs.

Since the user can define Compounds and set the fit attribute to some of the selected Elements, ERYA creates two auxiliary vector classes to handle the additional constraints:

1. The Compounds class handle a chain of Elements that share a unique Compound ID defined by the user on the main screen. This will assign a fixed stoichiometry to the compound, and if these elements are assigned with the fitting procedure, the ratio between their mass (or atomic) fractions will never change. Isolated elements are assigned independently to a special Compound ID 0 where the ratio rules are not obeyed.
2. The Fitting Parameters class is responsible to handle the array of elements that will be called by the fitting procedure, including the Compounds, which was set by the user on main interface. This happens because a single compound shares a single degree of freedom, while each isolated element had their own. This class also implements the code of the fitting procedure derived from the Levenberg-Marquardt algorithm.

If the number of elements to be fitted is zero, ERYA will evaluate only the yields corresponding to the sample composition introduced by the user, and ends here. If fitting of some (or all) the elements is chosen, ERYA will iteratively modify the sample composition in order to match the experimental yields given by the user.

A numerical integration method based on the Trapezoidal Method is employed for the yield evaluation, as this was the simplest method worked without numerical issues during development.

Based on the user selected initial and final energy values on main interface, the integration domain is divided by equal steps, which is the energy step of numerical integration. (The default is 1 keV.)

For simplicity, the stopping-powers are evaluated at the beginning of each individual step.

To minimize interpolation errors on the cross-section data, the function responsible to handle the cross-section takes the energy interval limited by the energy at the beginning of interval plus the additional energy step on it, and query for every point on the cross-section table

between those two boundaries. This will make an intermediate linear branch interpolation between successive tabulated points and return the weight average of the cross-section.
By summing all partial steps, a numerical approximation of the integral will give the theoretical yield and ERYA returns those values to the screen and ends the numerical procedure.
If due to the user selection requires a fitting, ERYA-Bulk, after the initial yield calculations done as descripted earlier, it will start the Levenberg-Marquardt algorithm. The method require some initial calculations, where the most important is the initial theoretical yield derived from the initial sample composition values as inserted by the user, which also need the experimental yields to be inserted to proceed.
Once started, it uses the Elements, Compound and Fitting Parameters vector classes to build numerical matrices needed to the fitting algorithm work. ERYA implements the Levenberg-Marquardt algorithm using the work of reference [17]. Once a suitable solution is determined within the numerical accuracy, the adjusted composition and the additional information related to numerical errors and yields are also displayed on the screen.
An optional table procedure to store the intermediate yield values of the numerical integration can be activated if the user selects a non-zero value for the Table Step. This procedure is activated when the fit ends, or when evaluating the yield if there is no fit. The results are displayed on an additional table, accessible from the tabbed interface.

2.7.4 ERYA Profiling simulation

Once ERYA-Profiling validates all inputs, the next step is to compile the sample in terms of memory data structures and import information from the databases.
The very first object created by the simulation procedure is the Element object that combines information from the Element, Stopping-Power and Detector's Efficiency Databases.
ERYA-Profiling considers that a Sample can be made by several Layers, where each layer has a certain amount of the chosen Elements.
Once all necessary Elements are created, the Layer objects combine the layer description table contents as defined by user input on Layer Tab interface, combined with the Element objects as descripted previously.
Due to the complexity of the distributions, all internal workings were implemented on a Distribution class which handles the mathematical model of the distributions, and their

operations such as, set the correct function approximation when required, or compute the distribution in function of energy.

The Yield vector class handles the actual yield evaluation, one of each Main Element, and uses the data from the Layers and Distributions objects to perform the calculations.

Once everything settled, the real numerical simulation begins, from the first initial energy point, until the last one, that makes the main cycle of the numerical evaluation.

At each step of main cycle, ERYA-Profiling evaluates the energy loss in each individual sublayer to evaluate several parameters in order to determine the correct straggling distribution. The partial yield of each sublayer is the result of the convolution of energy distributions (thermal Doppler, beam initial resolution and straggling) and the reaction cross section.

This particular step is the most numerically intensive routine, including the fact that the cross-section can be evaluated from the numerical database table or by Lorentz-like analytical function.

The process resumes for all sublayers or when the energy at a certain sublayer drops below zero.

The sum of all sublayer yields is the yield of the nuclear reaction at a certain energy, and the computation proceeds to the next energy point of the chosen interval.

Once the simulation is completed, the relevant information is displayed on graphic and table formats. This includes a graphical plot of the yield in function of the initial energy, accompanied with a tabular form. Also, a log table of partial yields and additional parameters are also displayed if the user activates the adequate program settings.

ERYA-Profiling also supports importing experimental data after a successful simulation for a visual comparison between experimental and simulated data on the main screen.

2.8 Presentation of Results

In this paragraph we give a brief presentation of the main results related to the set of papers of Chapter 3 (core of this thesis) about ERYA development. Additionally, a mention will be made to papers related to ERYA applications, beyond the scope of this thesis.

2.8.1 Resume of the main results of the papers presented on Chapter 3

"International Atomic Energy Agency inter-comparison of particle induced gamma-ray emission codes for bulk samples"

This meeting was intended to present and compare different codes to perform PIGE bulk analysis, ERYA was compared against SIMNRA, NDF and PiGreCo, using standard tests to check their differences and potential improvements. This exercise showed similar results from all the tested codes.

"ERYA–Profiling: A code for quantitative PIGE analysis of in-depth heterogeneous samples"

In context of this thesis, this is the first paper to deal with the physical model of PIGE analysis. This paper gives more detail about the new PIGE-profiling program rather than the bulk version.

Among several test exercises, one was done, using cross section values of the $^{9}Be(p,\gamma)^{10}B$ nuclear reaction, concerning the 1082 keV thin resonance which overlaps the 992 keV broad peak [1, 18], to simulate a resonance scan for a thin Be sample with eventual surface oxide layer.

This example was important to test ERYA-Profiling with a user defined Lorentzian with their parameters been fitted from the original cross-section data or using the experimental excitation function as well. Full straggling and Gaussian only approximations were also tested extensively.

The main important result was that ERYA-Profiling could predict and measure the presence of a thin beryllium oxide top layer when full straggling was enabled to properly fit the simulation with the experimental results.

"Fluorine depth profiling based on the $^{19}F(p,p'\gamma)^{19}F$ excitation function"

Even though the major focus of this thesis concerns resonance scan depth PIGE profiling, advantage can be taken of the use of the complete excitation function data, by the ERYA-profiling code.
This was done for ^{19}F non-resonant depth profiling with the reaction $^{19}F(p,p'\gamma)^{19}F$ which tested the program capacity to identify different fluorine conceptual depth profiles, by calculating the yield at a given incident energy.

"ERYA-Bulk and ERYA-Profiling: An application for quantitative PIGE analysis"

In accordance with the thesis development, the applications ERYA-Bulk and ERYA-Profiling inner workings and source-code were presented in a paper of a computational physics journal. Linked to this publication, the source-codes were published on GitHub repository source-code under a LGPL-v3 license to allow open access to community while safeguarding the original author rights.
This paper details the implementation of both programs, by first promoting the modularity and future-proofing by using open frameworks, and then detailing the numerical implementation of the physical routines, leaving the distributions to a separate paper.
The paper also refers to the easiness of portability of ERYA by running the same program from a smartphone to a desktop computer and shows some performance tests to compare the two extremes.

"PIGE depth profiling: Energy Straggling Distributions in ERYA-Profiling"

The implementation of a full straggling model in ERYA-Profiling was one of the main goals of this PhD thesis. The model mathematical robustness was tested in "extreme" conditions, namely sharp resonances, and the results were compared with the SPACES, a application that implements depth profiling using stochastic methods to perform the calculations. [19]

Those extreme conditions were valuable to test the numerical code implementation to handle the energy distributions convolution and the numerical integration. In these sharp-resonance conditions, different integration steps and lambda variables, which are user controlled, were tested in order to optimize each simulation time consumption.

The full straggling option is relevant to study resonance scans of sharp resonances, especially the 992 keV of ^{27}Al or the 1167 keV of ^{18}O thin resonances, which feature a phenomenon called Lewis Peak, heavily dependent on the beam resolution and resonance width. For beam resolution (and/or resonance width) larger than 400 eV this peak is not present and, for a in-depth uniform sample, a Gaussian approximation is enough to handle the beam straggling.

2.8.2 ERYA Applications

A short list of applications is briefly presented here.

2020 Summer School

The Summer School on Nuclear Physics 2020 served as a test-ground of ERYA-Bulk and ERYA-Profiling programs. Students enrolled in this School had projects related to composition analysis of a variety of samples.

Most of the samples were either thin or in-depth homogeneous samples, requiring the use of ERYA-Bulk for their analysis. Program support to associate any number of elements into chemical compounds was crucial for some cases.

This was also an opportunity to take notes on ERYA use and performance, without neglecting user feedback and test the code for real samples instead of ideal ones.

ERYA-Profiling was requested for the analysis of one heterogeneous sample, where some elements had a depth scan profiling experimentally measured, and the simulated yield profile curve delivered by ERYA-Profiling was within the experimental results.

Results of applied papers co-authored by the candidate

The candidate calculated fluorine amounts in bulk samples related to fluorine products for teeth health contributing to the papers listed below.

"Evaluation of the effect of fluorinated tooth bleaching products using polarized Raman microscopy and particle induced gamma-ray emission", Spectrochimica Acta Part A: Molecular and Biomolecular Spectroscopy, Volume 236, article id. 118378, https://doi.org/10.1016/j.saa.2020.118378

"Evaluation of enamel demineralization and fluorine uptake caused by gustatory stimulants of salivary secretion (GSSS) using Raman spectroscopy and proton induced gamma-ray emission (PIGE)", Journal of Raman Spectroscopy, vol. 50, issue 3, pp. 380-386, https://doi.org/10.1002/jrs.5532

Validation of Cross-Sections Measurements

In the context of measurements of gamma-ray cross-sections aiming at free-standard PIGE, thick target yields were obtained which, together with ERYA calculations, led to the validation of the nuclear reaction cross sections. This work was published in the following references.

"Gamma-ray cross-sections of the $^{27}Al(p,p`\gamma)^{27}Al$ reaction in the proton energy range 1490-3000 keV",The European Physical Journal A, Volume 58, Issue 10, article id.209, https://doi.org/10.1140/epja/s10050-022-00861-0

"Cross-sections of the gamma-producing $^{25}Mg(p,p\gamma_{1-0})^{25}Mg$ nuclear reaction at E_{lab} = 870-4020 keV", The European Physical Journal A, Volume 58, Issue 7, article id.128, https://doi.org/10.1140/epja/s10050-022-00780-0

"Measurement of gamma-ray production cross sections for nuclear reaction $^{31}P(p,p\gamma_{1-0})^{31}P$", Nuclear Inst. and Methods in Physics Research, B, Volume 452, p. 26-29, https://doi.org/10.1016/j.nimb.2019.05.060

Astrophysics Applications

A collateral application of ERYA-Profiling is related to the field of Astrophysics namely of nuclear reactions that occur in stars, which can be studied on nuclear physics laboratories, being LUNA, a GranSasso underground laboratory, one of the most important on this field.
LUNA primary focus are the nuclear reactions that happen on main sequence starts, specially the chain of reactions related to the CNO cycle like the $^{14}N(p,\gamma)^{15}O$ published on [20]. The

$^{14}N(p,\gamma)^{15}O$ reaction is being studied by LUNA at lower energies than before and ERYA-Profiling can be used to analyse the targets produced for this study.

The only real issue to use ERYA-Profiling to calculate nuclear reaction rate, is the necessity to perform conversions from experimental data (specially from LUNA, that follows the astrophysics standards), where the main one is the conversion from astrophysical S-factors to milibarn units related to cross-sections, while the resonance strength parameter may need some corrections related to the nuclear reaction rate and star core temperature. The use of a custom function for the resonance was more straightforward to use.

This example may be a slightly different problem within the PIGE analysis framework, but reveals to follow a certain universality of methods from one program to be quickly adopted to a different field.

3

MAIN THESIS PAPERS

The following contents on this chapter are a set of papers that represent the main work done on this thesis, and they are fac-similed as they had been published.

Nuclear Inst. and Methods in Physics Research B 468 (2020) 37–47

Contents lists available at ScienceDirect

Nuclear Inst. and Methods in Physics Research B

journal homepage: www.elsevier.com/locate/nimb

International Atomic Energy Agency inter-comparison of particle induced gamma-ray emission codes for bulk samples

N. Pessoa Barradas[a,*], J. Cruz[b], M. Fonseca[b,c], A.P. de Jesus[b], A. Lagoyannis[d], V. Manteigas[b], M. Mayer[e], K. Preketes-Sigalas[d], P. Dimitriou[a,1]

[a] International Atomic Energy Agency, Division of Physical and Chemical Sciences, Vienna International Centre, PO Box 100, A-1400 Vienna, Austria
[b] Laboratório de Instrumentação, Engenharia Biomédica e Física da Radiação (LIBPhys-UNL), Departamento de Física, Faculdade de Ciências e Tecnologia da, Universidade Nova de Lisboa, Monte da Caparica, 2892-516 Caparica, Portugal
[c] Universidade Europeia, IADE, Av. Carlos I, 4, 1200-049 Lisboa, Portugal
[d] Tandem Accelerator Laboratory, Institute of Nuclear and Particle Physics, NCSR "Demokritos", 153.10 Aghia Paraskevi, Athens, Greece
[e] Max-Planck-Institut für Plasmaphysik, Boltzmannstr. 2, 85748 Garching, Germany

ARTICLE INFO

Keywords:
Particle induced gamma emission
Data analysis
Intercomparison
NDF
SIMNRA
ERYA
PIGRECO

ABSTRACT

PIGE has been widely used in the analysis of bulk samples, with quantification of data made usually through the use of reference samples. With a growing database of experimental cross sections becoming available, the use of first-principles data analysis methods is gaining ground. Only few codes capable of first principles analysis of PIGE data were available, but new codes have been recently developed. However, their accuracy has not been verified so far. In this work, the results of an inter-comparison of PIGE data analysis codes organised by the IAEA are presented. The inter-comparison was made through simulations for well-defined conditions, for bulk samples. Five analytical codes participated in the exercise: ERYA-Bulk, ERYA-Profiling, NDF, PiGreCo and SIMNRA. It is concluded that, although some differences are observed for some calculations, particularly in the presence of sharp resonances in the cross section, all four codes are appropriate for analysis of PIGE experimental data.

1. Introduction

Ion Beam Analysis (IBA) techniques such as Rutherford backscattering (RBS), Elastic Recoil Detection Analysis (ERDA), Nuclear Reaction Analysis (NRA) or Particle Induced X-ray Emission (PIXE) rely on computer codes for data analysis and quantification of the results obtained. For decades, users of the codes relied on their assumed accuracy and on tests by manual calculations that can be easily done in simple systems, such as determination of concentration and areal density from signal heights and widths or of areal density from a peak area [1]. However, validation of the codes and determination of their numerical accuracy remained an issue.

The International Atomic Energy Agency (IAEA) conducted in 2000 an inter-comparison of PIXE spectrum analysis software, with the participation of seven codes [2,3]. In this case, only the capability to retrieve peak areas was tested, and actual calculations to determine elemental concentrations from the peak areas were not included in the inter-comparison.

The IAEA organised in 2002 a technical meeting on the "Status of Software for Ion Beam Analysis in Materials Development", which led to a review of the status of IBA particle-particle codes [4], i.e. not including techniques such as PIXE or Particle Induced Gamma-ray Emission (PIGE), and to an inter-comparison of seven particle–particle codes, including RBS, ERDA and NRA [5]. The inter-comparison included 28 theoretical calculations that tested basic calculations as well as advanced physics modelling. The inter-comparison also included four sets of experimental data. For simple ^{4}He-RBS and ^{7}Li-RBS, agreement between the NDF [6,7], RUMP [8,9] and SIMNRA [10,11] codes reached 0.3%. For ^{4}He-ERDA, agreement between NDF, RUMP and SIMNRA was 0.21%. For NRA with the D(^{3}He,p)α reaction, NDF and SIMNRA agreed within 0.2% and 0.6% for the alpha and proton yields, respectively.

In 2016, an inter-comparison of ion beam analysis software for the simulation of backscattering spectra from two-dimensional structures was presented, with four codes participating [12]. The codes were in good agreement for the single-scattering approximation and less so when plural and multiple scattering play an important role.

These inter-comparisons have led to the conclusion that the widely used particle-particle codes are compatible and provide consistent results.

* Corresponding author.
[1] Present address: Institute of Nuclear and Particle Physics, NCSR "Demokritos", 153.10 Aghia Paraskevi, Athens, Greece.

https://doi.org/10.1016/j.nimb.2020.02.019
Received 10 October 2019; Received in revised form 12 February 2020; Accepted 16 February 2020
0168-583X/

For PIGE analysis, although the technique is well-established since the 1960s, a systematic inter-comparison has not yet been performed. A limited first comparison of PIGE codes was reported in 2010 [13], which included NDF, ERYA [14,15] and SPACES [16]. However, this was done in the context of thin film depth profiling using multiple complementary techniques and was not an inter-comparison aiming to validate the codes or to quantify the differences between them.

As a consequence, the technique is normally applied by comparison with well-defined standard reference materials. The potential of standardless PIGE was already stressed by the IAEA Coordinated Research Project (CRP) "Development of a Reference Database for Particle-Induced Gamma-ray Emission (PIGE) Spectroscopy" (2013–2017) [17]. However, the lack of validated PIGE analysis codes has not allowed this to be fully exploited.

This paper reports on a systematic inter-comparison of PIGE data analysis codes, initiated by the IAEA in 2018 [18]. Known existing analytical codes participated, and one code implemented PIGE for the purposes of this exercise.

2. Methodology and participating codes

Developers of PIGE codes known to calculate yields by performing first principles calculations using known physical parameters such as scattering cross sections and stopping powers, were invited to participate. The codes that were finally considered in the inter-comparison were: ERYA, with initial versions already available in 2004 [14,15] but extensively modified within the scope of the IAEA CRP on PIGE [17]; NDF [6,7], that includes PIGE since 2008 via an open source routine, published in 2010 [13]; PiGreCo, a new code that was developed in 2016 [19]; and SIMNRA [10,11], which was extended to include a PIGE routine for the purpose of participating in the inter-comparison. Other well-known IBA codes, including Monte Carlo codes, that do not yet have PIGE implemented, were not considered. The code SPACES [16], dedicated to narrow resonance depth profiling (NRP), is directed at high resolution experiments in thin layers using isolated resonances, for which it assumes constant stopping power, and is therefore not suitable for analysis of thick bulk samples.

Two of the participating codes, NDF and SIMNRA, are IBA data analysis packages that implement a number of techniques besides PIGE. This means that they can rely on a number of methods and routines previously developed for other techniques, for instance for handling stopping power and scattering cross sections, but also for definition of sample and experimental conditions. They both participated in the IAEA inter-comparison of IBA software [5], where for simple cases such as ^{4}He RBS or ^{4}He ERDA with Rutherford or slowly changing cross sections, they agreed within better than 0.3% in calculation of yields and signal shapes. This was considered sufficient, since very few IBA experiments reach a 1% absolute accuracy [20]. For more advanced calculations, such as in the presence of sharp resonances, some larger differences between the two codes were observed, mainly in signal shapes due to different handling of the cross sections. However, both codes continued to be developed since that inter-comparison. The two other codes, ERYA and PiGreCo, are dedicated solely to PIGE. ERYA has two versions, ERYA-Bulk and ERYA-Profiling, which are in fact independent executable codes that share some routines. The main difference is that ERYA-Bulk only simulates bulk targets, so it does not implement energy straggling, while ERYA-Profiling includes advanced energy spread models and can simulate multi-layered targets. The current version of PiGreCo is dedicated to bulk samples only. An overview of the codes is given in Table 1.

It was decided to concentrate the inter-comparison on calculations that all codes are, in principle and by design, capable of performing. A set of simulations for well-defined conditions and parameters was agreed on, including: reactions with slowly-changing scattering cross sections and with resonances; single element and multielemental targets; and calculations with and without the effect of beam energy spread and straggling. In all cases, the scattering angle and scattering cross section was specified, with angular distributions assumed to be isotropic; stopping powers were specified to be taken from SRIM-2013 [21]; absorption of gamma-rays was not considered. Very importantly, it was agreed that the cross sections used in the calculations would have a threshold, i.e. they were be considered to be zero below a given energy, even if the experimental cross section included values below that given energy. Finally, in some calculations an initial yield for a pure target was given as input. All the calculations are described in detail in Table 2.

A first set of simulations was reported by ERYA, NDF and PiGreCo. The results were compared to each other, following which SIMNRA also implemented PIGE and joined the inter-comparison exercise. The participants had the opportunity to improve the algorithms, and in this inter-comparison exercise, all codes were changed and improved as a result. The final results are presented here, since the purpose of this work is to report on the current state of the codes, including all their best capabilities.

PIGE cross sections rarely have accuracy better than 10% [22]; and therefore that is the expected minimum uncertainty in most PIGE experiments. For the purposes of this inter-comparison exercise, good agreement between codes is taken to mean that the calculations do not introduce a significant extra uncertainty in the results. We take the difference between codes to correspond to the extra uncertainty in the final quantification introduced by the use of a given code. In this sense, let us consider a rather low 5% cross section uncertainty. A 2.3% code uncertainty, added in quadrature to this 5% (assuming random uncertainties), would lead to a combined uncertainty of 5.5%, i.e. a negligible increase. We conservatively consider a 2% agreement between codes as acceptable.

If one wishes to remove the cross section uncertainty from these considerations, one could consider that very few IBA experiments have been reported at a 1% uncertainty level [20]. If such a limit would be taken, then an additional 0.5% code uncertainty would lead to a 1.1% combined uncertainty, i.e. a negligible increase.

3. Model and calculations

The underlying concepts of PIGE are simple. An energetic ion interacts with a nucleus, leading to a nuclear reaction with emission of a γ particle. The ion is often a proton and therefore the reaction is often (p,p'γ), (p,$\alpha\gamma$) and also (p,γ). The yield coming from N_p protons with energy E interacting in a layer with areal density Nt of a given isotope species is:

$$Y(E,\theta) = \Omega(E_\gamma)\varepsilon_{abs}(E,E_\gamma)N_pNt\sigma(E,\theta), \quad (1)$$

where $\varepsilon_{abs}(E,E_\gamma)$ is the absorption of the γ rays with energy E_γ as they travel through the sample to the detector after being generated at a depth where the beam had energy E, $\Omega(E_\gamma)$ is the absolute efficiency of the detector for γ rays with energy E_γ, and $\sigma(E,\theta)$ is the cross section for emission of a γ ray at angle θ to the incident ion direction. However, a beam with initial energy E_0 will steadily lose energy as it crosses the sample, and the total yield will be:

$$Y(E,\theta) = \Omega(E_\gamma)Np\int_0^E \varepsilon_{abs}(E,E_\gamma)Nt\sigma(E,\theta)/S(E)dE, \quad (2)$$

where S(E) is the stopping power at energy E. Note that Eq. (2) assumes that, within a given layer, the beam energy is unique and constant. In fact, this is not true; in any given layer each ion loses energy, so the beam energy decreases as the protons cross the layers.

All participating codes implement Eq. (2) (while considering $\varepsilon_{abs}(E,E_\gamma) = 1$, i.e. no absorption of the gamma rays), but they do so in different ways, which can lead to differences in the calculated values. For instance, often the areal density of sub-layers is taken to be sufficiently small such that cross section and stopping power are considered to be constant within the sub-layer. However, in a given sub-layer, the

Table 1
Summary of codes.

Code and version	Status	Programming language	Distribution	Source code	Real number precision
ERYA-Bulk 4.50	Active development	C++ wxWidgets (GUI)	Freeware	Restricted to author.	Double
ERYA-Profiling 2.70	Active development	C++ wxWidgets(GUI)	Freeware	Restricted to author.	Double
NDF v9.7a	Active development	Fortran/C PIGE is Fortran	Commercial. PIGE routine open source	Restricted to author. PIGE routine open source	Single
PiGreCo 1,1	Active development	C++, Qt libraries	Free	Free	Double
SIMNRA 7.02	Active development	Delphi	Commercial	Restricted to author	Double

Table 2
Calculations.

#	Energy range (MeV)	Energy step (keV)	Reaction	E_γ (keV)	θ (°)	Target (at.%)	Cross section	Energy spread [1]	Initial yield (Nγ/sr/μC)
1-a	3–5	200	$^{10}B(p,p'\gamma)^{10}B$	718	165	^{nat}B 100	Lag2015	No	No
1-b	3–5	200	$^{10}B(p,p'\gamma)^{10}B$	718	165	^{nat}B 10O 40 Fe 50	Lag2015	No	No
2-a-i	3–3.8	100	$^{10}B(p,\alpha\gamma)^{7}Be$	429	150	^{nat}B 100	Lag2015	No	580,000 [2]
2-a-ii	3–3.8	100	$^{10}B(p,\alpha\gamma)^{7}Be$	429	150	^{nat}B 10O 40 Fe 50	Lag2015	No	580,000 [2]
2-b-i	3–3.8	100	$^{10}B(p,p'\gamma)^{10}B$	718	165	^{nat}B 100	Lag2015	No	580,000 [2]
2-b-ii	3–3.8	100	$^{10}B(p,p'\gamma)^{10}B$	718	165	^{nat}B 10O 40 Fe 50	Lag2015	No	580,000 [2]
3-a	1–2.7	1	$^{19}F(p,p\gamma_2)^{19}F$	197	130	^{nat}F 100	Jes2000	No	No
3-b	1–2.7	1	$^{19}F(p,p\gamma_2)^{19}F$	197	130	^{nat}F 10O 30 Cr 60	Jes2000	No	No
4-1-a	3–5	200	$^{10}B(p,p'\gamma)^{10}B$	718	165	^{nat}B 100	Lag2015	Yes	No
4-1-b	3–5	200	$^{10}B(p,p'\gamma)^{10}B$	718	165	^{nat}B 10O 40 Fe 50	Lag2015	Yes	No
4-2-a-i	3–3.8	100	$^{10}B(p,\alpha\gamma)^{7}Be$	429	150	^{nat}B 100	Lag2015	Yes	580,000 [2]
4-2-a-ii	3–3.8	100	$^{10}B(p,\alpha\gamma)^{7}Be$	429	150	^{nat}B 10O 40 Fe 50	Lag2015	Yes	580,000 [2]
4-2-b-i	3–3.8	100	$^{10}B(p,p'\gamma)^{10}B$	718	165	^{nat}B 100	Lag2015	Yes	580,000 [2]
4-2-b-ii	3–3.8	100	$^{10}B(p,p'\gamma)^{10}B$	718	165	^{nat}B 10O 40 Fe 50	Lag2015	Yes	580,000 [2]
4-3-a	1–2.7	1	$^{19}F(p,p\gamma_2)^{19}F$	197	130	^{nat}F 100	Jes2000	Yes	No
4-3-b	1–2.7	1	$^{19}F(p,p\gamma_2)^{19}F$	197	130	^{nat}F 10O 30 Cr 60	Jes2000	Yes	No

Lag2015: A. Lagoyannis et al., NIMB 342 (2015) 271–276, truncated to 0 below 3 MeV.
Jes2000: A.P. Jesus et al., Nucl. Instr. Meth. B 161–163 (2000) 186, truncated to 0 below 1 MeV.
[1] Energy spread includes 3 keV beam energy spread and Bohr straggling.
[2] Yield for a 3 MeV proton beam on a pure Boron reference target.

cross section and stopping power can be taken as the value on top or bottom of the layer, the average of those two values, or they can be integrated over the sub-layer. The calculated yield will be different depending on the option taken.

Furthermore, at a given depth the beam energy is not unique due to beam energy spread and energy straggling; the beam has an energy distribution Γ. The most important effect for PIGE is that, in a given layer, the effective interaction cross section is [23,24]

$$\sigma_{eff}(E,\theta) = \int_{-\infty}^{+\infty} \Gamma(E',\theta)\sigma(E-E',\theta)dE' \quad (3)$$

In cases where the cross section changes quickly with energy, the effective cross section in a given layer can be very different than the cross section for the average beam energy in the layer - up to one order of magnitude in multilayers in cases constructed to maximize the effect [23]. In bulk samples the effect is much lower, but can be significant near resonances in the cross section, whenever the beam energy spread is comparable to the resonance width. Not all participating codes implement Eq. (3), as detailed below for each code.

In summary, the most important points that influence calculated yields are: the handling of stopping power, interaction cross sections and energy straggling; how the target is divided in internal sub-layers for calculation purposes; and how calculations are made within one sub-layer.

In this section, some calculation details are given for each participating code. Further details can be found in the publications dedicated to each code [6,7,10,11,14,15,19].

3.1. ERYA-Bulk

ERYA-Bulk evaluates the yield taking the whole bulk sample and evaluating the integral of Eq. (2), using a constant energy step that is defined by the user. For calculation 1-a, different energy steps were used (from 0.01 keV to 200 keV) and no differences on the yield were obtained, which shows that the calculation is stable and that, for smooth varying cross sections, it does not depend on the definition of internal sub-layers.

ERYA-Bulk uses SRIM stopping powers. When a stopping power is needed for a given energy, linear interpolation from the two nearest tabulated values is used. This program evaluates the cross section at a given energy by performing also a linear interpolation from the two nearest excitation function tabulated values.

ERYA-Bulk takes the initial and final energy of each interval step to evaluate the stopping power, which is taken as the arithmetic average of the two boundaries values.

Inside each sub-layer the cross-section is evaluated by integrating the cross section tabulated data via an Adaptative Integration Method (Trapezoidal Method).

A stability test was made by calculating the yield for the conditions of calculation 1, but using constant stopping power and constant cross section. In this case, in principle the yield should be linear with beam energy. The cross section was set to 1 mb above 3 MeV and 0 below. Calculations were made for two different values of the stopping power, 1.2 and 1.77 eV/(10^{15} at./cm^2). The maximum deviation from linearity was 0.23%, being below 0.1% in most cases.

3.2. ERYA-Profiling

ERYA-Profiling is capable of calculating multi-layered samples.

Each real layer is split in equal sub-layers of constant areal density, whose value is user-defined.

ERYA-Profiling shares the same functions and routines from ERYA-Bulk to calculate stopping powers and cross sections.

ERYA-Profiling evaluates the yields with Eq. (2), taking for the energy distribution function $\Gamma(E', \theta)$ the convolution of three dispersion distributions (thermal, resolution and straggling) around the initial beam energy at the beginning of each sub-layer.

Once each layer is completed (with constant density), the energy losses are computed from a formula that depends on the stopping-power and updates the new beam energy for the next layer. The integration will continue until the last sub-layer is reached or when the energy beam drops to zero.

Given that ERYA-Profiling is designed for calculations with energy spread, the stability test for calculation 1, which does not include energy spread, was not made.

3.3. NDF

By default, NDF subdivides a bulk sample into internal sub-layers of equal areal density. This is the main integration step. The energy loss in each internal layer is different; therefore the internal layers do not have equal energy width. The actual areal density of the internal layers is problem-dependent, determined by NDF from the stopping power. For calculation 1, the default value was 1000×10^{15} at./cm^2. This value can be user-defined; by decreasing or increasing it one order of magnitude, the maximum difference in calculated yield was found to be 0.003%, which shows that the calculation is stable and does not depend critically on the definition of internal sub-layers.

NDF uses SRIM stopping powers in the following way. SRIM is used to calculate 5000 stopping power values covering the required energy range. When a stopping power value is needed for a given energy, linear interpolation on these 5000 values is made. To calculate the energy loss in a sub-layer, the stopping power is integrated over the beam energy within the layer, using a simple Simpson rule. Because the stopping power changes slowly, this is accurate for the sub-layer areal density values used in NDF.

Linear interpolation is made between tabulated values of cross section. The cross section is always integrated in each sub-layer, thus avoiding the need for very thin layers. Furthermore, by default NDF convolutes the cross section with the energy spread of the beam according to Eq. (3) whenever straggling is calculated.

NDF implements different straggling models. For this exercise, Bohr straggling was used in the required calculations and the Tschalär effect [25], which is calculated by default in NDF, was not included in the calculation.

The stability test for constant stopping power and constant cross section was also made, showing a maximum 0.0007% deviation from linearity. This is within the expected accuracy of single precision real numbers used in NDF.

3.4. PiGreCo

The code treats bulk samples by dividing them into equally energy-spaced sub-layers. The default value of the energy step is determined by the minimum energy step in the corresponding cross section to be used, but it can also be defined by the user if a different one is desired. The value used for the comparison calculations of the current work was set to 1 keV.

The stopping power for each sub-layer is calculated at the middle of the layer. In its current version PiGreCo implements two ways for calculating the stopping power at a given energy: either by using the well-known Ziegler, Biersak and Littmark [26] compilation or by using SRIM stopping powers. For SRIM calculations, the code uses as input tabulated values for a proton energy range between 10 keV and 20 MeV for each element between Z = 1–92. The stopping power at the desired energy is then calculated by a simple linear interpolation between the existing points. In the case of composite target materials, the Bragg rule is used.

Cross sections are read directly from R33 formatted files in a tabulated form. The cross section corresponding to a specific energy is determined by a linear interpolation between known values. The inclusion of straggling in the yield calculation is an option selected by the user. In the simple case where no straggling is selected, the cross section used is the one corresponding to the energy at the middle of the sub-layer. When straggling is included, Bohr straggling is used and is convoluted with the energy spread implemented in Eq. (3).

A stability test was performed for constant cross section and constant stopping power which in the worst case resulted in a 0.23% divergence from linearity.

3.5. SIMNRA

In the case of PIGE simulations SIMNRA subdivides a bulk sample into internal sub-layers with thicknesses so that the energy loss in each sub-layer is close to the FWHM of the energy spread of the incident particle beam. Alternatively the sub-layer thicknesses can be chosen to provide about constant energy losses in each sub-layer, the desired energy-loss being user defined.

SIMNRA uses SRIM stopping powers in the following way: SRIM is used to calculate 840 logarithmically spaced stopping power values from 1 keV to 50000 keV. The stopping power for a specific energy is obtained by linear interpolation of these values. The energy-loss in a sub-layer is obtained by solving the differential equation $S(E) = -dE/dx$ (with E(x) the mean beam energy in a given depth x and S(E) the energy-dependent stopping power) using a fifth order Runge-Kutta method with embedded fourth order Runge-Kutta with Cash-Karp parameters [27] for an error estimate and automatic step width control of the energy-loss calculation. The accuracy of the energy-loss calculation is of the order of a few times 10^{-6}, i.e. for energy losses of the order of 1 MeV the inaccuracy is only a few eV.

Tabulated cross-section values are linearly interpolated. The cross section is always integrated in each sub-layer and is convoluted by default with the energy spread of the beam according to Eq. (3). SIMNRA implements different straggling models, for this exercise Bohr straggling was used when required. The Tschalär effect [25] cannot be switched off and was always included in the calculations if straggling was considered.

The stability test with constant stopping power and constant cross section showed a maximum deviation from linearity of about 10^{-10}%.

4. Results and discussion

The yield as a function of beam energy often changes several orders of magnitude in the examples chosen. For the purposes of comparing the results of the different codes, all results were normalised to the average of the values calculated by all codes: first, the average value of the simulations done by the different codes was calculated. Then, the ratio between each code and that average was calculated. It is this ratio that is presented, except where otherwise noted.

4.1. Slowly changing cross section, monoelemental target, no energy spread

Simulation 1-a corresponds to the simplest case tested in this intercomparison. The $^{10}B(p,p'\gamma)^{10}B$ reaction, with emission of a 718 keV γ, was chosen because the cross section (Lagoyannis et al. 2015 [28]) changes slowly with energy. The cross section, shown in Fig. 1, was truncated to zero at 3 MeV. A pure boron target was considered, which simplifies stopping power calculations. Beam energy spread and straggling were not included in the calculation. Finally, calculations were made from 3 to 5 MeV initial beam energy, at 200 keV steps.

The yields calculated by all codes are shown in Fig. 2a). It is clear

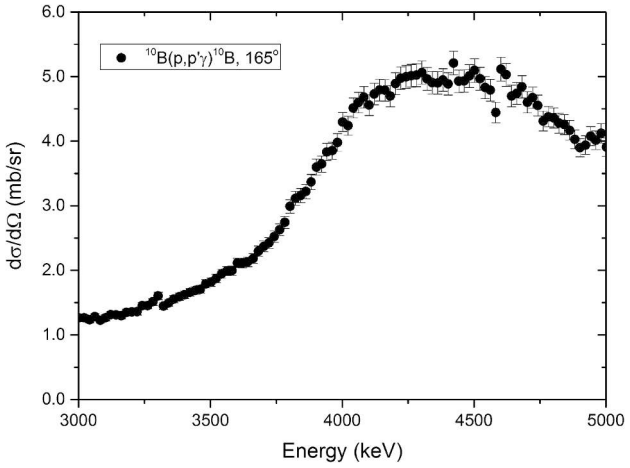

Fig. 1. Cross section for reaction ^{10}B(p,p'γ)^{10}B at 165° [28].

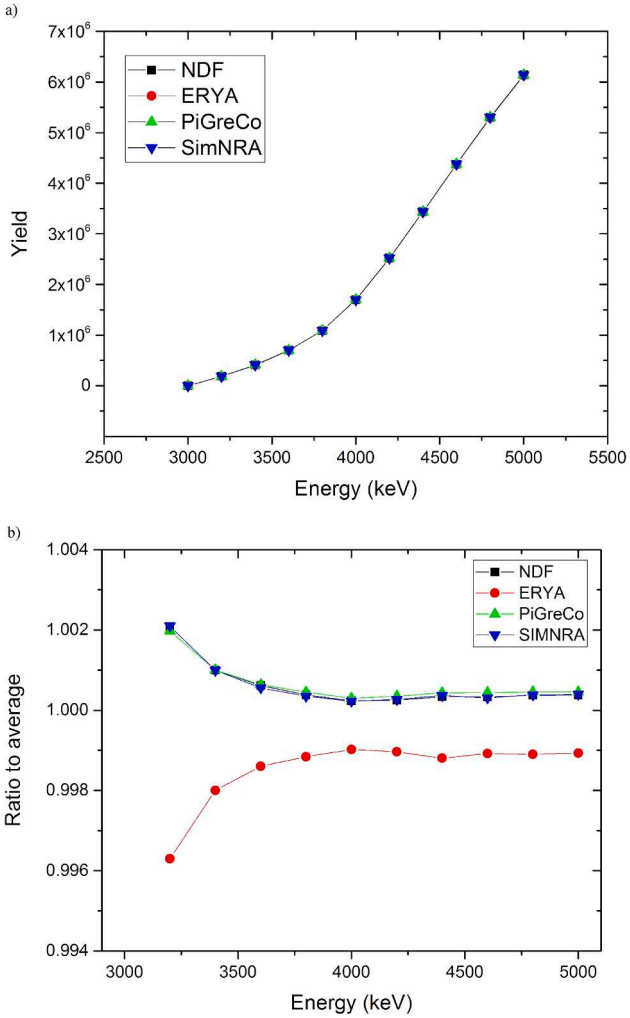

Fig. 2. Simulation 1-a: slowly changing cross section, monoelemental target, no straggling, for reaction ^{10}B(p,p'γ)^{10}B at 165°. a) Yield calculated by all codes. b) Results for all codes, shown as ratio to the average of the four calculations.

that the agreement is excellent, but details are difficult to observe because the differences between the calculations are much smaller than the yield values. The ratio of the codes to the average of all simulations is shown in Fig. 2b), where the differences are easily perceptible. Agreement is better than 0.6% in all cases. The ratio to average values

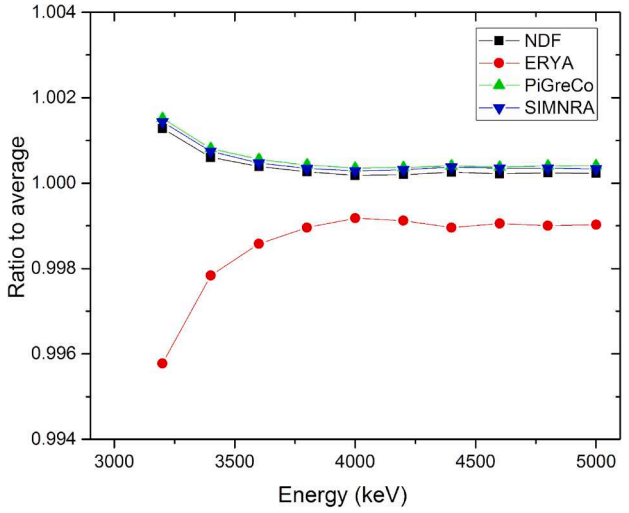

Fig. 3. Simulation 1-b: slowly changing cross section, multielemental target, no straggling for reaction ^{10}B(p,p'γ)^{10}B at 165°.

for ERYA-Bulk are lower in the low energy range close to 3 MeV, while it approaches the values for the other codes at higher energies. This initial difference may be due to the way the cross section is truncated at 3 MeV by the different codes. In fact, the difference in yield between ERYA-Bulk and the other codes is lowest at low energies in absolute terms (counts), but given the low yield at low energies, it becomes higher in relative terms (ratio). This agreement is similar to what was obtained for RBS and ERDA [5]. Agreement is 0.01% or better between NDF, PiGreCo and SIMNRA, which is extremely good and better than what was obtained for e.g. NDF and SIMNRA in RBS and ERDA [5].

4.2. Slowly changing cross section, multielemental target, no energy spread

Simulation 1-b is identical to 1-a, but with a multielemental target where boron is only 10 at.%. The results are shown in Fig. 3 and are very similar to those of calculation 1-a; all codes agree within a maximum difference of 0.6%. As in calculation 1-a, the values calculated by ERYA-Bulk near 3 MeV are lower than those calculated by the other codes and become less different at higher energies.

The difference between NDF, PiGreCo and SIMNRA is within 0.025%, with NDF values lying below the other two codes. One should keep in mind that in the IAEA inter-comparison of RBS and ERDA codes for the simplest problems, differences in yield of up to 0.3% between NDF and SIMNRA were found. The current results are one order of magnitude closer, and it is highly unlikely that any PIGE experiment will ever approach a total 0.025% uncertainty (or even 0.6%), even excluding systematic uncertainties such as that coming from the cross section.

4.3. Slowly changing cross section, monoelemental target, defined initial yield, no energy spread

Simulation 2-a-i is for a different reaction, ^{10}B(p,αγ)^{7}Be, with emission of a 429 keV γ, calculated at 100 keV intervals between 3 and 3.8 MeV. The cross section for this reaction, shown in Fig. 4, also changes slowly with energy, with no sharp resonances. A pure boron target was considered, and beam energy spread and straggling were not taken into account. The cross section is taken from [28] and is truncated to zero at 3 MeV. In this calculation, it was considered that a known yield exists for boron at 3 MeV, of 580,000 counts. This yield is supposed to account for the cross section at energies below 3 MeV.

The results for all codes are shown in Fig. 5. All results agree within better than 0.3%. As in the previous cases, the ERYA-Bulk result is lower than the other codes near the origin, becoming progressively

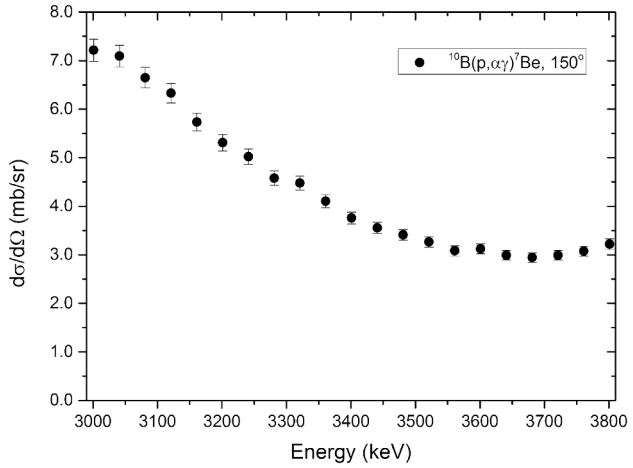

Fig. 4. Cross section for reaction ^{10}B(p,αγ)^{7}Be at 150° [28].

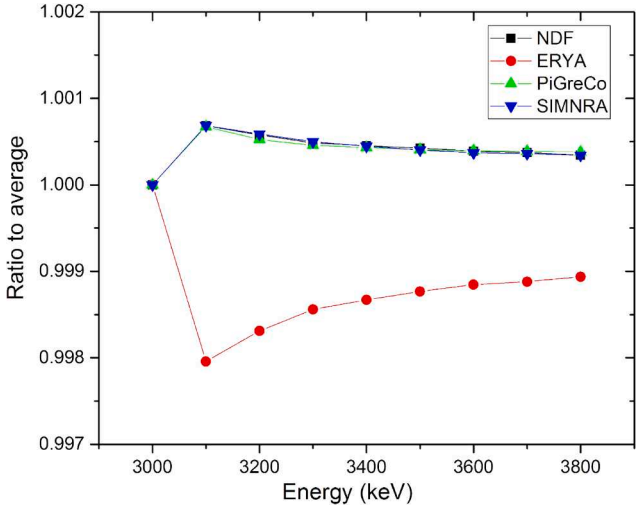

Fig. 5. Simulation 2-a-i: Slowly changing cross section, monoelemental target, defined initial yield, no straggling, for reaction ^{10}B(p,αγ)^{7}Be at 150°.

similar to the other results with higher initial beam energy. Agreement is 0.004% or better between NDF, PiGreCo and SIMNRA. This is extraordinarily good agreement.

A similar calculation, but for the ^{10}B(p,p'γ)^{10}B reaction between 3 and 3.8 MeV (simulation 2-b-i), led to agreement within 0.11% between all codes and within 0.04% between NDF, PiGreCo and SIMNRA, as shown in Fig. 6.

4.4. Slowly changing cross section, multielemental target, defined initial yield, no energy spread

Simulation 2-a-ii is identical to 2-a-i, but with a multielemental target where boron is only 10 at.%. The results are shown in Fig. 7. All codes agree within 0.3%. As in the previous cases, ERYA-Bulk shows the largest difference at low energy.

Agreement between NDF, PiGreCo and SIMNRA is within 0.04%. Note that at the origin, for a 3 MeV initial beam energy, there is some difference in the calculated value, with the results for SIMNRA results lying slightly below those for NDF and PiGreCo. This difference is due to the way the initial yield is calculated. In fact, the initial yield of 580,000 counts is given for a pure boron target. For a multielemental target, this yield has to be normalised to boron concentration and to the ratio of stopping power in boron and in the actual material (B 10O 40 Fe 50). An accurate calculation would require knowledge of the shape of the cross section below the 3 MeV threshold, which is not available.

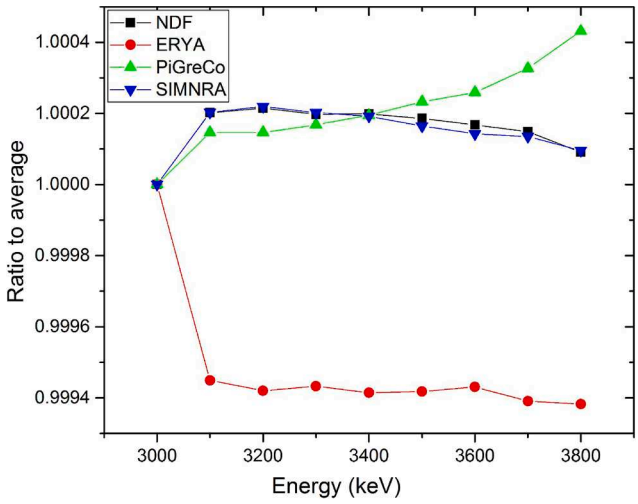

Fig. 6. Simulation 2-b-i: Slowly changing cross section, monoelemental target, defined initial yield, no straggling, for reaction ^{10}B(p,p'γ)^{10}B at 165°.

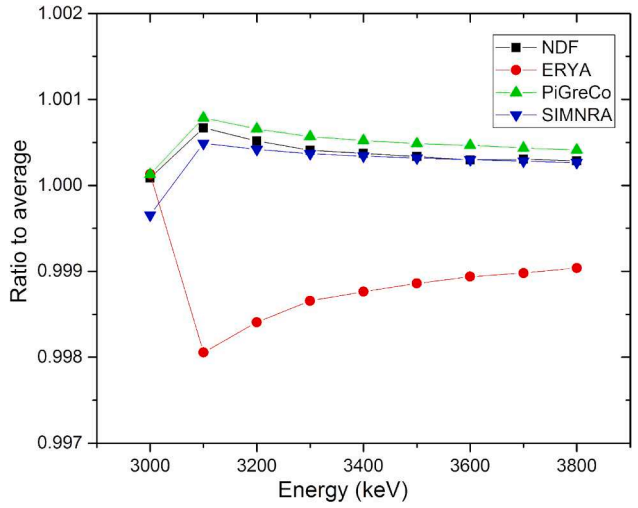

Fig. 7. Simulation 2-a-ii: Slowly changing cross section, multielemental target, defined initial yield, no straggling, for reaction ^{10}B(p,αγ)^{7}Be.

Therefore, different implementations make different assumptions, and it is not possible to say which method is preferable. All in all, the 0.04% agreement at 3 MeV (which includes ERYA-Bulk) must be considered excellent.

A similar calculation, but for the ^{10}B(p,p'γ)^{10}B reaction between 3 and 3.8 MeV (simulation 2-b-ii), led to agreement within 0.08% between all codes and within 0.05% between NDF, PiGreCo and SIMNRA , as shown in Fig. 8.

These six calculations demonstrate that, for simple cases where the cross section changes slowly and straggling is not considered, all participating codes agree within better than 0.6%, which is similar to what was obtained in the IAEA inter-comparison of IBA particle codes for RBS and ERDA [5]; considering NDF, PiGreCo and SIMNRA, the agreement is around 0.1%.

4.5. Cross section with resonances, no energy spread

Simulation 3-a is for the ^{19}F(p,pγ$_2$)^{19}F reaction, with emission of a 197 keV γ. This reaction was chosen because the cross section, shown in Fig. 9 (Jesus et al. 2000 [29]), has a number of sharp resonances. A pure fluorine target was considered. Beam energy spread and straggling were not included. Calculations were made at 1 keV steps between 1 and 2.8 MeV. The cross section was truncated to zero at 1 MeV. Note that

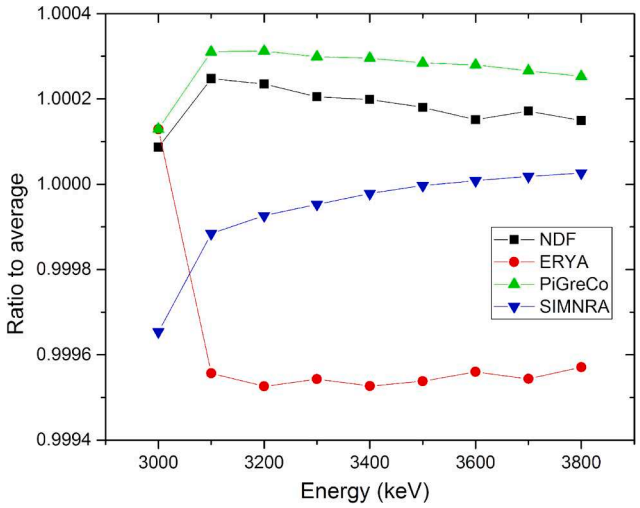

Fig. 8. Simulation 2-b-ii: Slowly changing cross section, multielemental target, defined initial yield, no straggling, for reaction $^{10}B(p,p'\gamma)^{10}B$.

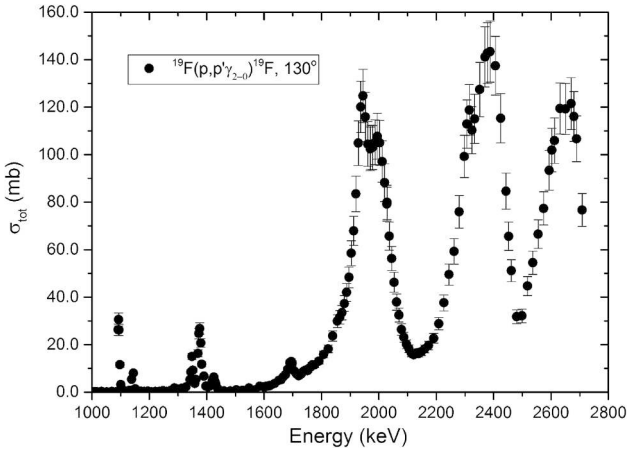

Fig. 9. Cross section for reaction $^{19}F(p,p\gamma_2)^{19}F$ at 130° [29].

this very narrow energy step is not realistic, as it would not be used in a real experiment. It was used to allow comparison of details in the calculations.

The results for all codes and for the entire energy range are shown in Fig. 10a). Despite the visible differences in the calculations, agreement between all codes is better than 0.25% in the entire energy range, which is much better than the accuracy of any PIGE experiment so far reported (or, for that matter, any RBS experiment).

The results are shown in selected energy ranges in Fig. 10b) to Fig. 10e). In the first 10 keV above the threshold, in the energy range 1000–1010 keV (Fig. 10b), the differences between codes are below 0.25%. In any case, in this range the yields are very low, and this relative difference corresponds to absolute differences below 0.2 counts, which is not significant.

Fig. 10c) shows the data calculated at energies around the 1093 keV sharp resonance. All codes agree within 0.15%. PiGreCo seems to show a small relative increase in yield with a large slope at the onset of the resonance, followed by an equally small and steep decrease, within 2 to 3 keV. The same energy range is shown in Fig. 10d), but the yield differences relative to NDF are plotted. These reach ± 6 counts at 1100 keV, for which the yield is around 20,000 counts. The associated statistical uncertainty, if this were experimental data, would be around 140 counts. Again, this shows that the uncertainty due to the code that is used is well below the expected experimental uncertainties. It is interesting to note that PiGreCo and SIMNRA results vary in a similar way and ERYA-Bulk results vary by approximately the same amount but towards negative values. As stated before, it is not possible to say which code is correct.

The results obtained at energies around the group of resonances at 1349, 1376 and 1425 keV, which are less sharp than that at 1093 keV, are shown in Fig. 10e). The codes agree within 0.04% in this energy range. Note that NDF seems to display very small fluctuations, around 0.001% in the 1 keV range. These are very likely due to the single precision real numbers used in NDF.

The results for simulation 3-b, made for exactly the same conditions but for a multielemental target, with composition ^{nat}F 10O 30 Cr 60, are shown in Fig. 11. The results are nearly identical to those of simulation 3-a, with maximum deviation between codes below 0.25%.

4.6. Slowly changing cross section, with energy spread

The calculation presented here, case 4-1-a. is identical to 1-a, presented in section 4.1, but in this case a 3 keV beam energy spread and Bohr straggling were included in the calculations.

The cross section is, as mentioned above, truncated to zero at energies below 3 MeV. In this case, in the absence of beam energy spread, the yield will be exactly zero for a 3 MeV initial beam energy. This was calculated by all codes in case 1-a. However, in the presence of beam energy spread, assumed to be Gaussian shaped, exactly half the beam particles have energy above 3 MeV, for which the cross section is above zero. In this case, a small but non-zero yield will be calculated. The yield at 3 MeV calculated by ERYA-Profile, NDF, PiGreCo and SIMNRA are 48.9, 64.5, 44.4 and 65.0 counts. As truncated cross sections are an artificial construct, these differences are not significant. As a comparison, the yield at 5 MeV is over 6.1 million counts.

The results for all codes are shown in Fig. 12. All codes agree within 0.3%, and NDF and SIMNRA are nearly undistinguishable.

The results for the same conditions but in a multielemental target (simulation 4-1-b) are very similar. In fact, there are no reasons to expect that energy spread should lead to different behaviour in calculations made for mono- or multielemental bulk targets.

For the calculations with given yield at the threshold energy (4-2-a-i, 4-2-a-ii, 4-2-b-i, 4-2-b-ii), the large initial yield is added to the small calculated yield for the threshold energy, which masks the effect of the beam energy spread. In all those calculations, the codes agree within 0.2%, with NDF and SIMNRA agreeing within 0.02%.

4.7. Cross section with resonances, with energy spread

The calculation presented here, case 4-3-a. is identical to 3-a, presented in section 4.5, but with a 3 keV beam energy spread and Bohr straggling included in the calculations. This is the most demanding calculation defined in the inter-comparison. At the threshold energy, 1 MeV, the beam energy spread leads to a non-zero calculated yield, which is 20.8, 11.1, 8.9 and 11.1 counts for ERYA-Profile, NDF, PiGreCo and SIMNRA, respectively. As for calculation 4-1-a above, these differences are not significant.. One should also note that for this simulation the yield for the maximum beam energy 2.7 MeV is around 9.5 million counts.

The results are shown in Fig. 13a) and b) for all codes. At the lower energies the resulting curves for ERYA-Profile and PiGreCo converge from values differing by around 15% different from NDF and SIMNRA to values differing by around 1%. The convergence occurs at 1020 keV for PiGreCo and at 1050 keV for ERYA-Profile.

Around the 1093 keV resonance, results for ERYA-Profile and

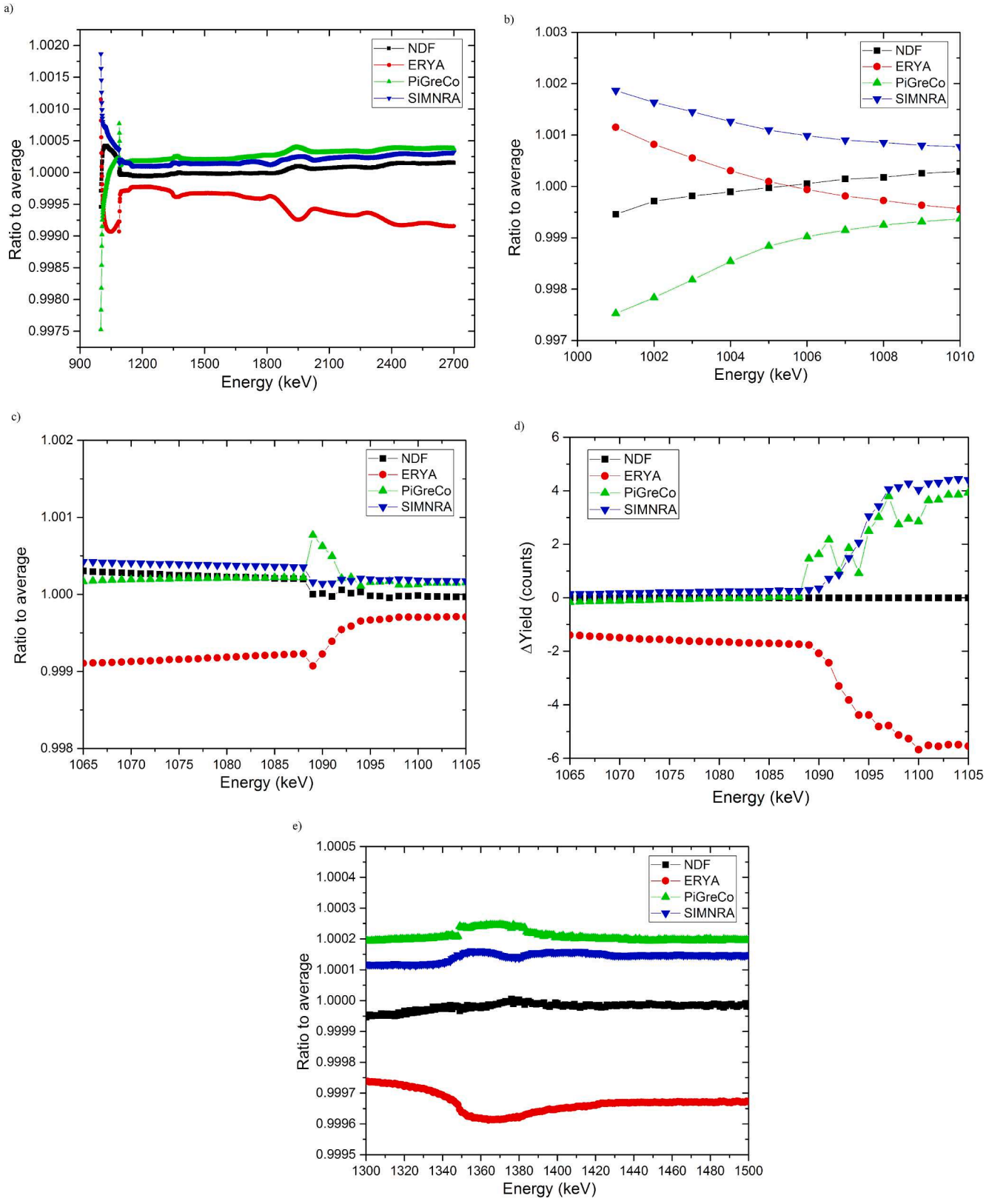

Fig. 10. Simulation 3-a: Cross section with resonances, monoelemental target, no straggling, for reaction $^{19}F(p,p\gamma_2)^{19}F$ at 130°. a) Results for all codes. b) Results for all codes in the energy range 1000–1010 keV. c) Results for all codes in the energy range 1065–1105 keV. d) Results for all codes in the energy range 1065–1105 keV, shown as yield difference towards NDF. e) Results for all codes in the energy range 1300–1500 keV.

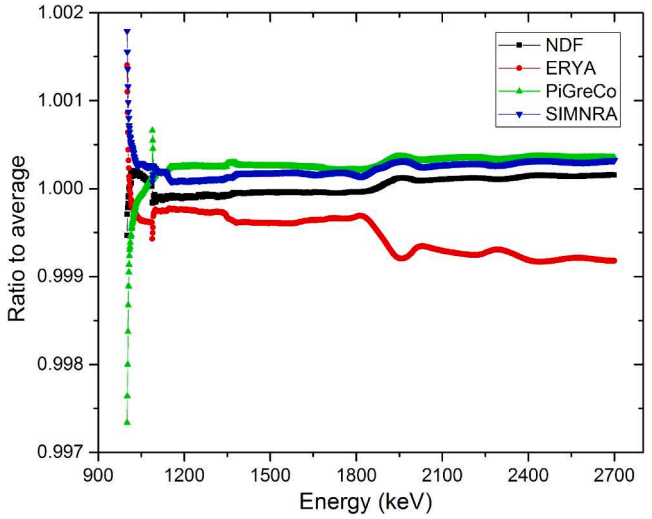

Fig. 11. Simulation 3-b: Cross section with resonances, multielemental target, no straggling, for reaction $^{19}F(p,p\gamma_2)^{19}F$ at 130°.

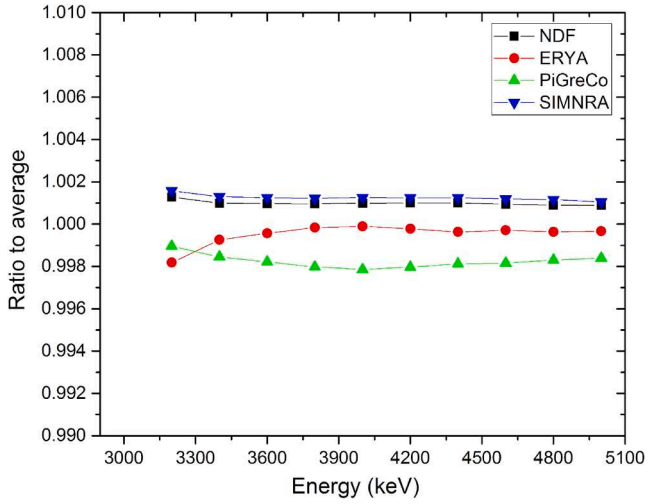

Fig. 12. Simulation 4-1-a: slowly changing cross section, monoelemental target, with beam energy spread and straggling, for reaction $^{10}B(p,p'\gamma)^{10}B$ at 165°.

PiGreCo deviate strongly from NDF and SIMNRA. The results are shown in absolute value in Fig. 13c), where it is clear that the observed differences must be due to the way the energy spread is handled by the codes. ERYA-Profiling leads to a calculated signal that is broader than NDF and SIMNRA at the high energy side of the resonance, while PiGreCo leads to a signal that is less broad than NDF and SIMNRA at the low energy side of the resonance. The difference is around 0.5 keV, which experimentally would be extremely difficult to observe. All in all, the large relative differences in the calculations do not arise from large differences in the magnitude of the yields calculated, but from the differences in calculated shape (energy width).

At energies above 1120 keV, the differences between the codes are within 1%. NDF and SIMNRA results are practically the same. ERYA-Profile and PiGreCo behave in a similar way, (Fig. 13b), but clearly different from NDF and SIMNRA. In any case, the difference is quantitatively within acceptable bounds; it can be concluded that, even in this demanding case, all participating codes are fit for the purpose of analysing experimental PIGE data.

The largest difference between NDF and SIMNRA, observed at low energies, is below 0.15%. It is noted that the ratio of SIMNRA to NDF presents a wave-like ripple. This ripple is not present in the ratios of ERYA-Profile and PiGreCo to NDF, which leads to the conclusion that it is likely due to the internal division of sub-layers in the SIMNRA code. The maximum amplitude is 0.02%, much below any detectable signal.

NDF and SIMNRA also present some differences near the 1093 keV sharp resonance. The maximum relative difference is however below 0.1%, which at this level of detail must be considered extraordinarily good agreement.

5. Conclusions

The IAEA organized the first systematic inter-comparison exercise of PIGE data analysis codes for bulk samples. Existing PIGE analytical codes participated, and other codes in active development, including analytical and Monte Carlo codes, were invited to participate. One of those codes under development implemented the technique and then participated. In total, five codes capable of first-principles analysis of PIGE data participated in this inter-comparison exercise: ERYA-Bulk, ERYA-Profiling, NDF, PiGreCo and SIMNRA.

A set of four exercises (some comprising sub-exercises) was defined by the participating code developers to test the performance of the codes on bulk analysis, starting from smooth cross sections and simple elemental compositions, then extending to cross sections with sharp resonances, including effects such as beam energy spread and straggling. The cross sections and stopping powers used, as well as details of the calculations, were agreed by the participants. The defined calculations included three different reactions, and concentrated on:

1. Smooth cross sections known down to the threshold energy (no beam energy spread)
2. Smooth cross section known down to a given energy (no beam energy spread)
3. Cross section with sharp resonance (no beam energy spread)
4. Straggling added to cases 1 to 3 using Bohr's model with a beam energy spread of 3 keV

Both monoelemental and multielemental targets were considered. Some of the exercises had a very fine energy step. Altogether, the calculations allowed to test the main issues affecting calculation of PIGE data for bulk target. Multilayered targets were not addressed.

When beam energy spread and straggling are not included in the calculations, all codes agreed with differences that reached a maximum of 0.6%, but which were generally below 0.3%. This is much lower than the uncertainties of the experimental cross sections used for PIGE, which are seldom below 5 to 10% and often larger [22]. In the absence of sharp resonances, NDF, PiGreCo and SIMNRA agree within 0.05%. In the presence of a cross section with sharp resonances, ERYA, NDF, PiGreCo and SIMNRA agree within 0.25%.

When beam energy spread and straggling are included in the calculations, differences in the calculated yields up to 20% were observed. However, we note that such large differences were confined to the vicinity of very sharp resonances, where the different implementation by the codes of the calculation of energy spread and straggling, as well as the numerical integration method, leads to a different shape of the energy-dependent yield (broader or less broad). In this case, it is the shape of the increase of the PIGE yield with beam energy that is the real difference between the codes, while the large relative differences in yield for one given beam energy are not significant; a sizeable part of this effect seems to be due to a shift in the energy axis of less than 0.5 keV.

When only NDF and SIMNRA are considered, the maximum difference is 0.2%. Given the complexity of the case, this must be considered excellent agreement.

In summary, all participating codes are fit for the purpose of analyzing experimental PIGE data. In general, the agreement between the codes is much better than the accuracy of available cross sections.

We note that these conclusions are valid for bulk samples only. For multilayers, particularly in the presence of thin layers and cross sections

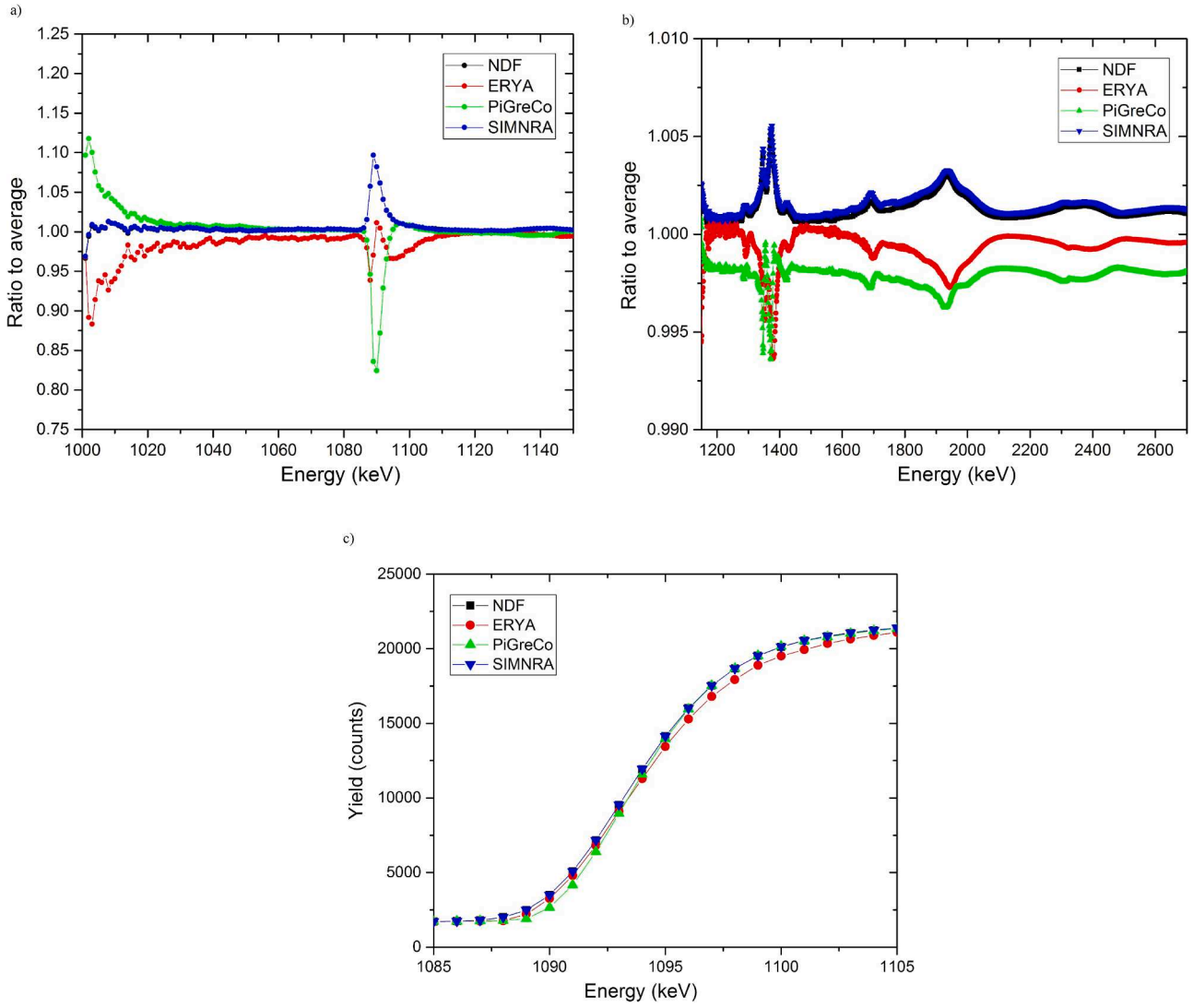

Fig. 13. Simulation 4-3-a: Cross section with resonances, monoelemental target, with beam energy spread and straggling, for reaction $^{19}F(p,p\gamma_2)^{19}F$ at 130°. a) Results for all codes. b) Results for all codes in the energy range 1150–2700 keV. c) Results for all codes in the energy range 1085–1105 keV shown as calculated yield.

with sharp resonances, it is expected that the handling of straggling and numerical integrations will play a larger role. This will be the subject of a future study.

Declaration of competing interests

The authors declare that they have no known competing financial interests or personal relationships that could have appeared to influence the work reported in this paper.

CRediT authorship contribution statement

N. Pessoa Barradas: Methodology, Investigation, Software, Writing - original draft, Writing - review & editing. **J. Cruz:** Methodology, Investigation, Software, Writing - review & editing. **M. Fonseca:** Software. **A.P. Jesus:** Software. **A. Lagoyannis:** Methodology, Investigation, Software, Writing - review & editing, Visualization. **V. Manteigas:** Software. **M. Mayer:** Software, Investigation, Writing - review & editing. **K. Preketes-Sigalas:** Software. **P. Dimitriou:** Conceptualization, Project administration, Funding acquisition, Data curation, Methodology, Writing - review & editing.

References

[1] Wei-Kan Chu, James W. Mayer, Marc-A. Nicolet, Backscattering Spectrometry, Academic Press, New York, 1978.
[2] Inter-comparison of PIXE spectrometry software packages, International Atomic Energy Agency TECDOC No. 1342 (2003), Vienna. ISBN: 92-0-101203-9.
[3] M. Blaauw, J.L. Campbell, S. Fazinic, M. Jaksic, I. Orlic, P. Van Espen, Nucl. Instrum. Methods Phys. Res. B 189 (2002) 113.
[4] E. Rauhala, N.P. Barradas, S. Fazinic, M. Mayer, E. Szilágyi, M. Thompson, Nucl. Instrum. Methods Phys. Res. B 244 (2006) 436.
[5] N.P. Barradas, K. Arstila, G. Battistig, M. Bianconi, N. Dytlewski, C. Jeynes, E. Kótai, G. Lulli, M. Mayer, E. Rauhala, E. Szilágyi, M. Thompson, Nucl. Instrum. Methods Phys. Res. B 262 (2007) 281.
[6] N.P. Barradas, C. Jeynes, R.P. Webb, Appl. Phys. Lett. 71 (1997) 291–293.
[7] N.P. Barradas, C. Jeynes, Nucl. Instrum. Methods Phys. Res. B 266 (2008) 1875.
[8] L.R. Doolittle, Nucl. Instrum. Methods Phys. Res. B 9 (1985) 344.
[9] L.R. Doolittle, Nucl. Instrum. Methods Phys. Res. B 15 (1986) 227.
[10] M. Mayer, AIP Conf. Proc. 475 (1999) 541.
[11] M. Mayer, Nucl. Instrum. Methods Phys. Res. B 332 (2014) 176.
[12] M. Mayer, P. Malinský, F. Schiettekatte, Z. Zolnai, Nucl. Instrum. Methods Phys. Res. B 385 (2016) 65.
[13] N.P. Barradas, R. Mateus, M. Fonseca, M.A. Reis, K. Lorenz, I. Vickridge, Nucl. Instrum. Methods Phys. Res. B 268 (2010) 1829.
[14] R. Mateus, A.P. Jesus, J.P. Ribeiro, Nucl. Instrum. Methods Phys. Res. B 219 (2004) 519.
[15] R. Mateus, A.P. Jesus, M. Fonseca, H. Luís, J.P. Ribeiro, Nucl. Instrum. Methods Phys. Res. B 264 (2007) 340.
[16] I. Vickridge, G. Amsel, Nucl. Instrum. Methods Phys. Res. B 45 (1990) 6.

[17] Development of a Reference Database for Particle Induced Gamma Ray Emission (PIGE) Spectroscopy, International Atomic Energy Agency TECDOC No. 1822 (2017), Vienna. ISBN:978-92-0-106317-5.
[18] IAEA Consultant's Meeting on Inter-comparison of PIGE Analysis Codes, 1-4 October 2018, IAEA, Vienna. https://www-nds.iaea.org/index-meeting-crp/CM-PIGE-analysis2018/.
[19] K. Preketes-Sigalas, A. Lagoyannis, M. Axiotis, Proc. 25th Hellenic Conference on Nuclear Physics, 3–4 June 2016, p. 162.
[20] C. Jeynes, N.P. Barradas, E. Szilagy, Anal. Chem. 84 (2012) 6061.
[21] J.F. Ziegler, J.P.Biersack, and M.D.Ziegler, SRIM – The Stopping and Range of Ions in matter, Maryland, SRIM Co., 2008. < www.srim.org > .
[22] IAEA Ion Beam Analysis Nuclear Data Library (IBANDL), < https://www-nds.iaea.org/exfor/ibandl.htm > .
[23] N.P. Barradas, E. Alves, C. Jeynes, M. Tosaki, Nucl. Instrum. Methods Phys. Res. B 247 (2006) 381.
[24] N.P. Barradas, E. Alves, Nucl. Instrum. Methods Phys. Res. B 249 (2006) 796.
[25] C. Tschalär, Nucl. Instrum. Methods 61 (1968) 141.
[26] J.F. Ziegler, J.P. Biersack, U. Litmark, The Stopping and Range of Ions in Matter, Pergamon Press, New York, 1985.
[27] W.H. Press, B.P. Flannery, S.A. Teukolsky, W.T. Vetterling, Numerical Recipes, Cambridge University Press, Cambridge, New York, 1988.
[28] A. Lagoyannis, K. Preketes-Sigalas, M. Axiotis, V. Foteinou, S. Harissopulos, M. Kokkoris, P. Misaelides, V. Paneta, N. Patronis, Nucl. Instrum. Methods Phys. Res. B 342 (2015) 271.
[29] A.P. Jesus, B. Braizinha, J.P. Ribeiro, Nucl. Instrum. Methods Phys. Res. B 161–163 (2000) 186.

Nuclear Instruments and Methods in Physics Research B 502 (2021) 142–149

Contents lists available at ScienceDirect

Nuclear Inst. and Methods in Physics Research, B

journal homepage: www.elsevier.com/locate/nimb

ERYA–Profiling: A code for quantitative PIGE analysis of in-depth heterogeneous samples

V. Manteigas, J. Cruz *, M. Fonseca, A.P. Jesus

Laboratório de Instrumentação, Engenharia Biomédica e Física da Radiação (LIBPhys-UNL), Departamento de Física, Faculdade de Ciências e Tecnologia da Universidade Nova de Lisboa, Monte da Caparica, 2892-516 Caparica, Portugal

ARTICLE INFO

Keywords:
PIGE
Computer code
ERYA-Profiling
Analysis of in-depth heterogeneous samples

ABSTRACT

The application entitled Emitted Radiation Yield Analysis (ERYA-Profiling) is a program for PIGE (Particle Induced Gamma-Ray Emission) analysis of in-depth heterogeneous samples.

Here, we present this code, which includes new features, functionalities, and direct handling of r33 and SRIM files, following the approach for a new version for ERYA-Bulk. Case studies are presented illustrating a good performance of the ERYA-Profiling program. ERYA-Profiling is currently compiled for Linux, Windows and Mac OS X operating systems and can be downloaded free from https://sites.fct.unl.pt/nuclear/software/erya-profiling.

1. Introduction

Particle Induced Gamma-Ray Emission (PIGE) has been widely used for the analysis of in-depth homogeneous samples, usually using reference samples for the quantification of data. With a growing database of experimental excitation functions and stopping powers, the use of computer codes based on these physical parameters is gaining ground. ERYA (Emitted Radiation Yield Analysis) is one of the few codes available for the analysis of PIGE data. The previous version [1–3] for bulk analysis (i.e. analysis of in-depth homogeneous samples), was recently replaced by a new version, renamed ERYA-Bulk [4–6], which improved in several features and functionalities related to: compatibility with several computer operating systems; input and output options, which import from IBANDL [7] and SRIM [8] files are examples; the user interface, offering additional options; the upgraded fitting procedure algorithm allowing to fix in relative terms the concentrations of elements, for example those belonging to the same chemical compound.

Resonant depth profiling makes use of resonances in the excitation function of particle-induced gamma-ray emitting reactions, particularly those resonances where the cross-section is significantly stronger than in the (non-resonant) region above and below the resonance energy. This means mainly (p,γ) reactions in isotopes with atomic number below 30. Depth profiling is performed by measuring the gamma-yield of the reaction as a function of the beam energy. Starting with energies near the resonance energy, the beam energy is increased in steps in order to scan the resonance along the depth of the sample. In the context of resonant profiling a mention to the pioneer work of Vickridge and Amsel and the development of the program SPACES must be done [9,10]. Although widely used for more than fifty years for a variety of light isotopes, other methods of material analysis have replaced (p,γ) profiling, being the (p,γ) applications in recent years mainly related to hydrogen analysis as may be appreciated in IBA Proceedings (2000–2020) and in recent reviews [11,12].

However, interest in proton-induced gamma-ray resonance profiling may raise again with the handling of its limitations and extension to a wider variety of isotopes. This may be accomplished by overcoming the need of isolate resonances (in order to simplify the calculations), allowing for the influence of more than one resonance and background to the gamma yield, as is done by the ERYA-Profiling code, which is presented in this paper. It also opens the possibility of using stronger (p,p'γ) and (p,αγ) resonances with natural widths near 1 keV, implying a faster experimental procedure.

In this work we present the ERYA-Profiling program, a version of ERYA developed for the analysis of in-depth heterogeneous samples, taking into consideration the beam initial energy resolution and energy straggling within the sample. As far as we know ERYA-Profiling is the most advanced program available for gamma resonant profiling with the capacity to include more than one resonance.

The approach followed by ERYA-Profiling is a direct one, where the user introduces a first guess of the compositions as function of the depth

* Corresponding author.
E-mail address: jdc@fct.unl.pt (J. Cruz).

https://doi.org/10.1016/j.nimb.2021.06.006
Received 7 January 2021; Received in revised form 2 April 2021; Accepted 8 June 2021

and optimizes it in comparison with the experimental results. In relation to the influence of more than one resonance, the uniqueness of response may seem in abstract an insurmountable problem. However, in concrete terms there will always be a scan of some layers done by just one resonance and this will allow to restrict the options. Case studies are presented to illustrate ERYA-Profiling capabilities and clarify this issue.

2. Yield calculation

The underlying concepts of PIGE are simple. Energetic ions (typically protons with energies up to 4 MeV) interact with a nucleus, leading to a nuclear reaction with emission of a gamma photon. The most common nuclear reactions are (p,p'γ), (p,αγ) and also (p,γ). The gamma yield $dY(E,\theta)$ emitted by an isotope *i*, resulting from the interaction of N_p protons with energy *E* with a thin layer having an areal density $N_i dx$ of the given isotope species is:

$$dY(E,\theta) = 4\pi\ \varepsilon_{\mathrm{abs}}(E_\gamma).N_p.\sigma(E,\theta).N_i \mathrm{d}x \tag{1}$$

where N_i is the number of isotopes per volume unit, d*x* is the thickness of the thin layer, $\varepsilon_{abs}(E_\gamma)$ is the absolute efficiency of the detector for γ rays with energy E_γ, and $\sigma(E,\theta)$ is the differential cross-section for emission of a γ ray at angle θ to the incident ion direction. Considering that a beam with initial energy E_0 will steadily lose energy as it crosses the sample, the total yield will be:

$$Y(E_0,\theta) = 4\pi\ \varepsilon_{\mathrm{abs}}(E_\gamma).N_p.f_m.f_i.N_{av}.A^{-1}\int_0^{E_0}\sigma(E,\theta)/S_m(E)dE \tag{2}$$

where $S_m(E)$ is the mass stopping power at energy *E*; f_m is the relevant element mass fraction; f_i, and *A* are the isotopic abundance and the atomic mass of the relevant element, respectively, and N_{av} is the Avogadro number. The factor $N_i/\ \rho = f_m\ f_i\ N_{av}\ A^{-1}$, where ρ is the mass density of the sample, transforms the atomic density into mass fraction also changing the linear stopping power to mass stopping power.

Equations (1) and (2), valid for ERYA-Bulk, may be rewritten in order to include a composition dependent on the depth and energy straggling and beam energy dispersion. Hence, eq. (2) becomes:

$$Y(E_0,\theta) = 4\pi\ \varepsilon_{\mathrm{abs}}(E_\gamma).N_{av}.f_i.A^{-1}\int_0^{E_0}\sigma(E,\theta).N_p(E).f_m(E)/S_m(E)dE \tag{3}$$

In general, a direct evaluation of eq. (3) is not viable due to the complexity of the simulation model. In order to accomplish the calculations the following approximations are applied:

(1) The integral is evaluated by a sum over small layers k, where the variation of composition along the depth (or energy) is negligible, and the stopping power may be assumed as constant.
(2) A constant average energy is assigned to each layer, $\overline{E}_k$.
(3) Within each layer protons display a distribution of energy *F*(*E*) and the cross-section may vary by several orders of magnitude, particularly for resonances that have a major interest to ERYA-Profiling.

Using these assumptions, the yield corresponding to a given element is given by the following sum:

$$Y(E_0) = \sum_{k=1}^{n} Y_k\left(\overline{E}_k\right) \tag{4}$$

And each term may be calculated from:

$$Y_k\left(\overline{E}_k\right) = 4\pi\ \varepsilon_{\mathrm{abs}}(E_\gamma).N_{av}.A^{-1}.f_{mk}.f_i/S_m\left(\overline{E}_k\right)\Delta E_k N_p\int F(E)\sigma(E)dE \tag{5}$$

The quantity ΔE_k represents the energy lost in layer k and is related to:

$$\overline{E}_{k+1} = \overline{E}_k - (\Delta E_k) \tag{6}$$

For each consecutive layer the beam energy will decrease until reaches zero or a cut-off energy, while evaluating (5) and (4).

The energy distribution *F*(*E*) on eq. (5) is given by a convolution of three separated distributions:

$$F(E) = F_D(E)*F_{Beam}(E)*F_S(E) \tag{7}$$

where $F_D(E)$ is the Doppler Distribution, proportional to the temperature, $F_{beam}(E)$ represents the beam initial energy dispersion, and $F_S(E)$, the Straggling Distribution, is the energy distribution resulting from the stochastic character of the energy loss suffered by the beam within the material. The first two distributions may be considered Gaussian distributions, and can be trivially merged in a single one, designated by DB.

$$F_{DB}(E) = F_D(E)*F_{Beam}(E) \tag{8}$$

and

$$F(E) = F_{DB}(E)*F_S(E) \tag{9}$$

As the following expression applies for a convolution:

$$(f*g)(E) = \int f(E')g(E-E')dE' \tag{10}$$

eq. (5), calculating the yield for each layer, becomes:

$$Y_k\left(\overline{E}_k\right) = 4\pi\ \varepsilon_{\mathrm{abs}}(E_\gamma).N_{av}.A^{-1}.f_{mk}.f_{ik}/S_m\left(\overline{E}_k\right)\Delta E_k N_p \int\int F_{DB}(E')F_S(E-E')\sigma(E)dEdE' \tag{11}$$

Depending on the energy lost by the beam till layer k, the program will fetch for the straggling distribution a Landau, Vavilov or Gaussian distribution.

A full numerical implementation of Vavilov would be overkill, due to the low convergence, and instead many authors approximate the Vavilov distribution by another ones more easily to implement numerically. ERYA-Profiling use a revision of a numerical method published by Rotondi and Montagna [13]. Several problems were found in this publication and dealt with and will be object of a separate publication.

Actually, a parameter κ was defined by Landau and Vavilov as the ratio between ξ, approximately equal to the average lost energy, and ϵ_{MAX} the maximum energy transfer per collision

$$\kappa = \xi/\epsilon_{MAX} \tag{12}$$

The parameter κ is assumed to be constant for each layer. According to the values of κ, the following distribution functions (table 1) come into play.

3. ERYA-Profiling features

The ERYA-Profiling code, following the approach used for the new version of ERYA-bulk, is written on C++11 language and uses a cross-platform library for the Graphical User Interface (GUI) and data structures called wxWidgets [14] (the program uses the wxWidgets 3.0.4 code branch). Since wxWidgets employs a unified Application Programming Interface (API) for GUI programs, it only requires coding once and

Table 1
Different energy distributions, due to energy straggling, used by ERYA-Profiling.

Landau κ -factor	Distribution
$\kappa = 0$	Dirac's Function
$0 < \kappa < 0.02$	Landau Function
$0.02 < \kappa < 0.24$	Vavilov-Moyal Function
$0.24 < \kappa < 22$	Vavilov-Airy Function
$22 < \kappa < 25$	Vavilov-Edgeworth Function
$\kappa > 25$	Gaussian Function

compile against the porting libraries to several operating systems. Currently it was compiled for Linux, Windows and Mac OS X without changing a single line of code.

The program expects the user to fill in the respective inputs all relevant information about the sample composition with some additional information related to the energy measurement range and energy beam resolution. Optionally, it is possible to define a Breit-Wigner resonance using the tools provided by the program interface, overriding the cross-section data delivered by the program databases related to the energy window selected by the user.

The program's main algorithm is pictured on Fig. 1, noticing that to calculate the yields, ERYA will start a double cycle, where the exterior one is related to the beam energy, while the inner one is related to the energy distribution in each layer, being the sublayer integration step chosen by the user, ranging from 1 to 1000 $\times$ 10^{15} at./cm^2).

To organize the user workflow, the program uses a tabbed interface for inputs and outputs (see Fig. 2):

"Elements editor" – this tab allows the user to select the elements and gammas, with the possibility to override the elements physical characteristics loaded from the database on the adequate columns. It also allows the introduction of calibration factors. The propagation of the uncertainties of the cross-section values, the absolute value of the collected charge, the detector efficiency and the stopping powers leads to an uncertainty of the determined mass fractions which may be larger than 20%. However, this may be reduced if calibrations are performed (as is typically done for standardless PIXE). The calibration consists of determining the ratio between the measured gamma-ray yield and the calculated gamma-ray yield for either (i) a pellet made of a pure inorganic compound that contains the element to be analyzed or (ii) a standard reference sample. These ratios may be used as external calibration factors (or correction factors) in future analyses of the given element, provided the same experimental conditions (e.g., ion beam, detector type and detector geometry) are used and that the same excitation function is used in the calculations.

"Layers editor" – in this spreadsheet, the user defines the number and atomic composition of each individual layer. With this approach, a non-homogeneous sample can be treated as a sum of individual homogeneous layers.

"Beam and Resonances" – the user defines the beam energy and its resolution, including the energy range for the profiling analysis. Optionally, the user may also define one or more Lorentzian resonances, or a custom function for the resonance at a finite energy range. By default, ERYA will perform the calculations with resource to the excitation function chosen in the elements editor. Most of the excitation functions of gamma-producing nuclear reactions published in the literature were not, for the case of very thin resonances, corrected for the thickness of the target used in the experiment. This must be done for profiling purposes and that is why we have implemented in ERYA-Profiling an input for "true" Breit-Wigner resonances (obtained by fitting the experimental results [17,18]) or resonance strengths.

"Graphical output" – displays the yield in function of energy in a graphical plot, optionally in comparison with the experimental yield, which may be introduced through this tab.

"Table output" – displays the yield in function of energy in table format.

"Log details" – displays partial yields and parameters of each layer. It is disabled by default but may be opened via the "Advanced Options" button.

At the bottom screen, some special buttons activate global events as making a quick save of the results or starting a new simulation. An additional applet to change the accuracy of the energy distributions and the sample depth integration step is accessible from the "Advanced" button.

The menu bar at the top screen contains the tools to handle the databases and the program settings. It also enables to save the sample contents to a file, and load again to avoid manual typing. The Database Management Tools from the ERYA's databases are accessible from the program's main menu. The user can freely change any database contents and settings or save to different files and swap on fly without restarting ERYA. wxWidgets framework also provides libraries to implement special routines for the database management tools to read and write text files with custom parsing rules, which enables to import data from files, for example those of IBANDL [7] and SRIM [8].

ERYA-Profiling works on three database sets: elements, stopping power and detector efficiency.

The Elements Database contains all the necessary elemental parameters, including the excitations functions, which were retrieved from IBANDL. Fig. 3 shows the elements database manager pop-up window,

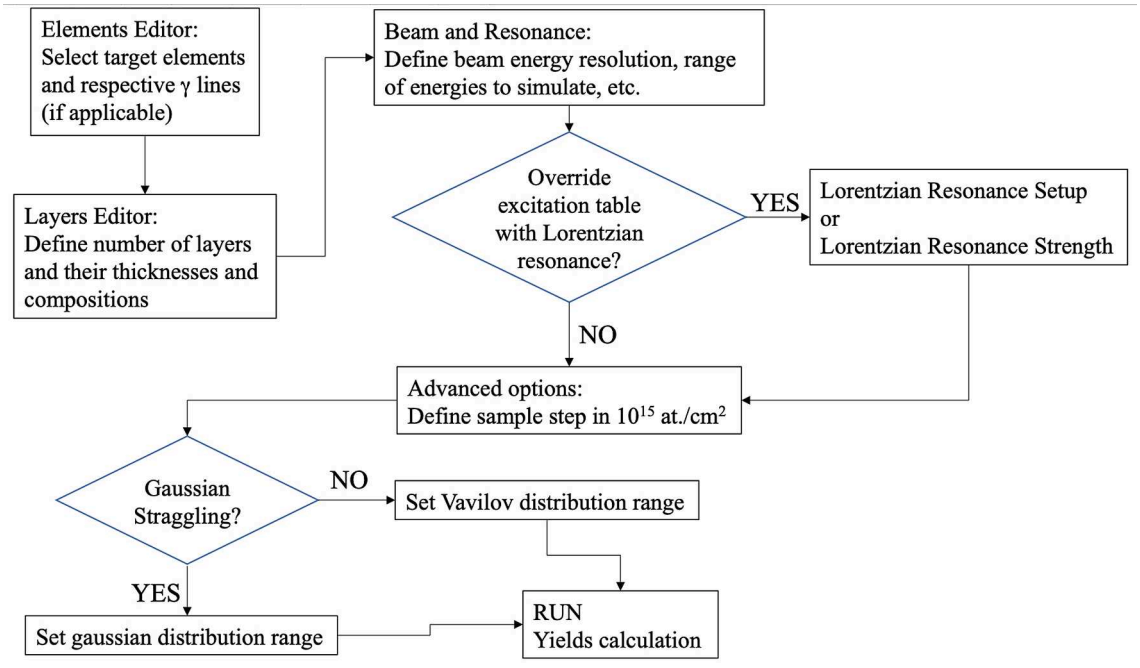

Fig. 1. ERYA-Profiling main algorithm.

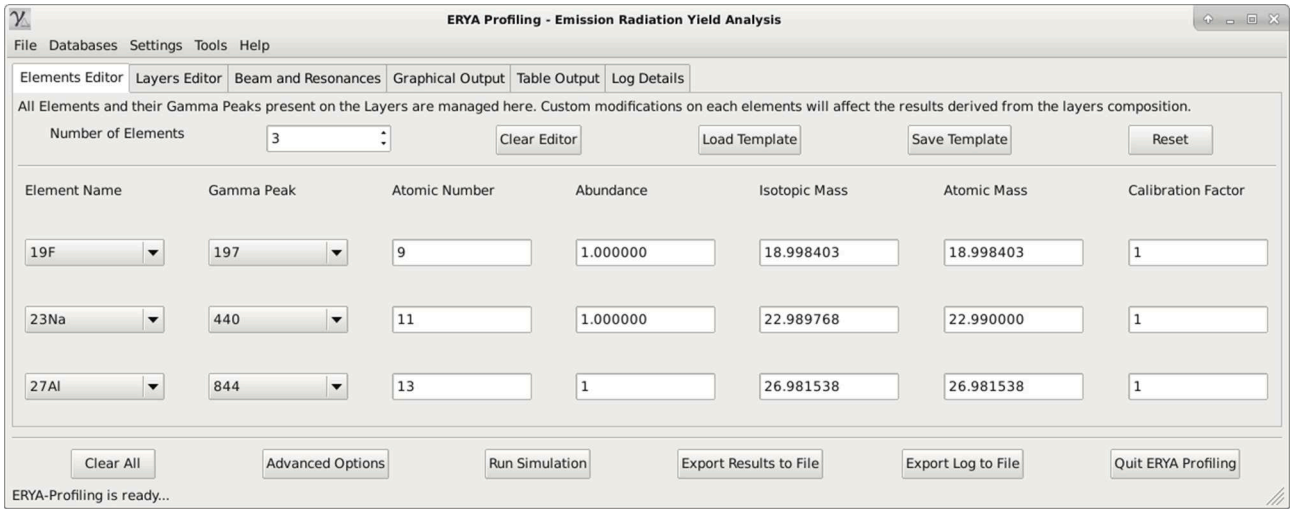

Fig. 2. ERYA-Profiling interface (rescaled for better visualization) running on Debian 10 Buster.

which allows not only the fast selection and visualization of different excitation functions, but also the upload of new excitation function files, for example in r33 format (as those in IBANDL).

The Detector Efficiency Database contains the data pertaining to the absolute efficiency of the gamma detector. Fig. 4 shows the Detector Efficiency database manager pop-up window. This window combines an editable text box, intended for the user to code an algebraic function (using a custom ERYA macro – see below), describing the variation of the Detector Efficiency with Energy, and a two-column table to fill any experimental values for the Detector Efficiency that will serve the same purpose. Both fields can be filled on the built-in editor and stored in the profile file. However, ERYA will choose the function field by default, if it is correctly defined, and will ignore the table.

The Stopping power database allows to choose between four options: the first two correspond to the Ziegler's model (either the 1977 or 1991 equations, hardcoded on program); the third option requires the user to type a function macro that represents the stopping power with eV/10^{15} at.cm^{-2} units in function of energy in keV; the last option (default) corresponds to SRIM tables (in units of eV/10^{15} at./cm^{2}) for all elements. The Stopping Power database manager pop-up window shown in Fig. 5, presents three options and a programmable custom

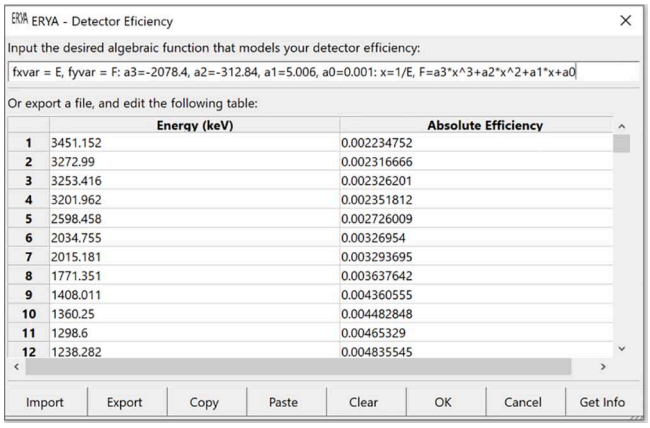

Fig. 4. ERYA-Profiling interface: Detector Efficiency database manager pop-up window.

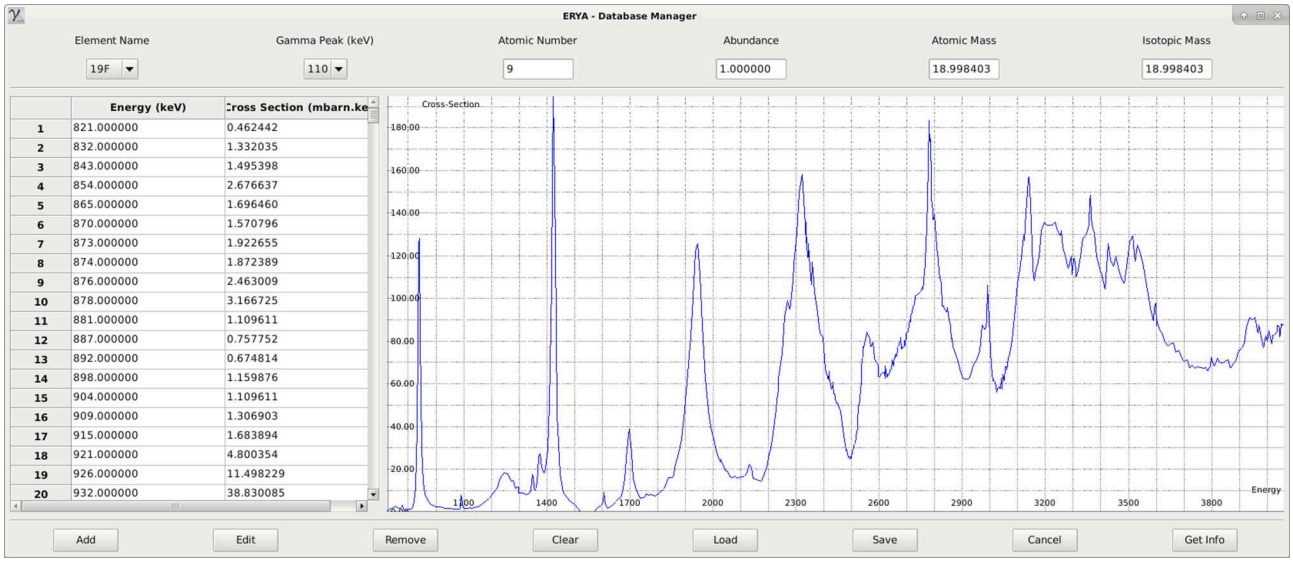

Fig. 3. ERYA-Profiling interface: Elements database manager pop-up window. In this case, it is plotted the excitation function for the 110 keV gamma peak of the ^{19}F (p,p' γ)^{19}F inelastic reaction.

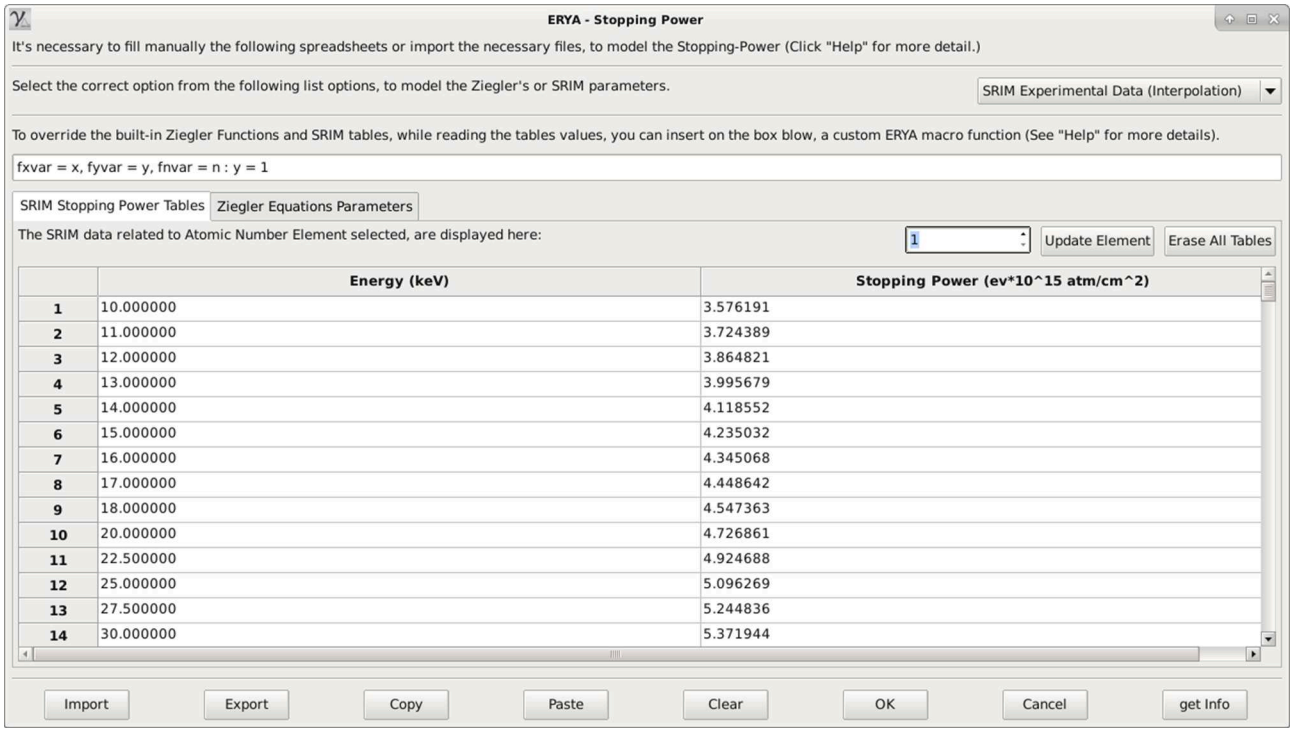

Fig. 5. ERYA-Profiling interface: Stopping Power database manager pop-up window.

ERYA macro – see below.

ERYA-Profiling has implemented a small programming language, derived from a BASIC dialect from high school programmable calculators, called ERYA function macro. This allows the user to write any custom algebraic function. The macro is then executed by an interpreter routine, without the need to recompile the entire program at each change. The user can use this feature on ERYA to define a custom algebraic function to model the Detector's Efficiency, or to code a Stopping Power custom function like the original 1977 or 1991 Zielger's Function. It also can be used to define a custom resonance function ("Detector and Resonances" tab).

As wxWidgets supports XML documents, all databases handled by ERYA are XML formatted documents, which store data within a hierarchic structure. This framework allowed the implementation of a basic routine to read and write Excel files with the xlsx format (2007 and later), since wxWidgets provides support for zip and xml files. ERYA uses this routine to save the results to an Excel file. ERYA can also import some tabular data from Excel files, as long it respects some structural rules.

Since the ERYA-Profiling databases have a combined size around 1 MB, the program will always load them into memory to the adequate C++ class structures on startup. Hence, the user has immediate access to the database contents and to the respective tools. ERYA-Profiling will access the loaded database structures together with the user inputs to evaluate gamma yields. All user inputs are checked to verify their consistency.

Full details concerning the operation of ERYA-Profiling can be found in the code's manual [15].

4. ERYA-Profiling – Case studies

In order to test the performance of ERYA-Profiling several studies were undertaken.

4.1. Beryllium on silicon

To validate the performance of the ERYA-Profiling program, we present a case study on the determination of the thickness of a thin film of Beryllium deposited on a slab of Silicon. This sample was part of an investigation related to the fusion program ongoing at our laboratory.

In order to fulfill the task, a resonant scan of the sample was performed using the thin 1082 keV ($\Gamma = 3.0$ keV) resonance of the ^{9}Be(p,γ)^{10}B reaction, being this resonance superimposed on the 992 keV broader ($\Gamma = 74$ keV) and weaker resonance, according to Fig. 6 a). The excitation function presented in this figure contains cross-section values measured in our laboratory, in particular those corresponding to the thin resonance, and results of Zahnow et al. [16] for the broader resonance renormalized to a few results obtained in our laboratory. As the experimental gamma-ray yield integrates the thin 1082 keV resonance along the thickness of the target used for the cross-section measurement (5.0 keV at the resonance), a modified resonance was obtained. A Breit-Wigner fit was done to this experimental resonance to extract the true unmodified resonance [17,18], as represented in Fig. 6 b). In the energy range of the 1082 keV resonance ERYA-Profiling replaced the excitation function obtained experimentally by the Breit-Wigner determined from the fit.

The experiment regarding the case study was performed at the CTN-IST Accelerator Laboratory, with a proton beam accelerated by a 3 MV Tandem accelerator. The beam current at the target was about 80 nA. The proton energy was calibrated by the 872 keV resonance of the ^{19}F(p,$\alpha\gamma$)^{16}O, the 1645.1 and 1930.7 keV resonances of the reaction ^{23}Na(p,p'γ)^{23}Na and by the 3470 keV resonance of the ^{16}O(p,p)^{16}O reaction. The reaction chamber was electrically insulated from the beam line working together with the target holder and beam stopper as one Faraday cup for beam charge collection. Gamma-ray detection of the 718 keV line, resulting from the ^{9}Be(p,γ)^{10}B reaction, was accomplished by a Ge(HP) detector placed at an angle of 130° with respect to the beam axis and at a distance of 55.5 mm from the target. The absolute efficiency was determined by means of calibrated sources ^{133}Ba, ^{152}Eu, and ^{56}Co placed at the target position.

To scan the 1082 keV resonance within the sample, a proton energy

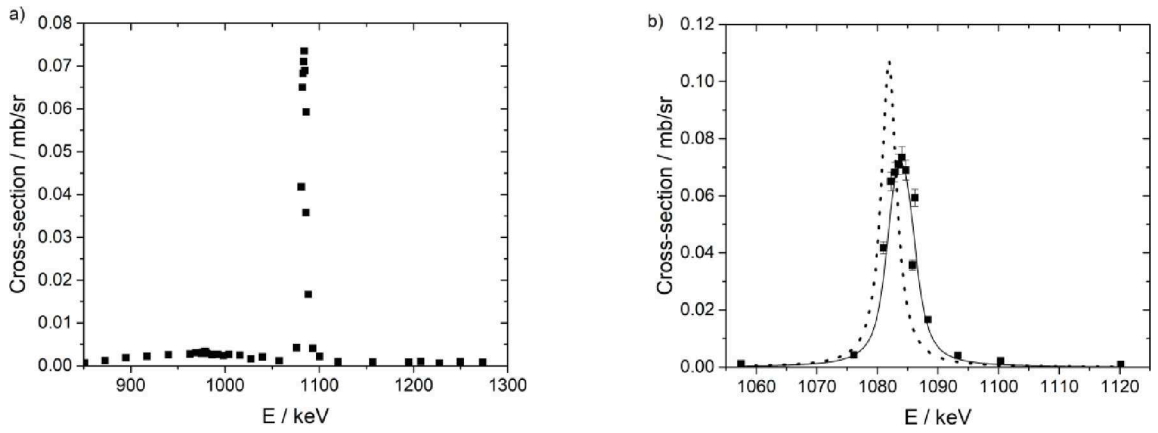

Fig. 6. a) Experimental excitation function for the reaction ^{9}Be(p, γ −718 keV)^{10}B; b) Experimental resonance (points), fit of the convolution of a true Breit-Wigner resonance with the thickness of the target (black line) and the Breit-Wigner corresponding to the best fit (dotted line).

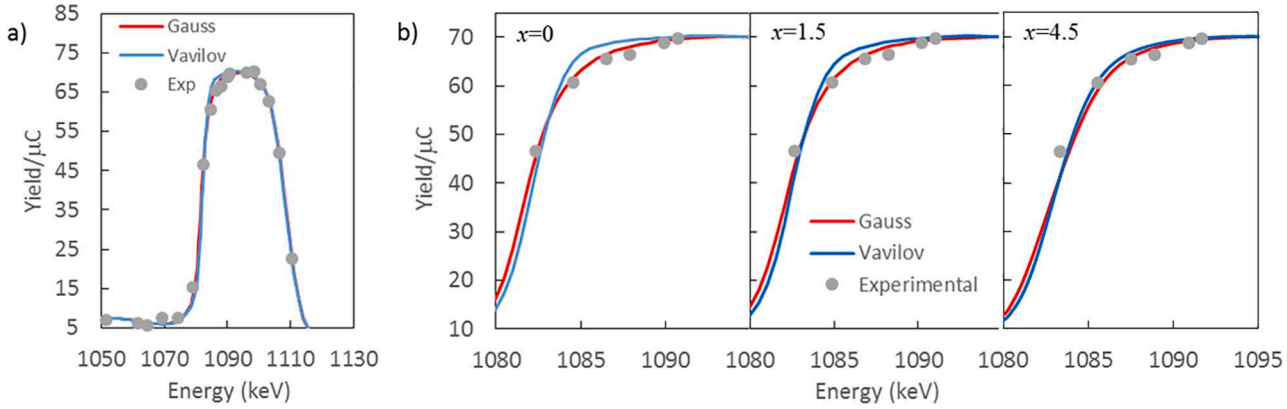

Fig. 7. a) Results obtained by ERYA using only Gaussian straggling (red line) or full straggling treatment including Vavilov (blue line), for a pure Be film, compared to the experimental results of gamma-yield versus incident proton energy; b) in an extended energy scale it is evident that the blue line does not agree with the red line and the experimental points for a pure Be film (with thickness, x, of a top oxide layer equal to zero); if a top layer of BeO is introduced in the simulation, with growing thickness up to 4.5×10^{17} at./cm^2, the agreement between the blue line and the experimental points improve, leading to the conclusion that the sample is not a pure Be film, but a surface oxide layer of 4.5×10^{17} at./cm^2 is part of the composition. (For interpretation of the references to colour in this figure legend, the reader is referred to the web version of this article.)

range from 1013 to 1123 keV was employed, with energy steps varying from 10 to 1 keV. The experimental detected yield per micro-Coulomb in function of proton energy is shown in Fig. 7 a), together with simulations performed by ERYA for a thin homogeneous film of Be with $(8.50 \pm 0.15) \times 10^{18}$ at./cm^2, employing only Gaussian straggling (red line) or full straggling treatment including Vavilov (blue line). In the first frame of part b) of Fig. 7 it becomes evident that the blue line does not agree with the red line and the experimental points for a pure Be film. The disagreement between the two simulations is predictable, because the non-Gaussian approximations used for a small energy loss which occurs at the sample surface leads to a smaller energy dispersion and hence a sharper increase of the yield. Adding a beryllium oxide layer at the surface improves the agreement (second and third frames of Fig. 7 b)); with an oxide layer of 4.50×10^{17} at./cm^2, the two lines are very close to each other and to the experimental points. Note that the stopping power of a BeO layer is higher than the one for a pure Be layer, implying that the simulation starts to use a Gaussian straggling approach for a thinner surface layer.

One may conclude from Fig. 7 that the full treatment of the straggling allows the perception of an oxide layer, while using only Gaussian straggling one would be happy with a conclusion of pure Be film. Note that, in this case, due to the silicon substrate, an oxide layer of 4.5×10^{17} at./cm^2 is near the detection limit of an EBS (Elastic Backscattering) analysis of our sample. It is also worth noticing that for (p,γ) profiling an oxide layer of 1.5×10^{17} at./cm^2 leads to a meaningful modification of the simulation with full straggling treatment.

The result of our (p,γ) profiling exercise is the following sample composition: 1st layer – BeO [$(4.5 \pm 1.0) \times 10^{17}$ at./cm^2]; 2nd layer – Be [$(8.20 \pm 0.15) \times 10^{18}$ at./cm^2]. The uncertainty corresponds to the minimum differential amount visually perceptible in the comparison with the experimental data. We may conclude also that the Be layer is uniform throughout its thickness.

The sample we have profiled was part of a batch of samples of the same origin. Some of them (unfortunately not the one we used) were, in the context of the fusion program, analysed by other ion beam techniques showing variability in the thickness of the Be layer. In order to confirm and quantify an oxidized layer TOF-ERDA, not available in our laboratory, was employed for a few of the samples, showing indeed a layer of surface oxidation [19].

4.2. *Aluminum implanted in titanium*

ERYA-Profiling was used to obtain the depth profile of Al implanted in Ti, at 140 keV energy and nominal fluence of 5×10^{17} at./cm^2. An experimental yield versus proton incident energy was obtained from 1680 and 1712 keV, scanning the 1683 keV (0.21 keV natural width) resonance of ^{27}Al(p,p'γ)^{27}Al nuclear reaction across the sample, by detecting the 848 keV gamma-line. This was part of an experimental

study published previously [20]. The experimental set-up and methodology were the same as used for the Be case.

The resonances closest to the 1683 keV resonance are situated at energies of 1664 and 1750 keV. The latest is too distant to influence the profiling, but the contribution from the 1664 keV resonance is seen at the first energy points (left tail of the yield Fig. 8), being nevertheless of no consequence for the scanning process. As these resonances are very thin, at the corresponding energy ranges, the excitation function was replaced by Breit-Wigner functions obtained by fitting to the experimental points considering the thickness of the target used for the excitation function measurement.

In order to obtain the real profile of the studied sample, eighteen layers were considered with Al contents following a Gaussian distribution, with a total amount of Al equal to 5×10^{17} at/cm^2. The corresponding titanium amounts were calculated to obey to two conditions: maximum yield at the depth corresponding to the range of Al ions in the sample, equal total numbers of atoms/cm^2 for the layers (1.2×10^{17} per layer), excepting the first layer composed by Ti only. A full straggling approach (including the Vavilov distributions) was followed in the calculations, as for the energy losses (and corresponding k factors) in play the Bohr Gaussian approach does not apply. For the proton energy distributions, sublayers of 2×10^{16} at./cm^2 were considered. A few attempts to optimize the layer composition were done, showing a good sensitivity to the depth of the first layer and depth of the maximum yield. The best fit was obtained for a Gaussian distribution up to the maximum, but a distorted enlarged one for the decreasing part, implying a diffusive process of aluminum into titanium. The layer compositions related to the best fit of the calculated and experimental yields versus incident energy, shown in Fig. 8, are given in table 2. The best fit corresponds to 5.5×10^{17} total amount of Al, close to the nominal fluence. An attempt of using only Gaussian straggling (also in Fig. 8) does not allow to describe the raising profile of the distribution and the maximum position and shows additional influence of the 1664 keV resonance.

4.3. Conceptual exercise – Fluorine deep seated in tungsten

Aiming at the evaluation of the uniqueness of response in case of contribution of two resonances, we developed a conceptual exercise featuring fluorine deeply seated in tungsten. Actually, the position of fluorine is irrelevant for the question of which resonances contribute to the yield in a depth profiling resonant scanning. However, the initial layer of W, if thick enough, allows to calculate the straggling using only the Gaussian approximation. This also justifies the use of a scanning resonance such as the 1345 keV resonance with 4.7 keV natural width of the ^{19}F(p,p'γ)^{19}F nuclear reaction. The fluorine profile was defined wide enough to guarantee the contribution of the 12 keV wide 1373 keV resonance to the 197 keV gamma ray line yield. Resonances of lower energy than 1345 are more than 100 keV distant, giving no contribution to the scanning.

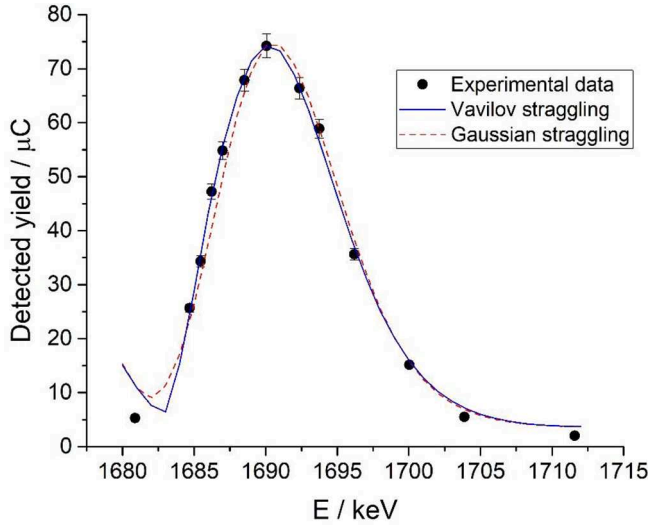

Fig. 8. Yield of the 844 keV gamma-line from the ^{27}Al (p, p'γ) ^{27}Al nuclear reaction as function of the proton incident energy for Al implanted in Ti at 140 keV and nominal fluence of 5×10^{17} at./cm^2. Points pertain to measurement and lines refer to ERYA-Profiling calculated yields, with full straggling including Vavilov distributions (full line) or just Gaussian straggling (dashed line).

Table 2
Depth profile correspondent to the best fit to experimental results of Al implanted in Ti at 140 keV with a nominal fluence of 5×10^{17} at/cm^2. Values in the table are given in units of 10^{15} at./cm^2, corresponding to a Gaussian distribution of fluorine up to the maximum (layer 9) and an enlarged distribution at deeper layers. All layers have the same thickness of 1.2×10^{17} at./cm^2, correspondent to a energy loss around 0.9 keV per layer.

	Ti	Al		Ti	Al
Layer 1	2.50E+01	0.00E+00	Layer 10	6.50E+01	5.50E+01
Layer 2	1.16E+02	3.68E+00	Layer 11	6.65E+01	5.35E+01
Layer 3	1.12E+02	7.58E+00	Layer 12	6.96E+01	5.04E+01
Layer 4	1.06E+02	1.40E+01	Layer 13	7.53E+01	4.47E+01
Layer 5	9.70E+01	2.30E+01	Layer 14	8.26E+01	3.74E+01
Layer 6	8.60E+01	3.40E+01	Layer 15	9.53E+00	2.47E+01
Layer 7	7.52E+01	4.48E+01	Layer 16	1.02E+02	1.84E+01
Layer 8	6.70E+01	5.30E+01	Layer 17	1.05E+02	1.50E+01
Layer 9	6.40E+01	5.60E+01	Layer 18	1.08E+02	1.20E+01

Three different profile configurations were tested. Configuration 1 and 2, with different widths, have for fluorine a Gaussian like distribution and configuration 3 has an exponential decay shape. The total and partial (by layer) amounts of W and the total amount of fluorine are the same in all configurations. The profile configurations are presented in table 3. ERYA-Profiling calculated the yield versus incident energy in the range 1380 to 1460 keV, considering for the proton energy distributions sublayers of 1×10^{17} at./cm^2.

Results of the 197 keV gamma-line yield versus proton incident energy are presented in Fig. 9, showing a clear distinction between Gaussian-like (configuration 1 and 2) and exponential decay (configuration 3) profiles. In the incident energy range used, the 1345 keV resonance is scanned across the sample from 1383 to 1440 keV, considering the energy straggling. The contribution of the 1373 keV resonance starts at around 1416 keV incident energy and goes up to 1460 keV. There is also a clear distinction between the two Gaussian-like profiles, being the second thinner than the first, except for the points with low fluorine content. However, this is not a consequence of superposition of the resonances as, except for layers 4 and 5, which have a contribution from both resonances, there is independent scanning of the other layers by a single resonance. The lack of sensibility to low fluorine content is due to energy straggling.

The information regarding resonance contributions as well as the

Table 3
Hypothetical depth profiles of three different configurations (1 and 2 – Gaussian-like shape, being 2 thinner than 1; 3 – exponential decay shape) of fluorine in tungsten, in units of 10^{15} at./cm^2. The total and partial (by layer) amounts of W and the total amount of fluorine are the same for all configurations.

	Configuration 1		Configuration 2		Configuration 3	
	W	F	W	F	W	F
Layer 1	3.0E+03	0.0E+00	3.0E+03	0.0E+00	3.0E+03	0.0E+00
Layer 2	3.2E+02	2.5E+01	3.2E+02	1.2E+01	3.2E+02	2.0E+02
Layer 3	3.2E+02	5.0E+01	3.2E+02	3.2E+01	3.2E+02	1.0E+02
Layer 4	3.2E+02	7.5E+01	3.2E+02	9.6E+01	3.2E+02	5.0E+01
Layer 5	3.2E+02	1.0E+02	3.2E+02	1.2E+02	3.2E+02	2.4E+01
Layer 6	3.2E+02	7.5E+01	3.2E+02	9.6E+01	3.2E+02	1.2E+01
Layer 7	3.2E+02	5.0E+01	3.2E+02	3.2E+01	3.2E+02	6.1E+00
Layer 8	3.2E+02	2.5E+01	3.2E+02	1.2E+01	3.2E+02	3.1E+00

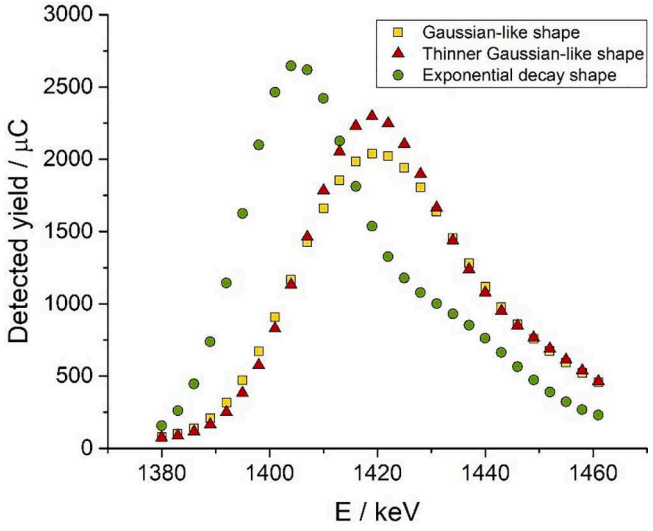

Fig. 9. Yield of the 197 keV gamma-line from the $^{19}F(p,p'\ \gamma)^{19}F$ nuclear reaction as function of the proton incident energy for fluorine in tungsten corresponding to the three configuration profiles given in Table 3.

yield obtained from each of the resonances may be taken from the log provided by the program at request from the user, providing additional insight on the profile scanning process. Hence, in conclusion, a unique response on the depth profile may be taken from the yield, in spite of the contribution for some layers of both resonances.

Although this is a conceptual exercise note that in a real exercise the yield related to the 110 keV gamma-line is available in the same spectra and the relative importance of the two resonances is different favoring the role of the 1345 keV resonance. This would contribute further to clarify the profile.

5. Conclusions

The ERYA-Profiling program developed for the analysis of in-depth heterogeneous samples was presented. As far as the authors know this is the most advanced program available for gamma resonant profiling with the capacity to include more than one resonance and the background. As another unique feature, the energy straggling within the sample is considered in a complete version using different energy distribution functions adequate to the amount of energy loss.

Case studies were presented in order to illustrate ERYA-Profiling capabilities:

1. A thin resonance superimposed on a broader and weaker resonance, belonging to the excitation of $^{9}Be(p,\gamma)^{10}B$ reaction was used to scan a Be thin film and determine its thickness and uniformity. Results obtained have shown that a full treatment of the straggling is necessary to have sensibility to surface modifications, as an oxide layer. A simulation with only Gaussian straggling misses the existence of a BeO layer of 4.5×10^{17} at./cm^2, while a full straggling treatment is meaningful sensitive to 1.0×10^{17} at./cm^2.
2. Depth profiling by resonant scanning was performed on Al implanted (energy 140 keV, nominal fluence $5x10^{17}$ at./cm^2) in Ti, using the 1683 keV resonance of the $^{27}Al(p,p'\gamma)^{27}Al$ nuclear reaction. The 1664 keV of the same reaction did not interfere with the scanning. ERYA-Profiling obtained the best fit for a depth profile Gaussian up to the maximum but enlarged for deeper distances from the surface, for a total amount of 5.5×10^{17} at./cm^2. Again a Vavilov approach for the straggling was necessary to describe the experimental results.
3. A conceptual problem to assess the issue of uniqueness of response in case of contribution from two resonances was designed featuring fluorine in tungsten, using the 1345 keV resonance of the $^{19}F(p,p'\gamma)^{19}F$ nuclear reaction, γ – 197 keV. Three fluorine profiles were defined wide enough to guarantee the contribution to the yield of the 1373 keV resonance. A clear distinction in the gamma-yield results of the different configurations was shown. Additionally a general conclusion may be drawn: taking into consideration that some layers are scanned only by one of the resonances and that in addition to yield in function of incident energy, ERYA-Profiling also provides an information log which allows to quantify the contribution of each resonance, we believe that in most cases of multiple resonance contribution the user will be able to find a unique answer regarding the depth profile.

CRediT authorship contribution statement

V. Manteigas: Investigation, Methodology, Software, Writing - original draft, Writing - review & editing. **J. Cruz:** Investigation, Methodology, Software, Writing - review & editing. **M. Fonseca:** Investigation, Methodology, Software, Writing - review & editing. **A.P. Jesus:** Conceptualization, Investigation, Methodology, Software, Writing - review & editing.

Declaration of Competing Interest

The authors declare that they have no known competing financial interests or personal relationships that could have appeared to influence the work reported in this paper.

Acknowledgments

The authors acknowledge LIBPhys (UID/FIS/04559/2019) and NOVA.ID.FCT. The authors also acknowledge LATR (CTN/IST), where the PIGE measurements were performed.

References

[1] R. Mateus, A.P. Jesus, J.P. Ribeiro, Nucl. Instrum. Methods Phys. Res. B 219 (2004) 519, https://doi.org/10.1016/j.nimb.2004.01.114.
[2] R. Mateus, A.P. Jesus, M. Fonseca, H. Luís, J.P. Ribeiro, Nucl. Instrum. Methods Phys. Res. B 264 (2007) 340, https://doi.org/10.1016/j.nimb.2007.09.030 >.
[3] M. Fonseca, R. Mateus, C. Santos, J. Cruz, H. Silva, H. Luis, A.P. Jesus, Nucl. Instrum. Methods Phys. Res. B 406 (2017), 144-147, <10.1016/j.nimb.2017.03.035>.
[4] N. Pessoa Barradas, J. Cruz, M. Fonseca, A.P. de Jesus, A. Lagoyannis, V. Manteigas, M. Mayer, K. Preketes-Sigalas, P. Dimitriou, Nucl. Instrum. Methods Phys. Res. B 468 (2020) 37–47, https://doi.org/10.1016/j.nimb.2020.02.019.
[5] IAEA-TECDOC- 1822, 2017.
[6] ERYA-Bulk webpage, < https://sites.fct.unl.pt/nuclear/software/erya-bulk >.
[7] IAEA Ion Beam Analysis Nuclear Data Library (IBANDL), <https://www-nds.iaea.org/exfor/ibandl.htm>.
[8] J.F. Ziegler, J.P.Biersack, and M.D.Ziegler, SRIM – The Stopping and Range of Ions in matter, Maryland, SRIM Co., 2008, <www.srim.org>.
[9] I.C. Vickridge, G. Amsel, Nucl. Instrum. Methods Phys. Res. B. 45 (1990) 6.
[10] I.C. Vickridge, G. Amsel, Nucl. Instrum. Methods Phys. Res. B. 108 (1996) 403.
[11] Y. Wang, M. Nastasi (Eds.), Handbook of Modern Ion Beam Material Analysis, 2nd Edition,, 2009.
[12] H. Fritzsche, J. Huot, D. Fruchart (Eds.), Neutron Scattering and Other Nuclear Techniques for Hydrogen in Materials, Springer, 2016.
[13] A. Rotondi, P. Montagna, Nucl. Instrum. Methods Phys. Res. B. 47 (1990) 215.
[14] wxWidgets webpage, <https://www.wxwidgets.org>.
[15] ERYA-Profiling webpage, < https://sites.fct.unl.pt/nuclear/software/erya-profiling >.
[16] D. Zahnow, C. Angulo, M. Junker, C. Rolfs, S. Schmidt, W.H. Schulte, E. Somorjai, Nuclear Physics A 589 (1995) 95, https://doi.org/10.1016/0375-9474(95)00077-E.
[17] A.P. Jesus, B. Braizinha, J.P. Ribeiro, Nucl. Instrum. Methods Phys. Res. B 161–163 (2000) 186, https://doi.org/10.1016/S0168-583X(99)00855-1.
[18] A.P. Jesus, B. Braizinha, J. Cruz, J.P. Ribeiro, Nucl. Instrum. Methods Phys. Res. B 174 (2001) 229, https://doi.org/10.1016/S0168-583X(00)00521-8.
[19] N.P. Barradas, N. Catarino, R. Mateus, S. Magalhães, E. Alves, Z. Siketić, I. Bogdanović Radović, Nucl. Instrum. Methods Phys. Res. B 346 (2015) 21, 10.1016/j.nimb.2015.10.062.
[20] R. Mateus, M. Fonseca, A.P. Jesus, H. Luís, J.P. Ribeiro, Nucl. Instrum. Methods Phys. Res. B 266 (2008) 1490, 10.1016/j.nimb.2007.11.042.

Eur. Phys. J. Plus (2021) 136:969
https://doi.org/10.1140/epjp/s13360-021-01954-3

THE EUROPEAN PHYSICAL JOURNAL PLUS

Regular Article

Fluorine depth profiling based on the $^{19}F(p,p'\gamma)^{19}F$ excitation function

J. Cruz[1,2,a], **M. Fonseca**[1,2,3], **D. Galaviz**[4,5], **A. Henriques**[4], **H. Luís**[6], **J. Machado**[1,2], **P. Teubig**[4,5], **P. Velho**[4], **V. Manteigas**[1], **A. P. Jesus**[1,2]

[1] Laboratório de Instrumentação, Engenharia Biomédica e Física da Radiação (LIBPhys-UNL), Caparica, Portugal
[2] Departamento de Física, Faculdade de Ciências e Tecnologia da Universidade Nova de Lisboa, Monte da Caparica, 2892-516 Caparica, Portugal
[3] HEI-Lab: Digital Human-Environment Interaction Lab, Lusófona University, Lisbon, Portugal
[4] Laboratório de Instrumentação e Física Experimental de Partículas, 1649-016 Lisboa, Portugal
[5] Departamento de Física, Faculdade de Ciências da Universidade de Lisboa, Campo Grande, 1749-003 Lisboa, Portugal
[6] Campus Tecnológico e Nuclear do Instituto Superior Técnico (CTN-IST), Estrada Nacional 10 (km 139,7), 2695-066 LRS Bobadela, Loures, Portugal

Received: 6 July 2021 / Accepted: 9 September 2021

Abstract Ion beam analysis of fluorine has applications in research on teeth and bones, materials science, geochemistry and archaeometry. A novel PIGE (particle induced gamma-ray emission) standard free methodology for fluorine content determination for in-depth heterogeneous samples based on the excitation function of the $^{19}F(p,p'\gamma)^{19}F$ nuclear reaction is presented. New precise cross section measurements of this reaction in the proton energy range 2.1 to 4.1 MeV have been performed. In addition, the ERYA-Profiling code, a computer program specially developed for PIGE analysis of in-depth heterogeneous samples, employed this new excitation function in a case study where different fluorine simulated depth profiles probed the capability of insight into fluorine distributions in a given sample, showing the potential of PIGE analysis.

1 Introduction

Fluorine is the most electronegative, reactive chemical element, and is also one of the most abundant in Earth's crust. Due to its chemical reactivity, it rarely occurs naturally in its elemental state; fluorine occurs in ionic forms (fluorides), or combined with other elements in minerals like fluorspar, fluorapatite, and cryolite.

Fluorine is highly toxic, but nonetheless it is widely used and forms an essential part of everyday life. Among other things, fluorides are used in the plastics industry (e.g., fluoropolymers and fluorine resins), and as additives to toothpaste and in LED bulbs to turn the cold LED light into a warm white. Fluorine compounds are also added to many pharmaceuticals to increase their effectiveness.

[a] e-mail: jdc@fct.unl.pt (corresponding author)

Published online: 24 September 2021

Over the years, the detection and characterization of fluorides, hydrogen fluoride, and fluorine has focused mainly on environmental and biological samples to understand and control the benefits and the potential toxicity that has been associated with fluorine uptake [1]. The standard detection method to analyze trace levels of fluorine in these samples is primarily the potentiometric (ion selective electrode, ISE) and gas chromatographic (GC) methods [2, 3]. There are, nonetheless, other analytical tools available, such as inductively coupled plasma mass spectrometry (ICP-MS), atomic absorption spectrometry (AAS) and molecular absorption spectrometry (MAS) [4].

In the last years, the IAEA (International Atomic Energy Agency) has encouraged the development of PIGE (particle induced gamma-ray emission) as a standard technique in the quantification of elements lighter than sulfur [5]. PIGE, an IBA (ion beam analysis) technique based on gamma-producing nuclear reactions, is particularly effective for fluorine detection and quantification in the outer few μm [6–13] due to the high sensitivity (below approx. 1 ppm) derived from high cross section values of the relevant nuclear reaction. Similar to PIXE (particle induced X-ray emission), another ion-beam based analytical technique which already benefits from a wide use worldwide, PIGE demands small samples, does not destroy them, and provides multi-elemental information in a single spectrum.

Although complementary to PIXE in the sense that it covers light element analysis with the same kind of experimental facilities, PIGE, for a while, did not follow the same steps as PIXE toward a standard free technique based on the physical parameters which determine the radiation yield. On one side, the negligible absorption of radiation by the sample allows for PIGE the use of standards in a straightforward reasonable approximation; on the other side, contrary to PIXE, nuclear reaction excitation functions are rarely smooth, displaying narrow and large resonances, which hindered the motivation to develop software for concentration calculations based on the cross sections.

In the last years, we have shown that if cross sections are available in numerical values at energy steps close enough to define in detail the resonances, trivial integration leads to elemental concentrations for bulk samples [14–17]. Thus, these advances have allowed for the development of standard free PIGE methodology. The ERYA (emitted radiation yield analysis) code [15] was specifically developed to integrate the relevant nuclear reaction cross sections along the depth of homogeneous samples.

Resonances make PIGE a suitable technique for profiling fluorine in the outer few μm. In a review paper, Coote [18] presented a comprehensive list of depth profiling results using the PIGE technique for the surface analysis of inorganic materials (geochemistry, meteoritic material and man-made materials such as alloys) and organic materials (bone, teeth and fish scales). These studies relied on isolated strong and narrow resonances from the $^{19}F(p,p'\gamma)^{19}F$ and $^{19}F(p,\alpha\gamma)^{16}O$ nuclear reactions and they were selected according to the required yield, depth capability and depth resolution at the surface. These studies were limited to proton energies not higher than 1.5 MeV because above this value, resonances are much broader. This considerably limits the depth probed by PIGE. However, this limitation can be overcome by considering the whole excitation function which, in turn, requires a complete mathematical treatment and a computer code that implements it. Our group, continuing its work on ERYA, developed new a computer code, named ERYA-Profiling [19], that allows a full PIGE analysis of in-depth heterogeneous samples from resonance scanning profiling of the sample with an isolate resonance or more than one resonance, also including the direct component, as the contribution from the whole excitation function is calculated. Additionally, a non-homogeneous depth distribution of a given element may be inferred from the measured yield, taking advantage of broad features of the excitation function, as will be shown later.

Examples of pratical situations which benefit from this solution are: the study of fluorinated high-performance coatings, the investigation of layered structures in paintings and other pieces of art, the diffusion of fluorine into the teeth from surface applied treatments and the uptake of fluorine from archeological bones. For such situations, where penetrating high energy beams may be required, insight into fluorine distribution in a given sample may be inferred from comparison between the calculated yield and corresponding measured gamma-ray yield at one or two different proton energies.

Naturally, a reliable output from ERYA-Profiling requires an accurate knowledge of nuclear reactions cross sections. For fluorine, the inelastic scattering reaction ^{19}F(p,p'γ)^{19}F is particularly relevant due to its high cross section values and to the fact that the main produced gamma-rays, 110 and 197 keV, are near the efficiency maximum of most gamma-ray detectors. From literature, we conclude that the available experimental results are scarce, and results of different authors show large discrepancies up to a factor of two [20], especially above 2.5 MeV, which is an energy region of high interest. Although at a proton energy of 2.4 MeV, a sensitivity of around 1 ppm may be reached [21], extending to higher energies up to around 4 MeV represents an upgrade as lower sensitivities may be obtained. Also, the sample may be probed at higher depths which may be relevant for in-depth heterogeneous samples.

To understand these discrepancies, a necessary step to give PIGE the role of a precise and reliable analytical technique, we present in this work results of new measurements of the gamma-producing cross sections of the ^{19}F(p,p'γ)^{19}F reaction for $\gamma_{1-0} = 110$ keV and $\gamma_{2-0} = 197$ keV, in the proton energy range 2.1 to 4.1 MeV. Compared to the existent data, these measurements were done with a smaller energy step, allowing a better definition of the resonances. These precise new cross section values were implemented into the ERYA-Profiling to infer PIGE sensitivity to different simulated fluorine depth profiles.

2 PIGE methodology

Qualitatively, PIGE is based on the bombardment of solid samples by ions (typically protons with energies up to 4 MeV) which interact with sample nuclei, leading to a nuclear reaction with emission of gamma photons.

The gamma yield $\mathrm{d}Y\ (E,\ \theta)$ emitted by an isotope i, resulting from the interaction of N_p protons with energy E with a thin layer with areal density $N_i \mathrm{d}x$ of the given isotope species is:

$$\mathrm{d}Y(E,\theta) = 4\pi\,\varepsilon_{\mathrm{abs}}\big(E_\gamma\big)N_p\frac{\mathrm{d}\sigma}{\mathrm{d}\Omega}N_i\mathrm{d}x \tag{1}$$

where N_i is the number of isotopes per volume unit, $\mathrm{d}x$ is the thin layer thickness, $\varepsilon_{\mathrm{abs}}(E\gamma)$ is the absolute efficiency of the detector for γ rays with energy $\mathrm{E}\gamma$, and $\mathrm{d}\sigma/\mathrm{d}\Omega$ is the differential cross section for emission of a γ ray at angle θ with respect to the incident ion direction. For a thick sample, the beam with initial energy E_0 will steadily loose energy as it penetrates through the sample. The total gamma-ray yield then becomes, assuming a constant mass fraction throughout the depth of the sample

$$Y(E_0,\theta) = 4\pi\,\varepsilon_{\mathrm{abs}}\big(E_\gamma\big)N_p f_m f_i\frac{N_{\mathrm{av}}}{A}\int_0^{E_0}\frac{1}{S_m(E)}\frac{\mathrm{d}\sigma}{\mathrm{d}\Omega}\mathrm{d}E \tag{2}$$

where $S_m(E)$ is the mass stopping power at energy E; f_m is the relevant element mass fraction; f_i, and A are the isotopic abundance and the atomic mass of the relevant element, respectively,

and N_{av} is the Avogadro number. The factor $N_i/\rho = f_m\, f_i\, N_{av}\, A^{-1}$, where ρ is the mass density of the sample, transforms the atomic density into mass fraction also changing the linear stopping power to mass stopping power.

If the assumption of in-depth homogeneous samples is not valid, the gamma-ray yield, considering that the mass fraction may vary with depth, modifies to:

$$Y(E_0,\theta) = 4\pi\,\varepsilon_{abs}(E_\gamma) N_p\, f_i \frac{N_{av}}{A} \int_0^{E_0} \frac{f_m(E)}{S_m(E)} \frac{d\sigma}{d\Omega} dE \tag{3}$$

If additionally, one considers that at a given depth, protons have an energy distribution $F_{\overline{E}}(E)$ with the mean proton energy equal to $\overline{E}$, the equation above turns into:

$$Y(E_0,\theta) = 4\pi\,\varepsilon_{abs}(E_\gamma) N_p\, f_i \frac{N_{av}}{A} \int_0^{E_0} \frac{f_m(\overline{E})}{S_m(\overline{E})} \int_0^{\infty} F_{\overline{E}}(E) \frac{d\sigma}{d\Omega} dE\, d\overline{E} \tag{4}$$

Hence, Eq. (4) calculates the gamma-ray yields for samples with mass fraction varying with depth and takes into consideration the beam energy spread and the energy straggling within the sample.

So, to quantify the amount of fluorine from Eq. (4), one requires the detector efficiency which depends on the energy of gamma-ray lines, the number of incident protons, i.e., the beam collected charge, the stopping powers corresponding to the main composition of the sample and finally the $^{19}F(p,p'\gamma_{1-0})^{19}F$ ($E\gamma = 110$ keV) or the $^{19}F(p,p'\gamma_{2-0})^{19}F$ ($E\gamma = 197$ keV) cross section values. To use Eq. (4), the proton energy distribution along the depth of the sample must be included.

ERYA-Bulk [22], a recent version of ERYA, calculates gamma-ray yields for in-depth homogeneous samples from Eq. (2), neglecting beam energy spread and energy straggling, since the effect of these on the bulk yield is negligible [23].

The ERYA-Profiling program, taking advantage of some functionalities and capabilities of ERYA-Bulk was developed for the analysis of in-depth heterogeneous samples from Eq. (4), including a full treatment for straggling by using different energy distribution functions adequate to the amount of energy loss.

3 Experimental procedure

The experimental work was carried out at the 3 MV Tandem accelerator of the Ion Beam Laboratory at CTN (Sacavém, Portugal) [24]. The proton beam, produced by a Duoplasmatron source is, after acceleration, deflected at a 90º analyzing magnet and a 25º switching magnet, passing through several focusing and steering electromagnetic devices before entering the target chamber. This configuration assured an energy resolution of 1 keV, measured by the 991 keV resonance of $^{27}Al(p,\gamma)^{28}Si$ reaction ($E\gamma = 1779$ keV, $\Gamma = 0.10$ keV).

Beams with current intensities between 100 and 200 nA were used. The proton energy was calibrated with the 1645.1 and 1930.7 keV resonances of the reaction $^{23}Na(p,p'\gamma)^{23}Na$ and the 3470 keV resonance of the $^{16}O(p,p)^{16}O$ reaction.

At the entrance of the chamber, the beam passes through a collimator composed of a nickel foil with an aperture of 1 cm diameter and 2 mm of thickness, a gold foil with 1 mm thickness and an aperture of 2 mm and last a stainless-steal foil with the same dimensions as the gold one. These foils are mounted onto PVC structure and are electrically insulated from the chamber. To assure a good reproducibility of beam charge collection, the chamber is insulated from the beam line and pumping system, to act together with the target holder and beam stopper as one Faraday cage.

Gamma-ray detection was accomplished by a 45% relative efficiency HPGe detector having a nominal resolution of 2.2 keV for the 1173 keV ^{60}Co gamma line, placed at an angle of 130º to the beam direction. The detector absolute efficiency was determined by means of radioactive sources of ^{133}Ba and ^{152}Eu (with several energy lines between 81 and 1.5 MeV), calibrated in activity with an uncertainty of 5%, placed at the target position.

Besides the gamma-ray detector, a PIPS detector, placed at an angle of 160° to the beam axis, was used in this experiment to collect backscattered particles from the target. With an intrinsic efficiency of 100% and a resolution of 15 keV for 5 MeV alpha particles, its solid angle was determined with 2% uncertainty by measuring with high accuracy the diameter of the aperture placed in front of the detector and the distance between the target and the detector.

The target was prepared by vacuum evaporating a thin sodium fluoride layer on a previously evaporated silver self-supporting film.

4 Results

4.1 Cross section measurement

To avoid the uncertainties associated to the measurement of the absolute number of incident protons (beam charge collection) and of the target thickness, it was measured simultaneously the Rutherford backscattering yield of a heavy component of the target, i.e., the Ag self-supporting film.

For thin targets as the one used in this work, and at off resonance or on resonances that are large when compared with the target energy thickness, the radiation yield, collected within a small solid angle, is given directly by Eq. (1), with $\mathrm{d}Y(E,\theta) \approx Y(E,\theta)$, becoming:

$$Y(E,\theta) = 4\pi\,\varepsilon_{\mathrm{abs}}\left(E_\gamma\right) N_p \frac{\mathrm{d}\sigma}{\mathrm{d}\Omega} n_F \tag{5}$$

where n_F is the number of fluorine nuclei in the target per surface unit, and the other quantities have been defined previously.

The number of protons elastically scattered by silver at an angle β, inside a small solid angle, may be determined by:

$$Y_p^{\mathrm{Ag}} = \varepsilon_p \Omega_p N_p \left(\frac{\mathrm{d}\sigma}{\mathrm{d}\Omega}\right)_{\mathrm{Ruth}}^{\mathrm{Ag}} n_{\mathrm{Ag}} \tag{6}$$

where N_p is the number of incident protons with energy E, n_{Ag} is the number of silver nuclei in the target per surface unit, Ω_p and ε_p are, respectively, the solid angle and the intrinsic efficiency of the particle detector and $\left(\frac{\mathrm{d}\sigma}{\mathrm{d}\Omega}\right)_{\mathrm{Ruth}}^{\mathrm{Ag}}$ is the proton Rutherford backscattering cross section on silver, which can be calculated analytically.

From the two previous equations, the differential cross sections for the 110 and 197 keV gamma-rays were calculated using:

$$\frac{\mathrm{d}\sigma}{\mathrm{d}\Omega} = \frac{Y(E,\theta)}{Y_p^{\mathrm{Ag}}} r \frac{\varepsilon_p \Omega_p}{4\pi\,\varepsilon_{\mathrm{abs}}\left(E_\gamma\right)} \left(\frac{\mathrm{d}\sigma}{\mathrm{d}\Omega}\right)_{\mathrm{Ruth}}^{\mathrm{Ag}} \tag{7}$$

where r is a stoichiometric factor which represents the relation between the density of atoms of silver and fluorine in the target ($r = n_{\mathrm{Ag}}/n_F$) and has been obtained by alpha particle RBS (Rutherford Backscattering Spectrometry) analysis of the sample: $n_F = 5.0 \times 10^{17}$ at./cm^2 and $n_{\mathrm{Ag}} = 3.2 \times 10^{17}$ at./cm^2. The Ag Rutherford cross section was calculated neglecting the

Table 1 Uncertainty budget for the measurements

Statistical uncertainties	
γ-ray peak area (statistics and area determination)	2%
Proton (Ag) peak area (statistics and area determination)	1%
Ruth. cross section (beam energy resolution = 1 keV)	<0.1%
Overall relative uncertainty	2.3%
Systematic uncertainties	
γ-ray detector efficiency	7%
Proton detector solid angle	2%
Ratio of F to Ag	3%
Overall absolute uncertainty	7.9%

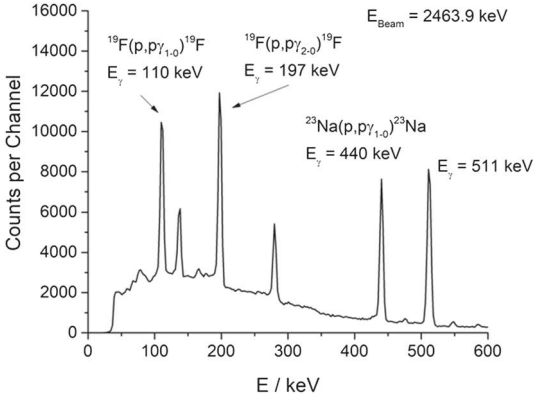

Fig. 1 Gamma-ray spectrum obtained at 2464 keV proton energy clearly showing the gamma-ray lines to be quantified

beam energy loss at the sodium fluoride layer, which amounts to a 0.6% variation at 2.1 MeV beam energy and 0.2% at 4.1 MeV.

The cross section uncertainties are listed in Table 1, where a separation between statistical and systematic uncertainties is made.

To keep the systematic uncertainties under control, the target stability, the beam charge collection, the detection system, and the background contributions to the gamma lines were monitored throughout the whole measurement. The choice of materials for the entrance collimator ensured that all detected 110 and 197 keV photons were coming from the target. Measurements were repeated at several energy points to ensure that experimental conditions were kept unchanged and to check target stability under proton bombardment. In the described conditions, systematic uncertainties affect only the overall scale of cross section values.

Figure 1 shows a gamma spectrum obtained at 2464 keV proton energy, where the 110 keV and 197 keV lines are clearly separated from other gamma lines. The corresponding scattered proton spectrum is presented in Fig. 2, showing that the peak relative to Ag is also separated from the other peaks, which are identified in the figure.

Excitation functions for the ^{19}F(p,p'γ)^{19}F reaction are presented in red in Fig. 3 for the 110 keV line and in Fig. 4 for the 197 keV line. Numerical values are available in the IBANDL database for PIGE [20].

Comparison of our results with the ones available in IBANDL database for PIGE [5, 25–30] is shown in Fig. 3 for the 110 keV line and in Fig. 4 for the 197 keV line. Despite

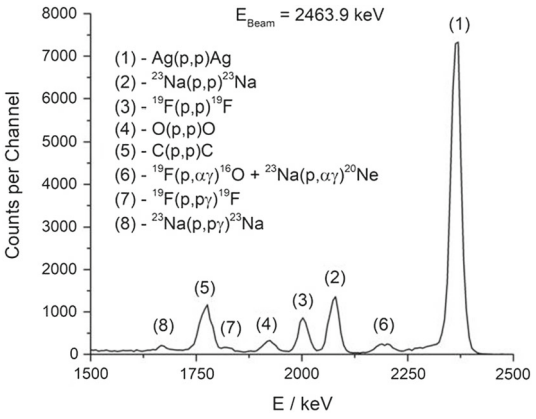

Fig. 2 Scattered proton spectrum obtained at 2464 keV proton energy showing the Ag peak separated from the other peaks

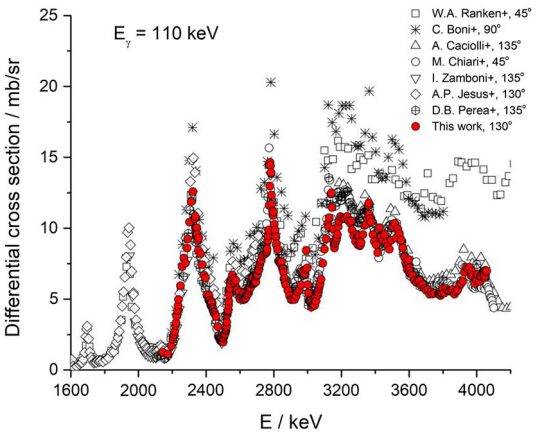

Fig. 3 Comparison of the results concerning the cross sections of the reaction ^{19}F(p,p'γ_{1-0})^{19}F measured in this work with those measured by other authors [5, 25–30]

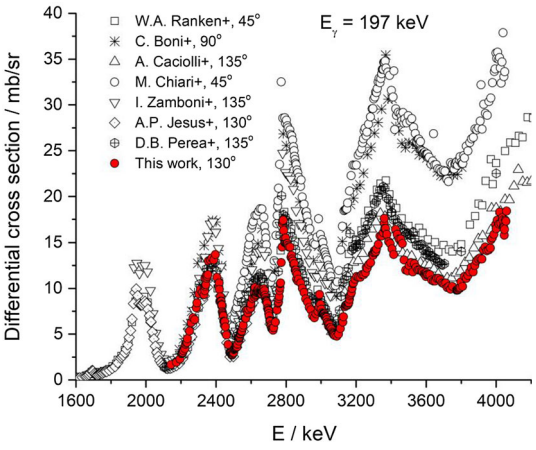

Fig. 4 Comparison of the results concerning the cross sections of the reaction ^{19}F(p,p'γ_{2-0})^{19}F measured in this work with those measured by other authors [5, 25–30]

the proton energy deviation from 5 to 10 keV among different authors, off resonance or in broad resonances, a quantitative comparison among authors may be done.

In relation to the 110 keV gamma-ray line, the results of the other authors are in fair agreement below 2.8 MeV, but above this energy C. Boni [30] and W.A. Ranken [25] results are around 50% higher than the other values. This work brings validation to the lower values, agreeing with them within the experimental uncertainty.

For the 197 keV gamma line, there is a larger scatter of values of previously published results. In the first large resonance, results of A.P. Jesus [29] and D.B. Perea [26] are in close agreement, but lower by 30% in relation to values of I. Zamboni [28] and C. Boni [30]. In the second and third resonances, the discrepancy of the values of these authors relative to A.P. Jesus [29] and D.B. Perea [26] increases, and values of M. Chiari [5] are still higher, reaching a factor close to two, trend that is kept through the whole energy range. Above 3 MeV there is a fair agreement between values obtained by A. Caccioli [27], W.A. Ranken [25] and D.B. Perea [26], but results of C. Boni [30] and M. Chiari [5] are almost a factor of two larger than those. Again, the values obtained in this work confirm the trend of lower cross sections, for the whole energy range. For authors displaying lower values of the cross sections (previous works and this work), the respective results are generally within the uncertainties in relation to the average.

Although the 110 keV line, originating at a $j = 1/2$ level is expected to be isotropic, the same does not apply to the 197 keV line coming from a $j = 5/2$ level. However, all the measurements were done at similar or equivalent angles, 130°, 135° and 45°, except for C. Boni [30] who measured at 90°.

Hence, for both gamma lines, the results obtained in this work give weight to a statistical rejection of C. Boni [30] and M. Chiari [5] values for the 197 keV line and C. Boni [30] and W.A. Ranken [25] (above 3.1 MeV) values for the 110 keV line.

4.2 Fluorine depth profiling with ERYA-profiling

With the ERYA-Profiling database updated with the new ^{19}F(p,p'γ_{2-0})^{19}F ($E_\gamma = 197$ keV) excitation function, an hypothetical case study, fluorine in silicon substrate, is presented to illustrate PIGE depth resolution sensitivity when the whole excitation function is considered. Technologically, fluorine in silicon has been studied to determine surface contaminants of silicon wafers after procedures such as etching and polishing or to investigate implanted silicon samples ([18] and references therein). Three different depth distributions with the same total amount of fluorine, in a silicon thick sample, were defined considering in ERYA-Profiling five layers, each with a fixed amount of fluorine and silicon (Table 2). In Fig. 5, the fluorine concentration per layer is represented as function of the proton energy, as a conversion from depth in at./cm^2 was made to proton energy, taking into consideration the energy thickness of each layer and the energy loss of the beam along the sample. The distributions are: a gaussian-like shape (red line), an exponential-like shape (blue line), and a see-saw shape (green line). These distributions were chosen to simulate a gaussian implanted profile (true for low fluence implantations), diffusion from the surface and a layered structure, respectively. In Fig. 5a, the layers correspond to 2.7×10^{19} at./cm^2 of Si per layer, i.e., 5.5 μm total thickness, and a total of 5.0×10^{18} at./cm^2 of F. In Fig. 5b, the layers correspond to 5.4×10^{18} at./cm^2 of Si per layer, i.e., 1.1 μm total thickness, and a total of 5.0×10^{17} at./cm^2 of F (so chosen to be of the same magnitude relative to Si as in the previous situation). Detailed information on F amounts per layer for the different distributions is given in Table 2. A fourth configuration is also shown in Fig. 5 (yellow line), corresponding to a in-depth homogeneous distribution of F (same total amount) in Si throughout the range of protons in Si.

In Fig. 5, the excitation function corresponding to the 197 keV gamma-ray line is also shown allowing the perception that different parts of the 197 keV gamma-ray excitation

Table 2 Layer amounts of F for three different in-depth distributions and correspondent calculated gamma-ray yields for the 197 keV line, coming from the inelastic scattering of protons by ^{19}F. For each case, the distributions have the same total amount of fluorine in silicon (thick sample). Si and F amounts are given in units of 10^{15} at./cm^2. Layers are numbered 1 to 5 starting from the surface of the sample, which is bombarded by protons with an energy of 3350 keV. The yields are calculated by ERYA-Profiling for our detection system and 1μC of collected charge. For comparison, the gamma-ray yield, corresponding to the same amount of fluorine with a homogeneous distribution throughout the range of 3350 keV protons in Si, is also given

Distributions	Layer 1	Layer 2	Layer 3	Layer 4	Layer 5	Calculated γ yield
	Figure 5a: in each layer 2.7×10^4 of Si; total amount of F: 5×10^3					
Gaussian-like	400	850	2500	850	400	54,844
Sea-saw-like	1670	0	1670	0	1660	113,424
Exponential	3210	1160	415	149	66	85,004
Homogeneous	Throughout the range of 3350 keV protons in Si					36,249
	Figure 5b: in each layer 5.4×10^3 of Si; total amount of F: 5×10^2					
Gaussian-like	40	85	250	85	40	9499
Sea-saw-like	167	0	167	0	166	10,487
Exponential	321	116	41.5	14.9	6.6	11,076
Homogeneous	Throughout the range of 3350 keV protons in Si					3625

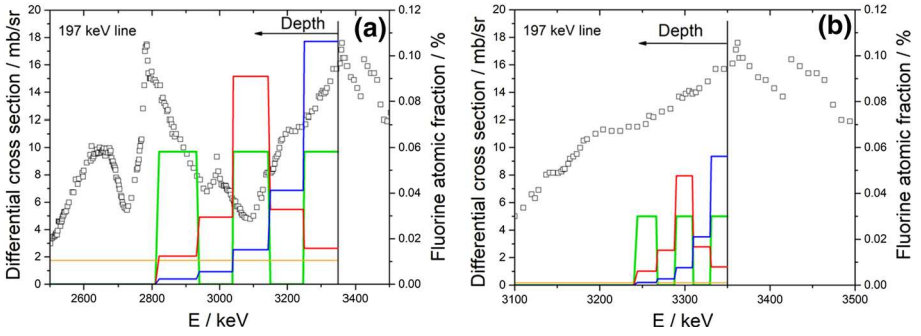

Fig. 5 Different in-depth distributions, with the same total amount of fluorine in silicon: gaussian-like shape (red line), exponential-like shape (blue line), and see-saw shape (green line). The yellow line corresponds to a in-depth homogeneous distribution of F in Si throughout the range of 3350 keV protons in Si. The excitation function corresponding to the 197 keV gamma-ray line, coming from the inelastic scattering of protons by fluorine, is also shown in both figures. In Fig. 5 **a,** the layers correspond to 2.7×10^{19} at./cm^2 of Si per layer, and a total of 5.0×10^{18} at./cm^2 of F. In Fig. 5 **b,** the layers correspond to 5.4×10^{18} at./cm^2 of Si per layer, and a total of 5.0×10^{17} at./cm^2 of F

function contribute to the gamma yield coming from fluorine. As the gamma yield is mostly proportional to the product of the cross section by the fluorine atomic concentration, a quick inspection of Fig. 5a is enough to understand that different yields will be obtained for the different distributions. Gamma yield values correspondent to the three distributions were calculated by ERYA-Profiling and displayed in Table 2, confirming a clear distinction among the distributions. Yields refer to 3350 keV proton energy, our detection efficiency (= 0.0181) and 1.0 μC of collected charge.

It is true that one distribution with one given fluorine total amount and another distribution with a different fluorine total amount may lead to the same value of the gamma yield. However, note that if the yields are the same at a given incident energy, they will differ at another energy and also differ for the 110 keV gamma line whose excitation function differs from the one corresponding to the 197 keV line (see Figs. 3 and 4).

Analyzing situations with narrower and narrower distributions of fluorine lead to the situation illustrated in Fig. 5b, where only a small part of the excitation function is responsible for the gamma-ray yield. This translates into a lower capacity of distinction, which in this case, and for 3350 keV proton energy, means yields that differ from each other by 10%, slightly higher than the experimental uncertainty of measured yields. This gives a perspective of the depth resolution (~ 1 μ for Si) that may be reached at this energy. However, moving to a lower portion of the excitation function with closer resonances and a steeper gradient of cross section per energy, this may be improved. Considering the proton incident energy of 2800 keV, one obtains for the Gaussian like, see-saw like, exponential like and homogeneous configurations yields, respectively, equal to 5811, 7245, 9560 and 2545. Notice that now the three first configurations differ by more than 25%.

5 Discussion

What are the implications of the excitation functions and their uncertainties and discrepancies for fluorine bulk and profiling analysis? An overall deviation factor in the cross sections translates (see Eqs. 2 and 4) directly in the same deviation of the corresponding calculated yield or mass fraction of the element. Also, the combined uncertainty of cross section values, of the absolute value of the collected carge, of the detector efficiency and of the stopping powers leads to an uncertainty of the determined mass fractions which may be larger than 20%, considering the quoted uncertainties of a given excitation function.

However, this may be improved if calibrations are performed (as it is also done for standardless PIXE). For each light element to be analyzed, the gamma-ray yield of a pellet made of pure inorganic compound containing the element or of a standard reference sample must be measured and compared with the corresponding calculated yield. The ratio of the experimental and calculated yield will then be used as an external calibration factor (or correction factor) in future analysis of that element, provided the same experimental conditions (e.g., ion beam, detector type and detector geometry) are used and also the same excitation function for the calculations. In order to confirm the stability of experimental conditions (mainly of the charge measurement), one might use a lithium or boron standard sample (the cross sections related to ^{7}Li(p,p'γ)^{7}Li and ^{10}B(p,$\alpha\gamma$)^{10}B reactions are smooth) and measure its yield before each analytical running time. An uncertainty around 5% which is the uncertainty of stopping power values is then attainable.

Notice that, compared to the true excitation function, one given experimental excitation function may exhibit deviations that are not constant within the whole energy range. We have seen it in the comparison shown before (Fig. 3 and 4). This implies that a calibration factor measured at a given energy may not be valid at another energy. Also, it is evident from the hypothetical case that absolute uncertainties will directly affect the values of fluorine amounts, and the relative uncertainties (portions of the excitation function versus another) will influence the distributions.

Hence, it is important to rely on a detailed and precise excitation function measurement (such as ours) where in relative terms (one energy range versus another) conditions were assured to keep constant any quantities leading to systematic uncertainties.

6 Conclusions

The excitation functions of ^{19}F(p,p'γ)^{19}F reaction for $\gamma_{1-0} = 110$ keV and $\gamma_{2-0} = 197$ keV, in the proton energy range 2.1 to 4.1 MeV were obtained in this work, with a careful experimental procedure to assure low absolute (in terms of the cross section values scale) and relative (among different points and portions of the excitation function) uncertainties. This experiment also brought in comparison with previous existing data a more detailed knowledge and resonance definition.

The capacity gained with an application (ERYA-Profiling) to deal with in-depth heterogeneous samples employing the whole excitation function was presented. Insight into fluorine distributions down to a depth resolution below 1 μm was demonstrated. This allows to handle specific problems where high energy beams to go deeper into the sample are required.

Acknowledgements The authors acknowledge LIBPhys (UID/FIS/04559/2019) and NOVA.ID.FCT.

Data availability This manuscript has associated data in a data repository. [Author's comment: Data are available on request from the authors.]

References

1. N.R. Johnston, S.A. Strobel, Arch. Toxicol. **94**, 1051–1069 (2020). https://doi.org/10.1007/s00204-020-02687-5
2. Toxicological profile for fluorides, hydrogen fluoride and fluorine (U.S. Department of Health and Human Services, 2003), https://www.atsdr.cdc.gov/toxprofiles/tp11-p.pdf. Accessed 6 July 2021
3. R. Fuge, Appl. Geochem. **100**, 393–406 (2019). https://doi.org/10.1016/j.apgeochem.2018.12.016
4. A. Dhillon, M. Nairb, D. Kumar, Anal. Methods **2016**(8), 5338–5352 (2016). https://doi.org/10.1039/C6AY01534D
5. Development of a Reference Database for Particle Induced Gamma Ray Emission (PIGE) Spectroscopy (IAEA-TECDOC-1822, Vienna, 2017)https://www.iaea.org/publications/12235/development-of-a-reference-database-for-particle-induced-gamma-ray-emission-pige-spectroscopy. Accessed 6 July 2021
6. M. Döbeli, A.A.-M. Gaschen, U. Krähenbühl, in *Advances in fluorine science*, vol. 2, ed. by A. Tressaud (Elsevier, Netherlands, 2006), p. 215
7. C.S. Sastri, A. Banerjee, T. Sauvage et al., J. Radioanal. Nucl. Ch. **298**, 311–315 (2013). https://doi.org/10.1007/s10967-012-2410-x
8. D.D. Cohen, E. Stelcer, O. Hawas, D. Garton, Nucl. Instrum. Meth. B **219–220**, 145–152 (2004). https://doi.org/10.1016/j.nimb.2004.01.043
9. R. Mateus, M.A. Reis, A.P. Jesus, J.P. Ribeiro, Nucl. Instrum. Meth. B **249**, 784–788 (2006). https://doi.org/10.1016/j.nimb.2006.03.139
10. P.S. Dhorge, R. Acharya, N.S. Rajurkar, V. Chahar, V. Tuli, A. Srivastava, P.K. Pujari, J. Radioanal. Nucl. Ch. **311**, 1803–1809 (2017). https://doi.org/10.1007/s10967-016-5118-5
11. F. Lucarelli, G. Calzolai, M. Chiari, S. Nava, L. Carraresi, Nucl. Instrum. Meth. B **417**, 121–127 (2018). https://doi.org/10.1016/j.nimb.2017.07.034
12. F. Lucarelli, Eur. Phys. J. Plus **135**, 538 (2020). https://doi.org/10.1140/epjp/s13360-020-00516-3
13. C. Heckel, K. Müller, R. White, S. Wolf, N.J. Conard, C. Normand, H. Floss, I. Reiche, Quatern. Int. **403**, 40–50 (2016). https://doi.org/10.1016/j.quaint.2015.11.105
14. R. Mateus, A.P. Jesus, J.P. Ribeiro, Nucl. Instrum. Meth. B **219–220**, 519–523 (2004). https://doi.org/10.1016/j.nimb.2004.01.114
15. R. Mateus, A.P. Jesus, J.P. Ribeiro, Nucl. Instrum. Meth. B **229**, 302–308 (2005). https://doi.org/10.1016/j.nimb.2004.11.019
16. R. Mateus, M. Fonseca, A.P. Jesus, H. Luís, J.P. Ribeiro, Nucl. Instrum. Meth. B **266**, 1490–1492 (2008). https://doi.org/10.1016/j.nimb.2007.11.042
17. M. Fonseca, A.P. Jesus, H. Luís, R. Mateus, J. Cruz, L. Gasques, D. Galaviz, J.P. Ribeiro, Nucl. Instrum. Meth. B **268**, 1806–1808 (2010). https://doi.org/10.1016/j.nimb.2010.02.079
18. G.E. Coote, Nucl. Instrum. Meth. B **66**, 191–204 (1992)

19. V. Manteigas, J. Cruz, M. Fonseca, A.P. Jesus, Nucl. Instrum. Meth. B **502**, 142–149 (2021). https://doi.org/10.1016/j.nimb.2021.06.006
20. IAEA Ion Beam Analysis Nuclear Data Library (IBANDL), https://www-nds.iaea.org/exfor/ibandl.htm
21. R. Mateus, A.P. Jesus, M. Fonseca, H. Luís, J.P. Ribeiro, Nucl. Instrum. Meth. B **264**, 340–344 (2007). https://doi.org/10.1016/j.nimb.2007.09.030
22. ERYA-Bulk webpage. https://sites.fct.unl.pt/nuclear/software/erya-bulk . Accessed 6 July 2021
23. N.P. Barradas, J. Cruz, M. Fonseca, A.P. de Jesus, A. Lagoyannis, V. Manteigas, M. Mayer, K. Preketes-Sigalas, P. Dimitriou, Nucl. Instrum. Meth. B **468**, 37–47 (2020). https://doi.org/10.1016/j.nimb.2020.02.019
24. E. Alves, K. Lorenz, N. Catarino, M. Peres, M. Dias, R. Mateus, L.C. Alves, V. Corregidor, N.P. Barradas, M. Fonseca, J. Cruz, A. Jesus, Eur. Phys. J. Plus **136**, 684 (2021). https://doi.org/10.1140/epjp/s13360-021-01629-z
25. W.A. Ranken, T.W. Bonner, J.H. McCrary, Phys. Rev. **109**, 1646 (1958). https://doi.org/10.1103/PhysRev.109.1646
26. B. Perea, P. Corvisiero, D.J. Rey, V. Joco, A.M. Vidal, A.M. Martin, A. Zucchiatti, Nucl. Instrum. Meth. B **406**, 161–166 (2017). https://doi.org/10.1016/j.nimb.2017.02.017
27. A. Caciolli, M. Chiari, A. Climent-Font, M.T. Fernández-Jiménez, G. García-López, F. Lucarelli, S. Nava, A. Zucchiatti, Nucl. Instrum. Meth. B **249**, 98–100 (2006). https://doi.org/10.1016/j.nimb.2006.03.089
28. I. Zamboni, Z. Siketic, M. Jakšic, I.B. Radovic, Nucl. Instrum. Meth. B **342**, 266–270 (2015). https://doi.org/10.1016/j.nimb.2014.10.022
29. A.P. Jesus, B. Braizinha, J.P. Ribeiro, Nucl. Instrum. Meth. B **161–163**, 186–190 (2000). https://doi.org/10.1016/S0168-583X(99)00855-1
30. C. Boni, E. Cereda, G.M.B. Marcassan, V. de Tomasi, Nucl. Instrum. Meth. B **35**, 80–86 (1988)

Computer Physics Communications 275 (2022) 108307

Contents lists available at ScienceDirect

Computer Physics Communications

www.elsevier.com/locate/cpc

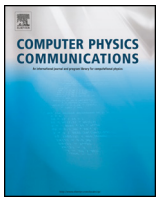

ERYA-Bulk and ERYA-Profiling: An application for quantitative PIGE analysis ☆,☆☆

V. Manteigas [a,*], L. Martins [a], J. Cruz [a], M. Fonseca [a,b], A.P. Jesus [a]

[a] Laboratório de Instrumentação, Engenharia Biomédica e Física da Radiação (LIBPhys-UNL), Departamento de Física, Faculdade de Ciências e Tecnologia da Universidade Nova de Lisboa, Monte da Caparica, 2892-516 Caparica, Portugal
[b] Lusófona University, HEI-Lab: Digital Human-Environment Interaction Lab, Lisbon, Portugal

ARTICLE INFO

Article history:
Received 6 September 2021
Received in revised form 12 January 2022
Accepted 6 February 2022
Available online 17 February 2022

Keywords:
PIGE
Computer code
ERYA-Bulk
ERYA-Profiling
Analysis of in-depth heterogeneous samples
Full stragling treatment

ABSTRACT

The applications entitled ERYA-Bulk and ERYA-Profiling (ERYA stands for Emitted Radiation Yield Analysis) are two programs which implement PIGE (Particle Induction Gamma-Ray Emission) analysis of samples which can be either homogeneous (handled by ERYA-Bulk) or heterogeneous (with multiple layers, which are simulated by ERYA-Profiling).
The homogeneous model uses an analytical method to evaluate the nuclear yield as function of the mass fraction of the element(s) of interest. A routine is available to fit the experimental yields in order to compute the correct sample atomic composition.
Otherwise, the heterogeneous model takes consideration of the physics with greater detail, including straggling in the energy lost by the projectiles, making a more realistic yield simulation, whose level of accuracy the user can control in exchange of computational time.
Here, we present the latest developments of these codes, which include new features, functionalities and direct handling of different source files. ERYA-Bulk and ERYA-Profiling are currently compiled and tested for Linux, Windows and Mac OS X operating systems.

Program summary
Program Title: ERYA-Bulk, ERYA-Profiling
CPC Library link to program files: https://doi.org/10.17632/gnrvm4jt5v.1
Developer's repository link: https://github.com/Arucard1983/ERYA-Bulk (*ERYA-Bulk*), https://github.com/Arucard1983/ERYA-Profiling (*ERYA-Profiling*)
Licensing provisions: LGPL-v3
Programming language: C++
External routines: wxWidgets [1], wxMathPlot [2]
Nature of problem: Compute the gamma-ray yield coming from a sample bombarded by a energetic (few MeV) beam of charged particles (namely protons). The yield corresponding to a given element depends on the mass fraction of this element and on the major composition of the sample which determines the rate of energy loss by the beam. It also depends on the detector efficiency, the collected beam charge (i.e., number of projectiles) and the cross-sections of the relevant gamma-producing nuclear reaction.
All data inputs can be loaded from a file or inserted by the user. The energy straggling along the beam interaction with the sample, irrelevant for bulk analysis, is determinant for depth profiling.
Solution method: The yield calculation is made by numerical integration of an analytical formula that depends on several quantities which can be analytical in nature or approximated by interpolation (the cross-section data interpolation is one example).
The straggling and energy dispersion also depends on energy distributions which have different numerical approximations. A modular approach using the object-oriented programming helps to implement different models to the main integration routine, and make the source code more readable and prone for future extensions.

☆ The review of this paper was arranged by Prof. Z. Was.
☆☆ This paper and its associated computer program are available via the Computer Physics Communications homepage on ScienceDirect (http://www.sciencedirect.com/science/journal/00104655).

* Corresponding author.
E-mail address: vm.manteigas@campus.fct.unl.pt (V. Manteigas).

https://doi.org/10.1016/j.cpc.2022.108307

A fitting feature was implemented on ERYA-Bulk to adjust the sample composition to the experimental yield results.

References

[1] wxWidgets webpage, https://www.wxwidgets.org.
[2] wxMathPlot webpage, https://wxmathplot.sourceforge.io/.

1. Introduction

PIGE has been widely used for the analysis of in-depth homogeneous (bulk analysis) and heterogeneous (profiling analysis) samples. Bulk analysis has proceeded usually with the use of reference samples for the quantification of data. The growing database of experimental excitation functions and stopping powers becoming available promoted the development of computer codes based on these physical parameters [1], as ERYA-Bulk [2] NDF [3–5], PiGreCo [6] and SIMNRA [7,8]. From these, ERYA-Bulk and PiGreCo are public freeware codes.

Analysis of in-depth heterogeneous samples has been used for more than fifty years for a variety of light isotopes in the field of material analysis, mostly focused on resonant depth profiling. This is performed by measuring the gamma-yield of the reaction as a function of the beam energy, scanning an isolated thin resonance along the depth of the sample. The program SPACES (not publicly available) was developed for this purpose [9,10].

ERYA-Bulk is a new version of the ERYA (Emitted Radiation Yield Analysis) program designed to evaluate the gamma-ray yields coming from homogeneous samples bombarded by charged particles (namely protons) using the theoretical framework derived first in [2], and later implemented by two different software versions: a MS-DOS version, and later a Windows version based on LabView Runtime, which are currently discontinued.

ERYA-Profiling is an extension of ERYA-Bulk designed to deal with depth-heterogeneous samples. Besides SPACES and ERYA-Profiling, NDF also performs resonant depth profiling simulations, but it is not a freeware code.

We decided to upgrade the former ERYA-bulk program rewriting it in order to get functional and portable software and also to implement the ERYA-profiling program within the same approach.

The new ERYA programs were implemented on C++11 language and use the cross-platform framework wxWidgets to implement the GUI and the data structures within.

The major advantage of wxWidgets was the possibility to ease the port to several operating systems, since it acts as a wrapper library to make the code compile to several computer architectures and native operating systems libraries. The original source code once compiled and linked to the wxWidgets libraries for each operating system, builds native programs without changing a single line of code. Also, wxWidgets provides additional frameworks to uniform data structure handling, making the code more portable across several operating systems.

Both ERYA-Bulk and ERYA-Profiling executables may be seen as a merge of three main modules:

1. The GUI handles all events for the several tools available to the user, using wxWidgets model framework.
2. A series of auxiliary routines, called *library* routines, dedicated to handle the ERYA databases operations on memory and also the files handling, using the wxWidgets libraries to implement this module.
3. The physics numerical evaluation routine, which is specific of each program. This module depends on GUI handling the user inputs, and the library functions to retrieve the database data, in order to run the numerical evaluation code.

2. The physics problem

When energetic ions (typically protons with energies up to 4 MeV) interact with a nucleus this may induce nuclear reactions with emission of gamma photons. The gamma yield $\mathrm{d}Y(E,\theta)$ emitted by an isotope i, resulting from the interaction of N_p projectiles with energy E with a thin layer having an areal density $N_i dx$ of the given isotope species is:

$$dY(E,\theta) = 4\pi\,\varepsilon_{\mathrm{abs}}\left(E_\gamma\right).N_p.\sigma(E,\theta).N_i.\mathrm{d}x \tag{1}$$

where N_i is the number of isotopes per volume unit, dx is the thickness of the thin layer, $\varepsilon_{abs}(E_\gamma)$ is the absolute efficiency of the detector for γ rays with energy E_γ, and $\sigma(E,\theta)$ is the differential cross section for emission of a γ ray at angle θ with respect to the incident ion direction.

Charged particles interact with the material medium mainly by Coulomb Interactions leading to a continuous energy loss of the particles. Considering that a beam with initial energy E_0 will steadily lose energy as it crosses the sample, the total gamma yield will be:

$$Y(E_0,\theta) = 4\pi\,\varepsilon_{\mathrm{abs}}\left(E_\gamma\right).N_p.f_m.f_i.N_{av}.A^{-1}\int_0^{E_0}\sigma(E,\theta)/S_m(E)\,dE \tag{2}$$

where $S_m(E)$ is the mass stopping power (i.e. the energy lost by unit of mass thickness of the sample) at energy E; f_m is the relevant element mass fraction; f_i, and A are the isotopic abundance and the atomic mass of the relevant element, respectively, and N_{av} is the Avogadro number. Equation (2) presumes that the sample composition does not change with depth, assumption valid for bulk analysis.

In order to include a composition dependent on depth and take also into account that the beam energy loss is accompanied by a beam energy dispersion, the number of projectiles with a given energy E is no longer constant and neither are the mass fractions. Then the gamma-yield is given by

$$Y(E_0,\theta) = 4\pi\,\varepsilon_{\mathrm{abs}}\left(E_\gamma\right).N_{av} .A^{-1}\int_0^{E_0}\sigma(E,\theta).N_p(E).f_m(E).f_i(E)/S_m(E)\,dE \tag{3}$$

In summary, for bulk analysis equation (2) must be solved, and for depth profiling analysis the program must solve equation (3). Both calculations need to be fed by data regarding several parameters: atomic numbers, atomic masses, isotopic abundances, cross sections in function of the projectile energy (i.e. excitation functions) of the relevant gamma-producing nuclear reactions, stopping powers correspondent to the major composition of the sample and detection efficiency. This data is compiled in databases provided by ERYA and shared by the Bulk and Profiling versions.

For bulk analysis, the user is supposed to provide a first guess of the sample major composition, identify the elements of interest, introduce the correspondent experimental gamma-yields and

receive as answer the mass fractions of these elements, after a fitting procedure using the Levenberg-Marquardt algorithm [11].

For depth profiling analysis, the user must assume a layered structure of the sample and give a first guess of number of layers and respective composition in terms of major composition and elements of interest; the program will give back, for a chosen energy range, the gamma-ray yield in function of projectile energy which will be optimized by the user in comparison with the corresponding experimental data.

In order to obtain the gamma-ray yield from eq. (2), ERYA-Bulk performs a division of the sample in n consecutive layers parallel to the sample surface, within which the stopping power can be taken as constant. All the layers have the same energy thickness, the energy step, which may be chosen by the user (an additional functionality). Then the integral in eq. (2) becomes the following sum:

$$\sum_{i=1}^{n}\left[\frac{1}{S_m(E_i)}\int_{E_i}^{E_{i+1}}\sigma(E,\theta)\,dE\right] \tag{4}$$

ERYA-Bulk uses by default SRIM [12] stopping powers, evaluated at the beginning of each layer. Inside each layer the cross-section is evaluated by integrating the cross section tabulated data via an Adaptive Integration Method (Trapezoidal Method). This program evaluates the cross section at a given energy by performing a linear interpolation from the two nearest excitation function tabulated values.

In general, a direct evaluation of eq. (3) is not viable due to the complexity of the simulation model. In order to accomplish the calculations, the following approximations are applied in ERYA-Profiling:

1. The integral is evaluated by a sum over small layers k. To each layer k, a constant energy is assigned, $\overline{E}_k$, which is the average energy at the beginning of that layer.
2. The variation of composition along each layer depth (or energy) is negligible, the stopping power is assumed to be constant, and it is calculated at $\overline{E}_k$.
3. Within each layer protons display a distribution of energy $F(E)$ and the cross-section may vary by several orders of magnitude, particularly for resonances that have a major interest to ERYA-Profiling.

Using these assumptions, the yield corresponding to a given element is given by the following sum:

$$Y(E_0)=\sum_{k=1}^{n}Y_k\left(\overline{E}_k\right) \tag{5}$$

And each term may be calculated from:

$$Y_k\left(\overline{E}_k\right)=4\pi\,\varepsilon_{\text{abs}}\left(E_\gamma\right).N_{av}.A^{-1}.f_{mk}.f_i \Big/ S_m\left(\overline{E}_k\right)\Delta E_k N_p\int F(E)\,\sigma(E)\,dE \tag{6}$$

The energy distribution $F(E)$ on eq. (6) is given by a convolution of three separated distributions: the Doppler Distribution, proportional to the temperature, the beam initial energy dispersion, and the Straggling Distribution, i.e. the energy distribution resulting from the stochastic character of the energy loss suffered by the beam within the material. The first two distributions may be considered Gaussian distributions and can be trivially merged in a single one. Depending on the energy lost by the beam till layer k, the program will fetch for the straggling distribution a Landau [13], Vavilov [14] or Gaussian [15] distribution.

3. Brief description of main program modules

In the following, we describe the main modules of ERYA-Bulk and ERYA-Profiling, which, as referred before, were implemented on C++11 language, and use the cross-platform framework wxWidgets to implement the GUI and the data structures within. The programs were developed under an object-oriented programming paradigm. Some details of the main classes pertaining to each module are given below.

3.1. The GUI module

The GUI module of both programs is implemented according to the wxWidgets coding Standards. Each major dialog and its contents are defined by its own C++ class, which contains the function handlers and events.

Without a cross-platform framework like wxWidgets, a native compiled software would require a different source code branch for the GUI code, including windows, events, handlers, and even native operating system calls. In this scenario one would need to use GTK or Qt toolkits for Linux, Win32 API or .NET for Windows, Cocoa for Mac OS X and this would be too costly to maintain, and would divert the focus from the real problem, which is implementing a working scientific software with a GUI.

3.2. The Library Module

The Library Module uses the wxWidgets framework libraries to create a series of specific routines for ERYA to handle special kinds of data, offloading from the GUI components code.

The major two library modules are related to the Databases and the File Formats, that depend on other components that we detail later.

3.2.1. Database library

The Databases classes handle the relevant database structures in memory while providing common functions to control contents access.

The “ElementDatabaseList” class contains in each individual register the information pertaining to the characteristic of an element, such as its name and corresponding gamma line and also abundance, isotopic or atomic mass, and atomic number. It also appends four numerical columns to store the experimental cross-section and their energies, including the measurement uncertainties.

The database also supports a remark field for the global database and for each individual element that the user can edit via the program interface, since it provides an ASCII text editor to make the changes and the program update this field automatically.

The vector class that handles the entire element’s database implements several operations needed for the program running, such as find an element by name or gamma line, add new elements, delete a specific element, find duplicates, or sort the database. Some of these functions are called by the user through a GUI handler (e.g. by clicking a button or filling in the inputs), others are called indirectly.

The database library also contains classes to handle stopping power data, the vector class “ElementSRIMList” and the single class “Stopping-Power” for approximations of stopping power calculation other than SRIM.

Also part of the database library, the single class “Detector Efficiency” stores the experimental data and the Detector’s Function object, which handles the efficiency calculation in function of energy.

3.2.2. File Format Library

The next important (and more complex in terms of code) library module is the File Format Library which contains a diverse set of C++ classes dedicated to handle the actual loading and saving of databases classes contents in memory to a storage device.

Both programs (ERYA-Bulk and ERYA-Profiling) support a common "DetectorFile", "DatabaseFile" and "ZieglerFile" classes to handle the respective detector, database and stopping power files.

Since wxWidgets provides support to create XML documents (as their own C++ classes and methods), ERYA stores all database files using this format. Support of IDF (Ion Beam Analysis Data Format) [16] standard will be implemented in the future.

The program configuration file is also a XML document, but the implementation code is embedded on the GUI's Main Screen class for simplicity.

For ERYA-Bulk all inputs and outputs, as displayed on the main screen, are handled by the "ERYAPIGEFile" class, which also provides the functions to load and save the files, derived from the XML document format.

ERYA-Profiling stores all inputs related to the first three tabs on the main screen in three XML documents, each one handled by a specific class: "ERYAProfilingSampleFile", "ERYAProfilingLayerFile", "ERYAProfilingResonanceFile". Later all these classes are merged to a single one, "ERYAProfilingGlobalFile", to handle the contents of the three separated files, while adding some additional parameters related to accuracy parameters. The user has access to the GUI separated files through specific buttons. The upper screen menu for managing files will use the global file instead.

ERYA-Profiling save the outputs to Excel or ASCII tables which are handled respectively by "XlsxFile" and "TextFile" classes.

3.2.3. Compatibility with non-native file formats

ERYA was programmed to load directly source files with different formatting rules, in order to avoid manual conversion or tedious manual typing on the program interface.

One of the supported formats is the plain ASCII text file. Some special ASCII files, such as r33 from the IBANDL database [17] and SRIM table files have special import routines to parse non-numeric and numerical data. ERYA can also store data on IBANDL r33 format, in order to ease interchanging to other applications or user needs.

ERYA also has the capacity to import or export tabular data on a Microsoft Excel file using the Xlsx format (introduced in Office 2007). Since Excel Xlsx files are in reality zip files with a strict structure of folders and specific files, it opened the possibility to implement a routine for ERYA to load and save Excel files directly using the wxWidgets library.

ERYA reads the first spreadsheet of any Excel files, and only parse strict number and strings to a temporary matrix on memory called "TableMatrix", that later will be processed by ERYA's library methods according to the program context. When the user opens an Excel file on ERYA, the "XlsxFile" class parses the relevant data to the "TableMatrix" data class, and ERYA copy its contents to the GUI elements.

ERYA can also save tabular data as Excel files, storing everything in a single spreadsheet, while using a special temporary matrix table class as an intermediate step required to obey the Microsoft own standards. Any Excel files created by ERYA use only a simple global formatting rule for the fonts and column size. When the user saves to Excel the tabular data are written to the "TableMatrix" class, and passes to the "XlsxFile" class that handles everything to make a viable Excel file.

3.2.4. ERYA Macro language

An additional library called "AlgebraicFunction", implements a small programming language called ERYA Macro to support algebraic functions as inputs for some special setups.

ERYA Macro implementation uses a BASIC-like language within a single line coding program, while internally employing a stack interpreter like FORTH with the RPN notation hidden from the user. The ERYA Macro syntax was inspired by the programmable calculators (CASIO and Texas Instruments), acting as a derivative of the Basic language, while the variable names follow the C standards [18].

When the ERYA program reads a string that should act as a macro, like the Detector's Efficiency custom function for example, it starts a one-time conversion which begins by parsing the original string into a chain of words (tokens). Automatically, the tokens are converted or rearranged to the postfix order using the Shunting-Yard algorithm [18], and stored in memory.

Each time the "AlgebraicFunction" class is called (by passing a function argument, or requiring a numerical result) the stored postfix chain is executed by the stack interpreter, until returning a numerical result or an error.

3.3. The physics module

The numerical calculation regarding PIGE analysis is handled by this module, and since ERYA-Bulk and ERYA-Profiling handle two different models, this component is specific of each program.

3.3.1. ERYA-Bulk calculation

The main architecture of the code involves a cycle in proton energy from the value defined by the user to the minimum existent in the pertinent excitation function with steps also defined by the user, or a minimum calculated from a target thickness specified by the user. In some cases it may be necessary to sum the yield pertaining to that minimum to the calculated yield. As this minimum yield is dependent on the experimental setup, this must be given by the user as an input.

The "ReactionYield" class interfaces the inputs on screen and the databases loaded in memory, controlling the entire process. The first step is to check potential inconsistencies, which cause the calculation to halt and alert the user for the error.

Since the user can define compounds and fitting constraints for the sample, ERYA creates two additional vector classes as follows: the "Compounds" class which handles group of Elements that share a unique Compound Number defined by the user on the main screen. This will assign a fixed relative atomic fraction between the compound's elements, not allowing it to change during the fitting procedure; the "Fitting Parameters" class is responsible to handle the fixed atomic fraction constraints from the "Compounds" class, while also mapping the correct element position of all selected elements to the numerical matrices during the Levenberg-Marquardt algorithm.

The calculation of nuclear gamma-yields is made by the Yields class for each individual element, using the functions from "Elements", "Compounds" and "Fitting Elements" classes. Some of these functions include the evaluation of the samples atomic mass, the renormalization of the atomic fractions considering the user's defined constraints and the evaluation of the Detector's Efficiency corresponding to the element's gamma peak.

The Yield's class implements the numerical integration using the Simpson's Rule with a constant integration step previously defined by the user. During the integration method, the stopping-power is evaluated at the beginning of each individual step. The cross-sections are evaluated by interpolating the values of the excitation function.

If the user does not choose any elements to be fit, ERYA will evaluate the yields corresponding to the initial guess composition. If the user selects some elements to be fit and introduce their experimental yields, the fitting procedure inside the "Yields" class is activated and starts the Levenberg-Marquardt algorithm, beginning with the yields corresponding to the initial guess composition.

Once reached a suitable solution, ERYA retrieves the relevant outputs and displays them on the screen. These outputs can be saved as an excel file, together with the corresponding inputs.

ERYA also provides a table of yields in function of energy if required by the user. This table is created on the program's main screen, and it can also be saved as an excel file.

3.3.2. ERYA-Profiling simulation

ERYA-Profiling fulfills two objectives: calculate, at a given proton energy, the gamma-ray yield of a given element which has a concentration dependent on the depth along the sample; calculate the produced yield of a layered sample, allowing the user to optimize the depth distribution of a given element's concentration, by scanning a given resonance of the excitation function along the depth of the sample.

The main architecture of the code involves a cycle in number of atoms per area from zero to a maximum consistent with the input in composition provided by the user with steps also defined by the user. As explained before, each layer is characterized by the mean proton energy lost till that layer, and a proton energy distribution consistent with the energy loss is assigned to that layer. In order to handle resonance scanning problems, an outer cycle in proton energy repeats the process from the incident energy to a maximum energy with an energy step, being all these parameters defined by the user.

ERYA-Profiling builds the "Elements" class with a logic similar to the ERYA-Bulk counterpart. The sample composition, which is defined by a combination of elements and layers is handled by a "Layers" class.

The simulation results are handled by "Yields" classes, each one of a specific element.

Regarding projectile energy straggling, the energy distribution may be a Landau, a Vavilov or a Gaussian distribution. The Vavilov distribution is implemented by a numerical approximation, based on a method published by Rotondi and Montagna [19] and modified to tackle some inconsistencies. We have in preparation a paper dedicated to this subject. The choice of distribution is based on a parameter κ, which was defined by Landau and Vavilov as the ratio between approximately equal to the average lost energy, and ϵ_{MAX} the maximum energy transfer per collision

$$\kappa = \xi / \epsilon_{MAX} \tag{7}$$

The parameter κ is assumed to be constant for each layer. According to the values of κ, the distribution functions, presented in Table 1 of a previous publication [20], come into play.

The relevant distributions are handled by appropriate classes which depend on functions (Dirac, Landau, Vavilov-Moyal, Vavilov-Airy, Vavilov-Edgeworth, Gaussian Function) encapsulated on C++ classes.

For scanning resonance purposes, the user may use, instead of the excitation function around a given resonance (experimental resonance values are modified by the thickness of the target used for the measurement of the excitation function), a Breit-Wigner resonance obtained from a fit to the experimental results. The user defined resonance is handled by the "ResonanceFunction" class which is called automatically by the "Yields" class.

A class called "ReactionProfiling" controls the numerical simulation from the initial incident energy to the maximum. Results are displayed on the user's interface in tabular and graphical format in comparison with experimental yields (if imported by the user).

Partial logs evaluated for each layer of yields and other relevant values are stored on "Sample" class and may be called to the GUI or stored in an Excel file.

4. User interface

4.1. ERYA-Bulk

The image of Fig. 1 shows the current ERYA-Bulk main screen running on Debian 11 Bullseye.

The program interface, recovering some concepts from the previous versions, adds several improvements. The main screen is composed by a matrix frame where the elements and gamma energies are aligned with the physical data associated. Some columns are editable to fill the necessary information that should model the sample while others are reserved for the results.

Outside the main frame, at the bottom screen, the user can define the yield integration parameters on the corresponding inputs. Some buttons are also available to the common tasks, including running the simulation and saving the results to a file.

The menu bar at the top screen contains the tools to handle the databases and the program settings. It also enables to save the sample contents to a file, and load again to avoid manual typing. The Database Management Tools from the ERYA's databases are accessible from the program's main menu. The user can freely change any database contents and settings or save to different files and swap on fly without restarting ERYA.

The Elements Database contains all the necessary elemental parameters, including the excitations functions, which were retrieved from IBANDL. Fig. 2 shows the elements database manager pop-up window, which allows not only the fast selection and visualization of different excitation functions, but also the upload of new excitation function files, for example in r33 format (as those in IBANDL).

The Detector Efficiency Database contains the data pertaining to the absolute efficiency of the gamma detector. Fig. 3 shows the Detector Efficiency database manager pop-up window. This window combines an editable text box, intended for the user to code an algebraic function (using the custom ERYA macro – previously mentioned), describing the variation of the Detector Efficiency with Energy, and a two-column table to fill any experimental values for the Detector Efficiency that will serve the same purpose. Both fields can be filled on the built-in editor and stored in the profile file. However, ERYA will choose the function field by default, if it is correctly defined, and will ignore the table.

The Stopping power database allows to choose between three options: the first two correspond to the ZBL model (either the 1977 or 1991 equations, hardcoded on program); the third option (default) corresponds to SRIM tables (in units of eV/10^{15} at.cm^{-2}) for all elements. SRIM is run beforehand and the output files are imported by ERYAs to their databases. The Stopping Power database manager pop-up window shown in Fig. 4, presents three options and a programmable custom ERYA macro.

4.2. ERYA-Profiling

The main interface of ERYA-Profiling (Fig. 5) keeping up some of the features of the one developed for ERYA-Bulk has several differences caused by the different inputs and outputs associated with the different physical problem to be solved.

In order to organize the user workflow, the program uses a tabbed interface for inputs and outputs (second line). Fig. 5 pertains to the "Elements" editor, where a selection of elements and gamma lines may be done, with the possibility to override the elements physical characteristics loaded from the database on the

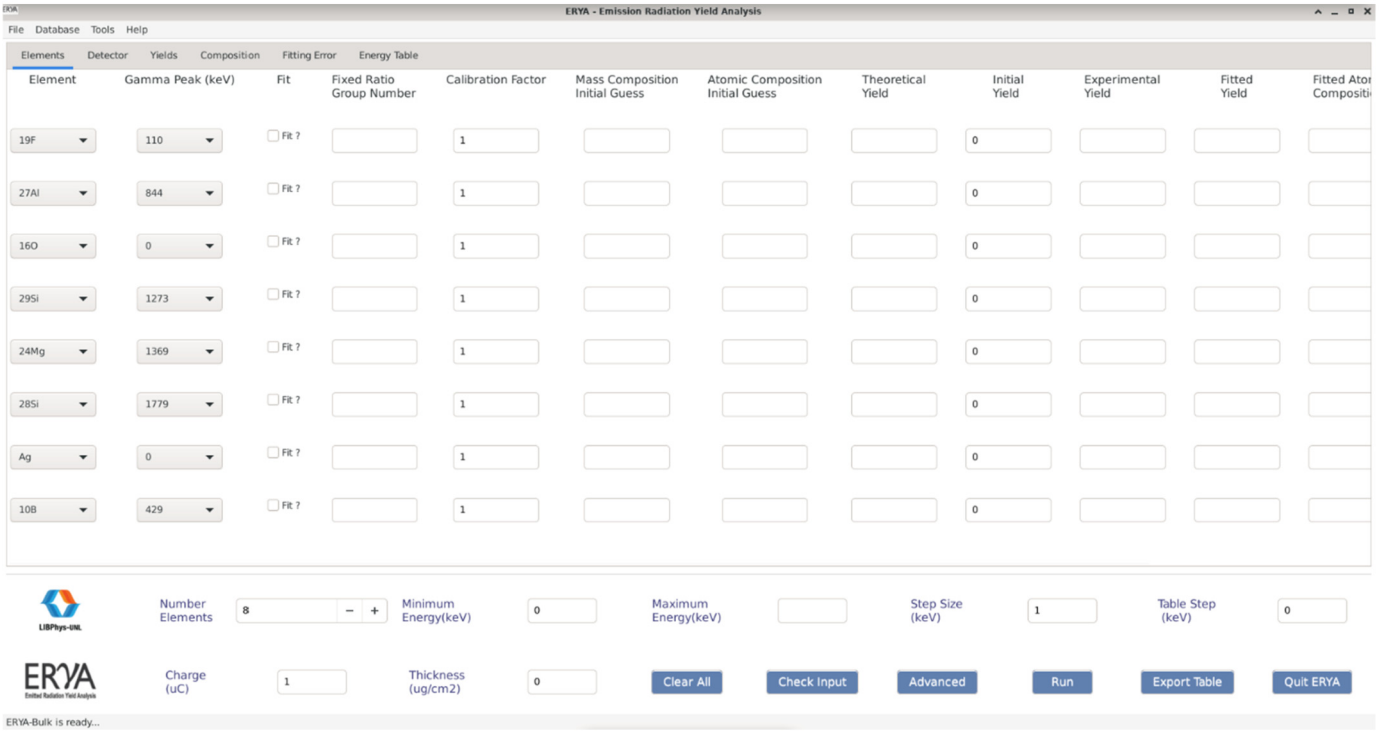

Fig. 1. ERYA-Bulk interface running on Debian 11 Bullseye.

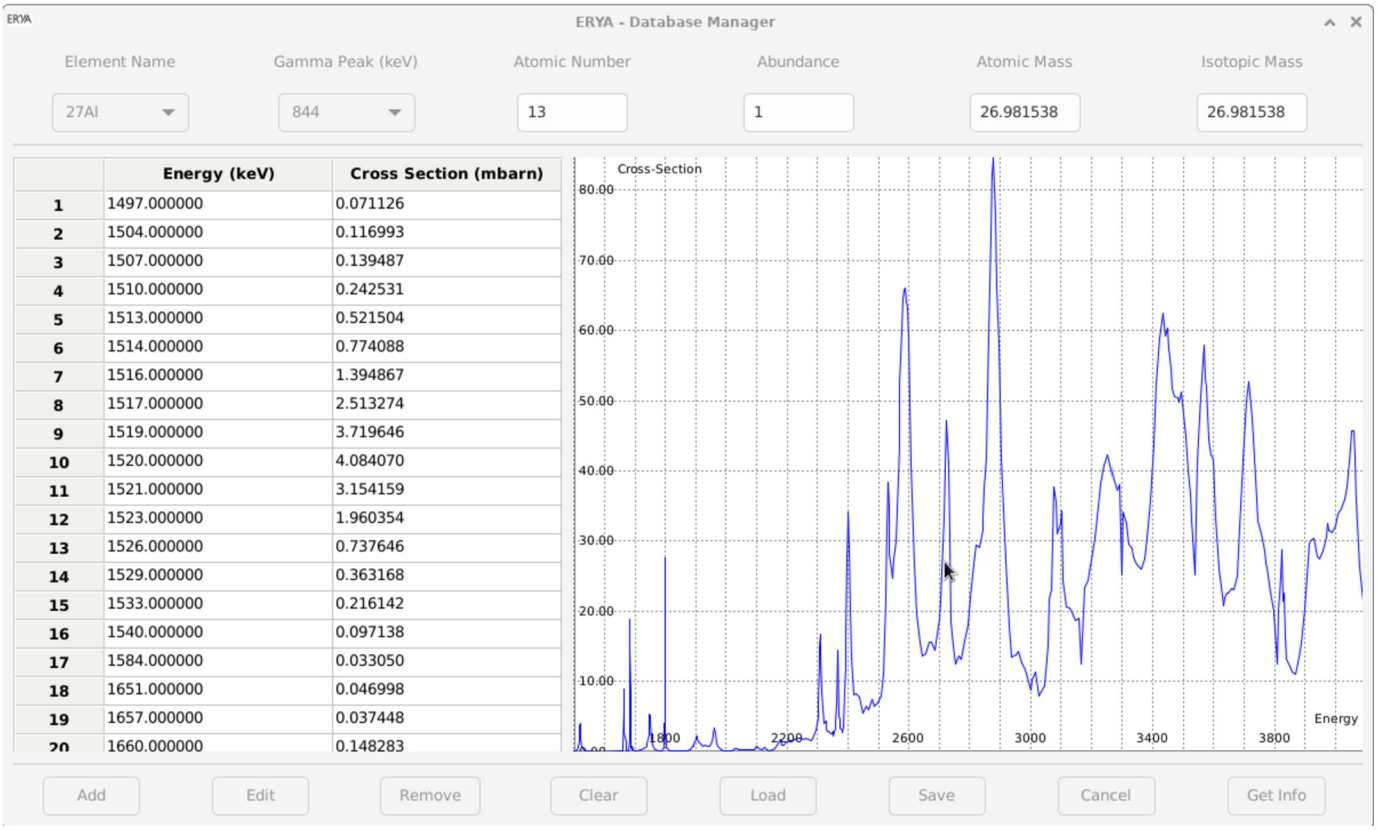

Fig. 2. Elements database manager pop-up window (running on Debian 11 Bullseye). In this case, it is plotted the excitation function for the 844 keV gamma peak of the ^{27}Al(p,p'γ)^{27}Al inelastic scattering reaction.

adequate columns. The “Layers” editor opens a spreadsheet where the user defines the number and atomic composition of each individual layer, treating a non-homogeneous sample as a sum of individual homogeneous layers. The user may define the beam energy and its resolution, including the energy range for the profiling analysis on the “Beam and Resonances” editor. Optionally, the user may also define one or more Lorentzian resonances, or a custom function for the resonance at a finite energy range. By default,

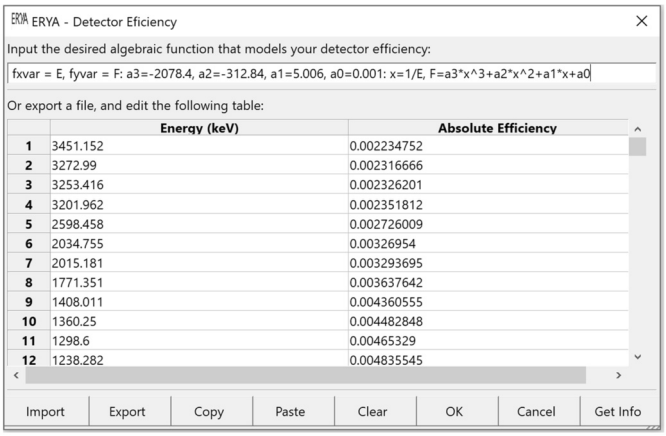

Fig. 3. Detector Efficiency database manager pop-up window (running on Windows 10).

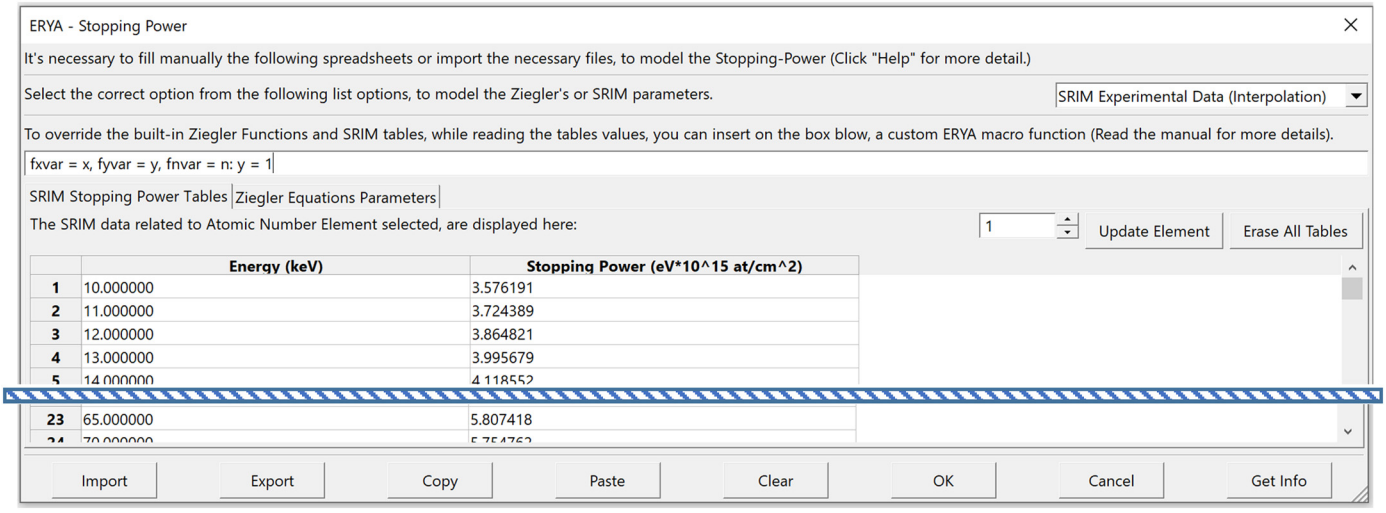

Fig. 4. Stopping Power database manager pop-up window. A breaking bar separates the upper and bottom parts of the window (running on Windows 10).

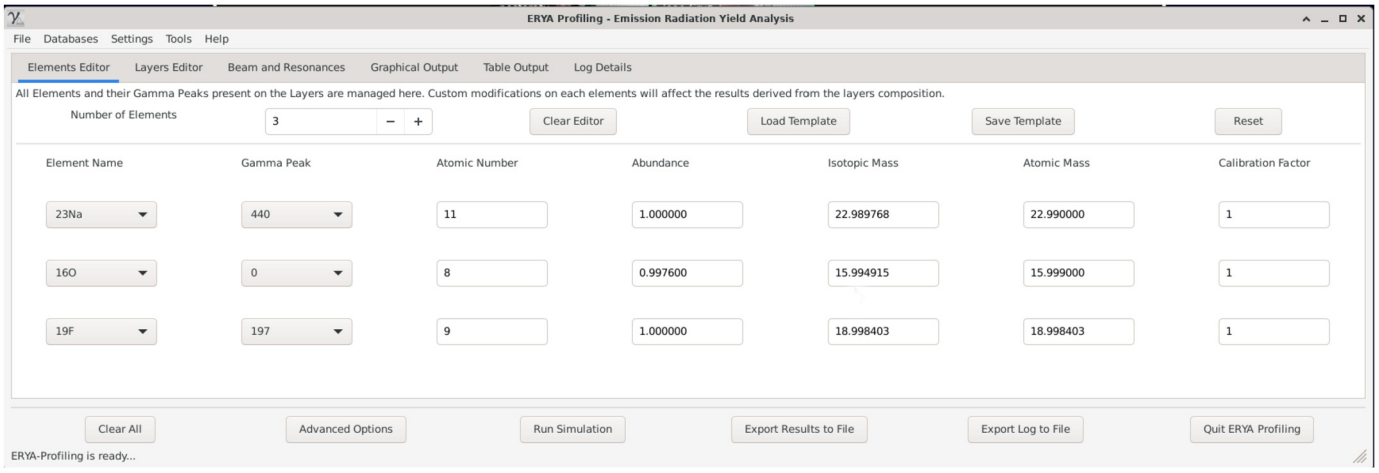

Fig. 5. ERYA-Profiling interface (rescaled for better visualization) running on Debian 11 Bullseye.

ERYA-Profiling will perform the calculations with resource to the excitation function chosen in the elements editor. The "Graphical output" editor displays the yield in function of energy in a graphical plot, optionally in comparison with the experimental yield, which may be introduced through this tab, providing also the results in a table format on "Table output".

After the calculation, access to partial yields and parameters of each layer may be seen in "Log details", which is disabled by default but may be opened via the "Advanced Options" button. At the bottom screen, some special buttons activate global events as making a quick save of the results or starting a new simulation. An additional applet to change the accuracy of the distributions

and the sample depth integration step is accessible from the "Advanced" button.

A progress bar, with the option to cancel the operation and return the control to the user with all inserted data left untouched, is provided to the user during the simulation. The menu bar at the top screen contains the tools to handle the databases and the program settings. It also enables to save the sample contents to a file, and load again to avoid manual typing. Access to databases and databases pop-up windows are the same as in ERYA-Bulk.

5. Case study

In order to test the ERYA programs and assess their performance, we present a simulation study to answer a question raised by another group at our laboratory working in gallium and aluminum nitrides deposited on sapphire (Al_2O_3). These materials are very interesting for optoelectronics and their properties can be changed by argon implantation. Particularly in the case of pure aluminum nitrides (without gallium) defects caused by the implantation may modify the composition of the first layers. This was verified for nitrogen by Elastic Recoil Detection Analysis (ERDA) and a combination of Rutherford and Elastic Backscattering Spectrometry (RBS/EBS) in the first implanted samples, but no clear information for aluminum came from this analysis. Hence, the question raised was if PIGE profiling could provide that information. The samples to be developed have the following structure: a film of AlN, with thickness between 0.9 μm and 1.2 μm, over another film of AlN (with the same thickness) or GaN with around 0.7 μm, over thick sapphire.

Considering future experiments, the best choice for a resonance to be scanned along the depth of the sample is the 1798 keV thin resonance of the ^{27}Al(p,p'γ)^{27}Al nuclear reaction, because the corresponding yields are much higher than the usual 992 keV resonance of the (p,γ) reaction in ^{27}Al, lowering the needed running time, and the natural thickness, 3.4 keV, is small enough for the layer resolution needed to handle samples with thickness of hundreds of nanometer. Also, the low energy of the resonance leads, for this sample, to a total yield that is not dominated by the contribution from the thick sapphire substrate.

In terms of the simulation, the yield of the sapphire was obtained from ERYA-Bulk for a range of pertinent energies, giving the expected energy loss in the first two layers. After the profiling exercise on the two first layers, this energy loss is provided by the ERYA-Profiling log file, allowing to sum the appropriate bulk yield from sapphire to the yield obtained for the two first layers. ERYA-Profiling could also be used to calculate the yield from sapphire but for a homogeneous thick target ERYA-Bulk is faster because no straggling distributions are used.

The excitation function of the ^{27}Al(p,p'γ)^{27}Al, with $E_\gamma = 844$ keV was loaded into ERYA-Bulk and ERYA-Profiling for the calculations. For the profiling simulation the energy range correspondent to the experimental 1798 keV resonance was replaced by the corresponding Breit-Wigner fit to the experimental points considering the thickness of the target used for the measurement of the referred excitation function. The energy range for the profiling scan was chosen to be from 1795 to 1832 keV.

For the surface layers corresponding to the energy range 1795 to 1810 keV (where modifications induced by implantation are expectable) the energy integration step was 1 keV and the thickness of the layers for the sake of energy distribution was 2×10^{17} at/cm^2, with a full treatment of the energy straggling (Landau, Vavilov, Gaussian). From 1810 to 1832 keV the steps were 2 keV and 5×10^{17} at/cm^2 and only a Gaussian approximation was used for the energy straggling, minimizing computation time.

The first test to be done concerns the sensitivity to the thickness of the first layers. Fig. 6 shows the yields versus incident energy obtained by ERYA-Profiling (summed up with the correspondent bulk yields of sapphire) for different combined thickness of the two layers of AlN, 1.8, 2.0 and 2.4 μm. As one can see, the trend of the curves obtained for the three situations are different, allowing to distinguish among them. This different trend is due to different contributions of the broad resonance of ^{27}Al(p,p'γ)^{27}Al at 1750 keV to the first layers and/or to the bulk sapphire, depending on the energy lost in the first layers. Again, this contribution may be assessed in the produced log file. In the same figure the configuration with AlN (1.2 mm) over GaN(0,7 mm) over sapphire is also presented, leading as expected to a completely different curve with lower yield due to the lack of Al in the second layer.

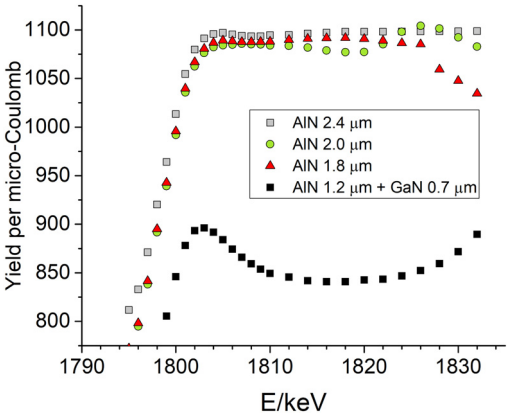

Fig. 6. Curves of gamma-ray yield versus incident energy; the detected gamma-ray line (844 keV) comes from the ^{27}Al(p,p'γ)^{27}Al nuclear reaction. The samples are composed of a superposition of aluminum nitride films (combined thickness indicated in μm in the legend) on sapphire or an aluminum nitride film (1.2 μm) over a gallium nitride film (0.7 μm) over sapphire.

As a second exercise a modification (decrease of Al) of around 10% and 4% was done to the AlN stoichiometry in the first 300 nm of AlN with 2.4 μm. The corresponding gamma-ray yields are presented in Fig. 7a) compared to the unmodified situation.

Although the 4% modification leads to a yield perceptible different from the one of the unmodified configuration, considering the uncertainties of the experimental yields to which the calculations will be compared, the decrease in yield is smaller than the experimental uncertainties. However, the 10% modification leads to values and trend of values outside the uncertainty range. In Fig. 7 b) the sapphire bulk contribution is not added to the yields of the AlN films in order to perceive the influence of this contribution to the total yield. One may see that sapphire contributes almost a half to the total yield, but does not modify the trend of values obtained for the first modified layer, giving in this energy range an almost constant contribution.

Hence, our answer to the question made to us is that PIGE profiling of Al, based on a resonance of the ^{27}Al(p,p'γ)^{27}Al reaction, taking also into account the whole excitation function, may indeed be sensitive to the thickness of the AlN films deposited on thick sapphire and to modifications larger than 10% in the stoichiometry of the first surface layers.

6. Performance

ERYA-Bulk and ERYA-Profiling were tested on a wide variety of computer hardware and operating systems.

An inter-comparison of ERYA-Bulk with NDF, PiGreCo and SIMNRA was done [21], without contemplating straggling, with very close results from all the programs for homogeneous samples. Still for the same kind of samples, Gaussian straggling was assessed, which implied in our case to use ERYA-profiling. Again, close results were obtained from all the programs.

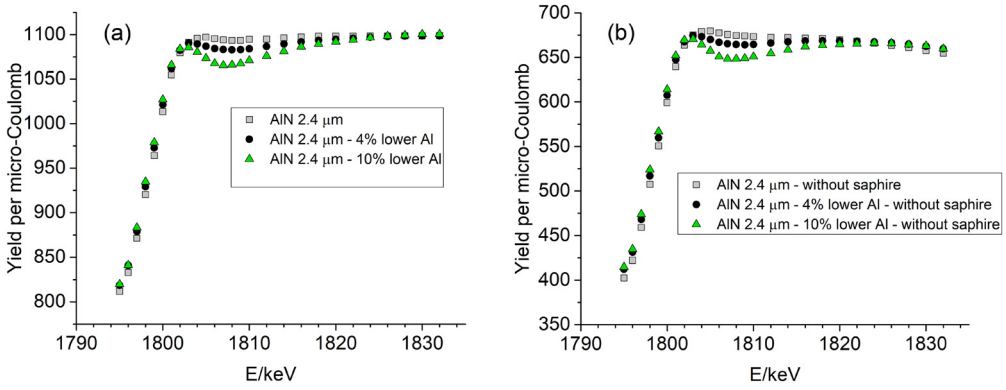

Fig. 7. Curves represent the same as in Fig. 6 for the case of a superposition of aluminum nitride films (combined thickness 2.4 μm) on sapphire a) and without sapphire b). The concentration of Al was lowered by 10% or 4% for the first 300 nm of the film.

6.1. Timing exercise

The exercise was undertaken with two different systems:

1. A Clevo branded laptop computer which runs the 64-bit Linux Debian 11 distribution and has an 8-core CPU from 7th generation Intel brand. (Intel(R) Core(TM) i7-7700HQ CPU @ 2.80GHz). All programs were installed on this computer using the manual guide for the Linux versions of these programs.
2. A smartphone branded CAT S62 Pro running Android 10. In order to run ERYA, it required the installation of a app called Debian No Root to install a limited Debian 10 (anything that uses low level access is not supported), including a partially working Desktop environment (XFCE 4). Since the CAT S62 use a 64-bit ARM processor (8-Core Qualcomm Snapdragon 660 @ 1.2 GHz.), the Debian No Root app installs the 64-bit ARM version of Debian 10. The installation of ERYA on this device is similar to the normal Linux installation, although it requires the user manage the touch screens controls that emulates the keyboard and mouse events to install and use the ERYA software.

It is expectable that the computation time of ERYA-Profiling may be estimated from the following formula:

$$T = T_l \times \#E \times \#L \times P$$

where $\#E$ is the number of elements, $\#L$ is the number of layers (L), P is the number of calculated energy points, and T_l is the elemental layer computational time, depending on the distributions and the number of points to define them. We employed in this exercise, optimized conditions related to this number of points (ERYA-Profiling default numbers), which corresponds to an accuracy in yield calculation better than $1/10^4$.

We registered the calculation times for the simulations done according to:

1. For AlN ($E = 2$) from 1795 to 1810 keV an energy step of 1 keV ($P = 15$) and a layer thickness of 1×10^{17} at/cm^2 ($L = 17$) were chosen with a full treatment of the energy straggling (Landau, Vavilov, Gaussian);
2. From 1810 to 1832 keV the steps were 2 keV ($P = 16$) and only a Gaussian approximation was used for the straggling; the number of elements was the same and the number of layers was 25.

The results are summarized in Table 1, showing a computation time for each singular calculation, inferior to 0.02 s for the Gaussian approximation and equal to 0.10 s for the full straggling treatment. These results correspond to the Clevo laptop computer; for the smartphone the computing times are higher as expectable, but still acceptable.

Table 1
Results of calculation times for two computing machines and conditions 1 and 2 as described in the text.

Computer	$\#E \times \#L \times \#P$	Straggling Distributions	T	T_l
Clevo 1	510	FullStrgl	51 s	0.10 s
Clevo 2	800	Gaussian	14 s	0.018 s
CAT 1	510	FullStrgl	143 s	0.28 s
CAT 2	800	Gaussian	77 s	0.096 s

7. Conclusions

In this work we presented the latest development of the ERYA-Bulk program, designed for PIGE analysis of in-depth homogeneous samples, which include new features, functionalities and direct handling of different source files (which import from IBANDL [17] and SRIM [12] files are examples) and a software approach providing it full compatibility with most of the operating systems.

Also presented is the ERYA-Profiling program, with the same approach, features and functionalities, but designed to deal with in-depth heterogeneous samples, i.e., PIGE profiling. As far as the authors know this is the most advanced program available for gamma resonant profiling with the capacity to include more than one resonance and the background. As another unique feature, the energy straggling within the sample is considered in a complete version using different energy distribution functions adequate to the amount of energy loss. A case study was presented to assess ERYA-Profiling performance, showing for a rather demanding case good capability.

Full details concerning the operation of ERYA-Bulk and ERYA-Profiling can be found on the code's manual [22,23].

CRediT authorship contribution statement

V. Manteigas: Methodology, Investigation, Software, Writing – original draft, Writing – review & editing. **L. Martins:** Methodology, Investigation, Software. **J. Cruz**: Methodology, Investigation, Software, Writing – review & editing. **M. Fonseca**: Methodology, Investigation, Software. **A.P. Jesus**: Conceptualization, Methodology, Investigation, Software, Writing – review & editing.

Declaration of competing interest

The authors declare that they have no known competing financial interests or personal relationships that could have appeared to influence the work reported in this paper.

Data availability

The raw/processed data required to reproduce these findings can be shared.

Acknowledgements

The authors acknowledge LIBPhys (UID/FIS/04559/2019) and NOVA.ID.FCT.

References

[1] International Atomic Energy Agency TECDOC No. 1822, Vienna, 2017, ISBN 978-92-0-106317-5.
[2] R. Mateus, A.P. Jesus, J.P. Ribeiro, Nucl. Instrum. Methods Phys. Res. B 219 (2004) 519, https://doi.org/10.1016/j.nimb.2004.01.114.
[3] N.P. Barradas, C. Jeynes, R.P. Webb, Appl. Phys. Lett. 71 (1997) 291–293.
[4] N.P. Barradas, C. Jeynes, Nucl. Instrum. Methods Phys. Res. B 266 (2008) 1875.
[5] N.P. Barradas, R. Mateus, M. Fonseca, M.A. Reis, K. Lorenz, I. Vickridge, Nucl. Instrum. Methods Phys. Res. B 268 (2010) 1829.
[6] K. Preketes-Sigalas, A. Lagoyannis, M. Axiotis, in: Proc. 25th Hellenic Conference on Nuclear Physics, 3-4 June, 2016, p. 162.
[7] M. Mayer, AIP Conf. Proc. 475 (1999) 541.
[8] M. Mayer, Nucl. Instrum. Methods Phys. Res. B 332 (2014) 176.
[9] I.C. Vickridge, G. Amsel, Nucl. Instrum. Methods Phys. Res. B 45 (1990) 6.
[10] I.C. Vickridge, G. Amsel, Nucl. Instrum. Methods Phys. Res. B 108 (1996) 403.
[11] K. Madsen, H.B. Nilsen, O. Tingleff, Methods for Nonlinear Least Square Problems, Technical University of Denmark, 2004.
[12] J.F. Ziegler, J.P. Biersack, M.D. Ziegler, SRIM – The Stopping and Range of Ions in Matter, Maryland, SRIM Co., 2008, www.srim.org.
[13] L. Landau, J. Phys. (USSR) 8 (1944) 204.
[14] P.V. Vavilov, Sov. Phys. JETP 5 (1957) 749.
[15] N. Bohr, Philos. Mag. 30 (1915) 581.
[16] N.P. Barradas, Nucl. Instrum. Methods Phys. Res. B 332 (2014) 148–151.
[17] IAEA Ion Beam Analysis Nuclear Data Library (IBANDL), https://www-nds.iaea.org/exfor/ibandl.htm.
[18] "ALGOL-60 Translation", Dr. E.W. Dijkstra, Stichting Mathematisch Centrum, Amsterdam, https://www.cs.utexas.edu/~EWD/MCReps/MR35.PDF.
[19] A. Rotondi, P. Montagna, Nucl. Instrum. Methods Phys. Res. B 47 (1990) 215.
[20] V. Manteigas, J. Cruz, M. Fonseca, A.P. Jesus, Nucl. Instrum. Methods Phys. Res. B 502 (2021) 142–149.
[21] N. Pessoa Barradas, J. Cruz, M. Fonseca, A.P. de Jesus, A. Lagoyannis, V. Manteigas, M. Mayer, K. Preketes-Sigalas, P. Dimitriou, Nucl. Instrum. Methods Phys. Res. B 468 (2020) 37–47.
[22] ERYA-Bulk webpage, https://sites.fct.unl.pt/nuclear/software/erya-bulk.
[23] ERYA-Profiling webpage, https://sites.fct.unl.pt/nuclear/software/erya-profiling.

ERYA-Profiling Energy Straggling Distributions

V. Manteigas[1,a], J. Cruz[1], L. Martins[1], A.P. Jesus[1]

[1] Laboratório de Instrumentação, Engenharia Biomédica e Física da Radiação (LIBPhys-UNL), Departamento de Física, Faculdade de Ciências e Tecnologia da Universidade Nova de Lisboa, **Monte da Caparica, 2892-516 Caparica, Portugal**

[a] e-mail: vm.manteigas@campus.fct.unl.pt

In Revision

Abstract

ERYA-Profiling is a program which calculates the yield of gamma-rays coming from nuclear reactions induced in materials, with in-depth heterogeneous compositions, by accelerated charged particles, namely protons. The particle energy straggling due to the statistical nature of energy loss, is an essential part of the calculation. The energy straggling may be described by energy distributions, Landau, Vavilov or Gaussian, depending on the amount of energy loss. In this work, the Vavilov regime for straggling is performed by a combination of Moyal and Airy functions. As far as the authors know this is the first time this approach was ever used to deal with the Vavilov straggling distribution. Comparison with SPACES, a well-known Stochastic code for gamma-ray yield profiling, is performed for a standard reference, the very thin 992 keV resonance of $^{27}Al(p,\gamma)^{28}Si$ nuclear reaction, showing a good agreement. Yield per layer versus the mean proton energy for that layer (which may be translated as depth), output provided by ERYA-Profiling, allowed the assessment of the different distribution functions, showing a good continuity between them.

Introduction

Methods of profiling in-depth heterogeneous samples by ion beam interactions have existed for decades. Among them, proton-gamma profiling, meaning the measurement of the yield of gamma-radiation coming from nuclear reactions produced by charged particles (namely protons) interacting with sample nuclei, has gained ground for the best depth resolution [1]. This is achieved by probing very thin resonances, with widths under 1 keV [usually from (p,γ) reactions] along the depth of the sample. If the resonance is isolated with yield value much higher than the background (integrated yield for proton energies lower than the resonance energy, E_R), the corresponding measured gamma-ray yield as a function of the proton energy translates directly into the mass fraction of the relevant element as function of the depth. This means mainly (p,γ) reactions in isotopes with atomic number below 30. Although widely used for more than fifty years for a variety of light isotopes, other methods of material analysis have replaced (p,γ) profiling, being the (p,γ) applications in recent years mainly related to hydrogen analysis as may be appreciated in IBA Proceedings (2000-2022) and in recent reviews [2,3]. In the context of resonant profiling, the pioneer work of Vickridge and Amsel and the development of the program SPACES must be mentioned [4-8].

ERYA-Profiling [9-11] performs gamma-profiling with non-isolated resonances and broad resonances (actually using the entire excitation function), which represents a wide generalization of the method to a larger number of elements and resonances which may be employed.

Due to the statistical nature of particle energy loss, large fluctuations can occur in the amount of energy deposited by a particle traversing an elemental medium. The fluctuations in relation to the mean energy loss, the energy straggling, are an important part of ERYA-Profiling calculation. They may be described by energy distributions, Landau, Vavilov or Gaussian, depending on the amount of energy loss. Actually, Landau and Gaussian approximations may be found as limits (for very small and very large energy losses, respectively) of the Vavilov approach.

Due to the complexity of the Vavilov analytical solution, leading to calculations which are computer-time consuming [12], different approaches have been used to include this distribution in Monte Carlo codes programs dealing with transport of charged particles trough matter [13-17].

We chose to follow the approach of Rotondi and Montagna [14], who derived several analytical expressions to cover the domain of energy loss where the Landau and Vavilov approximations are relevant. We found some continuity issues regarding the frontier between different functions, which motivated the development of several modifications. This was already mentioned in ref. 9. However, finding important to provide the details of our approach to the community dealing with code development of charged particle transport in matter, in this work we describe the Landau and Vavilov approximations implemented in ERYA-Profiling, as well as the integration method used to calculate the yield.

Also, in order to validate our approach we compare ERYA-Profiling calculations with those from SPACES, namely for the very thin 992 keV resonance of ^{27}Al(p,γ)^{28}Si.

1. Gamma Yield Numerical Integration

As may be seen in several publications [1, 9-10, 18-19], the gamma-ray yield of a relevant nuclear reaction, induced in a homogeneous sample by protons with an incident energy equal to E_0, may be written as follows, assuming there is no dispersion in the incident energy and in the energy loss,

$$Y(E_0,\theta) = 4\pi\,\epsilon_{\text{abs}}(E_\gamma) f_m f_i N_p N_{av} A^{-1} \int_0^{E_0} \frac{\sigma(E,\theta)}{S(E)}\,dE \qquad (1.1)$$

for a given element from the sample with mass fraction f_m, isotopic abundance f_i and atomic mass A. In equation 1.1 $\varepsilon_{abs}(E_\gamma)$ is the absolute efficiency of the detector for γ rays with energy E_γ, and $\sigma(E,\theta) = d\sigma/d\Omega$ is the differential cross-section for emission of a γ ray at angle θ to the incident ion direction. N_p and N_{av} are respectively the number of protons bombarding the sample and the Avogadro's number and $S(E)$ is the stopping power in units of energy per mass areal density.

If energy fluctuations and a mass fraction dependent on depth are assumed, the yield evaluation will be changed to:

$$Y(E_0,\theta) = 4\pi\,\varepsilon_{\text{abs}}(E_\gamma).N_{av}.f_i.A^{-1}\int_0^{E_0}\sigma\,(E,\theta).N_p(E).f_m(E)/S\,(E)\,dE \qquad (1.2)$$

Aiming at the simplification of the integration problem, ERYA-Profiling takes the following assumptions.

- It considers the sample as a composition of homogeneous layers, with mass fraction f_{mk}, where each layer is perpendicular to the beam direction.
- For each individual layer or integration layer k the variable E is approximately constant, equal to $\bar{E}_k$, which is the initial energy E_0 subtracted by the average energy loss of the protons till that specific layer, $\overline{\Delta E}_{0\to k}$.
- The stopping-power at an individual layer may be treated as constant, as the energy variation within each layer is small.

Using those three principles, the yield for a given element is represented by the following sum:

$$Y(E_0) = \sum_{k=1}^{n} Y_k\left(\overline{E}_k\right) \qquad (1.3)$$

where each partial yield may be calculated by:

$$Y_k\left(\overline{E}_k\right) = \varepsilon_{\text{abs}}(E_\gamma).N_{av}.A^{-1}.f_{mk}.f_i/S\left(\overline{E}_k\right)(\Delta E)_k N_p\int F(E)\sigma(E)dE \qquad (1.4)$$

where $F(E)$ refers to the proton energy distribution and the quantity ΔE_k represents the energy lost in layer k, which is related to:

$$\overline{E}_{k+1} = \overline{E}_k - (\Delta E)_k \qquad (1.5)$$

For each consecutive layer the beam energy will decrease until reaches zero or a cut-off energy.
The energy function, $F(E)$, is given by a convolution of three separated distributions:

$$F(E) = F_D(E) * F_{Beam}(E) * F_S(E) \qquad (1.6)$$

where $F_D(E)$ is the Doppler Distribution, proportional to the temperature, $F_{beam}(E)$ represents the beam initial energy dispersion or beam resolution, and $F_S(E)$, the Straggling Distribution, is the energy distribution resulting from the stochastic character of the energy loss suffered by the beam within the material.
Within plain mathematical rigor, the Doppler distribution is Maxwell type (which, for positive values, is similar to a Gauss Distribution) and the beam resolution may be considered a normal distribution. Since the first two terms of (1.6) may be assumed as Gaussian, they can be combined into a single Gaussian Distribution, that will be called the Thermal-Resolution Distribution, F_T:

$$F_D(E) * F_{Beam}(E) = F_T(E) \qquad (1.7)$$

Hence, we have the initial problem integration problem reduced to a two function convolution:

$$(F_T * F_S)(E) = F_T(E) * F_S(E) \tag{1.8}$$

since the convolution of two distributions can be evaluated by the integral:

$$(F_T * F_S)(E) = \int F_T(E')\, F_S(E - E')\, dE' \tag{1.9}$$

Plugin all these statements, the average cross-section value is calculable by the following double integral given by:

$$\sigma(\overline{E}_k) = \int_{-\infty}^{\infty}\int_{-\infty}^{\infty} F_T(E'')\, F_S(E' - E'')\sigma_j(\overline{E}_k - E')dE'dE'' \tag{1.10}$$

Due to the convolution symmetry, the integral may be evaluated by switching the variables of the distributions, obtaining the same result:

$$\sigma(\overline{E}_k) = \int_{-\infty}^{\infty}\int_{-\infty}^{\infty} F_T(E')\, F_S(E'' - E')\, \sigma_j(\overline{E}_k - E'')\, dE'dE'' \tag{1.11}$$

An approximation must be done for the numerical evaluation of (1.11) as the domains of integration are infinite. This implies the selection of a finite integration domain wide enough so that the integral of the distributions may be taken as equal to one.

An equivalent alternative to calculate (1.11) with infinite domains starts from the concept of average cross section as follows, calculated for finite domains.

$$\sigma(\overline{E}_k) \approx \langle\sigma(\overline{E}_k)\rangle = \frac{\int F_T(E'')\, F_S(E'-E'')\sigma(E_k-E'-E'')dE'dE''}{\int F_T(E'')\, F_S(E'-E'')dE'dE''} \tag{1.12}$$

Switching energy variables in eq. 1.12 will theoretically lead to the same result but, due to the asymmetry of the straggling distribution and the cut-off integration domain error, it is possible to obtain a small numerical difference between the two numerical evaluations.

All distributions cut-off were based on a 3-sigma approximation which will result in an error of 0.5% by the worst estimate.

2. Straggling Distributions (general)

The fluctuations in the energy loss may be characterized by the significance parameter κ, which is proportional to the ratio of mean energy loss to the maximum allowed energy transfer in a single collision with an atomic electron, ϵ_{MAX},

$$\kappa = \xi/\epsilon_{MAX} \tag{2.1}$$

$$\epsilon_{MAX} = \frac{2m_e\beta^2\gamma^2}{1+2\gamma\frac{m_e}{m_p}+\left(\frac{m_e}{m_p}\right)^2}\,[keV] \tag{2.2}$$

where m_e and m_p are the electron and projectile masses, respectively, β is the relativistic projectile velocity, v_p/c, and γ is the Lorenz factor, $\gamma = (1-\beta^2)^{-1/2} = E/m_p c^2$, being E the total energy of the particle (kinetic plus mass energy).

The parameter ξ comes from the Rutherford scattering cross section and is defined as:

$$\xi = 2\pi \left(\frac{e^2}{4\pi\varepsilon_0}\right)^2 \frac{{Z_1}^2 Z_2 N_A \rho x}{m_e \beta^2 c^2 A} = \frac{2.5496*10^{-10} {Z_1}^2 Z_2 n}{\beta^2}\,[keV] \tag{2.3}$$

where Z_1 and Z_2 are the atomic numbers of the projectile and medium respectively, N_A is the Avogadro´s number, and for the medium we have: ρ - density in g/cm^3, x - thickness in cm, A - atomic mass and n - number of atoms per area in units of 10^{15} at/cm^2.

The parameter κ measures the contribution of the collisions with energy transfer close to ϵ_{MAX}. For a given medium, κ tends towards large values if x is large and/or if β is small. Likewise, κ tends towards zero if x is small and/or if β approaches 1.

Generally, many collisions between the medium electrons and the incident particle occur during the traversal of the medium. If for each individual collision the energy transfer is small compared to the energy loss in the medium, the energy straggling may be described by a Gaussian distribution; this occurs for large values of κ (κ >22). If individual collisions make significant contributions to the energy loss in the medium, the straggling distribution is asymmetric; for very small values of κ (κ<0.01), the straggling is well described by the Landau distribution [20]; for 0.01 < κ < 22, the distribution derived by Vavilov [21] bridges the gap between the Landau and Gaussian distributions. Landau and Vavilov distributions are described as functions of the Landau variable defined by

$$\lambda = \frac{\Delta}{\xi} - 1 + \gamma_{EM} - \beta^2 - ln(\kappa) \tag{2.4}$$

where γ_{EM}=0.577 is the Euler-Mascheroni constant and Δ is equal to the difference between the average energy loss $\overline{\Delta E}$ and the actual energy loss ΔE, obtaining:

$$\Delta = \overline{\Delta E} - \Delta E \tag{2.5}$$

Since the energy loss is always a positive value, this means the following expression is positive:

$$\Delta E = \underbrace{\xi\left(\lambda + 1 - \gamma_{EM} + \beta^2 + ln(\kappa)\right)}_{\Delta} + \overline{\Delta E} > 0 \tag{2.6}$$

Combining the previous expressions together, the energy variable within the distribution domains is evaluated directly by:

$$E = \overline{E}_k - \Delta E = \overline{E}_k - \xi\left(\lambda + 1 - \gamma_{EM} + \beta^2 + ln(\kappa)\right) - \overline{\Delta E} \tag{2.7}$$

The probability distribution, $f(x, \Delta E)$, that a charged particle going through a distance x, suffers an energy loss between ΔE + dΔE is given by the transport equation [14,21]:

$$\frac{\partial f(x,\Delta E)}{\partial x} = \int_{\epsilon_{min}}^{\epsilon_{max}} \omega(\epsilon) f(x, \Delta E - \epsilon) d\epsilon - f(x, \Delta E) \int_{\epsilon_{min}}^{\epsilon_{max}} f(\epsilon) d\epsilon \quad (2.8)$$

where $\omega(\epsilon)$ is the probability density of energy loss per unit length, given:

$$\omega(\epsilon) = \frac{\xi}{x\epsilon^2}\left(1 - \frac{\epsilon\beta^2}{\epsilon_{max}}\right) \quad \text{for } \epsilon_{min} < \epsilon < \epsilon_{max} \quad (2.9)$$

and $\omega(\epsilon) = 0$ outside the previous defined interval.

Landau has derived his distribution by assuming $\epsilon_{min} = 0$ and $\epsilon_{max} = \infty$, obtaining a universal distribution depending only on the scaled energy-loss variable, λ. Vavilov used the maximum energy transfer as an upper limit, and indirectly (by the mathematical manipulation of equation 2.8) defined also a lower limit, described by equation 2.10; Vavilov's distribution is no longer universal, depending additionally on the particle velocity and on κ.

$$\epsilon_{min} = \frac{(1-\beta^2)I^2}{2mc^2\beta^2} \exp\left(\beta^2 + 2\frac{C}{Z} + \delta\right) \quad (2.10)$$

where I is the mean excitation energy of the medium, C/Z is the shell correction and δ is the density effect correction.

Vavilov followed Landau's approach, using as a first step the inverse Laplace transform of equation 2.8 and with additional manipulation arrived to:

$$f(\Delta E) d(\Delta E) = \frac{1}{\xi}\phi_v(\lambda, \kappa, \beta) d\lambda \quad (2.11)$$

with:

$$\phi_v(\lambda, \kappa, \beta) = \frac{exp\left(\kappa(1+\beta^2\gamma_{EM})\right)}{\pi} \int_0^\infty exp[\kappa f_1(y)] cos[y\kappa(ln(k) + \lambda) + \kappa f_2(y)]\, dy \quad (2.12)$$

with two auxiliary functions defined by:

$$f_1(y) = \beta^2\big(ln(y) + Ci(y)\big) - cos(y) - ySi(y) \quad (2.13)$$

$$f_2(y) = y\big(ln(y) + Ci(y)\big) + sin(y) + \beta^2 ySi(y) \quad (2.14)$$

These functions depend on sine and cosine integral functions defined by:

$$Si(y) = \int_0^y \frac{sin(u)}{u} du \quad (2.15)$$

$$Ci(y) = \int_{-\infty}^y \frac{cos(u)}{u} du = \gamma + ln(y) + \int_0^y \frac{cos(u)-1}{u} du \quad (2.16)$$

A full numerical implementation of Vavilov using those equations is not feasible due to the low convergence rates of the auxiliary functions, worsened by the oscillatory nature of the sine and cosine functions. Hence, several authors approximate the Vavilov distribution by others easier to implement numerically.

Taking the limit $\kappa \to 0$ of the Vavilov distribution, the two auxiliary functions (2.15) and (2.16) go to finite values, leading to a distribution that only depends on the Landau variable λ, the Landau distribution:

$$f(\lambda) = \frac{1}{\pi\xi}\int_0^\infty exp(-\pi\, x/2)cos\big(x(ln(x)+\lambda)\big)\, dx \tag{2.17}$$

When k>>1 the Vavilov Distribution goes to a Gaussian one:

$$f(\Delta,\kappa,\xi,\beta) = \frac{1}{\sqrt{\frac{2\pi\xi^2}{\kappa}\left(1-\frac{\beta^2}{2}\right)}}\, exp\left(\frac{-\left(\overline{\Delta E}-\Delta E\right)^2\kappa}{2\xi^2(1-\beta^2/2)}\right) \tag{2.18}$$

where the Gaussian mean is:

$$\mu = \overline{\Delta E} - \Delta E \tag{2.19}$$

and the Gaussian variance is given by:

$$\sigma^2 = \frac{\xi^2}{\kappa}\left(1-\frac{\beta^2}{2}\right) \tag{2.20}$$

3. Energy Distributions (this work)

3.1 Resolution-Thermal Distribution

The combined resolution-thermal distribution is evaluated on a finite integration domain that corresponds to a 3-sigma approximation. It means this domain is given by $[\mu - 3\sigma_T, \mu + 3\sigma_T]$, where μ is the mean value and σ_T the standard variation of the F_T distribution.

The combined standard variation is $\sigma_T = \sqrt{\sigma_{res}^2 + \sigma_{th}^2}$, where the beam initial energy standard deviation σ_{resl} is defined directly by a user input on the program interface, and the thermal standard deviation is evaluated from:

$$\sigma_{th} = 2.355\sqrt{\frac{2m_H kTE_k}{M}} \tag{3.1}$$

which is a consequence of the Maxwell average energy theorem. This may be evaluated from the initial energy at each individual sample layer. The equation also depends on the hydrogen's mass m_H, user-defined sample temperature T (Kelvin) and the molar mass of the layer M, which is evaluated internally by the ERYA-Profiling code using the databases loaded in memory.

Since the distribution energy variables (eqs. 1.9 and 1.10) are linear shifts from the mean energy the average thermal dispersion is set to zero.

3.2 Landau distribution

Physically, the Landau distribution models satisfactorily the energy straggling correspondent to the first layers of the sample.

When κ=0, the Landau distribution collapses to a single point, making a Dirac's Delta distribution. Due to coding constrains, the numerical Dirac's is implemented in a way to have the integral over his domain equal to one.

The numerical Dirac's Delta is defined only at x=0, where:

$$\delta(x) \approx \begin{cases} 1, |x| \leq 10^{-6} \\ 0, |x| > 10^{-6} \end{cases} \quad (3.2)$$

which assures:

$$\int_{-\infty}^{+\infty} \delta\,(x)dx = 1 \quad (3.3)$$

For values 0<κ<0.02, ERYA-Profiling implements the Landau distribution (eq. 2.17) by using the Wilkinson interpolation formulas, defining the finite integration domain of eq. 1.12 between λ=-3.4 and λ=25 [22].

3.3 Gaussian straggling distribution

The Gaussian straggling distribution is implemented for κ>22, by calculating from eq. 2.18 and defining the finite integration domain of eq. 1.12 as $[\mu - 3\sigma, \mu + 3\sigma]$, where μ and σ are given by eq. 2.19 and eq. 2.20 respectively. The Bohr formula for σ, giving values similar to eq. 2.20, is also available and may be selected at Advanced Options at the user interface.

3.4 Vavilov Distribution

For 0.02≤ κ <22, the energy straggling is described by the Vavilov theory. In order to implement his distribution, in this work we followed the approach of Rotondi and Montagna, but modifications had to be made to deal with discontinuities at the frontier of different functions they used to describe the Vavilov distribution in its entire domain. Some examples of discontinuities are given below and Table I resumes the situation regarding our options versus the ones of Rotondi and Montagna, which relates to different interval definitions and to the introduction of a new function. Note that table I differs slightly from the equivalent one of ref. 9, as we have proceeded with fine tuning of our distributions which led to different choices regarding the functions to employ.

Table I The different regimes and functions used to emulate the Vavilov distribution in the previous work of Rotondi and Montagna (where our work was based) and in our work.

Rotondi and Montagna	**Our work**
Moyal Function $0.02 \leq \kappa < 0.27$ Split in 3 intervals: $0.02 \leq \kappa < 0.12$ $0.12 \leq \kappa < 0.22$ $0.22 \leq \kappa < 0.29$	Moyal Function $0.02 \leq \kappa < 0.29$ Split in 3 intervals: $0.02 \leq \kappa < 0.11$ $0.11 \leq \kappa < 0.22$ $0.22 \leq \kappa < 029$
Edgeworth Expansion $0.29 \leq \kappa < 5$	Airy Function $0.29 < \kappa < 22$
Gaussian Distribution $\kappa > 5$	Gaussian Distribution $\kappa > 22$

With the exception of the alteration of a frontier value as shown in Table I, ERYA-Profiling implements the Moyal regime using exactly the expressions given by Rotondi and Montagna and defining the integration domain as $[\lambda_0, \lambda_{0.995}]$, where λ_0 corresponds to the λ value where the Moyal distribution starts to increase exponentially from zero and $\lambda_{0.995}$ is the λ value for which the integral of the distribution from λ_0 to $\lambda_{0.995}$ is equal to 0.995. These values are calculated by the formulas given also by Rotondi and Montagna.

Regarding the Airy function, we will explain later our motivation to use this function. We start now with the statement that, actually, Vavilov has shown that for $\kappa \geq 1$, his distribution could be approximated by a Airy function.

Defining the following parameters:

$$\eta = \frac{\left(1-\frac{2\beta^2}{3}\right)\xi}{(2k)^{\frac{2}{3}}} \tag{3.4}$$

$$a = \frac{(2k)^{\frac{1}{3}}\left(1-\frac{\beta^2}{2}\right)}{\left(1-\frac{2\beta^2}{3}\right)^{\frac{2}{3}}} \tag{3.5}$$

$$t = \frac{\overline{\Delta E}-\Delta E}{\eta} + a^2 \tag{3.6}$$

where all the quantities have been previously defined, and replacing on eq. 2.12 for k=1, we get a new function called the Airy-Vavilov distribution:

$$f(\eta, a, t) = \frac{1}{\eta\pi} exp(at - a^3/3) \int_0^\infty cos\,(ut + u^3/3)du \tag{3.7}$$

The Airy Function is oscillatory for negative values of its argument, and decay exponentially to positive values. Since the first zero occurs at t=-2.33811, it roughly corresponds to the value where that the Landau and Moyal distributions grow exponentially from zero (the λ_0 point).

The exponential term outside the integral of Airy-Vavilov's function for positive values (t>0) combined by the quick convergence of integral matches the long tail of the original Vavilov distribution.

Since the derivatives around the origin, including the function itself, are analytically evaluated using only the gamma function around the origin, it is possible to approximate the integral given on eq. 3.3 by the following power series:

$$Ai(t) = \frac{1}{\pi}\int_0^\infty cos(ut + u^3/3)\, du \approx a_0 + a_1 t + a_2 t^2 + \ldots = \sum_{n=0}^{\infty} a_n\, t^n \qquad (3.8)$$

where each coefficient can be calculated by a recurrence sequence:

$$a_0 = \frac{1}{3^{2/3}\Gamma(2/3)};\ a_1 = \frac{-1}{3^{1/3}\Gamma(1/3)};\ a_2 = 0;\ a_n = \frac{a_{n-3}}{n(n-1)}, n \geq 3 \qquad (3.9)$$

For function arguments $|t|>3$ about 100 terms are required to approximate the function value accurately, but for large function arguments, which corresponds to the long tail of Vavilov Distribution, an asymptotic expansion may be used instead, requiring the sum of fewer terms:

$$Ai(t) = \frac{1}{\pi}\int_0^\infty cos(ut + u^3/3)\, du \approx \frac{exp\left(\frac{-2}{3}t^{3/2}\right)}{\sqrt{4\pi}t^{1/4}}\left(\sum_{n=0}^{\infty}\frac{(-1)^n\Gamma(n+5/6)\Gamma(n+1/6)(3/4)^n}{2\pi n! t^{3n/2}}\right) \qquad (3.10)$$

For t>5 two sum terms are enough, leading to:

$$Ai(t) = \frac{1}{\pi}\int_0^\infty cos(ut + u^3/3)\, du \approx \frac{exp\left(\frac{-2}{3}t^{3/2}\right)}{\sqrt{4\pi}t^{1/4}}\left(1 - \frac{5}{48t^{3/2}}\right) \qquad (3.11)$$

While for -2.33841 < t < 5 ERYA-Profiling employs eq. 3.8 with recurrence terms (eq. 3.9), for $t \geq 5$, the approximation of eq. 3.10 is used. Otherwise, for larger negatives values of t, the function is set to zero.

The next step is to find a proper function domain to ensure the adequate approximation of Vavilov-Airy distribution. We start by taking the first zero of the Airy Function, t_0 = -2.33811, and use equations 2.4 and 3.6 to find the corresponding value of the Landau variable:

$$\lambda_0 = \frac{(t_0 - a^2)\eta}{\xi} - 1 + \gamma_{EM} - \beta^2 - ln(k) \qquad (3.12)$$

A similar reasoning should find $\lambda_{0.995}$ using a similar equation:

$$\lambda_{0.995} = \frac{(t_{0.995} - a^2)\eta}{\xi} - 1 + \gamma - \beta^2 - ln(k) \qquad (3.13)$$

where $\lambda_{0.995}$ has a broader meaning than before, being such as the integral of the distribution from λ_0 to $\lambda_{0.995}$ is close to 0.995.

In order to find $t_{0.995}$, we defined the corresponding energy value $E_{0.995}$ as given by the average energy $\bar{E}$ plus two terms: the first is the energy interval between $\bar{E}$ and E_0 (the energy corresponding to t_0)

and the second is the energy interval between $\bar{E}$ and E_{max}, the energy corresponding to the maximum of the distribution. We can write:

$$E_{0.995} = \bar{E} + (\bar{E} - E_0) + (\bar{E} - E_{max}) \tag{3.14}$$

Taking into consideration the asymmetry of the distribution (see fig.1), which, in consequence, determines that $\bar{E} > E_{max}$, at first impression the second term seems unnecessary for the definition of $E_{0.995}$. However, for low values of κ, where the asymmetry is very pronounced, adding to $\bar{E}$ only the first term in eq. 3.14, leads to an energy value which does not fulfill the condition of getting the integral of the distribution close to 0.995. Besides, the term $\bar{E} - E_{max}$ decreases as κ increases and the distribution gets more symmetrical.

Note that eq. 3.6 may be written as:

$$t = \frac{\bar{E}-E}{\eta} + a^2 \tag{3.15}$$

Using eq. 3.15, we may express t_0, t_{max} and $t_{0.995}$ in terms of E_0, E_{max} and $E_{0.995}$, and using eq. 3.14 we get:

$$t_{0.995} = 3a^2 - t_0 - t_{max} \tag{3.16}$$

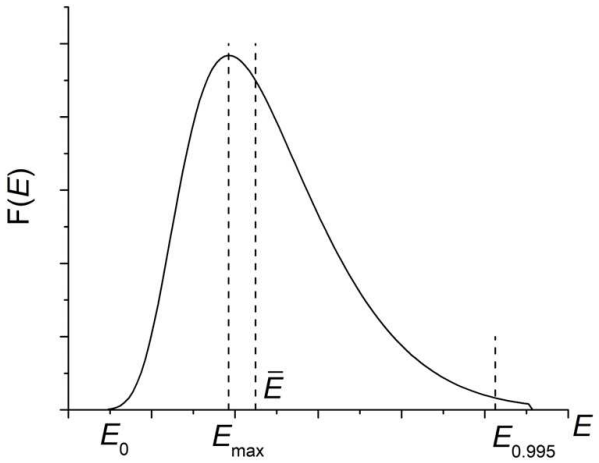

Fig.1 Scheme of an asymmetrical distribution, showing the condition $\bar{E} > E_{max}$ and the energy intervals mentioned in the text for the definition of $E_{0.995}$.

The value of t corresponding to the maximum of the distribution, t_{max}, is calculated from the derivative of $Ai(t)$ given by eq. 3.10, using the Golden Search Bissection Algorithm with t_0 = -2.33840 and $t_\infty = a^2$ as initial boundaries, where t_∞ is the t_{max} value for a symmetrical distribution. An accurate numerical integration of the Airy-Vavilov distribution was made using the software Maxima to compare with the boundary algorithm described here. It was shown that for k>0.3 the calculated $t_{0.995}$ lead to a value of the distribution integral equal or higher than 0.991.

Having obtained the boundary values of λ for the straggling distribution (Landau, Vavilov or Gaussian), since the domain of a convolution of two functions adds the domains of the two functions, the integration of the straggling (Landau, Vavilov or Gaussian) distribution convoluted with the resolution-thermal distribution is performed within a domain given by:

$$x_s, y_s \in [\lambda_0 - 3\sigma_T, \lambda_{0.995} + 3\sigma_T] \qquad (3.17)$$

For the numeric integration the user may define (at the user interface) the number of energy intervals to define the Landau, Moyal and Gaussian distributions, and the number of λ intervals to define the Airy distribution, io order to fine-tune the compromise between precision and computation time.

Rotondi and Montagna [14] describe the Moyal regime in terms of three different functions, with corresponding frontier κ values. The alteration of the frontier value κ = 0.12 by κ = 0.11 (see Table I) was done to improve the continuity of the distributions defined by functions 1 and 2.

Another problem appeared at the frontier value κ =0.29, where the maximum of the Edgeworth Expansion is displaced in relation to the maximum of the Moyal function (see Fig. 2a). In the same figure, it can be seen that the maximum of the Airy function is closer to the Moyal maximum, although with a lower amplitude. Note that the amplitude problem gets solved by normalization.

The displacement of the maximum of the Edgeworth distribution is due to the fact that it coincides with the average energy, behavior not expectable for low k values. The Airy distribution shows a good behavior at these values of κ and represents more accurately the gradual shift of the maximum of the distribution going slowly to the average energy as the κ-value increases.

Hence, we decided to use the Airy function instead of the Edgeworth Expansion. In order to improve the match between the maxima of the Moyal distribution near κ =0.29 and the Airy distribution, and also the continuity, we calculated the Airy distribution, in the κ-value range from 0.29 to 0.39, using a constant value of κ=0.39, and beyond 0.39 the calculation was done for the actual value of κ. The match improvement is shown in Fig. 2b. The continuity is discussed in relation to Fig. 5, featuring the yield per layer versus the average energy in each layer (equivalent to depth) at given proton incident energies.

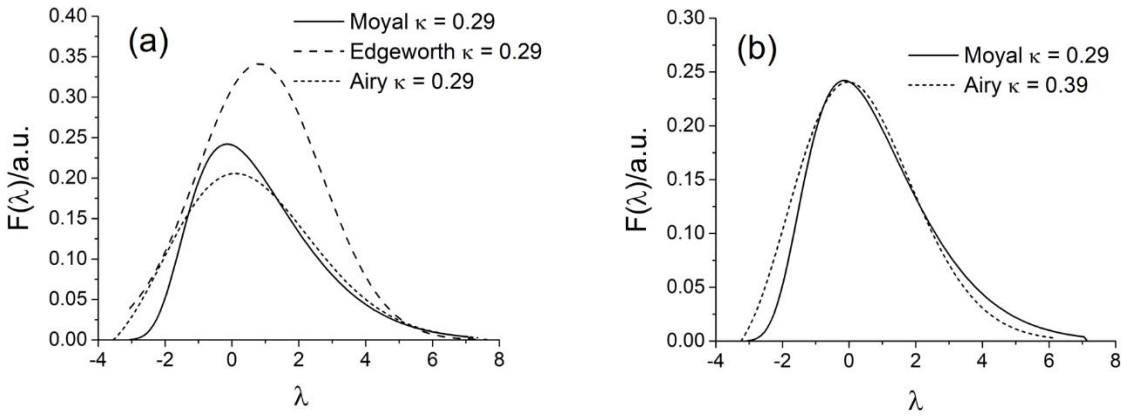

Fig. 2 a) Continuity of the straggling distributions Moyal, Edgeworth and Airy at κ =0.29, showing the displacement of the maximum of the Edgeworth in relation to Moyal and the better match between the maxima of Moyal and Airy distributions; b) calculating Airy for κ=0.39 improves the referred mach.

4. Comparison of ERYA-Profiling with SPACES

In order to assess the correctness of our approach, namely concerning the distributions, we decided to test it for extreme conditions (very thin resonances and well defined beam initial energy) by comparing ERYA-Profiling calculations with SPACES [2,8].

Although not in the public domain, SPACES is a code which is considered to describe adequately the interaction of accelerated ions with materials; within a stochastic approach ion energy loss and energy straggling are taken in detail. The developed stochastic theory assumes a $1/E^2$ energy loss distribution for a single ion-atom collision, as for Landau and Vavilov straggling distributions, but with different truncation and summation/integration rules, defining both a minimum and maximum energy transfer. This way, the distribution function is normalisable and has all moments defined. SPACES confirmed [4] an effect observed experimentally, for a beam with a very defined incident energy, on the gamma yield corresponding to sharp resonances, the so-called Lewis Peak [23]. This peak above the asymptotic yield is assumed to be caused by the stochastic nature of the energy loss. Having lower values of energy loss higher probability, projectiles with incident energy close or slightly higher than the resonant energy will have most probably, after the interaction with the first material layers, an energy equal to the resonant energy, leading to a high gamma-ray yield. As the incident energy increases, increasing also the energy dispersion within the material, this condition is no longer valid.

In Fig. 3 we apply ERYA-Profiling and SPACES for the simulation of the gamma-yield pertaining to the 1670 keV line of the $^{27}Al(p,\gamma)^{27}Al$ reaction at the 992 keV proton energy resonance, with a natural width of 70 eV. The sample is pure aluminum with 50 $\mu g/cm^2$ thickness and the beam incident energy is assumed to have a dispersion of 0.1 keV. Proton incident energies from 991 to 999 keV, with a 0.1 keV step, were used for the ERYA-Profiling simulation. A step ten times smaller was used by SPACES. SPACES results were normalized to ERYA ones at 996 keV. For ERYA-Profiling there are two curves. One using the version of ERYA-Profiling with straggling distributions as described in the previous paragraphs, namely using the Airy function; the other using the entire recipe of Rotondi and Montagna (as described in table 1) with the Edgeworth expansion.

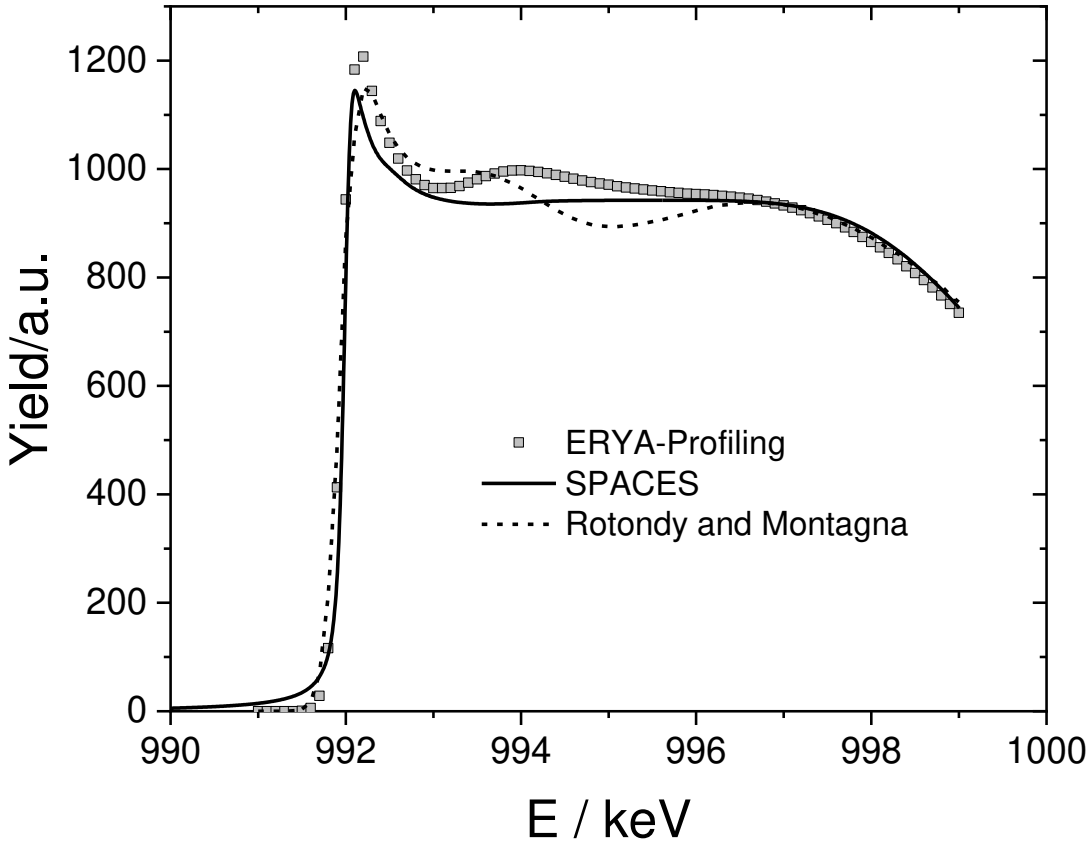

Fig. 3 Yield, obtained by the ERYA-Profiling and SPACES codes, of the 1670 keV line of the $^{27}Al(p,\gamma)^{28}Si$ reaction for proton energies from 991 to 999 keV, scanning the 992 keV (70 eV width) resonance across a pure aluminum sample with 50 $\mu g/cm^2$ thickness. The beam incident energy is assumed to have a dispersion of 0.1 keV. The Rotondi and Montagna curve pertains to a calculation done by ERYA employing the entire recipe of those authors, while the ERYA-Profiling curve uses the straggling treatment as described in this work.

As may be observed, both SPACES and ERYA simulations follow the same trend including the Lewis peak. Employing ERYA-Profiling an analytical approach, the prediction of an effect of stochastic nature might not seem expectable. However, for the first layers Vavilov/Landau distributions are very asymmetric, favoring small energy losses. Hence, the mathematics of the yield calculation should lead to a Lewis peak. And so it does.

Fig. 3 also shows features in ERYA calculations not existent for SPACES. For the Rotondi and Montagna approach there is a clear oscillation. The replacement of the Edgeworth expansion by the Airy function (and other adjustments mentioned before) introduces a big improvement. Still, a second lower and broader peak is present in the ERYA-Profiling curve. We believe there is no physical explanation for this peak which is related to a slight discontinuity (still remaining after an effort to reduce it to a minimum, as explained below) between the third Moyal function and the Airy function. For very sharp resonances and very defined incidence energy (necessary conditions to obtain experimentally a Lewis peak), we demonstrate in the appendix that the convolution between the Vavilov straggling distribution and the Lorentzian resonant distribution, leads to a yield around the

resonance which is higher than the asymptotic yield. The broad peak is again a consequence of the convolution as shown in the appendix.

As expected, the Lewis peak disappears as the beam dispersion and the resonance width are increased, as shown in Fig. 4 a) and b) and we point out that the same happens for the second peak. Believing, however, that this peak is a mathematical artifact, we note that this does not hinder the performance of ERYA-Profiling in terms of applied analytical work, as in practice the Lewis Effect is not routinely observed, since ion beam energy resolution is seldom of the few hundred eV necessary.

As ERYA-Profiling provides an output of the mean energy and the yield per layer (among other parameters calculated for each layer) a study of the yield per layer for a given incident energy may be performed which shows in more detail the role of the different straggling distributions.

In fig. 5 the yield per layer versus the mean proton energy for that layer (which may be translated as depth), pertaining to the same simulation exercise as shown in Fig. 3, is presented for different incident energies. Energy loss grows from right to left and, for each incident energy, the κ values at which the different distribution functions start to play a role are indicated. The frontier, between the Moyal and Airy distributions at $\kappa = 0.29$ shows a good continuity between these two regimes. Note that no discontinuity is seen in the frontiers of the different Moyal functions at $\kappa = 0.11$ and $\kappa = 0.22$.

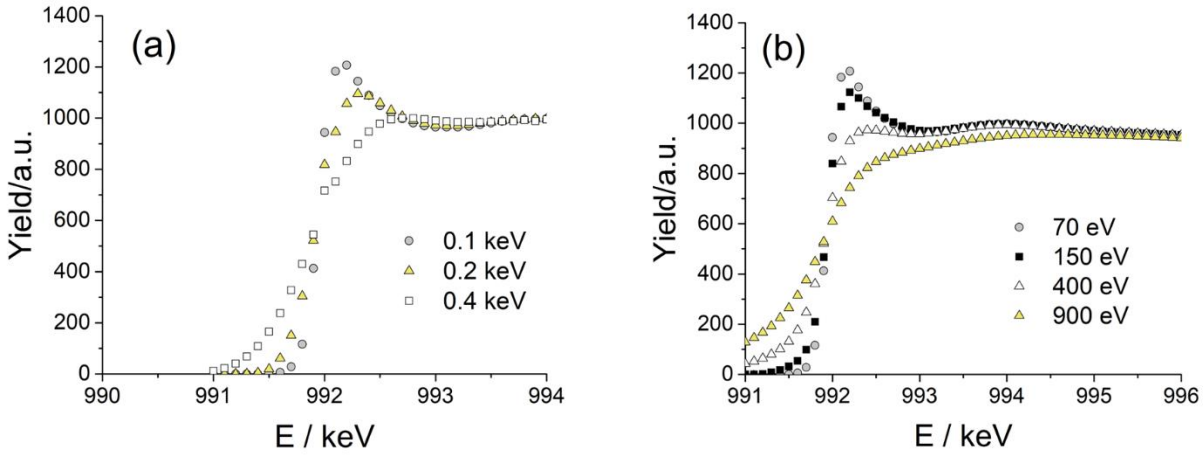

Fig. 4 The peaks seen in the ERYA-Profiling curve (fig.3) are a consequence of calculating for very sharp resonances and very defined incidence energy; with increased incident energy dispersion in a) and resonance width in b) these peaks disappear.

5. Conclusions

The Landau/Vavilov approximations implemented in ERYA-Profiling, as well as the integration method used to calculate the gamma-ray yield were presented. The Vavilov regime for straggling is performed by a combination of Moyal and Airy functions. As far as the authors know, ERYA-Profiling is the first code to employ this treatment of the Vavilov regime for straggling.

A detailed simulation was done for the gamma-ray yield of the 1670 keV line of the $^{27}Al(p,\gamma)^{28}Si$ reaction for proton energies from 991 to 999 keV, scanning the 992 keV (70 eV width) resonance across a pure aluminum sample with 50 μg/cm^2 thickness. ERYA-Profiling results clearly produce a Lewis peak of comparable amplitude and width to those calculated by SPACES for the 992 keV $^{27}Al(p,\gamma)^{28}Si$ resonance. To our knowledge this is the first calculation of a Lewis peak using Vavilov straggling, and it would be interesting to make a systematic comparison of the amplitude and width of Lewis peaks predicted by ERYA, with those predicted by the stochastic theory [24].

Yield per layer versus the mean proton energy for that layer (which may be translated as depth), output provided by ERYA-Profiling, allowed the assessment of the different distribution functions, showing a good continuity between them.

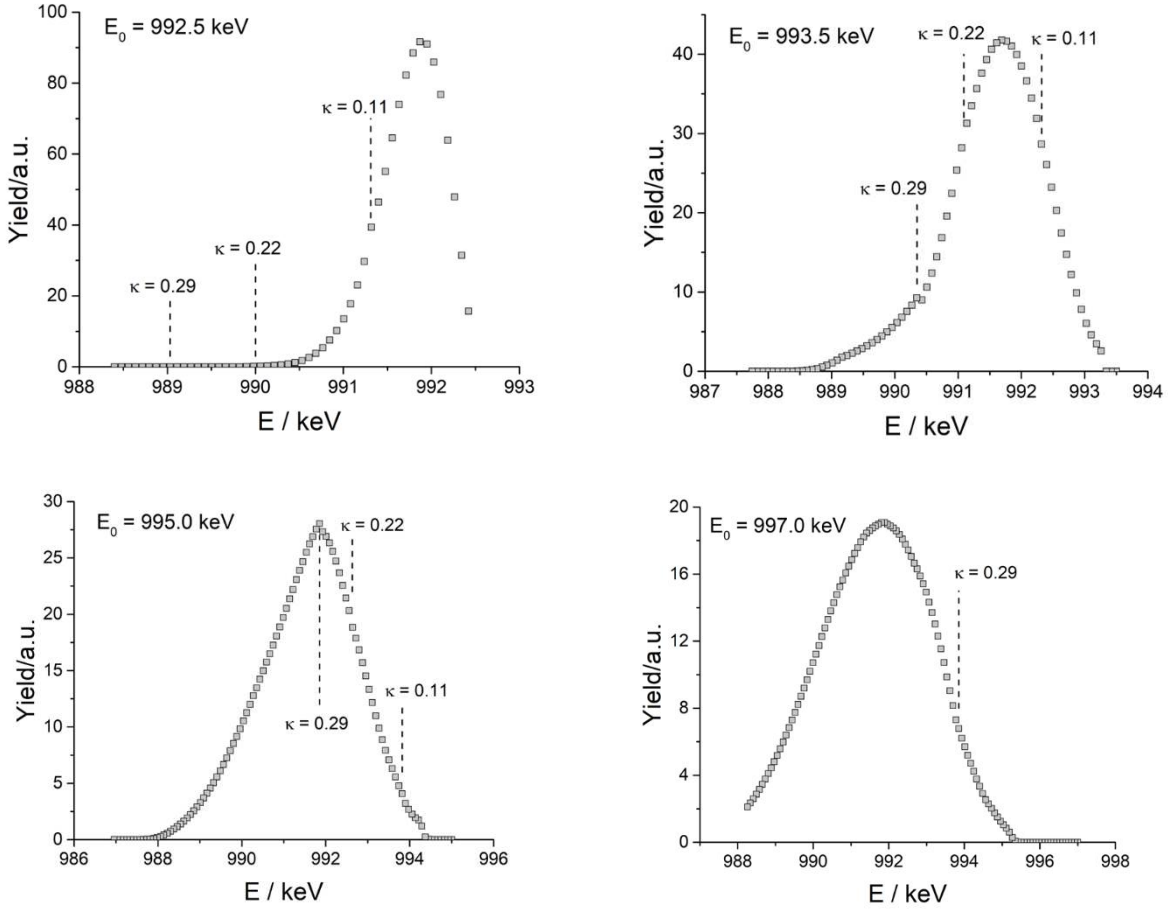

Fig.5 Yield per layer versus the average energy in each layer (equivalent to depth) at given proton incident energies; κ values related to the frontier between different distribution functions are indicated so that continuity may be assessed.

6. Acknowledgements

We are grateful to Prof. I.C. Vickridge for the SPACE results he kindly provided for us and for the profitable discussions with him. This work has been financially supported by Fundação para a Ciência e a Tecnologia through the LIBPhys funding UID/FIS/ 04559/2020,

Data Availability Statement

No Data Associated in the manuscript.

7. References

[1] International Atomic Energy Agency TECDOC No. 1822 (2017), Vienna. ISBN:978-92-0-106317-5, Chap. 2
[2] Y.Wang and M. Nastasi (Eds.), Handbook of Modern Ion Beam Material Analysis, 2nd Edition, 2009, ISBN-13: 978-1605112169
[3] H. Fritzsche, J. Huot, D. Fruchart (Eds.), Neutron Scattering and Other Nuclear Techniques for Hydrogen in Materials, Springer (2016), ISBN: 978-3-319-79429-7
[4] B. Maurel, G. Amsel and J.P. Nadai, Nucl. Instrum. Methods Phys. Res. 197 (1982) 1, https://doi.org/10.1016/0167-5087(82)90111-9
[5] I.C. Vickridge and G. Amsel, Nucl. Instrum. Methods Phys. Res. B 45 (1990) 6, https://doi.org/10.1016/0168-583X(90)90772-M
[6] I. Vickridge and G. Amsel, Nucl. Instrum. Methods Phys. Res. B 45 (1990) 16, https://doi.org/10.1016/0168-583X(90)90774-O
[7] I. Vickridge and G. Amsel, Nucl. Instrum. Methods Phys. Res. B 64 (1992) 687, https://doi.org/10.1016/0168-583X(92)95559-A
[8] I.C. Vickridge and G. Amsel, Nucl. Instrum. Methods Phys. Res. B 108 (1996) 403, https://doi.org/10.1016/0168-583X(95)01163-3
[9] V. Manteigas, J. Cruz, M. Fonseca, A.P. Jesus, Nucl. Instrum. Methods Phys. Res. B 502 (2021) 142-149, https://doi.org/10.1016/j.nimb.2021.06.006
[10] V. Manteigas, L. Martins, J. Cruz, M. Fonseca, A.P. Jesus, Computer Physics Communications 275 (2022) 108307, https://doi.org/10.1016/j.cpc.2022.108307
[11] J. Cruz, M. Fonseca, D. Galaviz, A. Henriques, H. Luís, J. Machado, P. Teubig, P. Velho, V. Manteigas and A. P. Jesus, Eur. Phys. J. Plus 136 (2021) 969, https://doi.org/10.1140/epjp/s13360-021-01954-3,
[12] Stephen M. Seltzer, Martin J. Berger, "Studies in Penetration of Charged Particles in Matter", (1964), Nuclear Science Series Report Number 39, p. 187, BibCode 1964spcp.conf..187S
[13] B. Schorr, Comput. Phys. Commun. 7 (1974) 215-24, https://doi.org/10.1016/0010-4655(74)90091-5
[14] A. Rotondi and P. Montagna, Nucl. Instrum. Methods Phys. Res. B 47 (1990) 215, https://doi.org/10.1016/0168-583X(90)90749-K
[15] O. Chibani, IEEE Transactions on Nuclear Science 45 (1998), 2288, https://doi.org/10.1109/23.725266
[16] Armando Lazaro Alaminos-Bouza, 2015, ffhal-02480024f
[17] S.K.L.Sjue, R.N.George and D.G.Mathews, Nucl. Instrum. Methods Phys. Res. B 407 (2017) 270, https://doi.org/10.1016/j.nimb.2017.06.013
[18] R. Mateus, A. P. Jesus, J. P. Ribeiro, Nucl. Instrum. Methods Phys. Res. B 219 (2004) 519, https://doi.org/10.1016/j.nimb.2004.01.114
[19] ERYA-Bulk webpage, https://sites.fct.unl.pt/nuclear/software/erya-bulk
[20] L. Landau, J. Phys. (USSR) 8 (1944) 204.
[21] V. Vavilov, Sov. Phys. JETP 5 (1957) 749.
[22] D.H. Wilkinson, Nucl. Instrum. Methods Phys. Res. A 383 (1996) 513, https://doi.org/10.1016/S0168-9002(96)00774-7
[23] W. L. Walters, D. G. Costello, J. G. Skofronick, D. W. Palmer, W. E. Kane, and R. G. Herb Phys. Rev. Lett. 7 (1961) 284, https://doi.org/10.1103/PhysRevLett.7.284
[24] I.C. Vickridge and G. Amsel, Nucl. Instrum. Methods Phys. Res. B 85 (1994) 566, https://doi.org/10.1016/0168-583X(94)95884-X

Appendix – The Vavilov – Lorentzian Convolution and the Lewis Peak

Let us consider a homogeneous material of infinite thickness. The gamma-yield corresponding to a single resonance at incident energy E_0 may be evaluated by:

$$Y(E_0) = Y_0 \int_0^{E_0} \sigma\,(E)dE \tag{A.1}$$

where the cross-section function may be described by a Breit-Wigner (Lorentzian) function:

$$\sigma(E) = \frac{\sigma_{max}}{(1+\epsilon^2)} : \epsilon = \frac{2(E-E_R)}{\Gamma} \tag{A.2}$$

The parameter σ_{max} is the maximum value of the resonance, and E_R and Γ are the resonance energy and the width of the resonance, respectively. Performing the integral under the assumptions that $E_0 = \infty$ and $(E_R - E) >> \Gamma$ one obtains, the asymptotic yield:

$$Y(E_\infty) = \frac{Y_0 \sigma_{max} \pi \Gamma}{2} \tag{A.3}$$

Considering that the beam incident energy has an uncertainty (beam resolution) that we may assume to be gaussian with variance Ω^2, we will have the convolution of the beam resolution and the Lorentzian and the yield at a projectile energy E may be given by:

$$Y(E) = \int_{-\infty}^{+\infty} \frac{1}{\sqrt{2\pi\Omega^2}} \frac{\sigma_{max}\Gamma^2}{4(E_R-E\prime)^2+\Gamma^2} exp\left(\frac{-(E-E\prime)^2}{2\Omega^2}\right) dE' \tag{A.4}$$

Defining

$$t = \frac{E-E\prime}{\sqrt{2\Omega^2}} \qquad \text{and} \qquad \Delta_R = \frac{E_R-E}{\sqrt{2\Omega^2}} \tag{A.5}$$

we may express the integral (eq. A.4) as a Voigt distribution:

$$Y(E) = Y_0 \int_0^E \sigma\,(E)dE = \frac{Y_0 \sigma_{max}\Gamma^2}{4\sqrt{\pi}} \int_0^{\infty} \int_{-\infty}^{+\infty} \frac{e^{-t^2}}{(\Delta_R-t)^2+\Gamma^2/4} dt\, d\Delta_R \tag{A.6}$$

Due to straggling, the projectile energy is not well defined, and an energy distribution must be considered. As may be perceived from fig. 5, for incident energies close to the resonance energy, the straggling distribution is the Landau distribution. Unfortunately its convolution with the resonance Lorentzian one has not an analytical solution. However, with some approximations, there is a solution (see below) if the Airy function is used. The Airy and Landau distributions share the characteristic of asymmetry, which seems to be a key ingredient to obtain peaks above the asymptotic yield. Note that if a gaussian distribution were assumed for straggling, similar equations to A.4 and A.6 would be obtained (being Ω^2, in that case, the combined variance of beam resolution and straggling). Since the Voigt distribution is a strict increasing function, the yield evaluated for any energy value would be smaller than the asymptotic yield.

Introducing the Airy function, attending to eq. 3.7 and eq. A.6, the yield will be given by:

$$Y = Y_0 \int_0^{\mathrm{E}} \sigma\,(E)dE = \frac{Y_0 \sigma_{MAX}\Gamma^2}{4\sqrt{\pi}\eta\pi} \int_0^{\mathrm{E}} \int_{-\infty}^{+\infty} \int_{-\infty}^{+\infty} \int_0^{+\infty} \frac{e^{-t^2} e^{au-a^3/3} cos(vu+v^3/3)}{(\Delta_R-t)^2+\Gamma^2/4} dt\, du\, dv\, d\Delta_R \tag{A.7}$$

The integral cannot be evaluated analytically, but it is possible to make some tricks and approximations that will prove the statement that the convolution between the Vavilov distribution and the Lorentzian cross section distribution can explain the Lewis effect.

The most obvious is to set η=1 due to (3.7) which normalize the integral (eq. A.7). Also, the integral of the Airy function around the positive real axis is given [The Handbook of Mathematical Functions, Section 10.12] by:

$$\int_0^\infty \int_0^\infty cos\,(vu + v^3/3)dudv = \frac{\pi}{3} \tag{A.8}$$

This means that the integral in eq. A.7 is maximized in a way that ηπ=1.

Furthermore, the two integrals related to t and Δ_R, which cannot be analytically evaluated may be approximated considering:

$$\left|\frac{e^{-t^2}}{(\Delta_R - t)^2 + \Gamma^2/4}\right| \leq \left|e^{-t^2}\right| \cdot \left|\frac{1}{{\Delta_R}^2 + \Gamma^2/4}\right| = e^{-t^2} \cdot \frac{1}{{\Delta_R}^2 + \Gamma^2/4} \geq 0, \forall t \in R \tag{A.9}$$

Then the integrals related to t and Δ_R can be evaluated which gives for $E = E_R$:

$$Y(E_R) \approx Y_\infty \int_0^\infty \int_0^{+\infty} e^{au - a^3/3} cos(vu + v^3/3)\, dudv \tag{A.10}$$

The more recent versions of *Mathematica* can handle the complicated integral (eq. A.10), considering that the exponential term $e^{-a^3/3}$is maximized as $\left|e^{-a^3/3}\right| \leq 1$, leading to:

$$Y(E_R) \approx \frac{4}{3} Y_\infty \tag{A.11}$$

by taking the approximations η=1, and a=0. Note that a=0 implies a projectile incident energy close to the resonant energy [low energy loss and low κ values (eq. 3.5)].

This means that, if we accept the Airy function as an approximate model of the Landau function, we may conclude that for incident energies close to the resonant energy and for sharp resonances, the yield around the resonance energy will be around 33% higher than the asymptotic yield at higher energies, explaining the Lewis Peak.

Additionally, in the regime of κ values where the Airy function is employed by ERYA-Profiling to describe the straggling, the condition will be a>0 and a fraction smaller than 4/3 would be obtained for A.11, but for the smallest values of the parameter a compatible with the regime, the fraction would be above 1, explaining the second peak (fig.3).

4

CONCLUSIONS AND FUTURE WORK

ERYA-Bulk and ERYA-Profiling are two complex programs designed to perform PIGE analysis for homogeneous and heterogeneous samples, respectively. Both programs share common features related to data management, while their physical models and related features are different.

It was a technical choice to make two specific programs for each kind of PIGE analysis and justified by the physical nature of the problem. Bulk sample analysis is expected to be fast, and ERYA-Bulk uses a simpler physical model which assumes that straggling and beam resolution effects are negligible (as verified during the IAEA comparative exercise – first paper of Chap.3), and the yield calculation is a straightforward integration of the excitation function.

On the other hand, PIGE profiling analysis quantifies the sample in terms of concentrations versus depth. Since the major contributions to the yield are from resonances and most measurements of depth profiling occur in a surface layer (the profiled sample being too thin to stop the beam), the straggling effects combined with the finite resolution of the beam will deviate from the ideal case of the bulk analysis. Therefore, the yield calculation on ERYA-Profiling must include the convolution of the excitation function with energy distributions related to straggling and beam resolution, implying mathematically a multiple integration problem.

The goals of this thesis work were to upgrade and improve previous versions of ERYA, implementing the programs ERYA-Bulk and ERYA-Profiling following requirements concerning portability, improved input/output, modular approach, refined version of profiling and distributions therein. The existing programs fulfill these requirements:

- Portability was verified by compiling the codes in different operating systems such as Windows, Mac OSX and Linux and by applied work done by different users (mainly the ERYA-Bulk version).

- Support of different types of data files was implemented, also in compliance with IAEA format data standards.
- The modular approach has already been useful by simplifying the development of the codes (mainly the ERYA-Profiling version).

In relation to a refined version of profiling, the ERYA-Profiling code aimed at:

- use of the entire excitation function besides the resonances of interest to perform resonant or non-resonant depth profiling;
- replacement of experimental resonances by fitted Briet-Wigner ones or resonance strengths;
- improved energy distributions.

The computational performance of the ERYA- Profiling code was assessed in the fourth paper of Chap. 3.

ERYA-Profiling performance related with resonant depth-profiling may be assessed by the exercises made in second and fourth papers of Chap. 3. From these exercises we concluded:

1. A thin resonance superimposed on a broader and weaker resonance, belonging to the excitation of $^{9}Be(p,\gamma)^{10}B$ reaction was used to scan a Be thin film and determine its thickness and uniformity. Results obtained have shown that a full treatment of the straggling is necessary to have sensibility to surface modifications, as an oxide layer. A simulation with only Gaussian straggling misses the existence of a BeO layer of 4.5×10^{17} at. /cm^2, while a full straggling treatment is meaningful sensitive to 1.0×10^{17} at/cm2.
2. Depth profiling by resonant scanning was performed on Al implanted (energy 140 keV, nominal fluency $5x10^{17}$ at/cm2) in Ti, using the 1683 keV resonance of the $^{27}Al(p,p'\gamma)^{27}Al$ nuclear reaction. The 1664 keV of the same reaction did not interfere with the scanning. ERYA-Profiling obtained the best fit for a depth profile Gaussian up to the maximum but enlarged for deeper distances from the surface, for a total amount of $5.4x10^{17}$ at/cm2. Again, a Vavilov approach for the straggling was necessary to describe the experimental results.
3. A conceptual problem to assess the issue of uniqueness of response in case of contribution from two resonances was designed featuring fluorine in tungsten, using the 1345 keV resonance of the $^{19}F(p,p'\gamma)^{19}F$ nuclear reaction, E_γ = 197 keV. Three fluorine profiles were defined wide enough to guarantee the contribution to the yield of the 1373 keV resonance. A clear distinction in the gamma-yield results of the different configurations was shown. Additionally, a general conclusion may be drawn: taking into consideration that some layers are scanned only by one of the resonances and that in addition to yield in function of incident energy, ERYA-Profiling also provides an information log

which allows to quantify the contribution of each resonance, we believe that in most cases of multiple resonance contribution the user will be able to find a unique answer regarding the depth profile.

4. A rather demanding case was presented concerning PIGE profiling of Al, based on a resonance of the $^{27}Al(p,p'\gamma)^{27}Al$ reaction, taking also into account the whole excitation function, showing good sensitivity to the thickness of AlN films deposited on thick sapphire and to modifications larger than 10% in the stoichiometry of the first surface layers.

In relation to non-resonant depth profiling employing the whole excitation function, a conceptual exercise was presented in the third paper of Chap.3. Insight into fluorine distributions, for a depth resolution from 1 to 5.5 μm, in a given sample from comparison between the calculated yield and corresponding measured gamma-ray yield was demonstrated. This allows to handle specific problems where high energy to go deeper into the sample and low resolutions are required.

The full straggling treatment mentioned earlier meant the implementation of Landau, Vavilov and Gaussian distributions, called upon by the code according to the energy lost by the beam.

The Rotondi-Montagna implementation of the Vavilov distribution (including Moyal and Edgeworth distributions) was chosen, but several issues had to be dealt with, issues driven by the discontinuity of the Moyal distributions (that still adapt fine with Landau) and the Edgeworth distributions (which only add an asymptotic expansion of a correction for the Gaussian distribution). The unmatching between Moyal and Edgeworth distributions and the abnormal oscillations caused by it, for situations involving sharp resonances with middle depth contributions, are shown in the fifth paper of Chap. 3. The chosen solution was to replace the Edgeworth distribution by the Airy function (suggested by Vavilov in earlier publications as a fair approximation), which required hard mathematical work to implement an adequate and fast numerical approximation. The accomplished improvement in continuity among distributions is also shown in the fifth paper of Chap. 3, along with the verification that the Airy function removed the abnormal oscillations seen with the Edgeworth function.

For sharp resonances seen with a beam with very good resolution such as the 992 keV, 70 eV width, resonance of the $^{27}Al(p,\gamma)^{28}Si$ reaction (also in the same paper), ERYA-Profiling calculation of the yield shows a Lewis Peak, as also predicted by SPACES. However, an unexpected small and broad peak appears at some distance (in terms of energy) after the Lewis Peak. The broad peak seems to be a consequence of the convolution between the excitation function and the Airy function as shown in the appendix of the same paper.

Noting that this peak (appearing only for sharp resonances and very well-defined initial beam energy) does not hinder the performance of ERYA-Profiling in terms of applied analytical work, as in practice

the ion beam energy resolution is seldom of the few hundred eV necessary, further and immediate work will pursue the resolution of this mathematical artifact problem.

Already a problem related to the Dirac's function, introduced to avoid the collapsing of the straggling distribution to a single point at the initial layer, was detected and a new strategy was to evaluate the straggling parameters in the middle of the layer instead at the beginning allowing the removal of the Dirac's function, leading to better results, still requiring additional tests.

Not with such an immediate nature, several goals for the near future are devised including the implementation of fitting capabilities in ERYA-Profiling to automatically obtain the best concentrations distribution with depth. Although not so demanding, input features already available in ERYA-Bulk related to density and mass fractions will also be implemented in ERYA-Profiling. Also, the fusion of the two programs in a single code will be contemplated.

REFERENCES

Chapter 1

[1] R. F. Sippel and E .D. Glover, “Sedimentary Rock Analysis by Charged Particle Bombardment”, Nucl. Instr. and Meth. 9 (1960) 37, https://doi.org/10.1016/0029-554X(60)90047-1

[2] J. M. Bewers and F.C. Flack, “Determination of fluorine by prompt γ-radiation from proton bombardment. Part I. Theory and experimental method”, The Analyst 94 (1969) 1, https://doi.org/10.1039/AN9699400001

[3] Y.Wang and M. Nastasi (Eds.), Handbook of Modern Ion Beam Material Analysis, 2nd Edition, 2009, ISBN-13: 978-1605112169 – Chapter 7, Appendix 12

[4] C. Boni, E. Cereda, Marcazzan Braga, G.M, and V. DeTomasi, “Simultaneous PIXE-PIGE analysis of thin and thick samples”, Nucl. Instr. Meth. B35 (1988) 80, https://doi.org/10.1016/0168-583X(90)90225-J

[5] A.P. Jesus, B. Braizinha and J.P. Ribeiro, "Excitation Function and Cross-sections of the Reaction 19F(p,αγ)16O", Nucl Instr. Meth. B 161-163 (2000) 186, doi:10.1007/s002180050244

[6] A.P. Jesus, B. Braizinha, J. Cruz, J.P. Ribeiro, “Influence of target thickness on resonant elastic scattering of protons by ^{19}F”, Nucl. Instr. Meth. B 174 (2001) 229, https://doi.org/10.1016/S0168-583X(00)00521-8

[7] J.P. Ribeiro, A.P. Jesus, B. Braizinha, J. Cruz, R. Mateus and J.V. Pinto, “Experimental study of the ^{19}F(p,αγ)^{16}O reaction”, Nucl. Phys. A 688 (2001) 468c, doi:10.1016/S0375-9474(01)00758-8

[8] R. Mateus, A.P. Jesus, B. Braizinha, J. Cruz, J.V. Pinto, J. P. Ribeiro, "Analysis of Lithium in thick samples", Nucl. Instr. Meth. B *190 (2002) 117-121, doi:*10.1016/S0168-583X(01)01222-8

[9] R. Mateus, A.P. Jesus, J. Cruz, J.P. Ribeiro, "Measurement of the Inelastic Scattering of protons by ^{23}Na in the Energy Range, 1.25-2.40 MeV", Nucl. Inst. and Meth. B 219-220 (2004) 307-311, https://doi.org/10.1016/j.nimb.2004.01.074

[10] J. Cruz, H. Luis, M. Fonseca, Z. Fülöp, G. Gyürky, F. Raiola, M. Aliotta, K. U. Kettner, A. P. Jesus, J. P. Ribeiro, F. C. Barker, C. Rolfs, "Experimental study of proton-induced nuclear reactions in ^{6,7}Li", Journal of Physics G: Nuclear and Particle Physics, Volume 35, Issue 1, pp. 014004 (2008), **doi:** 10.1088/0954-3899/35/1/014004

[11] R. Mateus, M. Fonseca, A. P. Jesus, H. Luís, J. P. Ribeiro, Nucl. Instr. Meth. Beam Int. Mat. Atoms B266 (2008) 1490, doi:10.1016/j.nimb.2007.11.042

[12] M. Fonseca, A. P. Jesus, H. Luís, R. Mateus, J. Cruz, L. Gasques, D. Galaviz, J. P. Ribeiro, "PIGE analysis of magnesium and beryllium", Nucl. Instr. & Meth. B 268 (2010) 1806-08.

[13] M. Chiari, B. Melon, L. Salvestrini, M. Fonseca, E. Alves, A. P. Jesus, "Measurement of proton induced gamma-ray emission cross sections on Al from 2.5 to 4.1 MeV", Nucl. Instr. & Meth. B 332 (2014) 355-358, https://doi.org/10.1016/j.nimb.2014.02.095

[14] P. Cabanelas, J. Cruz, M. Fonseca, A. Henriques, F. Lourenço, H. Luís, J. Machado, J. Pires Ribeiro, A. M. Sánchez-Benítez, P. Teubig, P. Velho, M. Zarza-Moreno, D. Galaviz, A. P. Jesus, "Cross sections for proton induced high energy γ-ray emission (PIGE) in reaction 19F(p, αγ)^{16}O at incident proton energies between 1.5 and 4 MeV", Nuclear Inst. and Methods in Physics Research, B 381 (2016) 110-113, https://doi.org/10.1016/j.nimb.2016.06.003

[15] P. Dimitriou, H. W. Becker, I. Bogdanović-Radović, M. Chiari, A. Goncharov,A. P. Jesus, O. Kakuee, A. Z. Kiss, A. Lagoyannis, J. Räisänen, D. Strivay, A. Zucchiatti, "Development of a Reference Database for Particle-Induced Gamma-ray Emission spectroscopy", Nuclear Inst. and Methods in Physics Research, B 371 (2016) 33-36, https://doi.org/10.1016/j.nimb.2015.09.052

[16] M. Fonseca, R. Mateus, C. Santos, J. Cruz, H. Silva, H. Luis, L. Martins, A. P. Jesus, "Quantitative analysis of Li by PIGE technique", Nucl. Instr. Meth. Beam Int. Mat. Atoms 406 (2017) 144, doi:10.1016/j.nimb.2017.03.035

[17] H. Silva, C. Santos, M. Fonseca, H. Luís, L. Martins, V. Manteigas, J. Cruz, A.P. Jesus, "Measurement of gamma-ray production cross sections for nuclear reaction ^{31}P(p,pγ1-0)^{31}P", Nucl. Instr. Meth. in Physics Research, B 452 (2019) 26, doi:10.1016/j.nimb.2019.05.060

[18] M. Chiari, E. Alves, I. Bogdanović Radović, J. Cruz, L. Csedreki, M. Fonseca, D. Galaviz, A. Henriques, M. Jakšić, A. P. Jesus, O. Kakuee, Z. Kiss, A. Lagoyannis, F. Lourenço, H. Luís, J. Machado, B. Melon, C. K. Nuviadenu, L. Salvestrini, N. SharifzadehZ. Siketić, G. Szíki, Z. Szikszai, P. Teubig, P. Velho, I. Zamboni, M. Zarza, "Measurement of proton induced γ-ray emission cross sections on Na from 1.0 to 4.1 MeV", Nucl. Instr. Meth. Beam Int. Mat. Atoms 441 (2019) 108, doi:10.1016/j.nimb.2017.01.043

[19] J. Cruz, M. Fonseca, D. Galaviz, A. Henriques, H. Luís, J. Machado, P. Teubig, P. Velho, V. Manteigas, A. P. Jesus, "Fluorine depth profiling based on the ^{19}F(p,p'γ)^{19}F excitation function", Eur. Phys. Jour. Plus 136 (2021) 969, doi: 10.1140/epjp/s13360-021-01954-3

[20] R. Mateus, M. Fonseca, J. Cruz, V. Manteigas, C. Santos, H. Luís, H. Silva, A. P. Jesus, "Gamma-ray cross-sections of the ^{27}Al(p,p`γ)^{27}Al reaction in the proton energy range 1490–3000 keV", Eur. Phys. Jour. A 58 (2022) 209, doi:10.1140/epja/s10050-022-00861-0

[21] "Development of a Reference Database for Particle Induced Gamma Ray Emission (PIGE) Spectroscopy", IAEA-TECDOC-1822, IBAN:978-92-0-106317-5

[22] IBANDL database, IAEA, 2023 at http://nds.iaea.org/ibandl/.

[23] E. Möller and N. Starfelt, "Microanalysis of flourine in zircaloy by the use of the ^{19}F(p,αγ)^{16}O Reaction", Nucl. Instr. and Meth. 50 (1967) 225, https://doi.org/10.1016/0029-554X(67)90044-4

[24] J.W. Mandler, R.B . Moler, E. Raisen and K.S . Rajan, "Determination of the flouride concentration profile in tooth enamel using a nuclear resonance technique", Thin solid Films 19 (1973) 165, https://doi.org/10.1016/0040-6090(73)90033-3

[25] I. Vickridge and G. Amsel, "Analytic calculation for some useful depth profiles of the linear expansion coefficients used in SPACES", Nucl. Instr. Meth. Phys. Res. B45 (1990) 6, https://doi.org/10.1016/0168-583X(90)90773-N

[26] M. Mayer, *SIMNRA User's Guide* , Report IPP 9/113, Max-Planck-Institut für Plasmaphysik, Garching, Germany, 1997

[27] N.P. Barradas, C. Jeynes, and R.P. Webb, "Simulated annealing analysis of Rutherford backscattering data", Appl. Phys. Lett. 71 (1997) 291, http://dx.doi.org/10.1063/1.119524 ; C. Jeynes, N.P. Barradas, P.K. Marriott, M. Jenkin, E. Wendler, G. Boudreault, R.P. Webb, "Elemental thin film depth profiles by ion beam analysis using simulated annealing - a new tool", J. Phys. D: Appl. Phys. 36 (2003) R97, **doi:** 10.1088/0022-3727/36/7/201

[28] N.P. Barradas, J. Cruz, M. Fonseca, A.P. de Jesus, A. Lagoyannis, V. Manteigas, M. Mayer, K. Preketes-Sigalas, P.Dimitriou, "International Atomic Energy Agency inter-comparison of particle induced gamma-ray emission codes for bulk samples", Nucl. Instr. Meth. Beam Int. Mat. Atoms B266 (2008) 1490, doi:10.1016/j.nimb.2020.02.019

[29] R. Mateus, A. P. Jesus, J. P. Ribeiro, "A code for quantitative analysis of light elements in thick samples by PIGE", Nucl. Instrum. Methods Phys. Res. B 219 (2004) 519, https://doi.org/10.1016/j.nimb.2004.11.019

[30] Micaela Fonseca, "Análise de elementos leves por reacções nucleares com produção de radiação gama", Ph.D Thesis (2011), https://run.unl.pt/handle/10362/6150

[31] Luis Martins, "Programa para análise em profundidade por técnicas nucleares", Grad. Thesis (2013), http://hdl.handle.net/10362/11047

[32] ERYA-Bulk manual at: https://github.com/Arucard1983/ERYA-Bulk/blob/master/manuals/ERYA%20Bulk%20Tutorial_v7.pdf

ERYA-Profiling manual at: https://github.com/Arucard1983/ERYA-Profiling/blob/master/manual/ERYA%20Profiling%20Tutorial%20APJv2.pdf

Chapter 2

[1] Micaela Fonseca, "Análise de elementos leves por reacções nucleares com produção de radiação gama", Ph.D Thesis (2011), https://run.unl.pt/handle/10362/6150

[2] E. Alves, K. Lorenz, N. Catarino, M. Peres, M. Dias, R. Mateus, L. C. Alves, V. Corregidor, N. P. Barradas; M. Fonseca, J. Cruz, A. P. Jesus, "An insider view of the Portuguese ion beam laboratory", The European Physical Journal Plus, Volume 136 (2021) Issue 6, article id.684 DOI: 10.1140/epjp/s13360-021-01629-z

[3] "Development of a Reference Database for Particle Induced Gamma Ray Emission (PIGE) Spectroscopy", IAEA-TECDOC-1822, IBAN:978-92-0-106317-5

[4] IBANDL database, IAEA, 2023 at http://nds.iaea.org/ibandl/.

[5] L. Landau, "On the energy loss of fast particles by ionization", J. Phys. (USSR) 8 (1944) 204, https://doi.org/10.1016/B978-0-08-010586-4.50061-4 (republished)

[6] V. Vavilov, "Ionization losses of high-energy heavy particles", Sov. Phys. JETP 5 (1957) 749.

[7] Stephen M. Seltzer, Martin J. Berger, "Studies in Penetration of Charged Particles in Matter", (1964), Nuclear Science Series Report Number 39, p. 187, BibCode: 1964spcp.conf..187S

[8] B. Schorr, "Programs for the Landau and the Vavilov distributions and the corresponding random numbers ", Comput. Phys. Commun. 7 (1974) 215-24, https://doi.org/10.1016/0010-4655(74)90091-5

[9] A. Rotondi and P. Montagna, "Fast calculation of Vavilov distribution", Nucl. Instrum. Methods Phys. Res. B 47 (1990) 215, https://doi.org/10.1016/0168-583X(90)90749-K

[10] O. Chibani, "New algorithms for the Vavilov distribution calculation and the corresponding energy loss sampling", IEEE Transactions on Nuclear Science 45 (1998), 2288, https://doi.org/10.1109/23.725266

[11] Armando Lazaro Alaminos-Bouza, 2015, https://hal.science/hal-02480024/document

[12] S.K.L.Sjue, R.N.George and D.G.Mathews, "Analytic saddlepoint approximation for ionization energy loss distributions", Nucl. Instrum. Methods Phys. Res. B 407 (2017), doi:10.1016/j.nimb.2017.06.013

[13] S. Krane; Introductory Nuclear Physics, John Wiley and Sons, ISBN 978-0-471-80553-3

[14] Claus E. Rolfs, William S. Rodney, Cauldrons on the Cosmos, ISBN-0-266-72457-3

[15] E. Merzbacher, "Quantum Mechanics", Third Edition, John Wiley and Sons

[16] Dr. E. W. Dijkstra, "ALGOL-60 Translation", Stichting Mathematisch Centrum, Amesterdam, also available at https://www.cs.utexas.edu/~EWD/MCReps/MR35.PDF

[17] K. Madsen, H.B.Nilsen, O. Tingleff, "Methods for Non-Linear Least Square Problems", Technical University of Denmark (2004)

[18] D. Zahnow, C. Angulo, M. Junker, C. Rolfs, S. Schmidt, W.H. Schulte and E. Somorjai, "Thermonuclear reaction rates of ^{9}Be(p,γ)^{10}B", Nuclear Physics A 589 (1995) 95, https://doi.org/10.1016/0375-9474(95)00077-E

[19] I. Vickridge and G. Amsel, "Analytic calculation for some useful depth profiles of the linear expansion coefficients used in SPACES", Nucl. Instr. Meth. Phys. Res. B45 (1990) 6, https://doi.org/10.1016/0168-583X(90)90773-N

[20] G. Imbriani, H. Costantini, A. Formicola, A. Vomiero, C. Angulo, D. Bemmerer, R. Bonetti, C. Broggini, F. Confortola, P. Corvisiero, J. Cruz, P. Descouvemont, Z. Fülöp, G. Gervino, A. Guglielmetti, C. Gustavino, G. Gyürky, A.P. Jesus, M. Junker, J.N. Klug, A. Lemut, R. Menegazzo, P. Prati, V. Roca, C. Rolfs, M. Romano, C. Rossi-Alvarez, F. Schümann, D. Schürmann, E. Somorjai, O. Straniero, F. Strieder, F. Terrasi, H.-P. Trautvetter, "S-factor of 14N(p,γ)15O at astrophysical energies", https://doi.org/10.1140/epja/i2005-10138-7

A

AIRY'S FUNCTION

A.1 Airy's Function Definition

Vavilov has shown that for κ≥1, his distribution could be approximated by a Airy function.
Defining the following parameters:

$$\eta = \frac{\left(1-\frac{2\beta^2}{3}\right)\xi}{(2k)^{\frac{2}{3}}} \qquad \text{(A.1)}$$

$$a = \frac{(2k)^{\frac{1}{3}}\left(1-\frac{\beta^2}{2}\right)}{\left(1-\frac{2\beta^2}{3}\right)^{\frac{2}{3}}} \qquad \text{(A.2)}$$

$$t = \frac{\overline{\Delta E}-\Delta E}{\eta} + a^2 \qquad \text{(A.3)}$$

where all the quantities have been previously defined, and replacing, for k=1, on Vavilov's equation (see "ERYA-Profiling Energy Straggling Distributions" paper, chapter 3, (2.1)), we get a new function called the Airy-Vavilov distribution:

$$f(\eta, a, t) = \frac{1}{\eta\pi} exp(at - a^3/3) \int_0^\infty cos\,(ut + u^3/3) du \qquad \text{(A.4)}$$

The Airy Function is oscillatory for negative values of its argument, and decay exponentially to positive values. Since the first zero occurs at t=-2.33811, it roughly corresponds to the value where that the Landau and Moyal distributions grow exponentially from zero (the λ_0 point).
The exponential term outside the integral of Airy-Vavilov's function for positive values (t>0) combined by the quick convergence of integral matches the long tail of the original Vavilov distribution.

Since the derivatives around the origin, including the function itself, are analytically evaluated using only the gamma function around the origin, it is possible to approximate the integral given on (A.4) by the following power series:

$$Ai(t) = \frac{1}{\pi}\int_0^\infty cos(ut + u^3/3)\, du \approx a_0 + a_1 t + a_2 t^2 + \ldots = \sum_{n=0}^{\infty} a_n\, t^n \qquad (A.5)$$

where each coefficient can be calculated by a recurrence sequence:

$$a_0 = \frac{1}{3^{2/3}\Gamma(2/3)};\ a_1 = \frac{-1}{3^{1/3}\Gamma(1/3)};\ a_2 = 0;\ a_n = \frac{a_{n-3}}{n(n-1)}, n \geq 3 \qquad (A.6)$$

For function arguments $|t|>3$ about 100 terms it is required to approximate the function value accurately, but for large function arguments, which corresponds to the long tail of Vavilov Distribution, an asymptotic expansion may be used instead, requiring the sum of fewer terms:

$$Ai(t) = \frac{1}{\pi}\int_0^\infty cos(ut + u^3/3)\, du \approx \frac{exp\left(\frac{-2}{3}t^{3/2}\right)}{\sqrt{4\pi}t^{1/4}}\left(\sum_{n=0}^{\infty}\frac{(-1)^n\Gamma(n+5/6)\Gamma(n+1/6)(3/4)^n}{2\pi n! t^{3n/2}}\right) \qquad (A.7)$$

For t>5 two sum terms are enough, leading to:

$$Ai(t) = \frac{1}{\pi}\int_0^\infty cos(ut + u^3/3)\, du \approx \frac{exp\left(\frac{-2}{3}t^{3/2}\right)}{\sqrt{4\pi}t^{1/4}}\left(1 - \frac{5}{48t^{3/2}}\right) \qquad (A.8)$$

While for -2.33841 < t < 5 ERYA-Profiling employs (A.5) with recurrence terms (A.6), for $t \geq 5$, the approximation of (A.7) is used. Otherwise, for larger negatives values of t, the function is set to zero.

A.2 Airy's Function of First Kind Definition

The Airy's Function of First Kind can be defined as one of the solutions from the following differential equation:

$$\frac{d^2y}{dx^2} - xy = 0 \qquad (A.9)$$

By applying the Fourier Transform on (A.9), it will result:

$$\int_{-\infty}^{\infty}\left(\frac{d^2y}{dx^2} - xy\right) exp(-2\pi i x t) dx = 0 \qquad (A.10)$$

$$-4\pi^2 t^2 \underbrace{\int_{-\infty}^{\infty} y\,(x) * exp(-2\pi i x t)dx}_{F(t)} - 2\pi i \frac{d}{dt}\underbrace{\int_{-\infty}^{\infty} y\,(x) * exp(-xt)dx}_{F(t)} = 0 \qquad \text{(A.11)}$$

Solving the differential equation with Fourier operators, it should give:

$$F(t) = exp(2\pi i\, t^3/3) \qquad \text{(A.12)}$$

And applying the inverse Fourier Transform will return the integral form of Airy Function:

$$Ai(x) = \int_{-\infty}^{\infty} exp\left(2\pi i(t^3/3 + xt)\right)dt = \frac{1}{2\pi}\left(\int_{-\infty}^{\infty} cos\,(t^3/3 + xt)dt + i\int_{-\infty}^{\infty} sin\,(t^3/3 + xt)dt\right) \qquad \text{(A.13)}$$

Since the sine function is odd and cosine is even, the imaginary integral vanishes, and then:

$$Ai(x) = \frac{1}{\pi}\left(\int_0^{\infty} cos\,(t^3/3 + xt)dt\right) \qquad \text{(A.14)}$$

A.3 Sketch proof of the Airy Function Power-Series Coefficients

In (A.5) the coefficients can be obtained from the Taylor series of the Airy Function, i.e.:

$$a_n = \frac{1}{n!}\frac{\partial^n f(x)}{\partial x^n} \qquad \text{(A.15)}$$

To evaluate the coefficients of Airy function, it is a straightforward integration.

$$a_0 = Ai(0) = \frac{1}{\pi}\int_0^{\infty} cos\,(u^3/3)du = \frac{\Gamma(1/3)}{2\sqrt[6]{3}\pi} = \frac{1}{3^{2/3}\Gamma(2/3)} \qquad \text{(A.16)}$$

$$a_1 = Ai'(0) = \frac{-1}{\pi}\int_0^{\infty} u\,sin(u^3/3)du = \frac{-\sqrt[6]{3}\Gamma(2/3)}{2\pi} = \frac{-1}{3^{1/3}\Gamma(1/3)} \qquad \text{(A.17)}$$

$$a_2 = \frac{Ai''(0)}{2} = \frac{-1}{2\pi}\int_0^{\infty} u^2\,cos(u^3/3)du = \lim_{u\to\infty}\frac{-1}{2\pi}sin(u^3/3) + \lim_{u\to 0}\frac{1}{2\pi}sin(u^3/3) = 0 + 0 = 0 \qquad \text{(A.18)}$$

The limits on (A.18) uses the Feynman mean theorem which states that the cosine and sine at infinite are set equal to zero, although they are mathematically indefinite. Also, the differential equation at (A.9) only makes sense if the second derivative at the origin is equal to zero.

For an arbitrary large *n*, it is expected that after integrations by parts it should result:

$$a_n = \frac{Ai^{(n)}(0)}{n!} = \frac{1}{\pi n!}\int_0^\infty u^n \cos(u^3/3)du = \frac{1}{n!\pi}\int_0^\infty (2-n)\,u^{n-3}\sin(u^3/3)du$$
$$a_n = \frac{1}{n!\pi}(n-2)(n-5)\int_0^\infty u^{n-6}\cos(u^3/3)du \quad \text{(A.19)}$$

The limits at infinity were set to zero due to Feynman theorem, and also noticing that:

$$a_n = \frac{1}{n(n-1)(n-3)(n-4)(n-6)!\pi}\int_0^\infty u^{n-6}\cos(u^3/3)du = \frac{a_{n-6}}{n(n-1)(n-3)(n-4)} \quad \text{(A.20)}$$

Thus, by direct comparison, the recurrence identity is the following:

$$a_n = \frac{a_{n-3}}{n(n-1)} \quad \text{(A.21)}$$

And this completes the sketch of proof, showing that only a numerical value of the gamma function and a simple recurrence formula are needed to evaluate any power-series coefficients.

A.4 Searching the Optimal Airy-Vavilov Function Domain

Like the Landau or Moyal functions, it is necessary to find a proper function domain to ensure the adequate approximation of Vavilov distribution fits within the 3-sigma domain range.

To find λ_0 from the first zero of Airy function, let's define t_0 = -2.33811 (the first zero of Airy function) and use:

$$\lambda_0 = \frac{\overline{\Delta E}-\Delta E}{\xi} - 1 + \gamma - \beta^2 - ln(k) \quad \text{with} \quad t_0 = \frac{\overline{\Delta E}-\Delta E}{\eta} + a^2 \quad \text{(A.22)}$$

Which by direct substitution, should give the following expression:

$$\lambda_0 = \frac{(t_0-a^2)\eta}{\xi} - 1 + \gamma - \beta^2 - ln(k) \quad \text{(A.23)}$$

A similar reasoning should find $\lambda_{0.995}$ using a similar equation:

$$\lambda_{0.995} = \frac{(t_{0.995}-a^2)\eta}{\xi} - 1 + \gamma - \beta^2 - ln(k) \quad \text{(A.24)}$$

Taking the Airy function alone and the asymptotic expansion (A.7), the integral becomes:

$$f(\lambda_{0.995}) \approx \int_{\lambda_{0.995}}^{\infty} Ai\,(t)dt = \frac{1}{\pi}\int_{\lambda_{0.995}}^{\infty}\int_{0}^{\infty} cos(ut + u^3/3)\,dudt$$
$$f(\lambda_{0.995}) \approx \int_{\lambda_{0.995}}^{\infty} \frac{exp\left(\frac{-2}{3}t^{3/2}\right)}{\sqrt{4\pi}t^{1/4}}dt = \frac{erfc\left(\frac{\sqrt{2}t_{0.995}^{3/4}}{\sqrt{3}}\right)}{\sqrt{6}} < \frac{1}{200\sqrt{6}} \quad \text{(A.25)}$$

which means that the $t_{0.995}$ value should be given by:

$$t_{0.995} \approx 5.6696 \quad \text{(A.26)}$$

Replacing (A.22) on (A.23) and (A.24), the interval boundaries should be given by:

$$\lambda_0 \approx \frac{t_0 - (2k)^{2/3}}{(2k)^{2/3}} - \frac{1}{2} - ln(k), \beta \approx 0 \quad \text{(A.27)}$$

$$\lambda_{0.995} \approx \frac{t_{0.995} - (2k)^{2/3}}{(2k)^{2/3}} - \frac{1}{2} - ln(k), \beta \approx 0 \quad \text{(A.28)}$$

The non-relativistic β=0 limit is justified due to the energy beam being in order of a few MeV.

Using these formulas, lambda interval for lower and higher k-value are approximately given by:

$$k = 0.02, t_{0.995} \approx 5.6696: \lambda_0 \approx -17.406, \lambda_{0.995} \approx 30.371 \quad \text{(A.29)}$$
$$k = 0.3, t_{0.995} \approx 5.6696: \lambda_0 \approx -3.582, \lambda_{0.995} \approx 7.673 \quad \text{(A.30)}$$
$$k = 22, t_{0.995} \approx 5.6696: \lambda_0 \approx -4.777, \lambda_{0.995} \approx -4.328 \quad \text{(A.31)}$$

According to Montagna approximation by Landau and Moyal distributions, the lower bounds should be around λ=-3.4, and using the universal Landau variable for lower k-factors delivers a much lower value, that can cause an unrealistic approximation of the Vavilov distribution.

By contrast the upper limit for Landau and Moyal are changing from λ=25 to Landau, and decrease during the Moyal approximation until λ=9, when k=0.29.

This not-so-optimal transitions between Landau and Airy for lower k are a sort of issues, that needs to be tackled.

As a side-note, the Landau can be approximated by the Moyal distribution around k=0.1 to k=0.3 according to Montagna, and to ensure a clean 3-sigma cut-off it is necessary to cut the lower bound by P=1/400=0.0025 and Q=1/400=0.0025. Then the function:

$$f(\lambda) \approx \frac{1}{\sqrt{2\pi}} exp\left(-\frac{\lambda + e^{-\lambda}}{2}\right) \quad \text{(A.32)}$$

This integral is analytically possible using the Gaussian error function, where for $\lambda_{0.995}$:

$$f(\lambda_{0.995}) \approx \int_{\lambda_{0.995}}^{\infty} \frac{1}{\sqrt{2\pi}} exp\left(-\frac{\lambda+e^{-\lambda}}{2}\right) d\lambda = erf\left(\frac{e^{-\lambda_{0.995}/2}}{\sqrt{2}}\right) = \frac{1}{400} \quad \text{(A.33)}$$

And the for λ_0 will get:

$$f(\lambda_0) \approx \int_{-\infty}^{\lambda_0} \frac{1}{\sqrt{2\pi}} exp\left(-\frac{\lambda+e^{-\lambda}}{2}\right) d\lambda = 1 - erf\left(\frac{e^{-\lambda_0/2}}{\sqrt{2}}\right) = \frac{1}{400} \Leftrightarrow erf\left(\frac{e^{-\lambda_0/2}}{\sqrt{2}}\right) = \frac{399}{400} \quad \text{(A.34)}$$

Evaluating numerically the (A.33) and (A.34) equations, the optimal boundary points will be:

$$\lambda_{0.995} = 11.531 \quad \text{(A.35)}$$

$$\lambda_0 = -2.212 \quad \text{(A.36)}$$

Which is a little offset compared to the Montagna model. When we assume that the lower bound are an infinitesimal, then the the upper bound are evaluated from:

$$f(\lambda_{0.995}) \approx \int_{\lambda_{0.995}}^{\infty} \frac{1}{\sqrt{2\pi}} exp\left(-\frac{\lambda+e^{-\lambda}}{2}\right) d\lambda = erf\left(\frac{e^{-\lambda_{0.995}/2}}{\sqrt{2}}\right) = \frac{1}{200} \quad \text{(A.37)}$$

Then the numerical value is a little better:

$$\lambda_{0.995} = 10.145 \quad \text{(A.38)}$$

While the lower bound for an error lower that e=10^{-6} it will give:

$$f(\lambda_0) \approx \int_{-\infty}^{\lambda_0} \frac{1}{\sqrt{2\pi}} exp\left(-\frac{\lambda+e^{-\lambda}}{2}\right) d\lambda = 1 - erf\left(\frac{e^{-\lambda_0/2}}{\sqrt{2}}\right) = 10^{-6} \quad \text{(A.39)}$$

$$\lambda_0 \approx -3.4 \quad \text{(A.40)}$$

This asymmetric boundary choice corresponds to the Airy approximation to use the first Airy zero for lower bound, and the upper bound are estimated by (A.24), and converted by (A.23).

A.5 Implementing the Optimal Domain of the Vavilov-Airy Distributions

The previous section justifies the following algorithm to find the best interval without using heavy computational procedures. It uses the fact that the asymmetry of the distribution, especially the gap between the maximum and average of the distribution could be used to find an optimal interval.

By taking account the lower bound energy E_0, the maximum loss energy E_p, the average energy ΔE, and the higher bound energy $E_{0.995}$, given by solving (A.3):

$$E_0 = \eta(t_0 - a^2) + \Delta E \quad \text{(A.41)}$$

$$E_p = \eta\left(t_p - a^2\right) + \Delta E \tag{A.42}$$

$$E_{0.995} = \eta(t_{0.995} - a^2) + \Delta E \tag{A.43}$$

The energy span between the lower bound and the average energy will be defined by solving the equation (A.41):

$$\Delta E = E_0 - \eta(t_0 - a^2) \tag{A.44}$$

And define the energy gap between the maximum loss and average energy by replacing (A.42):

$$\delta E_p = \Delta E - E_p = -\eta\left(t_p - a^2\right) \tag{A.45}$$

Notice that (A.41) can be rewritten as in function of initial energy gap:

$$\delta E = \Delta E - E_0 = -\eta(t_0 - a^2) \tag{A.46}$$

Where the gap between upper energy and maximum loss are defined by the following:

$$\delta U = \delta E + \delta E_p = E_{0.995} - \Delta E \tag{A.47}$$

Which follow our hypothesis that the gap from (A.45) can be added to upper interval by assuming a symmetry of distribution around the average like the Gaussian distribution.

However (A.48) by definition will also be equal to:

$$\delta U = \Delta E - E_{0.995} = -\eta(t_{0.995} - a^2) \tag{A.48}$$

Combining (A.46) and (A.47) with (A.48), the upper limit of distribution domain is given by:

$$\eta(t_{0.995} - a^2) + \Delta E = \Delta E + \delta E + \delta E_p \Leftrightarrow \eta(t_{0.995} - a^2) = -\eta(t_0 - a^2) - \eta\left(t_p - a^2\right) \tag{A.49}$$

$$t_{0.995} = 3a^2 - t_0 - t_p \tag{A.50}$$

Finally, the upper energy domain are given by this formula:

$$E_{0.995} = \eta\left(2a^2 - t_0 - t_p\right) + \Delta E \tag{A.51}$$

To determine the distribution maximum, it follows from Vavilov own derivation that:

$$\frac{Ai'(t_p)}{Ai(t_p)} + a = 0 \tag{A.52}$$

That can be integrated to a problem to find the maximum of the following function:

$$log\left(Ai\left(t_p\right)\right) + at_p = 0 \tag{A.53}$$

For larger values of k the Airy function are dominated by the asymptotic expansion of (A.8), then the derivative are given by:

$$Ai'(t) \sim -\frac{exp(-2t^{3/2}/3)t^{1/4}}{\sqrt{4\pi}} - \frac{exp(-2t^{3/2}/3)}{t^{5/4}\sqrt{64\pi}} \quad (A.54)$$

Replacing (A.54) into (A.52) the logarithmic derivative of Airy at larger value of t are then:

$$\frac{Ai\prime(t)}{Ai(t)} \sim \sqrt{4\pi}t^{1/4}exp(2t^{3/2}/3)\left(-\frac{exp(-2t^{3/2}/3)t^{1/4}}{\sqrt{4\pi}} - \frac{exp(-2t^{3/2}/3)}{t^{5/4}\sqrt{64\pi}}\right) = -\sqrt{t} - \frac{1}{4t} \sim -\sqrt{t} \quad (A.55)$$

This derive the asymptotic condition of the maximum of Airy distribution, which is:

$$\frac{Ai\prime(t_\infty)}{Ai(t_\infty)} + a = 0 \Leftrightarrow -\sqrt{t_\infty} + a = 0 \Leftrightarrow t_\infty = a^2 \quad (A.56)$$

Giving the fact that the Airy distribution for large k is indistinct from Gaussian one.
In fact, the maximum energy loss at that condition:

$$\overline{\Delta E} = \eta(t_\infty - a^2) + \Delta E = \eta(a^2 - a^2) + \Delta E = \Delta E, k \to \infty \quad (A.57)$$

With the algorithm done it was possible with *Maxima* to check the truncation error by making numerical calculation are represent the following values on the following table:

Table A.1: Vavilov-Airy Boundaries

K	a	t_p	$t_{0,995}$	λ_0	λ_p	$\lambda_{0.995}$	e	f
0.02	0.341	-0.624	3.311	-17.620	-2.877	30.963	7.8253e-4	3.3589
0.1	0.585	-0.256	3.621	-5.953	0.132	11.460	3.5660e-3	2.9142
0.2	0.737	0.015	3.953	-4.118	0.214	7.646	6.6314e-3	2.7310
0.3	0.834	0.206	4.219	-3.581	0.077	5.845	8.2282e-3	2.6428
1	1.260	1.224	5.877	-2.896	-0.652	2.279	2.1835e-3	3.0618
10	2.714	7.183	17.253	-4.043	-2.750	-1.383	3.2869e-4	3.5916
20	3.420	11.511	25.917	-4.619	-3.434	-2.203	2.6806e-6	4.6939
25	3.684	13.437	29.617	-4.814	-3.652	-2.459	2.7344e-7	5.1409

Note: The Airy function is used on ERYA-Profiling only for k>0.29, thus the lower lines were computed only for reference and control. Also, the factor $a=(2k)^{1/3}$ was assumed as an approximation.

The t_p was evaluated using *Maxima* since the Airy function are built-in on their mathematical library. Comparing with the ERYA code, the results are consistent within the numerical error, and the algorithm was fast to find the required root.

Additionally, it was computed the truncation errors of the distribution domain using *Maxima* by evaluating the following numerical integrals:

$$e = \int_{t_{0.995}}^{\infty} a^2 \, e^{at - \frac{a^3}{3}} Ai(t) dt \tag{A.58}$$

$$e = \frac{1}{\sqrt{2\pi}} \int_{-\infty}^{-f} e^{\frac{-t^2}{2}} dt + \frac{1}{\sqrt{2\pi}} \int_{f}^{\infty} e^{\frac{-t^2}{2}} dt = erfc\left(\frac{f}{\sqrt{2}}\right) \tag{A.59}$$

Which essentially determines the error "e" from integral (A.58), and then by an approximation of a Gaussian integral, which can be evaluated analytically using the error function, the sigma factor "f" are determined by solving (A.59).

The results show that for Airy domain around k=0.29 the upper domain are a little below the target 3-sigma, however as seen on chapter 3, The Airy function for lower values was set linear corrections to freeze the distribution on k=0.4, making the approximations errors within the satisfactory. For larger k it goes as high to 5-sigma, but in practice this error are not expected (as seen on many testing's) to lead numerical errors due to domain truncate.

A.6 The Airy Finding Maximum Algorithm

To solve (A.53) it uses the Golden Search Bisection Algorithm that can be sketched as the following:

Step 1: Define the Golden Ratio $\phi = \frac{1+\sqrt{5}}{2}$, the parameters from the initial values $a = t_0 = -2.33840$ **with** $b = t_\infty = a^2$ and the tolerance **ε=0.05**

Step 2: Define the transitory parameters: $c = b - \frac{b-a}{\phi}$ and $d = a + \frac{b-a}{\phi}$

Step 3: While $|b - a| > \epsilon$, set and follow the cycle, otherwise jump to Results.

Step 4: If f(c) > f(d), where f(t) are given by (A.53)

Then set **b=d**

or Else set **a=c**

Step 5: Recalculate the transitory parameters:

$$c = b - \frac{b-a}{\phi} \text{ and } d = a + \frac{b-a}{\phi}$$

Step 6: End of the **While** cycle, jump to Step 3.

Results: Once the while cycle breaks the maximum of the function are found and giving by: $t_p = \frac{b+a}{2}$, which is an average of the two leading parameters.

Once found a solution with this simple and fast algorithm, the domain boundaries are giving by (A.41) and (A.51) and the problem are solved.

B

FORMAL DERIVATION OF THE CROSS-SECTION OF RESONANCES

B.1 Deriving the Born's Approximation of the Differential Cross-Section

A more rigorous derivation of the cross-sections around resonances can be derived from the Quantum Mechanics theory. This is important to derive the general case for a resonance strength.

Starting from the general Schrodinger's Equation written below:

$$\left[-\frac{\hbar^2\nabla^2}{2m}+V(r)\right]\psi(r)=\frac{\hbar^2k^2}{2m}\psi(r) \tag{B.1}$$

and applying the scaled potential defined by:

$$U(r)=\frac{\hbar^2V(r)}{2m} \tag{B.2}$$

results the reduced Schrodinger's Equation or wave-equation:

$$(\nabla^2+U(r)-k^2)\psi(r)=0 \tag{B.3}$$

The general solution which is also known as Lippmann-Schwinger Equation is given by:

$$\psi(r)=exp(ikr)-\frac{1}{4\pi}\int\frac{exp(ik|r-r\prime|)U(r\prime)\psi(r\prime)}{|r-r\prime|}d^3r' \tag{B.4}$$

Using the far away observer approximation, the modulus on (B.4) is then:

$$|r - r'| \approx r - \frac{\partial r}{\partial r'} r' = r - f(r')r' \tag{B.5}$$

which motivates to make a spherical wave expansion of (B.5), where each partial wave which is solution of (B.4) is given by:

$$\psi_k(r) = exp(ikr) - \frac{exp(ikr)}{4\pi r} \int exp(-ik'r')U(r')\psi_k(r')\, d^3r' = \phi(r) + \frac{exp(ikr)}{r} f(\theta, \phi) \tag{B.6}$$

The main physical quantity is the wave amplitude given by the integral:

$$f(\theta, \phi) = \frac{-1}{4\pi} \int exp\,(-ik'r')U(r')\psi_k(r')d^3r' \tag{B.7}$$

From quantum mechanics, the wave current in tridimensional space is given by the formula:

$$j = \frac{\hbar}{2mi}\left(\psi^* \nabla\psi - \psi \nabla\psi^*\right) \tag{B.8}$$

And replacing (B.6) into (B.8), and assuming a far away observer approximation, it will give:

$$j = \frac{\hbar k}{m} + \frac{\hbar k}{m}\frac{|f(\theta,\phi)|^2}{r^2} + O(1/r^3) \approx \underbrace{\frac{\hbar k}{m}}_{j_T} + \underbrace{\frac{\hbar k}{m}\frac{|f(\theta,\phi)|^2}{r^2}}_{j_S} \tag{B.9}$$

which is general current conservation condition during scattering, where the outbound wave (total current) is the sum of the free (incident) particle current and the scattered current.

Then the scattered current balance can be reshaped as:

$$j_s = j - j_T \approx j \tag{B.10}$$

The approximation is justified since the scattered amplitude is higher than the free particle one.

The total number of scattered particles *N* is given by the scattered current term from (B.9):

$$N = 4\pi j_s r^2 d\Omega = 4\pi r^2 J \tag{B.11}$$

Using (B.9) to (B.11) the following propriety is derived:

$$\frac{d\sigma}{d\Omega} = \frac{N}{4\pi J} = \frac{4\pi j r^2 d\Omega}{4\pi j_T d\Omega} = \frac{\hbar k |f(\theta,\phi)^2| r^2}{m r^2}\frac{m}{\hbar k} = |f(\theta, \phi)|^2 \tag{B.12}$$

As expected, the cross-section depends on the wave amplitude, and using (B.7) results:

$$f(\theta,\phi) = \frac{-1}{4\pi}\int exp\,(-ik'r')U(r')\psi_k(r')d^3r' = \frac{-1}{4\pi}\langle\phi_{k'}|U(r')|\psi_k\rangle \qquad \text{(B.13)}$$

The previous result is the first order Born expansion that can be represented by an element of the transition matrix. The differential cross-section is then written as a quantum mechanics operator:

$$\frac{d\sigma}{d\Omega} = \frac{1}{(4\pi)^2}|\langle\phi_{k'}|U(r')|\psi_k\rangle|^2 \qquad \text{(B.14)}$$

B.2 Deriving the Born's Approximation of the Cross-Section

To derive the total cross-section requires to apply some calculations. (B.7) can be written in function of the momentum transfer:

$$q = k - k' \qquad \text{(B.15)}$$

and assuming the vector modules of k and k' are equal, the transfer momentum depends on the scattering angle θ:

$$q = 2ksin(\theta/2) \qquad \text{(B.16)}$$

and the Born's Approximation of the wave amplitude is given by:

$$f(q) = \frac{-1}{4\pi}\langle\phi_{k'}|U(q)|\psi_k\rangle = \frac{-1}{4\pi}\int exp\,(iqr)U(r)d^3r \equiv F_q\big(U(r)\big) \qquad \text{(B.17)}$$

which is equivalent to take the Fourier transform of the potential and evaluate the differential cross-section directly from (B.17), a common procedure in quantum mechanics.

The integral (B.17) can be evaluated in the perspective of a far-away observer and the assumption that the interaction is consistent with a central potential. The real ordeal will be spin and angular momentum, but for now it won't be necessary to take care yet. This means that the angular variables are a trivial integration and results:

$$f(q) = \frac{-1}{4\pi}\int exp\,(iq \cdot r)U(r)d^3r = \frac{-1}{q}\int_0^\infty r\,sin(qr)U(r)dr \qquad \text{(B.18)}$$

Around a resonance, the potential can be approximated by a constant value, which leaves a trivial integration respective to the angular variables as the following:

$$\sigma = \int_0^{2\pi}\int_0^{\pi} sin\,(\theta)\left(\frac{d\sigma}{d\Omega}\right)d\theta d\phi = \int_0^{2\pi}\int_0^{\pi}\theta\,sin(\theta)|f(q)|^2 d\theta d\phi \qquad \text{(B.19)}$$

where the potential depends only on the distance from the target nuclide:

$$\sigma = \int_0^{2\pi}\int_0^{\pi}\int_0^{\infty}\int_0^{\infty}\frac{rssin(qr)sin(qs)sin(\theta)U^+(r)U(s)}{q^2}d\theta d\phi dr ds \qquad \text{(B.20)}$$

Replacing q by (B.16) and making the angular variable integration:

$$\sigma = \frac{\pi}{k^2}\int_0^\infty\int_0^\infty\frac{(s-r)sin\big(2k(s+r)\big)+(s+r)sin\big(2k(s-r)\big)}{k(r^2-s^2)}U^+(r)U(s)drds \qquad \text{(B.21)}$$

This apparent complicated expression can be easily solved by first separating the integral:

$$\sigma = \frac{-2\pi}{k^2}\int_0^\infty\int_0^\infty\frac{sin\big(2k(s+r)\big)}{2k(s+r)}U^+(r)U(s)drds - \frac{2\pi}{k^2}\int_0^\infty\int_0^\infty\frac{sin\big(2k(r-s)\big)}{2k(r-s)}U^+(r)U(s)drds \qquad \text{(B.22)}$$

By applying the change of variables $s+r=x$ and $r-s=y$, while noticing that a point-wise potential can be approximated by a Dirac's delta function:

$$\sigma = \frac{4\pi}{k^2}U^2(E_x)\int_0^\infty\int_0^\infty\frac{sin(2kx)}{2kx}\delta(y)dxdy + \frac{4\pi}{k^2}U^2\big(E_y\big)\int_0^\infty\int_0^\infty\frac{sin(2ky)}{2ky}\delta(x)dxdy \qquad \text{(B.23)}$$

From the *Handbook of Mathematical Functions*, the Dirac's Integral is given by:

$$\int_{-\infty}^{\infty}\delta\,(x)dx = 1 \rightarrow \int_0^\infty\delta\,(x)dx = \frac{1}{2} \qquad \text{(B.24)}$$

Also from the *Handbook*, the Dirichlet's sine integral can be solved using the Laplace Transform:

$$\int_0^\infty\frac{sin(x)}{x}dx = \int_0^\infty\int_0^\infty e^{(-y\cdot x)}sin(x)\,dxdy = \int_0^\infty\frac{1}{1+y^2}dy = \lim_{y\to\infty} arctan\,(y) = \frac{\pi}{2} \qquad \text{(B.25)}$$

Then the total cross-section of a resonance is written by a simpler expression, that only depends on the matrix density states of the potential:

$$\sigma = \frac{\pi}{k^2}\left(\pi U^2(E_x) + \pi U^2\left(E_y\right)\right) \equiv \pi^2 \lambda\!\!\!^{-2} |\langle k'|U(E_R)|k\rangle|^2 \qquad \text{(B.26)}$$

using $\lambda\!\!\!^{-} = 1/k$ in the previous equation.

B.3 Quantum Statistics of the Spin on Cross-Section

According to Merzbacher (See Ch.2 [15]) an important scattering physical law describes for a vicinity of a resonance that the wave-function can be described by a complex parameter:

$$f(z) = x + iy = (E - E_R) + i\,\Gamma/2 \qquad \text{(B.27)}$$

which makes sense by treating $tan\left(\delta(E_R)\right) = \frac{\Gamma}{2(E_R - E)}$ as the polar angle of (B.27), introducing in an arbitary wave-function a decay parameter, since:

$$\psi \propto exp(ikz) = exp\left(ik(E - E_R + i\,\Gamma/2)\right) = exp\left(ik(E - E_R)\right)exp(-k\,\Gamma/2) \qquad \text{(B.28)}$$

By taking the Fourier Transform of (B.18) using the complex parameter of (B.27), the Lippmann-Schwinger operator is derived:

$$f(r) = \frac{-1}{q}\int_0^\infty r\,sin(qr)U(r)dr = \frac{-U(E_R)}{q}\int_0^\infty exp\left(iq(r + i\,\Gamma/2)\right)dq = \frac{U(E_R)}{r + i\Gamma/2} \equiv \frac{U(E_R)}{E - E_R + i\Gamma/2} \qquad \text{(B.29)}$$

as r is re-interpreted as the vicinity of $E - E_R$.

Using (B.29) result as template, it justifies the procedure to apply a small correction to the potential around its resonance energy,

$$U(E) = U(E_R) + \frac{A_{fi}^{\mu}}{E - E_R + i\Gamma/2} \qquad \text{(B.30)}$$

This adds a small dispersion with length Γ and represents the resonance width with a finite duration. The other "A" terms are amplitudes given by:

$$2\pi A_{fi}^{\mu} = exp\left(i\left(\delta_f + \delta_i\right)\right) exp\left(i\delta_\mu\right) g_{\mu f}(J) g_{\mu i}(J) \qquad \text{(B.31)}$$

Coupling (B.30) with (B.31), the interaction between the projectile and the target is represented. The "*f*" subscript shows the phase shift once the projectile finished the interaction, while "i" refers to the initial states of the system. The resonance is represented by a μ subscript.

This means that the resonance width can be separated into an initial and final width:

$$\Gamma = \Gamma_{\mu}^{f} + \Gamma_{\mu}^{i} \qquad \text{(B.32)}$$

and each "*g*" term (that depends on the quantum angular numbers J) squared is equal to each partial width:

$$\Gamma_{\mu} = \sum_k \Gamma_{\mu k} : \Gamma_{\mu k} = g_{\mu k}^2 \qquad \text{(B.33)}$$

Replacing (B.31) on (B.30), the potential expansion can be written as:

$$U(E) = U(E_R) + \frac{exp\left(i(\delta_f + \delta_i)\right)}{2\pi} \sum_k \frac{exp(i\delta_\mu) g_{\mu f} g_{\mu i}}{E - E_R + i\Gamma_{\mu}^{f}/2 + i\Gamma_{\mu}^{i}/2} \qquad \text{(B.34)}$$

Other important factors are the quantum angular momenta of the projectile, target and the resonance itself. We will assume that the quantum numbers for the target and projectile will be I_a and I_b respectively. The resonance spin will be named *J*.

Since the angular momentum wave-function is separable from the radial part, it means that the we can separate their contributions without affecting the other term:

$$\sigma = \pi^2 \lambda\!\!\!^{-2} |\langle k' | U(E_R) | k \rangle|^2 = \pi^2 \lambda\!\!\!^{-2} S(J, I_a I_b) |\langle f | U(E_R) | i \rangle|^2 \qquad \text{(B.35)}$$

The angular momentum part of (B.35) is a straightforward calculation that does not require more than some fundamental quantum mechanics operations.

First, the spins (or in general the quantum angular momentum) of the target and projectile nuclide can be summed as:

$$I_a + I_b = S \qquad \text{(B.36)}$$

This sum is called the channel spin S which together with the orbital angular momentum L, forms the resonance spin J, which means:

$$J = L + S = L + I_a + I_b \tag{B.37}$$

The channel and resonance spins S and J range over:

$$|I_a - I_b| \leq S \leq I_a + I_b \tag{B.38}$$

$$|L - S| \leq J \leq L + S \tag{B.39}$$

Since the target and the projectile are independent before the scattering, then according to (B.38), for each quantum number I_a or I_b will be a total of $2I_a+1$ and $2I_b+1$ projections of the spin.

The resonance spin J will also have $2J+1$ projections of the spin, since L is not changed.

This leads to define the statistical spin factor as the ratio between the resonance states and the projectile states, as the following:

$$\omega = \frac{(2J+1)}{(2I_a+1)(2I_b+1)} \tag{B.40}$$

To finish the derivation, it is known that all nuclide components (protons and neutrons) are fermions with spin-1/2, then we need to multiply the expression by a factor of 2 to take account of the two spin states. This enables to obtain the quantum spin density states formula:

$$S(J, I_a I_b) = 2\omega = \frac{2(2J+1)}{(2I_a+1)(2I_b+1)} \tag{B.41}$$

B.4 The Breit-Wigner with a Resonance Strength

Once replaced (B.41) on (B.37), the cross-section formula will be given by:

$$\sigma(E) = \frac{2\pi^2 \lambda\!\!\!^{-2}(2J+1)}{(2I_a+1)(2I_b+1)} |\langle f|U(E)|i\rangle|^2 \tag{B.42}$$

The bracket term will be evaluated by replacing (B.30) on (B.42), using the same integrals that involve Dirac's Delta function and the proprieties of (B.33)

The following expression after all replacements results in:

$$\sigma(E) = \frac{\pi\lambda^2(2J+1)}{(2I_a+1)(2I_b+1)} \int_0^\infty \int_0^\infty \sum_{\mu\nu} \frac{exp\left(i(\delta_\nu - \delta_\mu)\right) g_{\nu f} g_{\mu f} g_{\nu i} g_{\mu i}}{\left(E - E_\nu + i\left(\Gamma_\nu^f + \Gamma_\nu^i\right)/2\right)\left(\left(E - E_\mu + i\left(\Gamma_\mu^f + \Gamma_\mu^i\right)/2\right)\right)} d\delta_\nu d\delta_\mu \quad \text{(B.43)}$$

Using simple algebraic manipulation of Dirac's Delta proprieties to evaluate the integrals related to the phase shifts, the following important formula is derived:

$$\sigma(E) = \frac{\pi\lambda^2(2J+1)}{(2I_a+1)(2I_b+1)} \sum_{\mu\nu} \frac{\Gamma_f(E)\Gamma_i(E)}{(E-E_\nu)(E-E_\mu)+\Gamma^2(E)/4} \quad \text{(B.44)}$$

The previous equation is the cross-section with a General Breit-Wigner Resonance formula, and it shows that the initial and final resonance widths can be different and vary with the energy, while the initial and final resonance compound states also can be different.

For a well-defined sharp resonance, which is the case assumed by ERYA-Profiling physical model, the energy values subscripts with Greek letters are equal (the compound nuclide is in a specific energy state), which means that:

$$\sigma(E) = \frac{\pi\lambda^2(2J+1)}{(2I_a+1)(2I_b+1)} \cdot \frac{\Gamma_f(E)\Gamma_i(E)}{(E-E_R)^2+\Gamma^2(E)/4} \quad \text{(B.45)}$$

Using the definition of (B.40) one derives the Breit-Wigner resonance distribution for a strong coupled spin, also called, Breit-Wigner with a Resonance Strength:

$$\sigma(E) = \frac{4\pi\lambda^2\omega\Gamma_f(E)\Gamma_i(E)}{4(E-E_R)^2+\Gamma^2(E)} \quad \text{(B.46)}$$

Which can also be written as the following:

$$\sigma(E) = \frac{4\pi\lambda^2\omega\gamma\Gamma(E)}{4(E-E_R)^2+\Gamma^2(E)} \quad \text{(B.47)}$$

Notice that the resonance widths from the resonance and those related to all projectile channels are functions of energy, which is true for large energy intervals, but can be approximated as constants for the vicinity of the resonance energy, and (B.47) are applied by this reason.

It is possible to derive a more functional equation that are implemented on ERYA-Profiling, which requires first to derive an expression for the De Broglie's wavelength:

$$E = \frac{p^2}{2\mu}; \lambda\!\!\!^{-} = \frac{\hbar}{p} = \frac{\hbar}{\sqrt{2\mu E}} \tag{B.48}$$

Since the PIGE experimental setup uses proton beams with low MeV energies, it is fine to use classical kinematics, also it needs to evaluate the reduced mass μ are related to the projectile (a proton) and a target nuclide with mass M:

$$\frac{1}{\mu} = \frac{1}{m_p} + \frac{1}{M}; M \approx Am_p \rightarrow \mu = \frac{m_p M}{m_p + M} \approx \frac{Am_p^2}{(A+1)m_p} = \frac{Am_p}{A+1} \tag{B.49}$$

Squaring (B.48) and substitute to (B.49) result:

$$\lambda\!\!\!^{-2} = \frac{\hbar^2(A+1)}{2AEm_p} \tag{B.50}$$

And replacing (B.50) to (B.47) determine the resonance cross-section with resonance strength with all computable parameters, especially the dependence of energy:

$$\sigma(E) = \frac{4\pi\hbar^2(A+1)\omega\gamma\Gamma(E_R)}{(2AEm_p)(4(E-E_R)^2+\Gamma^2(E_R))} \tag{B.51}$$

With the additional condition that the resonance width is constant around the resonance energy.